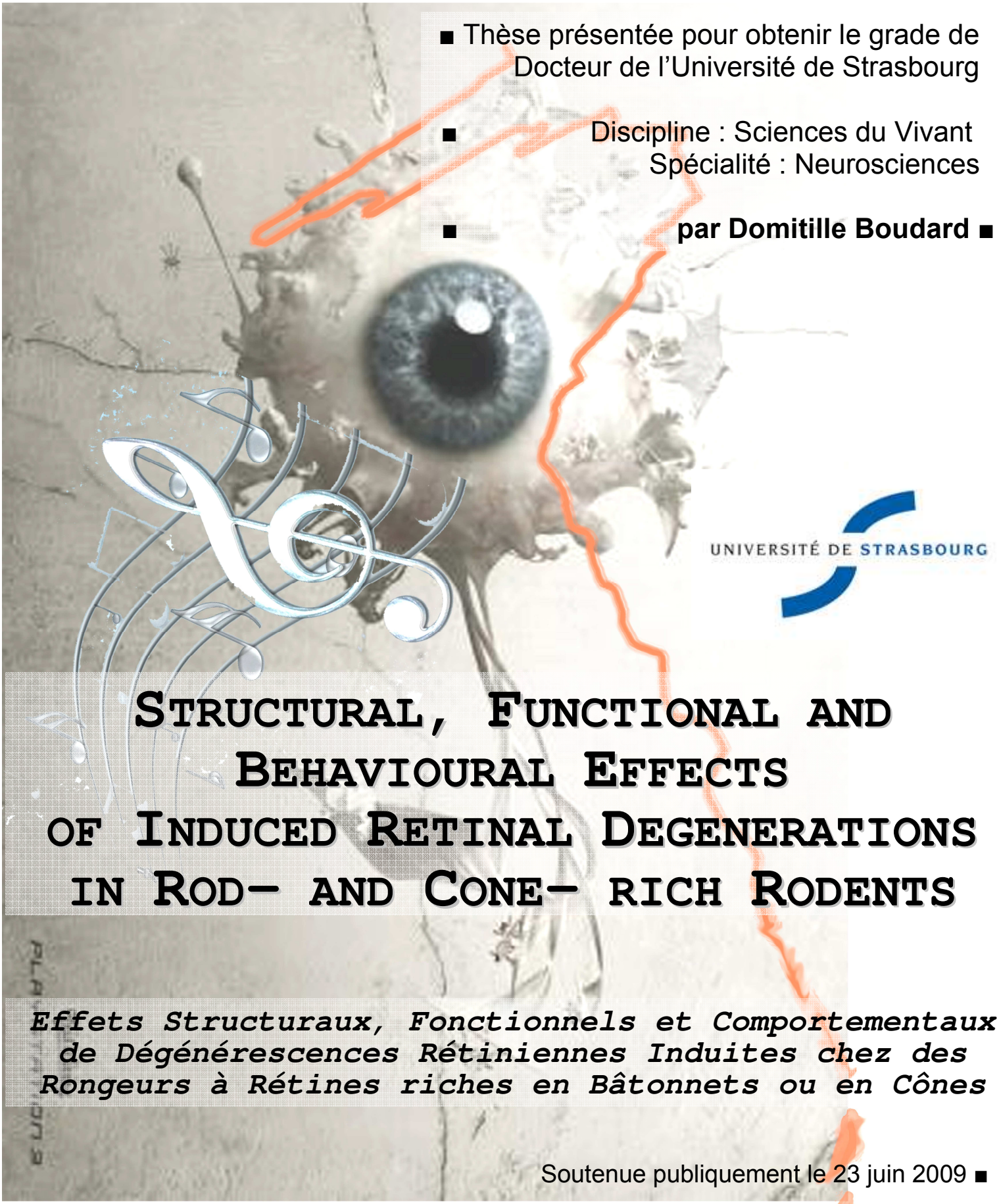

■ Thèse présentée pour obtenir le grade de Docteur de l'Université de Strasbourg

■ Discipline : Sciences du Vivant
Spécialité : Neurosciences

■ **par Domitille Boudard** ■

UNIVERSITÉ DE STRASBOURG

STRUCTURAL, FUNCTIONAL AND BEHAVIOURAL EFFECTS OF INDUCED RETINAL DEGENERATIONS IN ROD- AND CONE- RICH RODENTS

Effets Structuraux, Fonctionnels et Comportementaux de Dégénérescences Rétiniennes Induites chez des Rongeurs à Rétines riches en Bâtonnets ou en Cônes

Soutenue publiquement le 23 juin 2009 ■

Membres du jury ■

Directeur de Thèse	M. David Hicks, Directeur de Recherche, Strasbourg
Rapporteur Interne	Mme. Hélène Dollfus, PUPH, Strasbourg
Rapporteur Externe	M. Christian Grimm, Professor, Zürich
Rapporteur Externe	M. Howard Cooper, Directeur de Recherche, Bron

Membre invité ■

M. André Malan, Directeur de Recherche Emérite, Strasbourg

■ Thèse présentée pour obtenir le grade de
Docteur de l'Université de Strasbourg

■ Discipline : Sciences du Vivant
Spécialité : Neurosciences

■ **par Domitille Boudard** ■

UNIVERSITÉ DE STRASBOURG

STRUCTURAL, FUNCTIONAL AND BEHAVIOURAL EFFECTS OF INDUCED RETINAL DEGENERATIONS IN ROD- AND CONE- RICH RODENTS

Effets Structuraux, Fonctionnels et Comportementaux de Dégénérescences Rétiniennes Induites chez des Rongeurs à Rétines riches en Bâtonnets ou en Cônes

Soutenue publiquement le 23 juin 2009 ■

Membres du jury ■

Directeur de Thèse	M. David Hicks, Directeur de Recherche, Strasbourg
Rapporteur Interne	Mme. Hélène Dollfus, PUPH, Strasbourg
Rapporteur Externe	M. Christian Grimm, Professor, Zürich
Rapporteur Externe	M. Howard Cooper, Directeur de Recherche, Bron

Membre invité ■

M. André Malan, Directeur de Recherche Emérite, Strasbourg

A Mum, sis et PP…

Imagination is more important than knowledge.

Albert Einstein

The work presented here was carried out in 2006-2009 in the following laboratories:

- **Département de Neurobiologie des Rythmes** (actual Head: Dr. Valérie Simmoneaux), part of the Institut de Neurobiologie Cellulaire et Intégrative (UPR 3212 CNRS), Strasbourg, France;
- **« Eye and Nutrition » group** (Heads: Dr. Lionel Bretillon and Dr. Catherine Creuzot-Garcher), part of the FLAVIC laboratory (FLAveur Vision Comportement du consommateur) (UMR 1129 INRA), Dijon, France;
- **Laboratory for Retinal Cell Biology** (Head: Prof. Christian Grimm), University of Zurich, Dept. Ophthalmology, Zurich, Switzerland;
- **Division of Ocular Neurodegeneration** (Head : Prof. Mathias Seeliger), part of the Centre for Ophthalmology, Tübingen Institute for Ophthalmic Research, Tübingen, Germany.

This work was financially supported by:

- The Ministère de l'Enseignement supérieur et de la Recherche
- The Région Alsace
- Alcon®

Abstract in English

In the vertebrate retina, the cells whose role is to detect photons are called photoreceptors. Two types of "classical photoreceptors" (PRs) can be distinguished based on their structure and function: rods and cones. Because of their primordial role in visual acuity, integrity of cones is essential for good vision. The study of physiology and pathology of cones is hence crucial but hampered in classic laboratory rodents (mice and rats) due to their rod dominant retinas (97-99 %). Our laboratory possesses the world's only breeding colony of the diurnal rodent: *Arvicanthis ansorgei,* whose retina has 33 % of cones.

The aims of the study were: 1st, **to establish an *in vivo* model of retinal degeneration in which cone pathogenesis can be easily observed, permitting comparison with that of rods**; and 2nd, **to characterize the effects of degeneration at the structural, physiological and behavioural levels**.

To induce retinal degeneration, two types of published approaches were used: bright light exposure and *N*-methyl-*N*-nitrosourea (MNU) injections. Exposure of *Arvicanthis* to bright light, irrespective of the paradigm used, never induced any reproducible retinal damage either at the structural or functional level. In an alternative approach, high doses of MNU were injected into *Arvicanthis* to induce retinal degeneration. At the structural level, the degeneration commenced approximately 11 days after injection, and presented regional variability in that the upper hemisphere was damaged first, followed by the degeneration of the inferior one. Cones were markedly more resistant than rods during the degeneration process. ERG recordings at late post-treatment times showed decreased amplitudes of responses driven by either rods or cones, demonstrating that visual function is highly compromised. However, because retinal degeneration was never complete in Arvicanthis, in order to examine the effects of MNU-induced retinal degeneration on light-evoked behaviour, we chose to use rats in which photoreceptor loss is total. Abilities of control and MNU-treated rats to photoentrain to light/dark cycles of different light intensities were compared. Results showed that MNU-treated rats did not entrain their locomotor activity when light intensity was low whereas control rats were still synchronized.

The ensemble of this work has provided: 1st, **extensive characterization of *Arvicanthis ansorgei* retina, particularly at the functional level**; 2nd, evidence for remarkably **high resistance of *Arvicanthis* to retinal damage**; 3rd, establishment of a validated **model for the study of rod and cone degeneration** within the same retina; 4th, extensive description of **structural and functional characteristics of MNU-induced retinal**

degeneration in *Arvicanthis;* and 5th, evidence of an **impaired photoentrainment ability in MNU-treated rats.**

Résumé en Français

Introduction

L'œil est l'organe responsable de la détection, du traitement primaire et du transfert de l'information lumineuse aux structures cérébrales. L'ensemble de ces fonctions est réalisé en grande partie par un tissu tapissant l'intérieur de l'œil : la **rétine**. Ce tissu est structuré en plusieurs couches formées de différents types cellulaires. L'empilement de ces couches est perpendiculaire à la trajectoire du faisceau lumineux de sorte que la lumière traverse successivement l'ensemble des couches avant d'être détectée. L'information lumineuse arrive au niveau de la couche la plus externe, composée des **photorécepteurs (PRs)**. Ces cellules ont pour rôle de capter les photons et de traduire le message lumineux en un message nerveux qui sera éventuellement transmis aux cellules ganglionnaires dont les axones véhiculent l'information visuelle vers les centres supérieurs.

Deux types de PRs sont distingués, en fonction de leur structure, mais aussi de leurs fonctions. Les **bâtonnets** contiennent un seul pigment visuel (ou opsine) : la rhodopsine. Ils sont très sensibles à la lumière et sont sollicités lorsque l'intensité lumineuse est faible (à la tombée de la nuit ou à la pénombre). Ils sont essentiels à la détection des mouvements et des formes. Les PRs du deuxième type, les **cônes**, sont répartis en trois types en fonction de la longueur d'onde du pic d'absorption de leur opsine. Chez les rongeurs, il existe des cônes MW (*Middle Wavelength* ou longueur d'onde moyenne) qui absorbent principalement la lumière verte et des cônes SW (*Short Wavelength* ou longueur d'onde courte) qui absorbent principalement la lumière bleue. Chez l'Homme, un troisième type de cône absorbe principalement la lumière rouge. Etant donné leur faible sensibilité à la lumière, les cônes sont principalement sollicités dans des conditions où l'intensité lumineuse est forte. Chez l'Homme, les cônes permettent la détection des couleurs et une grande acuité visuelle; leur bon fonctionnement est le garant d'une bonne vision. En cas de dégénérescence des PRs, c'est d'ailleurs lorsque les cônes sont touchés que le handicap visuel est le plus important. **L'étude de la physiologie et de la pathologie des cônes s'avère donc indispensable.** Cependant, il existe très peu de données à l'heure actuelle sur la physiopathologie des cônes. Ceci est lié en grande partie au fait que les modèles animaux utilisés le plus fréquemment dans les laboratoires, généralement des rongeurs tels que rats et souris, ont des rétines très pauvres en cônes (seuls 1 à 3 % des PRs sont des cônes, le reste étant de type bâtonnet). Il

existe des espèces à rétines riches en cônes, comme l'écureuil, le porc, ou la musaraigne, mais elles ne sont pas faciles à élever en laboratoire et les outils biologiques ne sont pas forcément applicables à l'étude de ces espèces (sondes, anticorps, généralement développés chez le rat ou la souris). Au laboratoire nous possédons une espèce de Muridés diurne dont le nom scientifique est ***Arvicanthis ansorgei*** et dont la rétine a été caractérisée récemment (Bobu et al., 2006). L'analyse immunohistochimique avec des anticorps spécifiques des différentes opsines a révélé une **forte proportion de cônes** : environ 33 % des PRs (soit 10 fois plus que dans les rétines de rat ou de souris).

Les dégénérescences rétiniennes sont une cause fréquente de cécité dans les pays développés. L'étude de l'induction et de la cinétique de l'apoptose des cônes et des bâtonnets lors de la dégénérescence rétinienne est une étape clef de la recherche sur la prévention des pathologies rétiniennes et la protection de la rétine. La plupart des modèles de dégénérescences rétiniennes sont des modèles génétiques de mutations naturelles ou induites par génie génétique. Parmi les protéines dont la mutation entraîne une dégénérescence rétinienne, on trouve notamment des protéines de la phototransduction (comme la rhodopsine : mutations *rd*) et des protéines nécessaires au recyclage des pigments visuels (comme la RPE65). Ces modèles génétiques ont été très utilisés pour étudier les mécanismes de la dégénérescence rétinienne et tester des approches thérapeutiques. Cependant, ils présentent plusieurs inconvénients qui rendent leur utilisation difficile. Les mutations génétiques sont, à l'heure actuelle, principalement effectuées sur des souris, espèce dont la rétine possède très peu de cônes ce qui rend ces modèles difficilement adéquats pour l'étude de la physiopathologie de ce type de PR. De plus, en fonction des gènes invalidés, une mutation peut avoir des conséquences non seulement sur la rétine mais aussi sur d'autres organes compromettant la survie de l'animal ou les études au niveau comportemental. Enfin, il est difficile, avec les modèles génétiques, de moduler le moment auquel la dégénérescence apparaît et d'étudier sa progression à l'âge adulte, étant donné que la plupart des dégénérescences liées à des mutations ont une initiation précoce. Des modèles non génétiques de dégénérescences rétiniennes permettent de pallier ces inconvénients. Parmi les approches couramment utilisées, on trouve les dérégulations métaboliques par hypo- ou hyper- glycémie ou les lésions mécaniques par augmentation de la pression intraoculaire, pour mimer les caractéristiques du glaucome par exemple. La **toxicité induite par la lumière** a été expérimentalement établie en 1966 (Noell et al., 1966) et, depuis, les mécanismes de dégénérescence rétinienne suite à une exposition à la lumière ont été amplement étudiés. Il

existe aussi des modèles liés à la toxicité d'une substance. En effet, de nombreuses substances toxiques entraînent des dommages rétiniens. C'est le cas des agents alkylants, connus pour induire la formation de tumeurs, mais qui peuvent aussi entraîner la dégénérescence des photorécepteurs. En 1967, Herrold découvrait les effets délétères d'une injection de ***N*-méthyl-*N*-nitrosourée (MNU)** sur la rétine du hamster doré (Herrold, 1967). La MNU entraîne notamment une dégénérescence complète des PRs sous 7 jours, et ce, chez de nombreuses espèces (Tsubura et al., 2003a).

La rétine a la propriété de capter la lumière et de transmettre un message préalablement traité aux centres supérieurs. La fonction la plus classiquement connue de la rétine est la **fonction de formation d'images** dont le but final est la perception de l'environnement par la modalité visuelle. Cette fonction est rendue possible grâce aux PRs, aux cellules de la couche nucléaire interne et aux cellules ganglionnaires (RGCs). Les axones de ces dernières forment le nerf optique qui conduit l'information visuelle aux corps genouillés latéraux et aux feuillets intergéniculés latéraux du thalamus. Ces informations sont par la suite envoyées au cortex visuel pour un traitement plus approfondi. L'intégrité de la fonction visuelle peut être évaluée chez l'animal par l'utilisation de tests basés sur des tâches de placement, de repérage spatial ou sur les réactions d'anxiété des animaux face à des environnements visuels nouveaux. La rétine a aussi une deuxième fonction : la **capacité de détecter la présence ou l'absence de lumière**, appelée aussi message photique, nécessaire à la synchronisation des processus rythmiques circadiens (dont la période est d'environ 24 h), mais aussi au fonctionnement normal du réflexe pupillaire qui permet de réguler la quantité de lumière arrivant au niveau de la rétine. L'évaluation de la synchronisation photique de l'horloge circadienne peut être établie en enregistrant par exemple l'activité locomotrice d'un animal maintenu en cycle obscurité/lumière de 12-h/12-h. Dans ces conditions, un animal nocturne sera actif principalement pendant la nuit, et un animal diurne, pendant le jour. En cas de détérioration du système détectant et intégrant les signaux photiques, le rythme de l'activité peut s'en trouver perturbé. Au niveau comportemental, les effets d'une dégénérescence rétinienne peuvent donc être évalués, soit via l'étude de fonctions visuelles, soit via l'étude de fonctions non visuelles.

Les caractéristiques d'une dégénérescence rétinienne ou les effets thérapeutiques d'agents protecteurs peuvent être évalués à la fois aux niveaux structural, physiologique et comportemental. Au niveau structural, les techniques d'histologie peuvent être combinées à

des techniques d'imagerie *in vivo* en temps réel, type SLO (Ophtalmoscopie par balayage Laser) qui permettent d'avoir une vue globale du fundus et d'observer notamment la vascularisation rétinienne en utilisant des sources d'excitation différentes, ou par OCT (Tomographie par Cohérence Optique), une technique qui permet d'avoir une vue transversale de l'épaisseur de la rétine. L'enregistrement des réponses électrophysiologiques (ERG) de l'ensemble de la rétine suite à un stimulus visuel permet quant à lui d'évaluer l'intégrité de la rétine au niveau fonctionnel.

Objectifs

Les objectifs du travail de thèse étaient : 1, la **mise en place d'un modèle *in vivo* de dégénérescence rétinienne** dans lequel les cônes soient facilement repérables et l'étude de leur apoptose possible et comparable à celle des bâtonnets ; 2, l'établissement des **caractéristiques des effets de la dégénérescence rétinienne aux niveaux structural, fonctionnel et comportemental.**

1. Résistance de *Arvicanthis* à la Dégénérescence Rétinienne induite par la Lumière (?)

Lors de nos travaux, nous avons utilisé deux types d'induction de dégénérescence : l'exposition à la lumière intense et l'injection d'un composé toxique**.**

Dans un premier temps, les *Arvicanthis* ont été exposés à différents types de sources lumineuses en modulant les paramètres expérimentaux. Les premières expositions ont été réalisées à la lumière blanche en s'appuyant sur les paramètres trouvés dans la littérature. L'étude histologique des coupes de rétines des animaux exposés n'a révélé aucune différence structurale ou morphologique par rapport à celles des animaux témoins élevés en cycle de lumière/obscurité avec une intensité lumineuse de 200 lux. Nous avons alors varié la durée entre le moment de l'exposition et celui du sacrifice afin de détecter des événements précoces de la dégénérescence comme l'initiation de l'apoptose 36-h après exposition, ou des événements tardifs tels que la diminution de l'épaisseur de la couche nucléaire externe (généralement visible au bout d'une semaine). L'aspect structural des rétines contrôles et des rétines exposées était similaire pour tous les temps testés. Nous avons augmenté la durée d'exposition à une semaine sans pour autant observer de modifications structurales. Des études ont montré une influence du temps circadien auquel l'exposition avait lieu sur

l'apparition ou non d'une dégénérescence (Organisciak et al., 2000). Nous avons donc exposé les *Arvicanthis* à différentes périodes de leur temps circadien. Pour toutes les périodes étudiées, l'ensemble des rétines étaient structurellement intactes. Des paramètres d'exposition plus extrêmes ont par la suite été utilisés comme une exposition sous anesthésie avec un éclairage à fibre optique pouvant générer une intensité d'environ 20 000 lux. Là encore, aucune dégénérescence des rétines des *Arvicanthis* n'a été mise en évidence.

Afin d'étudier si les éventuels dommages induits par la lumière pouvaient avoir des conséquences au niveau physiologique et si l'intégrité structurale de la rétine ne cachait pas une altération fonctionnelle, nous avons analysé les réponses électrophysiologiques d'*Arvicanthis* exposés à la lumière et les avons comparées à celles d'*Arvicanthis* contrôles. Cette étude a révélé une physiologie rétinienne non altérée.

Enfin, nous avons utilisé la lumière bleue, connue pour avoir des effets plus délétères sur la rétine. Chez la souris, la lumière bleue induit une dégénérescence sévère après 5 minutes d'exposition. Des *Arvicanthis* exposés pendant 15 ou 30 minutes à cette même source lumineuse ne présentaient aucun dommage au niveau de leur rétine. Seul l'animal exposé pendant 45 minutes présentait une lésion rétinienne sur une zone limitée.

L'ensemble de ces résultats suggère une **grande résistance de *Arvicanthis* à la dégénérescence induite par la lumière**. Cette résistance peut être liée au fait que *Arvicanthis* est un animal pigmenté et que son épithélium rétinien offre donc une protection naturelle contre la toxicité induite par la lumière. Mais cette résistance peut aussi être liée à l'écologie de l'*Arvicanthis* qui nécessiterait au niveau oculaire une protection face aux agressions lumineuses. *Arvicanthis* est une espèce diurne et qui est donc active principalement dans des conditions de forte luminosité. Un mécanisme de défense face aux dommages de la lumière à forte intensité paraît indispensable. Il est aussi probable que les cônes soient moins sensibles à la phototoxicité que les bâtonnets, étant donné qu'ils sont actifs de jour et beaucoup moins sensibles à la lumière à faible intensité. Des études ont aussi montré que le mécanisme d'action de l'effet néfaste de la lumière sur la rétine passait par l'activation du pigment visuel des bâtonnets : la rhodopsine (Grimm et al., 2000b). *Arvicanthis* possédant une forte proportion de cônes, cela expliquerait qu'il soit moins sensible et particulièrement épargné face à la phototoxicité par rapport à des espèces à rétine riche en bâtonnets. En clinique la relation causale entre exposition à la lumière et apparition de dégénérescence rétinienne, type dégénérescence maculaire liée à l'âge, n'a jamais été clairement établie et les résultats des études épidémiologiques restent controversés. La lumière ne constitue sûrement pas un

facteur initiateur de dégénérescence, mais reste sans aucun doute un facteur aggravant d'une pathologie préexistante.

2. Caractérisation de la Dégénérescence Rétinienne induite par la MNU chez *Arvicanthis ansorgei*

Afin de déterminer si *Arvicanthis* est une espèce particulièrement résistante à la phototoxicité ou résistante à tout type de stress rétinien de manière générale et dans le but de poursuivre notre quête d'un modèle de dégénérescence des cônes, nous avons décidé d'utiliser une approche alternative pour endommager la rétine.

Nous avons utilisé le modèle MNU, décrit pour induire une dégénérescence rapide et complète des PRs. La MNU a déjà été utilisée chez de nombreuses espèces (souris, hamster, rat, musaraigne, macaque) en tant qu'inducteur de dégénérescence rétinienne (Herrold, 1967 ; Tsubura et al., 2003a). Lors de nos travaux, nous avons remarqué que la MNU injectée à la même dose que celle généralement utilisée chez le rat (75 mg/kg) n'entraînait aucune modification de la rétine de *Arvicanthis*, même après 25 jours. En revanche, cette dose de MNU injectée chez le rat Long Evans (souche pigmentée) induisait une dégénérescence complète des PRs après 7 jours.

Lorsque la MNU était utilisée à plus forte dose (100 ou 150 mg/kg) chez *Arvicanthis*, elle entraînait une dégénérescence continue des PRs observable par histologie, commençant 11 jours après l'injection et continuant après 25 jours. Afin d'évaluer les effets physiologiques généraux de la MNU sur *Arvicanthis*, la masse corporelle et la prise alimentaire quotidienne des animaux ont été mesurées à partir de J-5 avant injection et jusqu'au jour du sacrifice. L'analyse des résultats a montré, chez les animaux traités à la MNU, une prise alimentaire et une prise de poids identiques à celles des animaux témoins, une dizaine de jours après injection. Les effets structuraux rétiniens de la dégénérescence suite à une injection de MNU chez *Arvicanthis* ont été évalués sur des coupes histologiques. A 3 jours après injection, les segments externes des PRs se sont révélés plus courts. Jusqu'à 25 jours post-injection l'épaisseur de la couche nucléaire externe diminuait jusqu'à disparaître totalement. En revanche, les couches internes de la rétine (couche nucléaire interne et couche des cellules ganglionnaires) ne semblaient pas affectées par l'injection. Le même constat a été fait à 3 mois après une injection de MNU à 100 mg/kg. La MNU semblerait donc endommager sélectivement les PRs au sein de la rétine. Cette sélectivité a aussi été détectée

in vivo par la technique OCT où l'observation transversale de la rétine mettait en évidence une diminution drastique de l'épaisseur des PRs et une épaisseur des couches rétiniennes internes non modifiée.

Afin d'évaluer si la dégénérescence des PRs était homogène au niveau de la rétine, une étude topographique de la dégénérescence a été réalisée sur des coupes histologiques en mesurant l'épaisseur de la couche des photorécepteurs (segments externes et internes, et couche nucléaire externe) par rapport à l'épaisseur de la couche nucléaire interne. Cette analyse a permis de mettre en évidence une évolution non homogène de la perte des PRs le long de l'axe inférieur/supérieur. Au 11ème jour après injection, l'épaisseur de la couche des PRs des rétines traitées à la MNU était sensiblement réduite par rapport aux rétines contrôles. Cette réduction s'amplifiait les jours suivants avec une réduction plus marquée dans l'hémisphère supérieur, comparativement à l'hémisphère inférieur, notamment aux niveaux médian et central. L'observation des fundi de ces mêmes animaux par SLO avait aussi montré que l'atteinte était plus importante au niveau de l'hémisphère supérieur où des inclusions lipidiques et du matériel fluorescent étaient visibles.

En utilisant des anticorps dirigés contre les protéines spécifiques des cônes et des bâtonnets, nous avons montré que les bâtonnets étaient les premières cellules touchées, et que la dégénérescence des cônes suivait. L'analyse de la distribution de cellules apoptotiques marquées par la méthode TUNEL a permis de montrer que dans un premier temps les cellules apoptotiques se trouvaient au niveau interne de la couche cellulaire externe (emplacement des corps cellulaires des bâtonnets) et notamment dans l'hémisphère supérieur au niveau central, puis, que toutes les cellules de la couche nucléaire externe étaient touchées et que la progression s'étendait ensuite à l'ensemble du pôle supérieur et à une partie de l'hémisphère inférieur. La dégénérescence tardive des cônes par rapport à celle des bâtonnets a aussi été mise en évidence par immuno-empreinte où le ratio de la quantité de rhodopsine par rapport à la quantité d'arrestine des cônes a été comparé dans des rétines contrôles et des rétines traitées à la MNU. Ce ratio est réduit de plus de 84 % après injection de MNU, signifiant qu'à un moment donné de la progression de la dégénérescence, la perte des bâtonnets est plus importante que celles des cônes. Au niveau fonctionnel, nous avons montré par ERG que les amplitudes des ondes a et b étaient réduites aussi bien dans des conditions dans lesquelles le système des bâtonnets était sollicité que dans celles où seule la réponse générée par l'activation des cônes était observable. Ce dernier résultat signifie que, bien que les cônes semblent être relativement épargnés par l'injection de MNU au niveau structural, leur intégrité fonctionnelle est cependant compromise.

L'étude de la dégénérescence rétinienne suite à une injection de MNU chez *Arvicanthis* a permis : 1, de confirmer la relative résistance de la rétine de *Arvicanthis* déjà observée lors d'un stress lumineux ; 2, d'établir un modèle de dégénérescence induite des deux types de PRs ; 3, de caractériser cette dégénérescence aux niveaux structural et fonctionnel ; 4, de mettre en évidence une dégénérescence relative des cônes plus lente que celle des bâtonnets ; 5, de mettre en évidence une progression régionale de la dégénérescence, avec des dommages plus importants au niveau de l'hémisphère supérieur.

3. Effets de la Dégénérescence Rétinienne induite par la MNU sur le Photoentraînement chez le Rat

La dégradation drastique des PRs chez le rat et *Arvicanthis* et la faiblesse des réponses de l'ERG chez *Arvicanthis* suggèrent une perte notable de la fonction visuelle après une injection de MNU. Nous avons souhaité évaluer l'effet de cette dégénérescence marquée par une perte des PRs sur une autre fonction de la rétine : la **synchronisation de l'activité locomotrice à l'alternance lumière/obscurité** aussi appelée le photoentraînement. Nous avons choisi d'utiliser le rat traité avec la MNU comme modèle d'étude, espèce chez laquelle la dégénérescence des PRs est quasi-totale après quelques jours. Des rats Long Evans injectés avec le solvant seul ou une solution de MNU à 75 mg/kg ont été placés dans des cages individuelles munies d'une roue dont le nombre de révolutions est enregistré en temps réel. Le rythme de l'activité locomotrice des animaux a été enregistré au cours de 3 cycles LD successifs d'intensité lumineuse décroissante : 300, 15 et 1 lux.

L'analyse des enregistrements par actimétrie a montré que les rats contrôles synchronisaient leur activité locomotrice pendant les 3 cycles, mais que leur angle de phase lors du cycle de 1 lux était plus important que celui qu'ils présentaient à 300 et 15 lux. La capacité de photoentraînement des rats traités avec la MNU n'était pas altérée à 300 lux. A 15 lux, les rats MNU avaient toujours la capacité de se synchroniser, mais leur angle de phase était plus important que celui trouvé à 300 lux et que celui des animaux contrôles pour le même cycle. A 1 lux, les rats MNU perdaient totalement leur capacité à synchroniser leur activité locomotrice. Après le cycle de 1 lux, un dernier cycle de 300 lux a été mis en place afin de vérifier que la perte de la synchronisation observée à 1 lux n'était pas liée à une évolution de la dégénérescence, mais plutôt à un effet spécifique de l'intensité lumineuse.

Dans cette condition, les animaux MNU étaient à nouveau photoentraînés. On sait que dans des conditions de luminosité très faible (comme c'est le cas pour 1 lux), seuls les bâtonnets sont photosensibles. Ce résultat important met donc en évidence le fait que dans des conditions de faible luminosité le système des bâtonnets serait sollicité pour la fonction de photoentraînement, alors qu'à forte intensité d'autres cellules photosensibles pourraient intervenir, comme les cellules à mélanopsine.

Les animaux ont ensuite été sacrifiés et les rétines ont été prélevées pour évaluer et quantifier l'expression de protéines spécifiques des bâtonnets et des cônes (pigments visuels et protéines de la phototransduction) et de la mélanopsine, une protéine synthétisée par une sous-population de cellules ganglionnaires et dont le rôle dans le photoentraînement a déjà été démontré (Panda et al., 2002). L'analyse histologique des rétines de rats traités à la MNU a confirmé la dégénérescence complète des PRs au moment du sacrifice. Afin de confirmer que la rétine était déjà dégénérée au début des enregistrements, une coupe de rétine de rat sacrifié 9 jours après injection a aussi été comparée aux rétines contrôles et a montré que la disparition des PRs était déjà quasi complète dès 9 jours post-injection. L'étude histologique a aussi révélé une préservation de l'intégrité structurale des couches internes de la rétine. L'analyse histologique de l'expression des protéines spécifiques des bâtonnets et des cônes a montré une disparition presque totale des bâtonnets, une perte des cônes et une dégradation de leur segment externe. De plus l'expression des protéines de la phototransduction des bâtonnets et des cônes était significativement réduite. Le nombre de cellules marquées positivement avec un anticorps anti-mélanopsine sur coupes et sur rétines montées à plat a été déterminé et les cellules à mélanopsine se sont révélées moins nombreuses dans les rétines traitées avec la MNU. L'expression de la mélanopsine a été quantifiée par la méthode d'immuno-empreinte et l'expression totale de la protéine était réduite de plus de 80 % après traitement à la MNU. **L'ensemble des résultats a montré qu'une perte des PRs associée à une diminution de l'expression de la mélanopsine après injection de MNU chez le rat entraînait une perte de la synchronisation au cycle LD à basse intensité lumineuse.**

En conclusion, l'ensemble de ce travail de thèse a permis :

1 : La caractérisation plus en détail, aux niveaux structural et fonctionnel, de la rétine d'un modèle de rongeur à forte proportion de cônes: *Arvicanthis ansorgei*.

2 : La mise en évidence de la relative résistance de la rétine de *Arvicanthis* à deux types de stress aux mécanismes différents.

3 : La mise en place d'un modèle pour l'étude de la dégénérescence induite des cônes permettant de comparer au sein du même animal la cinétique de dégénérescence des deux types de photorécepteurs.

4 : La détermination des caractéristiques rétiniennes, structurales et fonctionnelles, du modèle MNU chez *Arvicanthis*.

5 : La mise en évidence de la perte du photoentraînement, une fonction réalisée par la rétine, chez le rat tarité à la MNU.

Acknowledgments / Remerciements

Firstly, I would like of course to thank you, **David**, for your ability in recycling lost PhD students… You taught me what I know about retinal anatomy and physiology, and certainly more that I already forgot! Thank you also for your way of supervising my work, it was drastically different from what I have experienced previously! It was very enjoyable to have such freedom and possibility to experiment my own ideas. Thank you finally for your personality which renders any situation informal and easy.

Merci à **Marie-Paule**, deuxième pilier de l'équipe rétine ! Ta vivacité d'esprit et ton intérêt pour le travail des autres ont su faire des réunions d'équipe des moments hyper enrichissants. Merci pour ta gentillesse, ta générosité, ton sourire et ta capacité à faire des critiques constructives et pertinentes sans jamais froisser ; qualités très rares et que j'admire. J'espère que tu vas obtenir tous les résultats que tu mérites.

Je souhaite remercier pleinement **Mireille Masson-Pévet** pour m'avoir accueillie au sein du laboratoire. Merci aussi pour votre support généreux lors de la « pér iode de transition ».

Je souhaite aussi remercier fortement **Paul Pévet** pour sa capacité fédérer les personnes autour de projets communs, et notamment les doctorants en Neurosciences de Strasbourg, qui ont bénéficié de son support constant par l'intermédiaire de Neurex et de l'IFR des Neurosciences et ont pu ainsi mener à bien leurs projets.

I would like to sincerely acknowledge the members of the Jury. Merci au **Professeur Hélène Dollfus**, danke **Professor Christian Grimm** and thank you **Doctor Howard Cooper** for giving me some of your time to judge my work. I am also grateful to Christian Grimm for his help with retinal degeneration issues.
Merci au **Docteur André Malan** pour avoir accepté de relire ce manuscrit, pour ses commentaires toujours très avisés et grâce auxquels j'ai pu découvrir mon travail sous des angles nouveaux.

I also wish to acknowledge people who contribute to this work:

Thank you to the group of **Professor Mathias Seeliger** for the *in vivo* data of MNU-treated *Arvicanthis*. Vielen dank **Naoyuki**, **Edda**, **Regine**, **Gesine** und **Susanne**.
Thank you to the group of Christian Grimm in Zürich, particularly to **Doctor Andrea Wenzel** and **Professor Charlotte Remé** whose kindness and extensive knowledge in the retinal degeneration matter where of great help. Danke schön.
Merci beaucoup à l'équipe Œil et Vision et aux **Docteurs Lionel Bretillon** et **Catherine Creuzot-Garcher** pour avoir accepté d'accueillir temporairement les *Arvicanthis* (et moi-même !). Ma gratitude va notamment au **Docteur Niyazi Acar** qui m'a initiée aux joies des ERG avec tellement de patience et de gentillesse, moi qui n'étais pas particulièrement au fait des techniques électrophysiologiques !

Merci **Dom'** pour t'occuper si dynamiquement d'une grande partie de l'animalerie. Merci aussi pour avoir pris de ton temps pour m'avoir initiée aux injections intraveineuses. Enfin, merci pour m'avoir épaulée et avoir su défendre mes intérêts pour les manips d'actimétrie… tu vois, ça a porté ses fruits !

Merci **Sophie** pour ton aide en matière de formalités administratives concernant les transports transfrontaliers d'animaux, ton aide pour l'obtention des produits ophtalmiques et aussi pour les injections intraveineuses (pas si faciles que ça en a l'air quand tu le fais toi !). Merci aussi pour ta réactivité et ta sympathie, comme la fois où tu m'as mise en contact avec une clinique de Strasbourg possédant un appareil à ERG.

Un énorme merci à **Aurore** et **Anita**, les fées du Chronobiotron ! Merci aussi à **Olivier**. Merci pour vous être occupés de tous les petits locataires du 5ème. Merci aussi et surtout à **Daniel B.** qui, en plus d'avoir la lourde tâche de gérer tous les arvis, m'a aidée à administrer les gouttes ophtalmiques aux *Arvicanthis* au risque de se faire mordre méchamment ! Merci beaucoup !

Mes remerciements vont aussi à **Paul K**., gardien féroce de la salle d'immuno', dont les conseils en or et l'étendue des connaissances rendent les manips' un peu moins mystérieuses… et beaucoup plus abordables !

A tous les membres de notre dynamique équipe :

Merci **Cristina** (alias Tudor !) pour ton amitié, mulțumesc ! Ta personnalité originale et ton sens du contact ont fait de toi une personne indispensable à la cohésion de l'équipe. Merci pour avoir écouté mes coups de gueule, brefs, mais intenses. Merci aussi pour la surprise le jour de mon anniversaire… inoubliable ! Ne perds surtout pas ta capacité à rire de tout et ton art du discernement… it is so Cristinish !

Un gros clin-d'œil à toi **Corina**, parce que c'est pas parce que tu nous as quittés pour des contrées moins clémentes qu'on t'a oubliée ! La vie dans le bureau avec toi a été très agréable. Je n'oublierai pas notre voyage transatlantique, un moment riche en aventures, vraie bouffée d'air dans le train-train laborantin ! J'en profite pour faire un gros bisou à Gregor dont les sourires nous manquent atrocement !

J'ai aussi une grande pensée pour **Sandrine**, exilée dans le Sud. Ton dynamisme, ton énergie et ton sens de l'humour manquent au bureau ! Ta capacité à gérer plusieurs tâches en même temps en ont rendu admiratifs plus d'un ! Merci pour ton aide en western-blot aussi ; tu n'hésitais pas à laisser tomber toutes tes manips pour venir me filer un coup de main ! Je n'oublierai jamais la recherche des œufs de Pâques !

Au camarade **Jean-Georges**, ta fougue et ta pugnacité pour exprimer les idées qui te tiennent à cœur ont su faire du bureau un véritable lieu d'échanges pas forcément très scientifiques mais pour le moins animés ! *Hasta la victoria!* Pour ce qui est de la part scientifique, merci beaucoup de m'avoir initiée aux joies du *western-blot*… oups, pardon… de *l'immuno-empreinte* je devrais dire ! Désolée par avance pour la soutenance en anglais, je sais que ça ne te plaira pas beaucoup. Mais je sais aussi que ton ouverture d'esprit et que ton intérêt pour les langues étrangères te permettront d'excuser cet écart !

Virginie, je te souhaite beaucoup de succès dans tes manips, beaucoup d'arvis attrapés les doigts dans l'nez et de phagosomes comptés (ceux-là aussi on les aime sans les compter…) ! Merci aussi pour toutes les délicieuses petites attentions franc-comtoises qui fleuraient bon les hauts-plateaux du Jura (…), tellement revigorantes et qui me permettaient de ne pas trop avoir le mal du pays.

Ouafaa, j'espère que tes westerns ne te feront plus jamais enrager ! J'espère aussi que ta peur des animaux te quittera peu à peu (ils sont si gentils…). Garde ton sourire et ta capacité à prendre du recul, ils sont ta force !

Arthur, j'espère que tu trouveras ta voie… Ne perds pas ta gentillesse et ta générosité au contact de plus brutes ! Ceux-ci te les envieront sûrement plus tard… Je compte sur toi pour l'écriture…

Madah: *Kiya haal hai?* Good luck with phagosomes! You'll probably need more time and energy (and chocolate…) ! I hope rhythms will move as you wish…

Tounes… hé Tounes ! Petite boule d'énergie en éternel mouvement dans le labo le matin, et épuisée dans l'après-midi. J'espère que tu réussiras à canaliser toute cette énergie dans une direction fructueuse ! Je croise les doigts pour que toutes ces captures puissent être exploitables.

Catherine. Merci pour les lames colorées sur le pouce ! Ça m'a bien dépannée ! En espérant que ta route parmi nous soit encore longue… compatriote !

Je n'oublie pas bien sûr **Claudine** qui nous rend la vie au laboratoire très facile grâce à sa capacité à gérer les stocks de solutions indispensables, et depuis peu la gestion des commandes aussi.

Good luck also to **Diana** with the electrophysiological measurements.

Fafa… hum Fafa… Alors toi, j'dois féliciter pour ta bonne humeur et l'ambiance enjouée que tu sais créer quotidiennement au labo ! J'espère que tu arriveras à acquérir la confiance en toi dont tu auras besoin, notamment pour ta validation visée. Merci aussi pour la surprise à l'occasion de mon anniversaire… difficile d'oublier tous ces ballons accrochés à mon bureau ! Un souvenir mémorable… *You're butterfly Fafa !*

Merci aussi à tous ceux qui ont su faire du labo un lieu agréable…

Dominique S., pour ton contact facile et toujours serein, et pour ton très grand sens de l'humour !
Rouliane, j'espère que tu ne t'épuiseras pas dans les manips… ou ailleurs… Merci pour tous les efforts déployés à l'occasion de mon anniversaire. Attention aux vampires qui risquent de te rendre visite au Chronobiotron entre ZT12 et ZT24 ! J'espère aussi que tu réussiras à surmonter tes crises psychotiques, parce que mettre le ketchup dans le micro-ondes, c'est vraiment pas drôle !
Laura, mon modèle de classe vestimentaire ! Félicitations pour ton dynamisme et ta capacité à maintenir tes engagements que j'ai pu apprécier en organisant avec toi le Jeu des Hormones ! J'espère que tes hamsters ne te décevront pas et que tu continueras à progresser avec le danois !
Sylviane, pour être une personne si agréable et pour ton sens de l'analyse original, qui font de toi un être indispensable à la bonne humeur générale.
Laurent, pour avoir la capacité d'observer le monde environnant avec une loupe si personnellement nexonienne !
Merci **Daniel C.** pour tes nombreux coups de main, tes corrections et ta grande générosité.
Stéphanie, pour ton rire tellement ravivant qui force à rester éveillé…
Patrick, pour ta propension, comme tout vrai Franc-Comtois, à ne pas te prendre la tête.
Stefanie, vielen glück für die Zukunft und Danke für Deine vielen Helfer mit germanischen Schwierigkeiten!
Ibtissam, bon courage pour la suite. Merci pour ta gentillesse.
Etienne, merci pour tes conseils en matière de problématique actimétrienne.

Et pour les anciens du labo qui ne sont plus là, merci pour votre accueil chaleureux ! Une pensée toute particulière à **Ben** (j'ai gardé ton petit mot de bienvenue dans le labo !), et **Céline**, pour son organisation de fêtes internationales !
Une pensée aussi pour **Mathieu**, vrai gentil tellement attachant, et **Florent**, deuxième gentil, dont je dois avouer avoir copié un peu le style pour présenter mon manuscrit.

Et comme la thèse, c'est aussi l'aboutissement d'un travail commencé bien en amont, je remercie aussi toutes les personnes rencontrées avant mon arrivée au Département de Neurobiologie des Rythmes.

Je pense aux personnes de l'IPCB et notamment à **Viviane** pour ton aide pour les tests comportementaux, même si mon TR a pu pas mal te déstabiliser ! **Betty** une éternelle maman si pleine de vie ! **Nina** pour ton soutien. **Francine** pour ta gentillesse. **Pierre**, fameux musicien ! **François** parce que vous faire des blagues me manque. **Michel** pour ton aide en matière de siRNA et t'être inquiété dans une période trouble. **Dilec** pour ta gentillesse quotidienne. **Jean-Luc** pour ton aide en informatique. **Pascal Darbon** pour les informations à propos du MEA. Merci aussi à **Marie-José Freund-Mercier** et **Rémy Schlichter** pour avoir été présents.

Une pensée aussi pour **Olive**, **André Dufour** et **Victor Candas**, grâce auxquels le DEA a pu être une réussite. Merci d'avoir été là pour mes débuts dans la recherche !

Une très forte pensée aussi à **Eve** et **Cindy**, mes camarades de fac' avec lesquelles la biologie devenait tellement hilarante!

Et comme ma thèse ne peut pas se résumer au travail scientifique pur, je n'oublie pas tous les membres de DoctoNeuro avec lesquels on a réalisé tellement de belles choses, indispensables à un bon équilibre psychique!
Je pense à **Etienne** notre ingénieur hyper talentueux et toujours prêt à filer un coup de main, **Anne-So'** dont le calme et la gentillesse offrent une grande bouffée d'air dans ce tourbillon de la vie, à **Christophe**, un vrai Hippocrate qui s'est honoré de ses serments, **Jenny** tellement attachante dans son rôle de Mini-Poussosse, **Matei** qui a pu réaliser ses fantasmes, **Delphine** et ses qualités de co-pilote, **Pedro** un troubadour qui nous manque, **Sophie** qui a repris l'organisation des NeuroTéléthoniens avec brio, **Alex**, **Elise**, **Marie**, **Nabila**, **Hugues**, **Peiman**, **Laure**, **Joëlle**, **Isa**, **Samir**, **Roomi**, **Fred**, **Clara, PH** … et tous ceux qui ont contribué à la réalisation de nos projets en apportant un petit quelque chose, une petit pierre, de la petite poussière… d'étoiles… neuronales !
Merci aux personnes qui ont permis à nos projets de se réaliser : **Catherine Duportail** et **Delphine Picamelot** de la Mission Culture Scientifique et Technique de l'ULP, **Delphine LeDelliou** du Vaisseau, **Stéphanie Klipfel** pour Neurex et **Kerly Ilves** de Ahhaa (*tere Tartu !*).

Une pensée aussi pour les super cops de Stras' :

Fannette, pour ton soutien pendant la période de rédac' et pour nos délires multiples.

Aurélie, parce qu'écrire mes remerciements, ça m'fait bien rire, tu sais… Parce que nos parcours se sont sans cesse croisés et que l'on a vécu plein plein de choses ensemble… heureusement que tu étais là !

Aurore, un mystère freudien tellement attachant. Merci pour tes bisous à répétitions, pour ta folie régulée, pour ta spontanéité !

Une grosse pensée très très particulière pour ma **kikinette**, amie de choc, amie de toujours, toujours à l'écoute, toujours tellement préoccupée par le bonheur des autres. J'ai eu une chance énorme de croiser ton chemin !

Une pensée finalement à ma Franche-Comté natale et à mes amis de toujours :

¡**Elsa**, mi gran amistad de la juventud! Te admiro mucho por tus capacidades lingüísticas, lo sabes…
Camille, qui mérite la médaille de l'amitié. Toujours tellement au fait de tout… et **Jérém'**, futur papa gâteau, ma main à couper !
Méla, notamment pour nos délires aquatiques.
Benoît, le Casanova casé… que de déceptions…
… mais que de joies pour **Fanny** ... Excuse-moi d'avoir failli te faire redoubler parce que tu rigolais trop !
Moumou, un vraie Dr. de choc, hein collègue ?
Delph' et **John-Paul**, bon courage pour cette nouvelle aventure parisienne !
Nanou, esprit créatif par définition, merci pour ton intérêt pour mon travail, ça m'a toujours beaucoup touchée.
Ari' : un tourbillon d'émotions, un exemple pour l'ensemble de notre troupe de théâtre !
Ad' : bonne nouvelle route à deux… je te souhaite tout le meilleur !
Et bien sûr **Lydou Didou** et sa petite bande basque… *Egunon !*

Merci aux personnes de ma famille qui m'ont soutenue, encouragée, aidée : **Edith**, **Chantal D.** et **Jean-Marc**, **Henri** et **Chantal B.** et mes **grands-parents**.
Merci aussi à **Marie-Antoinette** qui a bien assuré dans son rôle de stagiaire improvisée ! Merci pour le coup de main !
Une pensée particulière pour **Jojo**, dont j'ai pu goûter les délices de sa correspondance. Merci pour ton intérêt à mon travail de thèse. Ton regard et ton jugement m'ont beaucoup encouragée.

Finalmente, gracias a ti, el Caifan, **el guapito**, porque sin ti, nada de todo esto seria posible. Me has ayudado tanto con los experimentos, con los animales, con la redacción (y con los espíritus del cuarto obscuro!). La vida de cada día es un sueño, aun si somos tan diferentes. Esta tesis es un poco tuya también.
El viaje no se termina aquí… ¿Que te parece?
A quien todavia no llega pero ya esta tan presente, **Chicharin**… Gracias por todo lo que me das cada dia…

Table of Content

List of Figures and Tables

INTRODUCTION

MATERIALS AND METHODS

RESULTS

Recurrent Abbreviations

aa: amino-acid
***Aa*:** *Arvicanthis ansorgei*
AF: autofluorescence
AMD: age related macular degeneration
APS: ammonium persulfate
BSA: bovine serum albumin
b.w.: body mass
c-arr: cone arrestin
cGMP: cyclic guanosine monophosphate
CCB: cone cell body
Cnga3: cyclic nucleotide gated channel alpha 3
***cpfl1*:** cone photoreceptor function loss 1
COS: cone outer segment
DAPI: 4',6-diamidino-2-phenylindole dihydrochloride
DD: permanent darkness
DNA: deoxyribonucleic acid
d.p.i.: days post injection
DTT: dithiothreitol
EDTA: ethylenediaminetetraacetic acid
ERG: electroretinogram
EW: Edinger Westphal nucleus
FL: fluoresceine
$G_{\alpha t1}$: rod transducin
$G_{\alpha t2}$: cone transducin
GC: guanylate cyclase
GDP: guanosine diphosphate
GFAP: glial fibrillary acidic protein
Gnat1: Guanine nucleotide binding protein (G protein), alpha transducin activity polypeptide 1
GTP: guanosine triphosphate
H/E: haematoxylin/eosin
HCl: hydrochloric acid
ICG: indocyanin green
IGL: intergeniculate leaflet
INL: inner nuclear layer
i.p.: intraperitoneal
IPL: inner plexiform layer
ipRGC(s): intrinsically photosensitive retinal ganglion cell(s)
IR: infra-red
IS: inner segment(s)
LD: cyclic light/dark
LL: light/light
LW: long wavelength
MNU: *N*-methyl-*N*-nitrosourea
mRNA: ribonucleic acid messenger
MW: mid-wave
NIF: non image forming
nr: nervous (mutation)
Nrl: neural retina leucine zipper
OCT: optical coherence tomography
ONH: optic nerve head
ONL: outer nuclear layer.
OPL: outer plexiform layer
OPN: olivary pretectal nucleus
***Opn4*:** opsin 4 (melanopsin) gene
OS: outer segment(s)
P23H: histidine substituted for proline at aa sequence position 23
PBS: phosphate buffered saline
***pcd*:** purkinje cell degeneration
PDE: phosphodiesterase
PLR: pupillary light reflex
PR(s): photoreceptor(s)
PVDF: polyvinylidene fluoride
RCB: rod cell body
Rdta: attenuated diphtheria toxin gene fused to a promoter for rhodopsin
rd: retinal degeneration 1 mutation
rds: retinal degeneration slow mutation
RD(s): retinal degeneration(s)
RF: red free
RGC(s): retinal ganglion cell (s)
RGCL: retinal ganglion cell layer
RHT: retinohypothalamic tract
RIS: rod inner segment
ROS: rod outer segment
RPE: retinal pigment epithelium
SD: standard deviation
SD-OCT: Spectral domain Optical Coherence Tomography
SDS: sodium dodecyl sulfate
SEM: standard error of the mean
SCN: suprachiasmatic nucleus
SLO: scanning laser ophthalmoscope
SW: short wavelength
TBS: tris buffered saline
TdT: terminal deoxynucleotidyl transferase
TEMED: tetramethylethylenediamine
TUNEL: TdT-mediated dUTP nick end labelling
UTP: uridine-5'-triphosphate
UV: ultraviolet
VLGN: ventral lateral geniculate nucleus
ZT: *Zeitgeber* ("time giver") time

INTRODUCTION

A. INTRODUCTION

1. Down to Basics: Anatomy and Physiology of the Vertebrate Retina

2. In Quest of a Cone Model

3. Retinal Degenerations and their Mammalian Models

4. Retina Visual and Non Visual Functions

5. Evaluation of RD and RD Protective Treatment Effects

1. Down to Basics: Anatomy and Physiology of the Vertebrate Retina

In Vertebrates, only two organs can undergo biochemical changes in the presence of light: skin, which to the delight of many people will turn brown after sun bathing, and eyes. Nevertheless, the eye is the only real gate of light into the body and allows the transformation of photic energy to an electric signal. Light rays are focussed through the transparent cornea and lens upon the retina (Figure 1). Although all parts of the eye are important for perceiving light, the most crucial ocular structure is the **retina**, an essential region of the brain (derived from the neural tube) that gets direct stimulation from the outside world of light and images.

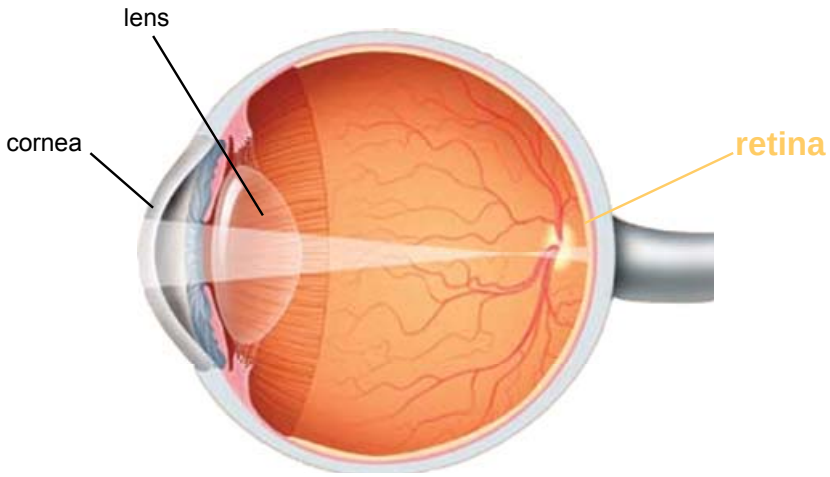

Figure 1 Drawing of light rays pathway through the eye.

Light rays enter the eye through the cornea and are refracted twice with help of the lens to finally be focused on the retina, lining the posterior wall of the eye.

Modified from © Mayo Foundation for Medical Education and Research.

1.1. Basic Anatomy of the Retina

The retina is a thin (500 µm in human and 200 µm in mice) tissue that lines the inner surface of the eyeball (Figure 1).

With the use of electron microscopy, microelectrode recording techniques, and pharmacology, retinal structure and function are nowadays very well understood. The first anatomical description of the retina was performed more than a century ago by Santiago Ramón y Cajal who used Golgi silver staining to describe the cell types constituting the retina in a number of vertebrate species (Cajal, 1892). Even if the detailed connections of the different cell types were wrong, the overall anatomical structure of the layers was very accurate (Figure 2A).

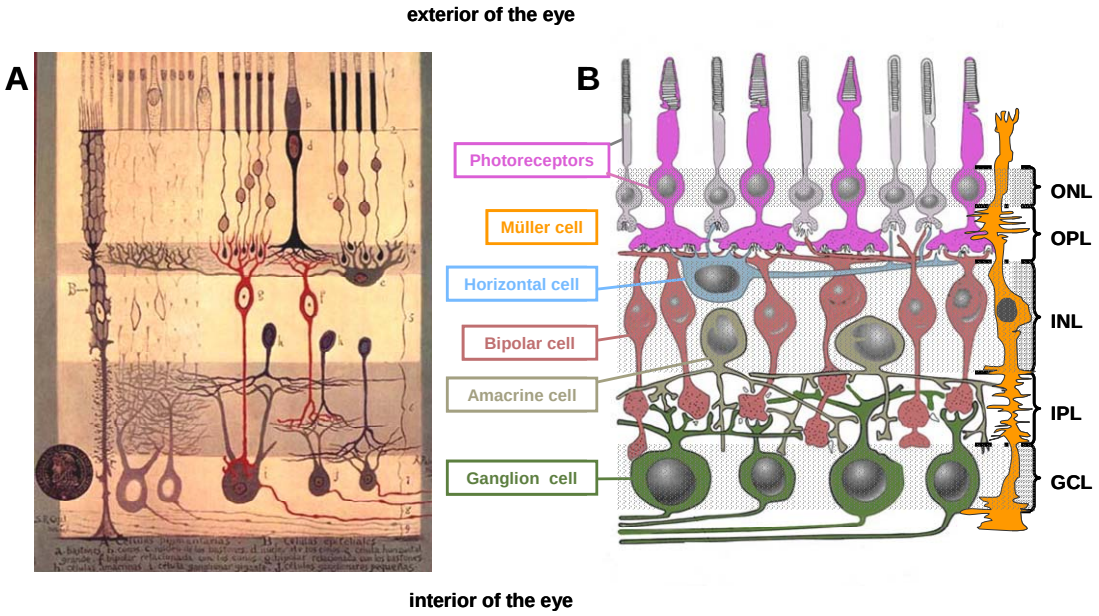

Figure 2 Radial section of the mammalian retina tissue.

Representation of the retinal structure with: **A**: a drawing made by Cajal around 1880; and **B**: a schematic representation of the structure of the retina as viewed nowadays.

GCL, ganglion cell layer; INL, inner nuclear layer; IPL, inner plexiform layer; ONL, outer nuclear layer; OPL, outer plexiform layer.
A. From "Structure of the Mammalian Retina" c. 1900 by Santiago Ramón y Cajal. **B**. Modified from www.skidmore.edu.

As clearly described by Cajal, we now know that vertebrate retinas are composed of three layers of cell bodies and two layers of synapses (Figure 2B). The **outer nuclear layer (ONL)**, located nearest the sclera, contains the cell bodies of the **classical photoreceptors (PRs)** (rods and cones). The **inner nuclear layer (INL)** contains the cell bodies of the **bipolar**, **horizontal** and **amacrine cells**, as well as those of the principal glial cells of the retina, the **Müller cells**. The most internal nuclear layer, the **ganglion cell layer (RGCL)**

contains cell bodies of **ganglion cells (RGCs)**, displaced amacrine cells and retinal astrocytes. Dividing these cell layers are two interplexiform layers where synaptic contacts are made between the different neurons. Most externally is the **outer plexiform layer (OPL)** where connections between PRs in the ONL, and bipolar and horizontal cells in the INL occur. The **inner plexiform layer (IPL)** is formed of synapses made between bipolar amacrine and ganglion cells.

1.2. Light Signal Transmission, the Classic Pathway

Vertebrate PRs respond to light by virtue of their apical specialisation: the **outer segment (OS).** This structure is filled with stacks of plasma membranes containing **visual pigments**: molecules composed of a protein called **opsin** and a chromophore derived from vitamin A and known as **retinal**. Each OS contains millions of visual pigment molecules.

The first event in light perception is **absorption of a photon by retinal**. Upon absorption of a photon of light, the retinal isomerizes from the 11-*cis* form to all-*trans* retinal which triggers conformational changes in the molecule resulting in bleaching. Opsin undergoes a conformational change to metarhodopsin II. Metarhodopsin II dissociates into opsin and all-*trans* retinal. The opsin activates transducin located in the cytosol, causing it to exchange bound guanosine diphosphate (GDP) for guanosine triphosphate (GTP), leading to dissociation of the alpha subunit from the beta and gamma subunits of transducin, with the GTP still bound to the alpha subunit. The alpha subunit-GTP complex activates phosphodiesterase (PDE) that hydrolysis cyclic guanosine monophosphate (cGMP) to 5'-GMP, lowering the concentration of intracellular cGMP which in turn leads to closure of the sodium channels within the plasma membrane. Closure of the sodium channels causes hyperpolarization of the cell due to the ongoing potassium current (Figure 3).

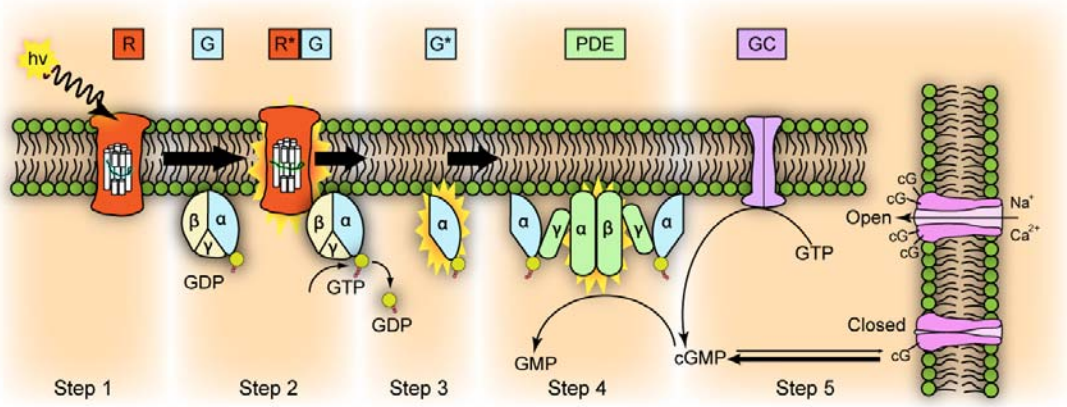

Figure 3 Representation of molecular steps in photoactivation.

Drawing of an OS disk in a rod. Step 1: A photon (hv) is absorbed and activates a rhodopsin molecule (R*) resulting in a conformational change in the disk membrane to R*. Step 2: Next, R* makes repeated contacts with transducin molecules, catalyzing their activation to G* by the release of bound GDP in exchange for cytoplasmic GTP. The α, β and γ subunits separate. Step 3: G* binds inhibitory γ subunits of the phosphodiesterase (PDE), releasing the active its α and β subunits. Step 4: Activated PDE hydrolyzes cGMP. Step 5: Guanylyl cyclase synthesizes cGMP, the second messenger in the phototransduction cascade. Reduced levels of cytosolic cGMP cause cyclic nucleotide gated channels to close preventing further influx of Na^+ and Ca^{2+}.

cGMP: cyclic guanosine monophosphate; G*: transducin; GC: guanylyl cyclase; GDP: guanosine diphosphate; GTP: guanosine triphosphate; OS: outer segment; PDE: phosphodiesterase; R*: rhodopsin.
Modified by J.J. Corneveaux from (Leskov et al., 2000).

Hyperpolarisation of the photoreceptor results in a decrease in release of the neurotransmitter glutamate in the OPL, which constitutively released in the dark. The effect of glutamate is to close a glutamate-activated Na^+ channel at the synaptic contact between PRs and depolarizing bipolar cells. Therefore, during a light stimulus, lowered release of glutamate onto the bipolar cell reduces the number of glutamate-activated Na^+ channels that are closed and the **bipolar cells** subsequently **depolarize**. This depolarization causes increased transmitter release onto the **RGCs which depolarize** and **produce action potentials** which are relayed to cortical visual processing centres via the optic nerves. This pathway (PR – bipolar cells – RGCs) is known as the **vertical pathway** of light signal transduction (Figure 4).

PR signals can also be transmitted laterally **using a horizontal pathway** by **horizontal** and **amacrine cells** that intermix, combine and modify the synaptic signal prior to final transmission to RGCs. These changes allow adjustment of sensitivity for bright and dim light vision, and permit shaping of visual responses by such processes as lateral inhibition, that increase contrast and sharpness of the image.

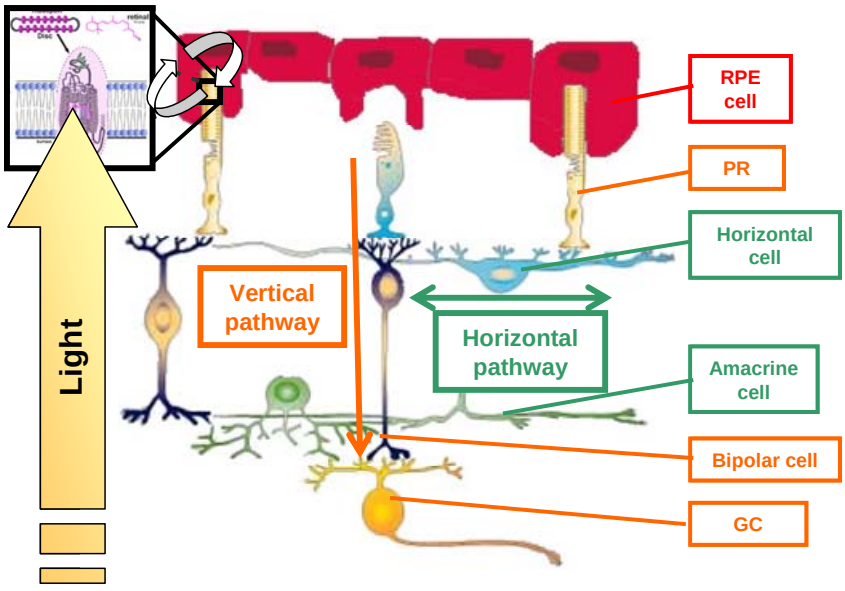

Figure 4 **Representation of vertical and horizontal phototransduction pathways.**

Light hits the visual pigment located in the OS of the PR (highlight). Upon this reaction, PRs activate bipolar cells that subsequently activate RGCs. Once the visual pigment has been activated, it requires regeneration through the visual cycle in the apposing RPE cells. The horizontal pathway is composed of horizontal and amacrine cells.

OS: outer segment; PR(s): photoreceptor(s); RGCs: retinal ganglion cells; RPE: retinal pigment epithelium. Modified from www.mitre.org.

The cells acting as photon detectors are the PRs which OS are oriented vertically towards the exterior of the eye. The cells whose role it is to transmit the light message out of the retina are the RGCs, located at the inner part of the retina. Therefore light must **travel through the thickness of the retina** before striking and activating the PR (Figure 4). This arrangement is necessary because OSs have to be in contact with the **retinal pigment epithelium (RPE)**, a monolayer located behind the retina that is vital for photosensitivity. Isomerisation of a visual pigment upon light absorption renders the protein insensitive to further light stimulation, and restoration of light sensitivity requires chemical re-isomerization of retinal via a multistep enzyme pathway, called the **visual cycle,** that takes place in part in the RPE. Hence, RPE cells are essential for the recycling of retinal molecules. Also, RPE cells are loaded with melanin granules that absorb stray photons and free radicals, providing an important protective shield.

In this classic view of the light signal transmission pathway, uniquely rods and cones are able to detect photons. We will later see that a sub-population of RGCs is also capable of light detection.

2. In Quest of a Cone Model

Two types of classic PRs exist in the vertebrate retina: **rods** and **cones**. They can be distinguished by their structure, their physiology and their respective roles.

2.1. Rods vs. Cones: Different Equipment, Different Functions

Rods and cones share a **common property**: they **detect photons** and undergo subsequent biochemical and physiological changes upon their absorption. But these two PRs differ in **structure**, **topography** and **roles**.

2.1.1. Different (Ultra) Structures

The PR cell consists of: an **OS** that - as seen previously - is filled with stacks of membranes containing the visual pigments, an **inner segment (IS)** containing the apparatus necessary for protein synthesis and ATP formation (mitochondria, Golgi apparatus, ribosomes…), a **cell body** containing the nucleus, and an **axon** extending to a **synaptic terminal** where neurotransmission to bipolar and horizontal cells occurs. Rods and cones both possess the same overall morphology but fine structure differs in several respects.

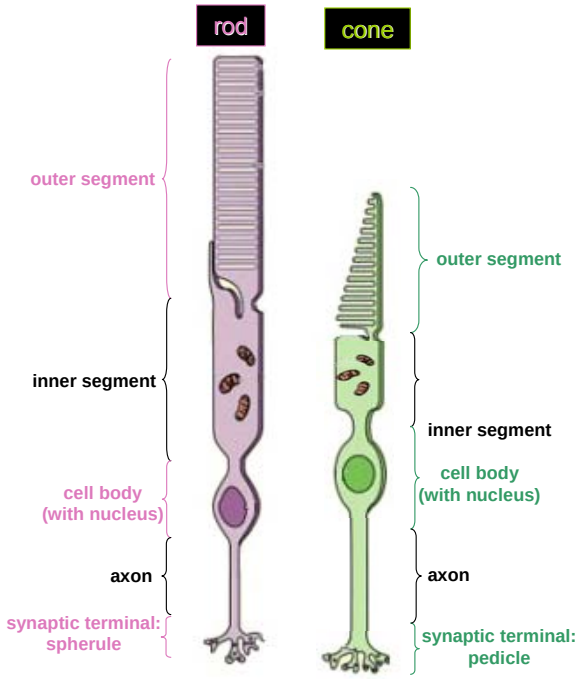

Figure 5 Rod and cone structures.

Both types of PRs contain an outer segment, an inner segment, a cell body, an axon and a synaptic terminal that can be distinguished for rods and cones.

Modified from thebrain.mcgill.ca.

First, whereas **rod OS (ROS)** are **slim cylindrical** structures reaching to the RPE, **cone OS (COS)** are **shorter**, **robust** and more **conical** with a wider base and tapering shape (Figure 5).

Second, ROS are **filled entirely with closed discs of double membranes** enveloped by a separate plasma membrane, whereas COS are composed of successive folds in a single **plasma membrane**, and thus are open to the extracellular space on one face (Figure 5).

Third, rod synapses are known as **spherules** are different to those of cones called **pedicles**. Rod spherules are **small round enlargements** of the axon (3-5 µm diameter) or extensions of the cell body. The less numerous cone pedicles, in contrast, are large, conical, flat end-feet (8-10 µm diameter) of the axon. Rod spherules lie packed between and above the cone pedicles (Figure 6).

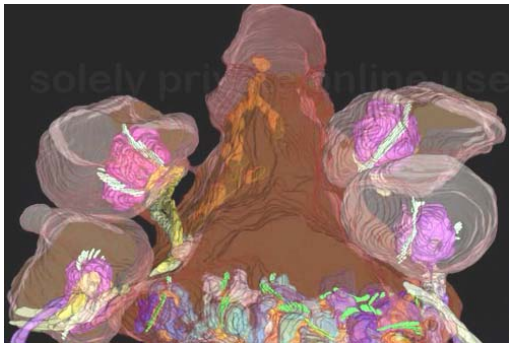

Figure 6 Synaptic terminations of rods and cones.

Reconstruction from electronic microscopy of a cone pedicle (centre) surrounded by rod spherules (sides).

From H. Jastrow (University of Mainz, Germany).

2.1.2. Different Topographies

Besides their structure, rods and cones also differ by their distribution within the retina.

Cone cell bodies (CCBs) lie along the scleral border of the ONL, with rod cell bodies (RCBs) making up the remainder of the ONL between and below the cone cell bodies. Cone inner segments are massive compared to the thin rod IS (Figure 4).

Rods and cones also have different lateral distributions that vary depending on the species considered. In the human retina, rods are distributed **all over the retina** except for a small spot totally devoid of rods where 100 % of the PRs are cones (Figure 7). This region, called the foveola, corresponds to the central point for image focus. In a radius of 1 mm around the foveola, the fovea, cones constitute over 50 % of the PRs, while over the entire retina cones average 5 % of total PRs (Curcio et al., 1991). Instead of a fovea, some vertebrate retinas have other specializations of the central retina, as the ***area centralis*** or the **visual streak**. These are regions with high density of ganglion cells located within a central field. Unlike the visual streak whichs forms a horizontal band, the area centralis is arranged in a spot. The visual streak is present in many vertebrates and particularly in reptiles.

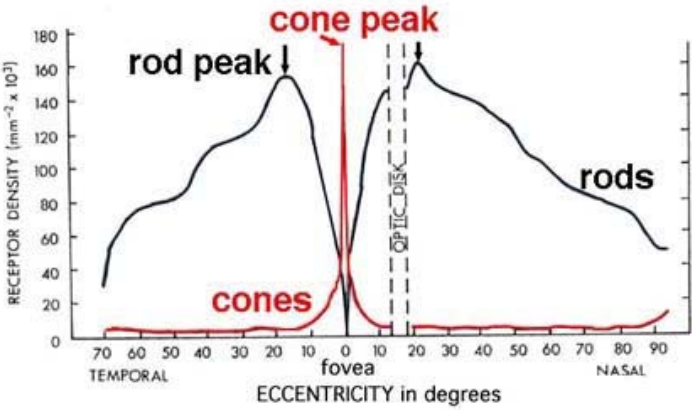

Figure 7 Distribution of rods and cones on the horizontal meridian of the human retina.

In the foveola, only cones are present, whereas in the rest of the retina, most of the PRs are rods.

From (Osterberg, 1935).

2.1.3. Different Connections

Rod and cone pathways are strictly separated in the outer retina; rods connect to rod bipolar cells and cones to cone bipolar cells. In the inner retina, cone bipolar cells form synapses with RGCs. Rod bipolar cells do not directly contact RGCs but feed into cone bipolar cells via a population of amacrine cells in the inner retina. The **wiring connection systems** of rods and cones with RGCs, in the peripheral and central retina, are different. In the periphery, there is a high convergence of the rods onto their postsynaptic neurons: one RGC carries information of a large number of photoreceptors (Figure 8, left panel). In contrast, in the cone-rich fovea, a low ratio of PRs to ganglion cells is found: one cone cell is connected to one bipolar cell itself contacting one RGC (Figure 8, right panel).

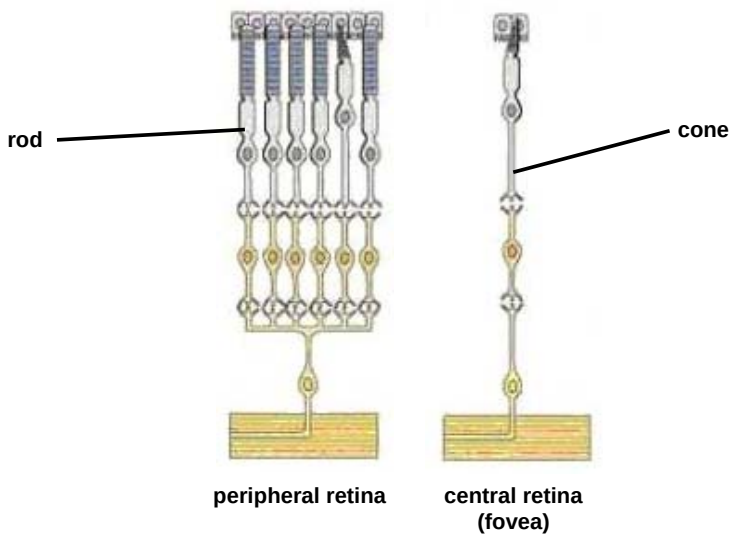

Figure 8 Connectivity of rod in the peripheral- and cone in the foveal retina of human.

In the peripheral retina, one RGC is contacted by several rods via the bipolar cells. In contrast, in the fovea, one cone contacts one bipolar cell which in turn contacts one RGC.

Modified from thebrain.mcgill.ca.

2.1.4. Different Pigments

Visual pigments of rods and cones belong to two different families of vertebrate opsins depending on their evolutionary histories. Rods contain the visual pigment **rhodopsin** and cones contain **cone opsins**. Also, they possess different homologous proteins and amplification factors of the phototransduction cascade (Curcio et al., 1991; Nathans, 1999; Roorda and Williams, 1999).

The spectral sensitivity of a given pigment is determined by the amino acid sequence of the opsin. Rhodopsin is sensitive to **one wavelength range only** with peak sensitivity around **498 nm**. Cones can further be subdivided depending on the exact structure of their opsin molecule. Three classes of mammalian cone opsins are named by acronyms roughly reflecting their spectral sensitivity maxima (Figure 8). Cones are either maximally sensitive to **long wavelength** light: LW cones (564 nm); **medium wavelength** light: MW cones (533 nm); or **short wavelength** light: SW cones (437 nm). Most mammalian species are dichromats, containing as well as rods only MW and SW sensitive cones in their retinas. Human and Old World primates possess all three types of cone opsins (Nathans et al., 1986; Jacobs, 1998).

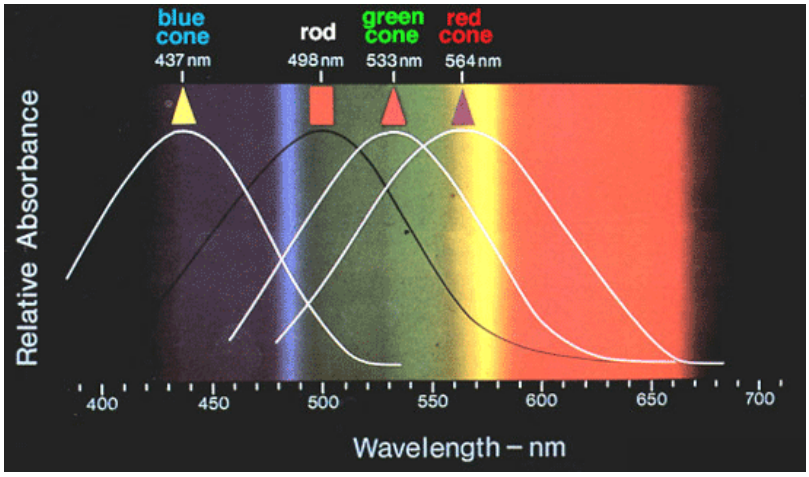

Figure 9 Absorption spectra of visual pigments in humans.

Rhodopsin, the visual pigment of rods has a maximum sensitivity around 498 nm. SW opsin, the visual pigment of blue cones has a maximum peak around 437 nm, MW for green cones has a peak at 433 nm and LW opsin for red cones has a maximum at 564 nm.

From (Bowmaker and Dartnall, 1980)

2.1.5. Different Roles

The high convergence of rods onto RGCs in the more peripheral retina causes image resolution to suffer. By contrast, the low convergence of cones improves the signal-to-noise ratio. Therefore, cones are responsible for **high visual acuity**, and are of utmost importance in human eyesight. Improving acuity is the fact that in the macula, bipolar and ganglion cells displaced laterally allowing the light rays to fall directly on cones with no loss of light intensity. Moreover, the difference of convergence, renders rhodopsin **exquisitely light sensitive** (Cicerone, 1976; Rodieck and Rushton, 1976) and operational under dim light

environments, whereas cone opsins require **relatively high light levels** to be activated (Sugita and Tasaki, 1988). Hence, rods are functional in dim light and cones are used in daylight.

Cones of different wavelength sensitivity and consequent pathways of connectivity to the brain are, of course, the basis of **colour discrimination** in the human visual world. In primates, three different cone types can be detected with behavioural, psychophysical and physiological testing. This is the basis of the so called trichromatic vision of humans.

2.2. Focus on Cones: Why Studying Cones is such a Major Concern…

As seen in the previous section, rods and cones are different cell types and useful human vision is very largely afforded by cones, which permit **high acuity** in the macula and **chromatic eyesight**.

Due to these particular functions, the **major visual handicap** encountered in hereditary blindness occurs through loss of cones, even though these cells are often not the site of the genetic lesion. This is the case for Retinitis Pigmentosa and age-related macular degeneration (AMD) (Curcio et al., 1996; Adler et al., 1999; Bhatti, 2006).

In other diseases such as the macular dystrophy known as Stargardt's disease, macular cones are very damaged whereas there is only little structural or functional damage to surrounding rods (Cibis et al., 1980; Zhang et al., 1995). The molecular basis of Stargardt's disease is not entirely known, and how the mutation of a gene expressed in both rods and cones (Allikmets et al., 1997; Rozet et al., 1999; Papaioannou et al., 2000) leads to such clinically specific lesions in the macula, is still **not understood**. It is known that the mutation results in build-up of toxic lipid adducts in the RPE (Mata et al., 2000). The biochemical pathways underlying genesis of these lipids is quite well understood in rod PR (Sparrow and Boulton, 2005), but it is currently unknown how such adducts may form in cone PR, or why cones should be so vulnerable to RPE malfunction. Molecular events during cone pathological processes need to be further investigated.

Also, factors influencing cone survival are largely unknown - even if a diffusible factor produced by rod PR which may be critical for cones has been identified (Leveillard et al., 2004), the mechanism by which this effect occurs is currently unknown. Moreover, there is currently very little information available on direct effects of neurotrophic factors or environmental insults (e.g., intense light exposure) on cone survival (Cicerone, 1976; Cortina et al., 2003).

There is therefore a **great need for a model permitting scrutiny of cone pathophysiology** under controlled experimental conditions, in order to obtain basic information that may help prevent or reduce visual handicap caused by cone death.

2.3. Models for Cones Studies

2.3.1. Why Classical Rodents don't – entirely – Make the Cut?

Mice (*Mus musculus*) and **rats** (*Rattus norvegicus*), the traditional species used for experimental research, are often **attractive models** for studies involving genetic manipulation, development, or electrophysiological experiments. These species are the most popular models as transgenic technology is far advanced, breeding is rapid and prolific, and animal housing is inexpensive. Another advantage is the rapid progression of the disease process, which can be measured in weeks as opposed to years in humans.

As for other fields of biology, use of mice and rats has led to **great advances in vision research**, such as the description of cellular and molecular mechanisms underlying rod cell degeneration in a wide range of blinding diseases, and potential avenues of therapeutic neuroprotection or gene replacement (Faktorovich et al., 1990; Humphries et al., 1990; Bennett, 2000; Travis et al., 2007).

However, **mice and rats have an important drawback for investigations directed at vision**, especially cone-based vision. Both of these species are nocturnal, burrowing animals that do not rely heavily on vision and have poor natural visual acuity (Prusky et al., 2000).

Moreover, if rodents - and particularly mice - are not generally considered to be a "visual animal", this is also because of the widespread occurrence of the retinal degeneration (*rd1*) mutation in mice, which induces rapid degeneration of rods followed by cones PR (Chang et al., 2002). This mutation (in cGMP-PDE) occurs in many common laboratory strains and renders all of the mice in these strains incapable of normal responses to light (Low, 1987).

Also problematic for the use of mice and rats in cone pathophysiology research is the **low cone to rod ratio** and the **lack of a macula** in their retinas, rendering them less suitable for questions regarding cone disease. Mice possess a number of cones estimated at 2.8 % total PRs (Carter-Dawson and LaVail, 1979b; Jeon et al., 1998) and at < 1 % for rats (Szel and Rohlich, 1992).

Although this has not prevented the study in these species of several important aspects of cone biology, including differentiation (Kelley et al., 1995), phenotype (Szel et al., 1993), function (Biel et al., 1999) and degeneration (Usukura et al., 1994; Xu et al., 2000), it has nevertheless hindered cone studies on a large scale and rendered very difficult the study of reproducible principal features of cone pathological processes. For example, even if several transgenic mice models manifest different salient features of AMD (Ambati et al., 2003; Rakoczy et al., 2006), none of them recapitulate the entire spectrum of pathological changes seen during the progression of the pathology. This is maybe due to the fact that rods actually die prior to cones even in macular diseases such as AMD (Jackson et al., 2002), or that the particular structure of Bruch's membrane, the basal membrane of the RPE, somehow sensitizes particularly the macula to metabolic stress (Chong et al., 2005). Both of these characteristics are difficult to evaluate in cone-poor retinas.

2.3.2. Cone Cell Lines

Photoreceptor cells are terminally differentiated, specialized neuronal cells with a limited capacity for cell division. Hence, to establish a line of photoreceptor cells, it has been essential to transform tumour cells with viruses.

Two immortalized human retinoblastoma cell lines: **Y-79** and **WERI-Rb11,** are available for the study of photoreceptors. Initially, it was thought that the Y-79 cells were of cone cell origin (Bogenmann et al., 1988) but more recently it has been shown that these cells express rod-specific antigens, such as rhodopsin, rod transducin, PDE, and recoverin (Di Polo and Farber, 1995; Wiechmann, 1996). A mouse photoreceptor-derived cell line, designated **661W** has been immortalized by the expression of a simian virus under control of the promoter of interphotoreceptor retinoid-binding protein (al-Ubaidi et al., 1992). Cellular and molecular analyses have shown that these cells **express cone but not rod photoreceptor markers**, which suggests that the cells arise from a cone photoreceptor lineage (Tan et al., 2004). Interestingly, 661W cells respond to light and can undergo light-induced cell death (Krishnamoorthy et al., 1999) and have been used successfully to study molecular events involved in the apoptotic process (Kanan et al., 2007). Kanan *et al.* showed the activation of multiple proteases by light-induced stress, a relevant finding for studies conducted to investigate the use of pharmaceutical agents to retard or cure the loss of cone photoreceptors observed in AMD and other degenerative retinal diseases.

However, even if these results appear promising for *in vitro* studies of cone death, the 661W cell line exhibits some **drawbacks** as a model of cone cells. Cells derived from this

cell line do not exhibit cone PR morphology, such as formation of OS-like membranes, and expression of some OS structural proteins. Moreover, cone opsins are distributed all over the cell and not restrained to OS as *in vivo*. A potential explanation for these unnatural PR characteristics could be that RPE would be essential to establish polarity and form OS through production of factors or proper physical contact with PR.

Therefore, even if cone cell lines could be a useful tool for studying cone pathophysiology, there are still some **inherent potential limitations**, including loss of native tissue architecture, selective loss of specific cell phenotypes/functions, tumoral nature of the cells, lack of functional feedback from other retinal cell types, and the potentially questionable relevance of *in vitro* findings.

2.3.3. Naturally Cone-Rich Animal Models

As seen previously, mice and rats possess a low cone to rod ratio, probably due to the fact that both of these species are nocturnal animals. In such an ecological niche, rod-mediated vision is advantageous in allowing detection of very dim light. Even though many diurnal mammals still possess excess rods compared to cones (such as in humans, still 20:1), higher cone numbers would be predicted in such organisms. In the wild, several species with rich or even "pure" cone retinas have been identified. Many diurnal teleosts, reptiles, and birds possess four cone types. Within the fish taxon, **goldfish** (*Carassius gibelio)* and **zebrafish** (*Brachydanio rerio*) are interesting laboratory species whose cone types (Robinson et al., 1995) are arranged in a mosaic pattern (Larison and Bremiller, 1990). Among **amphibians**, *Xenopus laevis* possesses 47 % of cones (Wilhelm and Gabriel, 1999). These three species have served to study rod-cone interaction (Frumkes and Eysteinsson, 1987; Witkovsky et al., 1989; Joselevitch and Kamermans, 2007; Ribelayga et al., 2008), cone visual cycle (Trevino et al., 2005; Fleisch et al., 2008), rhythmic processes such as cone OS shedding (Yacob and Kunz, 1977) and cone opsin expression (Halstenberg et al., 2005). Also, they have been widely used for studies involving cone degeneration after mutation (Ulshafer et al., 1990; Nishiwaki et al., 2008), or after light or chemical exposure (Hyatt et al., 1996; Vihtelic and Hyde, 2000). Fish retinas have also been studied for their unique property of regeneration (Cameron and Carney, 2000; Vihtelic and Hyde, 2000). Among birds, cones of **chicken** (*Gallus gallus*) retinas have been isolated in culture for *in vitro* studies (Okano et al., 1989) and their survival capacity has been investigated (Coleman et al., 2004) along with identification of cone survival factors (Leveillard et al., 2004).

Even if use of these species has generated interesting results, non-mammalian cones may be difficult to use as a model of human cones due to different physiological characteristics. For example, most non-mammalian cones possess coloured oil droplets at the outer end of their IS. These droplets are coloured filters that modify the spectral content of light reaching the visual pigments (Graf and Norren, 1974; Bowmaker et al., 1997) and are totally absent in mammalian cones. Moreover, use of non-mammalian species may also be difficult for practical reasons as they are not easy to rear and because biological tools available for rodents or primates can hardly be used on non-mammalian material.

All mammals possess rods and cones, and diurnal species show a large range of cone proportions from 8 % to 95 % cones (Ahnelt and Kolb, 2000; Peichl, 2005). Most diurnal mammals that have been examined still have rod-dominated retinas, such as **pigs** (*Sus domestica*) who possess 15 % – 20 % cones (Hendrickson and Hicks, 2002). Only a few diurnal species are known to have more cones than rods: the **ground squirrel** (*Spermophilus beecheyi*) has about 85 % (Kryger et al., 1998), and **tree shrew *(Tupaia belangeri)*** about 95 % (Muller and Peichl, 1989). Most non-primate mammals possess two spectral cone types: LW and SW that show a centro-peripheral density gradient, coinciding with the ganglion cell density gradient. Highest densities are present in the *area centralis* and lowest densities in the retinal periphery. **Cats** (*Felis catus*) who possess a real macula with a rod/cone ratio of 10.6 (Steinberg et al., 1973) were used to study the fate of cones in rod/cone degeneration (Narfstrom et al., 2001) during which the cone system is morphologically abnormal in young cats at an earlier stage of disease. **Rabbit** (*Oryctolagus cuniculus*) is another highly visual species and has been used as a model of cone-rich retina (Poznanski, 2005; Yasukawa et al., 2007). **Non-human primate** retinas are of course a very good model of human retina, but they have experimental and ethical constraints that limit their applications.

All these mammalian species have aided in exploring cone degeneration (Farber et al., 1983), trophic factor effects (Traverso et al., 2003), turnover (Long et al., 1986), visual cycle (Wolf, 2004), basic principles of cone function and cone-specific circuitry (DeVries et al., 2002; Li and DeVries, 2004; Rebrik and Korenbrot, 2004) and recovery of cone function following injury such as retinal detachment (Jacobs et al., 2002; Linberg et al., 2002). However, these models **present certain drawbacks**, such as difficulties in husbandry (pig) or surgery, drawbacks to breeding in captivity (cats, squirrel), and lack of genetic information and utilisation of pre-existing antibodies or databank sequences (cats, squirrel).

2.3.4. TRANSGENIC ANIMAL MODELS

Two strains of functionally rodless mice have been generated with a deletion of the gene for rod transducin alpha-subunit or for rod arrestin (Xu et al., 1997). These strains are interesting to study cone-driven electrophysiological responses, without interference of rod-driven responses but are not ideal for histological and biochemical studies. Cone-rich transgenic mouse models are also available in the form of $Rho^{-/-}$ mice (Humphries et al., 1997) or $Nrl^{-/-}$ mice (Mears et al., 2001). **Several disadvantages** of these transgenic models have emerged. First, cones in such strains may not be fully normal: in $Rho^{-/-}$ mice the "cone-rich" state lasts only a short time before they die secondarily to rods, and $Nrl^{-/-}$ are SW cones formed through a default developmental programme. In the latter case, recent data shows they display typical cone features by a wide range of structural and functional criteria: (Pugh et al., 2005). Second, as rods are completely absent or non-functional, it is impossible to compare pathological features of the two photoreceptor populations within the same animal.

2.4. *Arvicanthis ansorgei* (Thomas 1910): a "Gold Standard" for Cone Studies?

The considerations above argue strongly for the need for new animal models are required to facilitate experimental research into cone function and survival and to examine cone degeneration.

Ideal models would of course exhibit the key feature of possessing a large percentage of easily identifiable cones. They should also be suitable for a wide variety of experimental techniques including monitoring of behavioural patterns, studying whole animal physiology, slice physiology, ease of performing anatomical and molecular studies, and investigations involving genetic or anatomical experimentation. Finally, they should also possess practical advantages such as ease of handling, housing and breeding in captivity. One group of our laboratory is interested in the molecular mechanisms regulating diurnality and nocturnality (Dardente et al., 2004; Mendoza et al., 2007; Tournier et al., 2007). For these purposes, a breeding colony of a diurnal rodent species ***Arvicanthis ansorgei*** Thomas 1910 (Figure 10), was initiated in Strasbourg in 1998, from animals trapped in the southern and central part of Mali. This West African species ranges from Senegal to Niger and Burkina Faso in subtropical or tropical scrubland. The diurnal activity has been confirmed in our laboratory by actimetry measurements (Challet et al., 2002).

Figure 10 *Arvicanthis ansorgei* in its natural environment.

Picture of an adult *Arvicanthis ansorgei* in semi-captivity by B. Sicard (Institut de Recherche pour le développement, Mali).

Cytogenetic and molecular analyses have demonstrated the monophyly of this genus with estimated times of divergence from other Muridae divisions ranging from 4 to 13 million years (Ducroz et al., 1998). The phylogenetic match to laboratory mice and rats is crucial to optimize exploitation of existing databanks and available antibody probes of mice and rats. So far, many *Arvicanthis* homologues of neurotransmitter and visual pigment genes, have been cloned successfully based on the closeness of match to murine sequences. Also, all tested

antibodies, raised against either mouse or rat sequences of retinal proteins, cross-reacted fully with *Arvicanthis* (Bobu et al., 2006).

An **initial characterization of the retina** of *Arvicanthis ansorgei* performed in our group (Bobu et al., 2006) revealed that this species possesses 33 % cones, that is approximately 10 times more than mice and rats. Moreover, it was shown that cones are arranged in two regularly aligned cell layers at the scleral surface of the ONL, distributed uniformly across the entire retina and easy to distinguish from rods by their position and nuclear morphology. The presence of both rods and cones greatly facilitates comparison of the two populations in the face of stress and injury, and in their responses to prospective neuroprotective treatments.

Importantly, *Arvicanthis ansorgei* **can be bred successfully in captivity** (5-7 young per litter). The gestation and weaning times are similar to other laboratory-housed rodents (21 days and 1 month respectively), and their estimated lifespan is approximately 2.5-3 years.

Recently, the retina of another *Arvicanthis* species has been described: *Arvicanthis niloticus* (Gaillard et al., 2008). The two species are very similar in terms of retinal architecture. To conclude we can say that even if existing animal models will continue to be important, *Arvicanthis ansorgei* constitutes a very promising experimentally-accessible mammalian model with a cone-rich retina. However, the histological and functional characterization of its retina needs to be completed.

In this manuscript, for convenience, I will use indifferently the terms *A. ansorgei*, *Aa* or *Arvicanthis* to refer to *Arvicanthis ansorgei* species or animals.

3. RETINAL DEGENERATIONS AND THEIR MAMMALIAN MODELS

3.1. Human Retinal Degenerations

Retinal degenerations (RD) constitute the leading cause of blindness in Western countries. We will mention just a few examples of prevalent forms that concern PR.

Age related macular degeneration (AMD) is a common retinal pathology of the elderly. It affects a very significant percentage of the ageing population, and constitutes the largest threat to vision-related public health in the industrialized world (Gehrs et al., 2006). The macular area including the central fovea becomes compromised due to the degeneration of the RPE and the formation of drusen (the lipidic material built up in Bruch's membrane), with ensuing cone death and central visual loss.

Retinitis pigmentosa is a family of hereditary retinal diseases for which there is no cure at present. Large numbers of genetic mutations have been identified, most of which are located in **rods** that begin to degenerate in early stages of the disease. Patients become night blind as more and more of the peripheral retina becomes damaged, eventually reduced to tunnel vision.

Macular dystrophies, such as **Stargardt's disease,** are dominated by severe cone degeneration, with often little structural or functional damage to surrounding rods (Cibis et al., 1980; Zhang et al., 1995).

3.2. Genetic Animal Models of RD

Numerous genetic animal models of RDs have been described over the years. Studies using animals that have **naturally-occurring mutations** affecting specific populations of cell types have been useful for analysing visual function and the phototransduction process, as well as pathogenic mechanisms underlying death. The most well studied inherited mutant strains are the "retinal degeneration" (now termed rd1) and "retinal degeneration slow" (rd2) mice, both autosomal recessive conditions implicating respectively mutations in rod-specific cGMP, PDE and peripherin/rds proteins (Farber et al., 1989; Travis et al., 1991). In addition, the Royal College of Surgeons (RCS) rat (Bourne et al., 1938) harbours a mutation in the mertk tyrosine kinase receptor involved in retinal phagocytosis (D'Cruz et al., 2000).

Although most of the mutations affect rods, **some mutations concern cones**. The cone photoreceptor function loss 1 (*cpfl1*) mutation is the first naturally-arising mutation in

mice to cause cone function loss. Electrophysiological responses of *cpfl1*$^{-/-}$ mice show no cone-mediated response but normal rod-mediated responses from 3 weeks to 15 months of age (Chang et al., 2002). Histological studies of *cpfl1*$^{-/-}$ mice at parallel ages show an overall normal retinal structure with cone photoreceptor cell degeneration.

More recently, **transgenic engineering** has been used. Mutations of protein of the phototransduction as rhodopsin are commonly used: P23H mutation in mice (Olsson et al., 1992) and rat (Machida et al., 2000), or *Rdta* mutation (McCall et al., 1996). Targeted cone cell loss has also been performed (Soucy et al., 1998).

Although genetic models have already provided a wealth of data in understanding the process of retinal degeneration, they present certain **disadvantages**. First, transgenic technology is almost entirely restricted to mice, even if other transgenic species including rats and pigs have been engineered. Mice and rats, as seen previously, do not possess many cones and therefore are not so suitable as models for cone pathologies. Second, genetic models present some technical difficulties such as the constant need for checking the genotypes. Third, some drawbacks inherent to transgenic models do not allow full comparisons with human degenerations. Indeed, genetic models of RD can be associated with degeneration of structures important for cognitive functions and whose alterations could be a problem for visual behavioural testing. This is the case for the *pcd* mutants which exhibit a moderate ataxia beginning at 3 to 4 weeks of age. Also, with both natural and genetically induced mutations, cell degeneration occurs often very early in development (*Rd1, pcd, nr*), and even when progression is slow (*rds*), such features do not reflect most examples of human blindness that usually appear in adulthood.

3.3. Non-Genetic RD Animal Models

3.3.1. Generalities

As seen in the previous section, although genetic models of RD are very useful, they present certain drawbacks. Some of these disadvantages may be prevented using non-genetic induced RD models. These latter models mimic most of the risk factors that can influence the progression of a genetic based RD. For example, models based on metabolic impairment like hyper- or hypo-glycaemia have been used to induce RD (Rabin et al., 1973; Umino et al., 2006). Advantages of these types of protocols are that dosage and post-injection time can be varied to obtain differential effects on visual structure and function. For our studies, we used

two different approaches to induce acute RD: bright light exposure and toxic chemical injection.

3.3.2. The Light-Induced RD Model

"People may injure their bodily eye
By observing and gazing on the sun during an eclipse
Unless they take the precautions
Of only looking at the image reflected
In the water or some similar medium"

This citation of Socrates in Phaedo shows that 380 BC the harm caused to the eye by directly looking at the sun was already known. Blindness caused by looking at eclipses and the reflection of light on snow have also been commonly reported. About forty years ago, major concerns were expressed about retinal damage caused by high intensity light, laser or thermal radiations. At that time, only very high intensity light or emissions with particular wavelengths were known to cause eye damage. It was only **in 1966** that **Noell *et al.*** discovered that albino rats exposed to constant illumination at normal light intensity undergo dramatic retinal degeneration (Noell et al., 1966). In humans, light is considered as a very crucial key factor for the progression of inherited RD. Light exposure was found to accelerate RD in various animal models (Hafezi et al., 1997; LaVail et al., 1999). Since then, the animal light damage model has been widely used to study the mechanisms of stress-induced PR cell death, with the goal of obtaining insight into the mechanisms of cell death in human RD.

3.3.3. Chemicals and MNU Models

The mammalian eye is also highly sensitive to toxic substances, and several chemicals have been shown to cause RD in animals (Heywood and Gopinath, 1990). Most commonly recognized drug-induced retinopathies have a particular affinity for the RPE, such as anti-malarials (Matsumura et al., 1986; Das et al., 2008), the phenothiazines (Alkemade, 1968), ethambutol (Spekreijse et al., 1991) and sodium iodate (Kiuchi et al., 2002). Even, sildenafil, the active molecule of Viagra®, has been shown to induce retinal dysfunction (Gonzalez et al., 1999). However these compounds are not suitable for all species and delivery is not always easy.

***N*-methyl-*N*-nitrosourea (MNU)** is an alkylating agent of S_N1 type (reacting by nucleophilic substitution with an unimolecular rate-determining step) classically used in biology as a potent tumour-inducing agent in mammals (Bernard et al., 1986). Herrold was

the first to report PR degeneration in Syrian golden hamsters after systemic administration of MNU (Herrold, 1967). Later, it was shown that RD can be induced by a single systemic administration of MNU in a variety of adult animals, including mice (Smith and Yielding, 1986), rats (Murthy et al., 1972; Nakajima et al., 1996a) shrews, but also non-human primates (Tsubura et al., 2003a). The mechanisms underlying cell degeneration after MNU injection have been studied, and it is now known that pro-apoptotic factors are up-regulated (Yoshizawa et al., 2000; Grimm et al., 2001) while anti-apoptotic factors are down-regulated (Doonan et al., 2003; Yang et al., 2005; Oka et al., 2007; Yang et al., 2007), and that the degeneration occurs via apoptotic processes (Yoshizawa et al., 1999; Grimm et al., 2000b). Although the triggering mechanisms of pathogenesis are different from human RP, MNU-induced PR degeneration may be useful for testing of therapeutic strategies since the drug can be delivered easily via systemic injection and induces RD in several species.

3.4. Fate of Cones in RD

As mentioned previously, data regarding the pathology of cones during RD are very limited. The few existing studies regarding cone fate give conflicting results demonstrating either increased (Cortina et al., 2003) or decreased (Cicerone, 1976) vulnerability compared to rods.

4. Retina Visual and Non Visual Functions

Photosensitive cells of the retina detect light and relay this information through a multi-synaptic pathway to higher cortical structures via RGCs. These retinal outputs support not only pattern vision but also non-image-forming (NIF) functions.

4.1. The World as seen by the Eye: Image Forming Function of the Retina

Eyes are tremendous sensory organs allowing us to appreciate all the beauty (or not…) of the world we live in, to explore and gain knowledge and to express and receive thoughts and desires through visual expression and visual arts. For humans, vision is the most fundamental of our senses. A certain degree of integration of visual information is achieved within the retina, at the level of the OPL where cone pedicles pass electrical messages between each other and with rod spherules so that a small amount of rod and cone signal mixing occurs at this layer (Kolb and West, 1977; Nelson, 1977). Amacrine and horizontal cells play also great roles in the integration of the retinal visual message as they help to extract certain features of interest such as contrast and spatial patterning of the environment, and transmit the result of these computations through the optic nerve to the brain. Another important aspect of human vision is colour, due to the different cone opsins. Shape and motion perceptions are mostly integrated in the visual cortex.

4.2. Retina Beyond Images

Even if retina can accomplish very complex processes, it has also a more "modest" role as a light sensor for processes not related to image construction.

4.2.1. Non-Image Forming Functions: Which?

Daily rhythms of almost 24-h in mammalian physiology and behaviour are called **circadian rhythms** (from the Latin *circa* = about and *dies* = day). These rhythms are controlled by a tiny cluster of cells of the ventral hypothalamus: the suprachiasmatic nuclei (SCN). **SCN** neurons possess a unique molecular clock that allows them to autonomously generate oscillations with a period of almost 24-h, which ultimately leads to daily changes in animal behaviours such as sleep/wake cycles. However, as periodicity of this clock is not exactly 24-h, the SCN must be entrained (or reset) in order to adjust to the daily light/dark (LD) cycle. This latter process, which adjusts circadian rhythms, is known as

photoentrainment. In circadian studies, activity cycles are represented as actograms which for convenience sake are mainly double-plotted and the time at which the synchronizer (also called *Zeitgeber* for "time giver" in German) is given is called "Zeitgeber 0" or ZT 0. In the case of photoentrainment, ZT 0 corresponds to the time of lights on.

In order to make constant the amount of light entering the eye, the diameter of the pupil is negatively correlated with light intensity. At high light intensity, the iris decreases the area of the pupil by 95 % (full constriction) in comparison with dark-adapted conditions (full dilation). This mechanism is known as the **pupillary light reflex (PLR)**. The structures involved in PLR control are **the olivary pretectal nucleus (OPN)** that sends projections to the **Edinger Westphal nucleus (EW)** (Hultborn et al., 1978), and the **ventral lateral geniculate nucleus (VLGN)** and the **intergeniculate leaflet (IGL)** (Harrington, 1997).

Photoentrainment and PLR are both light-regulated mechanisms and - not surprisingly - they both disappear after bilateral enucleation in humans and animals (Nelson and Zucker, 1981; Foster et al., 1991; Czeisler et al., 1995), proving that both mechanisms are under the control of ocular photoreception.

4.2.2. Non Cone, Non Rod Photoreception?

For the greater part of the last 150 years, it was assumed that the mammalian retina contained only two types of photosensitive cells: rods and cones. However, in 1923, **Keeler** made a number of interesting observations from mice that had severe RD. Though they lacked most of their rods and cones, and were considered functionally blind, these mice were still able to generate a number of visual reflexes, including constriction of their pupils in response to light (Keeler et al., 1928). A similar observation was made later by Foster *et al.* who showed, 70 years later, that *rd/rd* mice had circadian responses to light that were indistinguishable from mice with normal retinas (Foster et al., 1991). The same group used genetically engineered mice with no rods or cones to show that these mice maintained the ability to shift their daily biological rhythms in accordance with shifting light cycles (Freedman et al., 1999). Also, some blind patients with no conscious perception of light, and supposedly no rod or cone photoreception, maintain **melatonin suppressio**n, a phenomena directly under photic input control (Czeisler et al., 1995).

This series of observations strongly suggested that, besides rods and cones, some other photosensitive ocular cell type must be present in the retina.

4.2.3. Melanopsin Pigment Discovery

While studying the dermal melanophores of frogs, **Provencio** *et al.* cloned a novel opsin molecule responsible for redistribution of skin pigmentation in direct response to light (Provencio et al., 1998b). Orthologues of this opsin, which they called **melanopsin**, were also found to be selectively expressed in a small subset (1-3 %) of the RGCs in the mouse retina (Provencio et al., 1998a; Provencio et al., 2000).

4.2.4. Arguments in support of Melanopsin as a Potential Component of the Photoreceptive System

1. Due to their RGC nature, these photoreceptive cells have the ability to **communicate directly with other structures of the brain**. These cells send their projections directly to the **SCN** (Gooley et al., 2001; Hannibal et al., 2002), forming the **retinohypothalamic tract (RHT),** an anatomically, developmentally and physiologically distinct route from the visual pathway. Melanopsin RGCs also project to the **OPN** and onto the **EW,** the retino-recipient sites responsible for PLR. These anatomical projections were confirmed by Hattar *et al.*, who used transgenic mice in which the reporter gene galactosidase was fused to the melanopsin promoter (Berson, 2003; Hattar et al., 2006).

2. Patch-clamp recordings in absence of rod and cone signals (after mechanical isolation or with the use of pharmacological blockers) showed that melanopsin-immunopositive cells were **intrinsically photosensitive** (Berson et al., 2002; Hattar et al., 2002). Therefore, the melanopsin expressing cells are also called **ipRGCSs**. Early controversies regarding melanopsin's ability to function as a true photopigment have been laid to rest with a series of experiments in which the melanopsin gene was expressed in multiple normally light-insensitive cell types. When these cells express the melanopsin gene, they become able to robustly respond to light, indicating that melanopsin functions as a true photopigment (Melyan et al., 2005; Panda et al., 2005; Qiu et al., 2005).

3. ipRGCSs express specific physiological features not found in other PRs and RGCs. They have **sustained light responses** under conditions of continuous bright illumination, faithfully encoding stimulus energy over relatively long periods of time, and are also **much less sensitive to light** (Barlow and Levick, 1969; Berson, 2003). Another remarkable physiological feature of ipRGCS is the ability of their dendrites to respond directly to light (Berson et al., 2002), which, combined with their **large overlapping dendritic fields** (Provencio et al., 2002), leads to poor **spatial resolution but wide field coverage**. These unique functional and anatomical properties of ipRGCSs all match perfectly with their role in

signalling diffuse ambient light levels **for tonic behaviours** such as **photoentrainment** and **PLR,** that require long integration times of ambient light levels (Panda et al., 2002; Lucas et al., 2003). Finally, ipRGCSs depolarize in response to light with a spectral sensitivity that closely matches the behavioural action spectrum of circadian photoentrainment and PLR, with a maximum of sensitivity between 460 and 481 nm (Lucas et al., 2001; Berson et al., 2002; Hattar et al., 2003).

4.2.5. PHOTOENTRAINMENT AND PLR AFTER MELANOPSINERGIC SYSTEM ALTERATION

The generation of **melanopsin knock-out animals (*Opn4*$^{-/-}$)** (Panda et al., 2002) has provided direct support in favour of a role of melanopsinergic cells in the regulation of circadian photoentrainment and PLR. Melanopsin knockout animals (*Opn4*$^{-/-}$) display a **significantly attenuated phase shifting response** to brief flashes of light (Panda et al., 2002) (Figure 11) and have **diminished PLR** at high light intensity levels (Lucas et al., 2003).

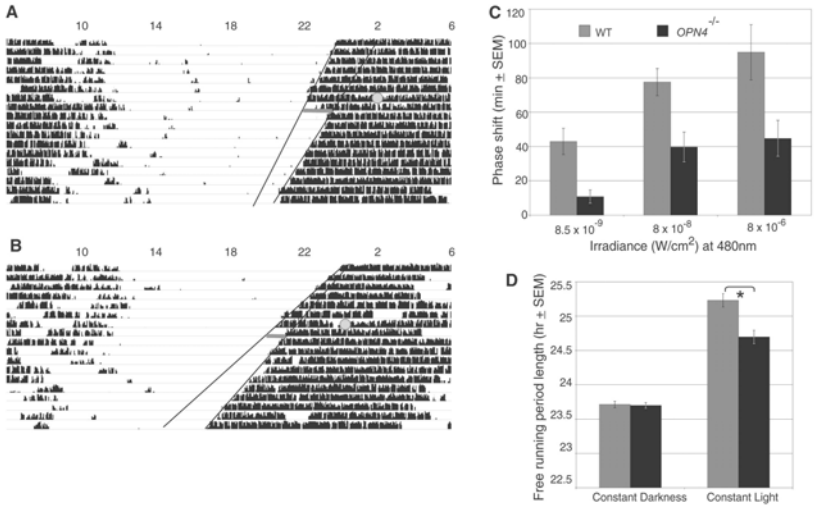

Figure 11 Attenuated circadian light input in *Opn4*$^{-/-}$ mice.

A single 15-min pulse of monochromatic light of 480 nm (circle) was administered 3 h after the onset of activity, which produced a smaller phase shift in the activity rhythm of the *Opn4*$^{-/-}$ animal (**B**) than in the wild-type littermate (**A**). The phase shift (gray bar) on the day after the light pulse was determined with Clocklab software (Actimetrics, Evanston, IL). (**C**) The light-induced phase-shift defect in the null mice is evident at all irradiance levels tested. Means (±SEM) of phase-shift measurements for the *Opn4*$^{-/-}$ mice (black) and the littermate wild-type mice (gray) are shown (n = 5 to 17 mice per group). Data were analyzed by t test (two tailed, equal variance), and a statistically significant difference ($P < 0.05$) was observed between the genotypes at all irradiances tested. Sham animals handled in the same way but that did not receive a light pulse show no significant difference between genotypes. (**D**) An attenuated lengthening of period was observed in *Opn4*$^{-/-}$ mice (black) relative to wild-type mice housed in constant light but not in constant darkness. Asterisk indicates a statistically significant difference ($P < 0.05$). SEM: standard error mean.

Opn4$^{-/-}$: melanopsin knock-out. From (Panda et al., 2002).

However, melanopsin defective animals retain relatively normal circadian rhythms, and do not display any overt dysfunction in their **ability to entrain to light** (Panda et al., 2002) (Figure 12).

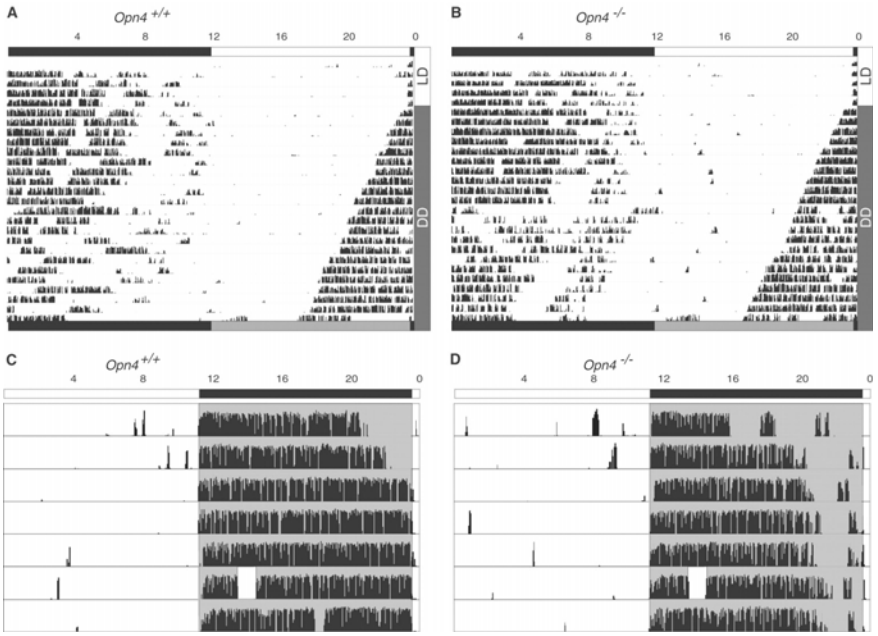

Figure 12 ***Opn4*$^{-/-}$ mice exhibit normal photic entrainment and light suppression of activity.**

Littermate *Opn4*$^{+/+}$, *Opn4*$^{+/-}$, and *Opn4*$^{-/-}$ mice were entrained to a LD cycle and then allowed to free run under constant darkness. The respective period lengths (means ± SD) under constant darkness were 23.7 ± 0.14 (*Opn4*$^{+/+}$), 23.6 ± 0.14 (*Opn4*$^{+/-}$), and 23.7 ± 0.12 (*Opn4*$^{-/-}$) hours with no significant difference among genotypes (two-tailed, equal variance *t* test; *n* = 6 to 12 per genotype group). Representative activity traces of *Opn4*$^{+/+}$ (**A**) and *Opn4*$^{-/-}$ (**B**) mice are shown. Activity traces from the last 4 days of entrainment (LD) and 22 days of constant darkness (DD) are shown. Each horizontal line represents data from a single day. Con- secutive days are plotted beneath each other, and 1-min bins of activity are represented as deflections from the horizontal line. Normal light suppression of activity in *Opn4*$^{+/+}$ (**C**) and *Opn4*$^{-/-}$ (**D**) mice is shown. A 300-lux white light pulse (18) was administered during the dark phase of entrainment. The light pulse acutely suppressed activity compared with activity at a similar phase in the preceding or following days (9 *Opn4*$^{+/+}$ and 11 *O*pn4$^{-/-}$ animals tested). Representative records from one *Opn4*$^{+/+}$ and one *Opn4*$^{-/-}$ animal are shown. White background indicates the light phase and gray background indicates the dark phase. The light pulse was administered on day 6 at 2 hours after lights off.

Opn4$^{-/-}$, melanopsin knock-out; SD, standard deviation. From (Panda et al., 2002)

The insignificant change in photoentrainment of melanopsin knockout animals can be explained by **rod and cone inputs** to ipRGCSs, adding a second source of photic input to the SCN. This idea was tested directly by evaluating photoentrainment abilities of **melanopsin knockout mice that lack both rod and cone photodetection systems** (Hattar et al., 2003). Triple knock-out animals were unable to entrain to LD cycles or to constrict their pupils in response to light (Hattar et al., 2003) (Figure 13).

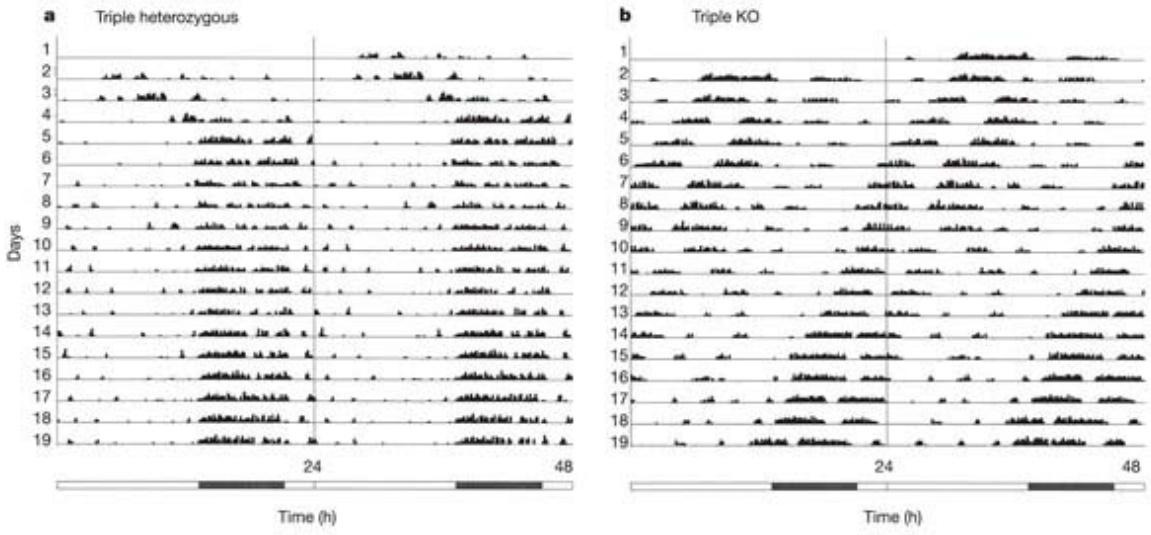

Figure 13 Triple knock out mice do not photoentrain their activity rhythm to LD cycles.

The illumination was approximately 800 lx white light. The numbered lines represent successive days. Activity levels (in total number of revolutions in 10-min bins) are given in 15 quantiles, with the first being 1–55 revolutions, the second 56–110, and so on. The bar below the actograms indicates light (white) and dark (black) periods. **a**, Triple heterozygote (*Opn4*$^{+/-}$*Gnat1*$^{+/-}$*Cnga3*$^{+/-}$). The locomotor activity had a cycle very close to 24 h and was phase-locked to darkness, showing photo-entrainment. **b**, Triple-knockout (*Opn4*$^{-/-}$*Gnat1*$^{-/-}$*Cnga3*$^{-/-}$). The animal free-ran with a period of less than 24 h, showing lack of photo-entrainment.

Cnga3: cyclic nucleotide gated channel alpha 3 ; Gnat1: Guanine nucleotide binding protein (G protein), alpha transducing activity polypeptide 1From (Hattar et al., 2003).

A last argument in favour for a role of melanopsin in non-visual functions is that ectopic expression of melanopsin in *rd/rd* mice has recently been shown to restore the PLR (Lin et al., 2008).

This ensemble of evidence strongly suggests that ipRGCSs constitute the mysterious third PR type predicted by Keeler almost 80 years earlier, and that melanopsin is its associated visual pigment.

5. Evaluation of RD and RD Protective Treatment Effects

The function of the mouse visual system and integrity of its anatomical structures can be tested in a variety of ways. As for any living tissue, retina can be analyzed with classical biological techniques using anatomical, biochemical, molecular, physiological and behavioural approaches. These techniques are useful to determine gross loss of cells, up or down-regulation of expression of structural proteins or factors and their corresponding mRNA in different tissues, to test functional electrical responses of circuit and ability of the circuit to drive a particular behaviour. Interestingly for RD studies, some tests are dedicated to detect particular forms of degenerations associated with apoptotic processes (*in situ* cell death detection, DNA ladder formation).

In this section only specific techniques related to retinal analysis will be discussed. The retina offers several advantages for the study of neural processing. It constitutes a well-defined neural circuit, the general function of which is well known. It can be removed from the eye without damage to internal connections, and continues to survive and function *in vitro* for many hours (even days or weeks). The retina is one of the few regions of the central nervous system for which the natural input, light, is fully known and easily controlled and retina generates a clearly defined output, namely action potentials in the RGC axons.

5.1. Retina Structural Evaluation

5.1.1. Classical Histological Staining Technique

It is important to keep in mind that the pioneering studies of Cajal using Golgi techniques form the basis of retinal anatomy still used today (Figure 2A). All the descriptions of cells and circuits that have followed have been achieved using modern techniques but always with the morphological data from Golgi staining as a basis.

Histological examination of the retina can be performed after serial sections through the optic nerve head (ONH), a preparation that allows comparison on the same section of central and peripheral retina characteristics, as for example numbers of cells or thickness of the different layers. Examination of the retina can also be made on flat-mounted preparations.

Also, with the advent of electron microscopy, histological, immunochemical staining techniques and electrophysiological single cell recording and staining, neural circuits in the retina can now be directly elucidated.

5.1.2. Scanning Laser Ophthalmoscopy (SLO)

The Scanning Laser Ophthalmoscope (SLO) was invented by Webb, Pomeranzeff, and Hughes in 1979. The SLO provides real-time images of the ocular fundus. Basically, it uses a very narrow moving beam which has the ability to bypass most ocular media opacities (i.e. corneal scars, cataracts, vitreous haemorrhage) to reach the surface of the retina and observe its structure. Some devices use the Doppler laser interferometry principle to provide a two-dimensional mapping of ocular perfusion and an accurate measurement of blood flow. Angiographies performed using the SLO are recorded at 30 images per second, producing a real-time video sequence of ocular blood flow. With these new devices, features not seen with fundus inspection are readily detectable. Macular drusen, for example, appear as yellow spots on SLO. Angiography using SLO allows tracking of cells such as leukocytes that play a central role in the pathogenesis of retinal and choroidal inflammatory disease. The infiltration of these cells into retinal and choroidal tissues may lead to tissue destruction and vision loss. A confocal SLO system has been designed with blue (488 nm) and infrared (795 nm) lasers exciting fluoresceine and indocyanine green. As an example of advantages and limitations of the approach, SLO can highlight **macular holes** (Figure 14) and the fluid surrounding them, but does not provide a quantitative assessment of the degeneration.

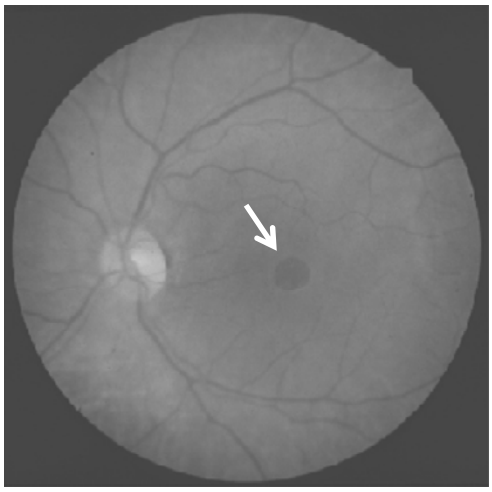

Figure 14 SLO imaging of a human fundus.

Fundus photography of a patient with a macular hole (arrow).

SLO: scanning laser ophthalmoscopy. From (Rudolph et al., 2002).

5.1.3. Optical Coherence Tomography (OCT)

Optical Coherence Tomography (OCT), is a non-contact, non-invasive imaging technique used to obtain high resolution cross-sectional images of the retina. OCT is analogous to ultrasound B-scan imaging except that light rather than sound waves are used in order to obtain a much higher longitudinal resolution of approximately 10 µm in the retina. OCT has been shown to be clinically useful for imaging thickness of macular holes, macular edemas, retinal detachment and retinal inflammatory diseases (Figure 15). In addition, OCT allows *in vivo* measurements of the thickness of the different retinal cell layers that might be different from histology in which tissue shrinkage or modifications due to treatment can hinder correct evaluation. The topographic mapping protocol is useful for longitudinally monitoring animals and for evaluating the progression of RD or the action of a protective treatment.

Figure 15 OCT imaging of a human retina.

Optical coherence tomography of a human retina showing serous, foveal neurosensory detachment. Note the high signal areas intraretinally and subretinally, corresponding to intraretinal exudates (arrow) and subretinal fibrinous material noted clinically (arrowhead).

OCT: optical coherence tomography. From (Olson et al., 2006).

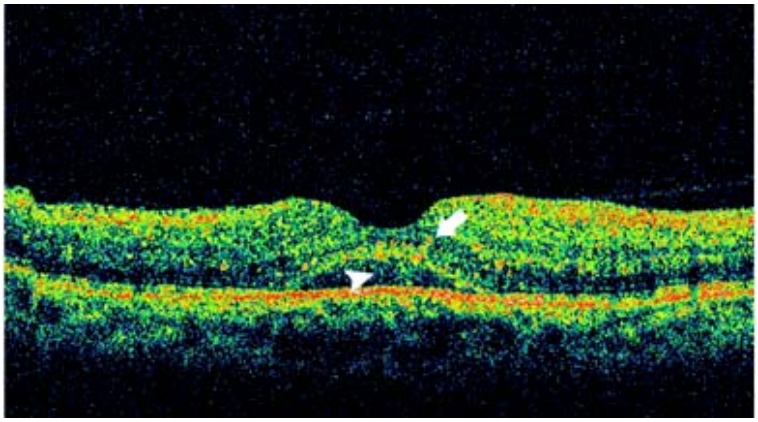

Although these techniques provide a good indication of retinal health, the anatomy of the retina does not provide a reliable measure of retinal function. For example, structural evaluation will not reveal defects at the molecular level or in the apparatus responsible for synaptic transmission. Therefore, the use of electrophysiological approaches is crucial to assess normal or pathological functional status.

5.2. Retina Electrophysiological Evaluation

Electroretinography records the full-field light-evoked diffuse electrical response - or **electroretinogram** (ERG) - generated by retinal cells after light stimuli. It was first identified in recordings from a frog eye in 1865 by the Swedish physiologist Alarik Frithiof Holmgren. It is now established that ERG represents the combined electrical activity of various cell types in the retina, including the PR (rods and cones), inner retinal cells (bipolar and amacrine cells), RGC and glial cells.

The retinal potential can be recorded by means of **corneal electrodes** in all vertebrate species. During a recording session, animals are exposed to standardized light stimuli and the resulting signal is displayed showing the time course of the signal's amplitude (voltage). Signals are very small, and typically are measured in microvolts or nanovolts.

ERG can be recorded under **different stimulus conditions** in order to elicit stronger responses from certain components. Retinal responses can be recorded under two conditions of light adaptation, either adapted to darkness: **scotopic conditions**; or adjusted to bright light: **photopic conditions** (Figure 16). In the mouse, under scotopic conditions the a-wave will mostly result from the activity of rods (Lyubarsky et al., 1999), whereas under photopic conditions it will reflect the activity of the cone system. In addition, two patterns of light stimulation can be used: wholefield illumination or patterned illumination (multifocal ERG) used to record separate responses for different retinal locations. Dynamic properties of the ERG can also be assessed by repetitive stimulation (flicker) of a certain frequency. Most alterations of retinal function can be appropriately analyzed by applying the flash and flicker protocols (Tanimoto et al., 2009).

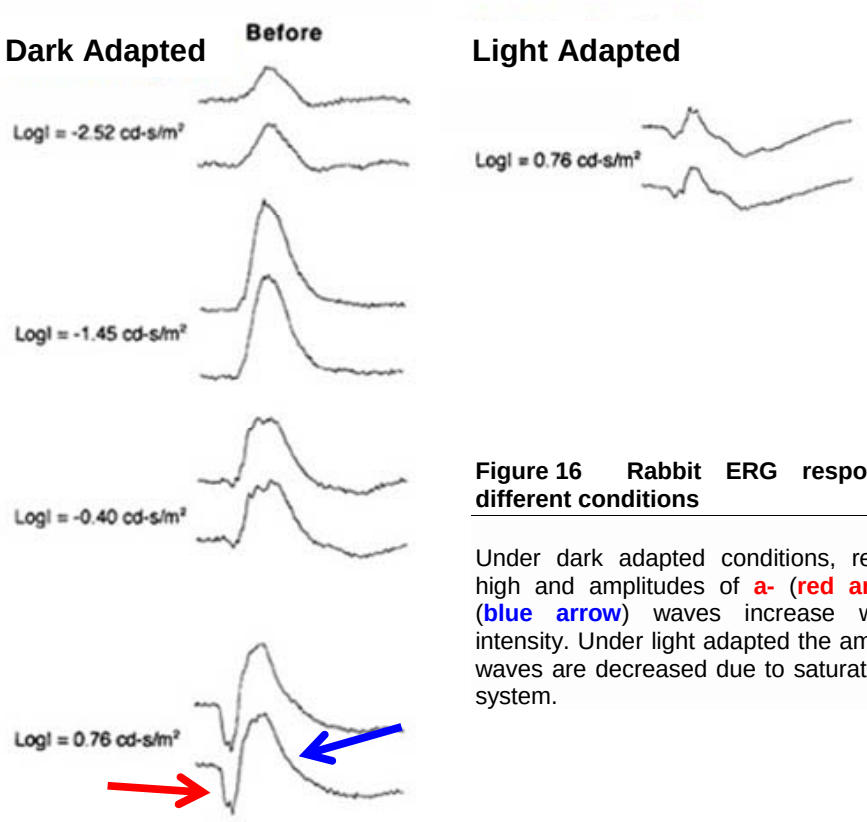

Figure 16 Rabbit ERG responses under different conditions

Under dark adapted conditions, responses are high and amplitudes of **a-** (**red arrow**) and **b-** (**blue arrow**) waves increase with stimulus intensity. Under light adapted the amplitude of the waves are decreased due to saturation of the rod system.

By adjusting the adaptation conditions and the type of light stimulation, the characteristic ERG wave components can be used to assay the activity of restricted sets of neurons. The relationships between ERG and neuronal activity have not been as well characterized in the mouse as in some other species. The scotopic ERG measured at the corneal level of a fully dark-adapted mouse in response to a bright whole-field flash stimulus consists of an initial negative deflection at the cornea, the **a-wave**, followed by a positive **b-wave** of short duration, followed by a larger, longer-lasting, positive **c-wave**. The c-wave is well understood and results from hyperpolarisation originating in the RPE. The a-wave can be used as a highly quantitative monitor of the electrical activity of the rod and cone PR (Peachey et al., 1995; Goto et al., 1996; Lyubarsky and Pugh, 1996). The cellular basis for the b-wave is not as well defined as those of the a- and c-waves, and subsequent work has led to the conclusion that the b-wave arises largely from the activity of bipolar cells (Gurevich and Slaughter, 1993; Robson and Frishman, 1995; Tian and Slaughter, 1995; Hood and Birch, 1996; Robson and Frishman, 1996). Even though the b-wave originates from neurons that are postsynaptic to the PRs, it can serve as a useful indirect measure of certain aspects of rods and cones. Under the appropriate conditions, the b-wave may be particularly useful in the

investigation of murine cone function (Lyubarsky et al., 1999), since the cone a-wave is very small and difficult to measure.

AIMS OF THE STUDY

B. AIMS OF THE STUDY

The **first goal** of our study is to **complete the characterization of the *Arvicanthis* retina**. The structure and constitution of the ONL has been well characterized with histological and immunohistochemical approaches (Bobu et al., 2006; Bobu et al., 2008). We intend to extend these analyses of fixed tissue through the use of real time *in vivo* imaging techniques to analyze the morphology of the retina in the living animal. Secondly, there are currently no data on light-evoked electrophysiological responses of *Arvicanthis ansorgei* retina. Therefore it is essential to acquire baseline visual response information from this species displaying a high percentage of cones and compare it with mice and rats whose cone percentage is low.

The **second goal** of the project is to **produce a standardized, reliable and reproducible RD model in which rod and cone degeneration and death can be followed** as separable events. For this purpose, we used two approaches to induce RD in *Arvicanthis ansorgei*. The first consisted of a phototoxic approach, the second of a chemical approach, using alkylating agent MNU. We sought to define the environmental (time), chemical (drug concentration) and physical (light intensity, duration, spectral quality) parameters necessary to induce quantifiable damage and death of cone (and rod) photoreceptors by the two techniques

The **third goal** of the study was to **analyse the impact of a RD on photic entrainment**. Specifically, these experiments were designed to evaluate whether stimulus strength could have a differential effect on synchronizing the circadian clock of the SCN. Even if the role of melanopsinergic cells in photoentrainment has now been fully demonstrated, the roles of cones and rods are still not clear. As RD was not complete in *Arvicanthis* (see the Results section), this study was realized on Long Evans rats.

MATERIALS

AND

METHODS

C. Materials and Methods

1. Animals

2. Bright Light Exposure

3. MNU Preparation and Injection

4. Morpho-Structural Analysis

5. Western Blot Analysis

6. Electroretinography

7. Actimetry

8. Light Intensity Measurements

1. ANIMALS

All animals used were 2 to 6 months old at the time of experiments.

Animals were housed in a temperature-controlled environment (22 ± 2°C) and had access to water and standard rat chow *ad libitum*. Animals were kept under LD 12:12 cycle conditions (lights on 7 h-19 h in summer and 8 h-20 h in winter). Light intensity at the level of cages was between 50 and 300 lux, depending on their location on the shelf and their proximity to the light source. During the dark phase, animals were exposed to a constant dim red light with intensity inferior to 5 lux. For light-induced degeneration and ERG recording experiments animals were dark adapted for at least 12-h. Also, for some light-induced degeneration experiments, animals were reared in dim light during the light period for 2 months prior to experimentation.

For our experiments, three species of rodents of the Muridae family were used: *Arvicanthis ansorgei*, rats (*Rattus norvegicus*) and mice (*Mus musculus*). *Arvicanthis ansorgei* came from our own breeding colony in the laboratory. Two strains of rats were used: pigmented Long-Evans rats were purchased from Janvier Laboratories (le Genest-Saint-Isle, France) and albino Wistar rats were supplied by our own colony. Two strains of BALBc albino mice were used ordered either from Charles River (l'Arbresle, France) or from Harlan Laboratories (Gannat, France). Animals delivered from laboratories were always left for 48-h adaptation before experiment.

Animals were sacrificed by decapitation following CO_2 intoxication or isoflurane anaesthesia.

Experiments were performed according to international (Association for Research in Vision and Ophthalmology Guide for Use of Animals in Vision Research: www.arvo.org) and institutional guidelines (David Hicks, the principal investigator, possesses a current animal experimentation licence, #67-132, issued by the Chief Veterinary Inspector, Ministry for Agriculture).

2. BRIGHT LIGHT EXPOSURE

2.1. General Procedures

Animals were dark adapted for at least 12-h prior to exposure. Unless otherwise indicated, bright light exposure started 3-h after lights on and animals were kept in clear plastic cages wrapped on the outside with aluminium foil to increase light intensity within the cages.

For all light exposure experiments with pigmented animals, pupils were previously dilated. Pupillary dilation was done by serial topical application onto the cornea in red light. To obtain full midriasis (pupil dilation/iris constriction) and cycloplegia (paralysis of the ciliary muscle), a drop of cyclopentolate 0.5 % (Skiacol®, Alcon Laboratories, Houston, TX, USA) was first applied to the cornea 30 min before exposure. Fifteen minutes later (or 15 min before exposure) a drop of phenylephrin 5 % (Neosynephrine Faure, Europhta, Monaco, France) or tropicamid 2 mg/0.4 mL (Tropicamide® Faure, Novartis Pharma, Bern, Switzerland) was put on the cornea. Dilation was effective for about 8-h.

For high light intensity and blue light exposure experiments, animals were anaesthetised. *Arvicanthis ansorgei* were anaesthetised with a mixed solution of ketamine (Ketamine Virbac, Carros, France) at 150 mg/kg and xylazine (Rompun® 2 %, Bayer Pharma, rue Jean Jaurès, Puteaux, France) at 10 mg/kg injected at 0.5 mL/100 g body weight (b.w.). Rats were anesthetised with a mix of tiletamin/zolazepam (Zoletil® 20, Virbac, Carros, France) at 0.4 mg/kg and xylazine (Rompun® 2 %) at 0.67 mg/kg injected at 0.25 mL/100 g b.w. Injections were given intraperitoneally; the body was stretched by pulling the tail and injection was made in the lower left quadrant of the abdomen to avoid vital organs.

Following light exposure, animals were returned to darkness for one night.

Control groups were maintained under the same conditions as each experimental group, and underwent the same anaesthetic procedure, but did not receive pupil dilation treatment and were not exposed to bright light.

2.2. White Fluorescent Lamp

The illumination apparatus was manufactured according to the same specifications as used by another group working on light damage (Laboratory of Retinal Cell Biology, University Hospital, Zürich, Switzerland; Head: Prof. Grimm). It consists of a custom-made aluminium frame with an overhead lamp housing two cool white Philips TL-D 36W/965 fluorescent lamps (Figure 17). The frame can be adjusted in height to vary light intensity without varying the spectral composition of the light. Light intensity was measured by a hand-held luxmeter at the base of the cage (see Light Intensity Measurement section below).

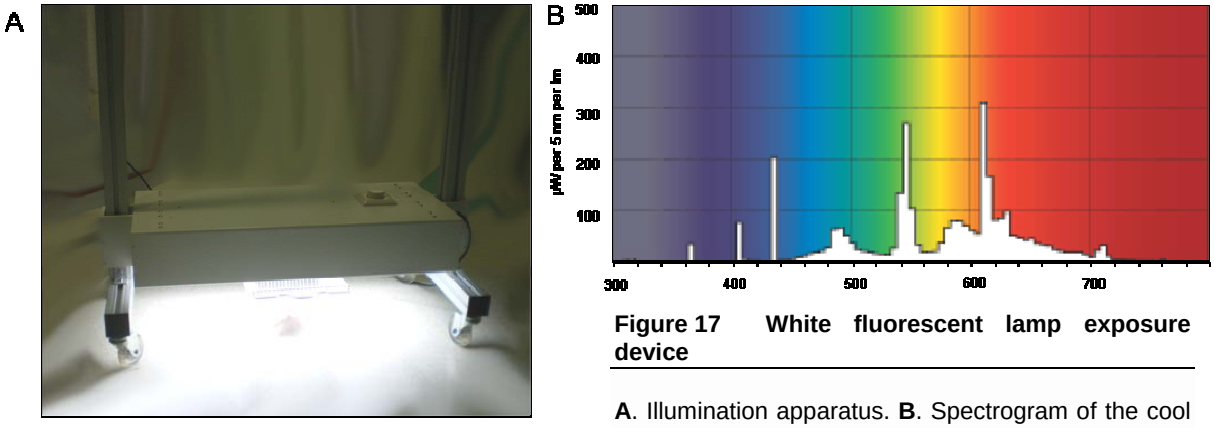

Figure 17 White fluorescent lamp exposure device

A. Illumination apparatus. **B**. Spectrogram of the cool white Philips TL-D 36W/965 fluorescent lamp.

2.3. Fibre-Optic Light

To increase light intensity at the corneal level, we used a fibre-optic cold light source (CL 1500 ECO, Carl Zeiss MicroImaging GmbH, Gottingen, Germany). With a twin-arm goose neck for oblique reflected light, fibre-optic illuminates the cornea precisely with intensive infrared-free light (Figure 18). A wide range of intensities can be achieved at the corneal level (from a few lux to more than 20,000 lux), depending on the distance between the light source and the cornea.

Figure 18 Fibre-optic light exposure.

Animals lay on the side with one eye exposed to the fibre-optic lights and the controlateral one hidden.

2.4. Blue Light Exposure

The experiments with blue light were realised in the Laboratory of Retinal Cell Biology under the kind supervision of Prof. Charlotte Remé. The blue light exposure system (Figure 19) consisted of a xenon short-arc reflector lamp (230 V, 50 Hz, 120 W; Intralux MDR 100; Volpi, Schlieren, Switzerland) with interference filters to eliminate ultraviolet (UV) and infrared radiations and a liquid fibre-optic light guide (8 mm in diameter) to the animal's cornea (Grimm et al., 2000a). The optical system included a switch holder for blue 403 ± 10 nm bandwidth interference filter. A heat sink was also provided to maintain animal body temperature constant during the time of light exposure.

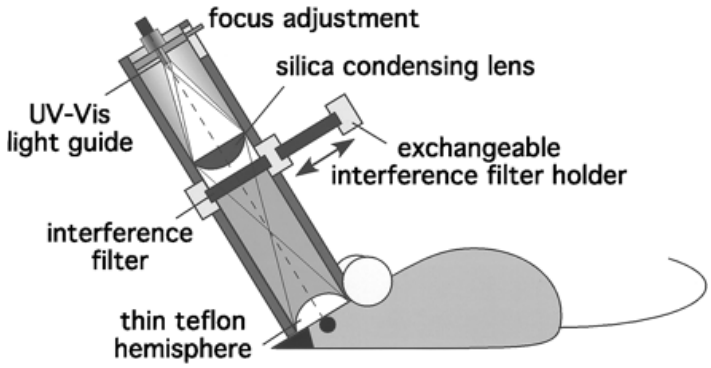

Figure 19 Illumination device for blue light exposure.

Light generated by a xenon short-arc reflector lamp with interference filters to eliminate UV and IR radiation was condensed by a silica lens and uniformly distributed on the cornea by a thin Teflon hemisphere. To evenly illuminate the retinas, the device is placed directly above the moisturized eye of an anesthetized animal.

IR: infra-red; UV: ultraviolet.
From (Grimm et al., 2000a).

3. MNU PREPARATION AND INJECTION

N-methyl-*N*-nitrosourea (MNU) was purchased from Sigma-Aldrich Chimie S.a.r.l. (Saint-Quentin Fallavier, France) and kept at 4°C in the dark.

MNU solution was freshly prepared in NaCl 0.9 % immediately prior to injection. Vehicle was prepared using a combination of 0.9 % NaCl solution with a 0.05 % acetic acid solution (as the data sheet of MNU indicates that the commercial solution contains 2.3 % of acetic acid).

Solutions of MNU were prepared at 10 mg/mL concentrations (solubility: 1.4 %). They were given by intraperitoneal (i.p) injections with 25 G 5/8" needles. *Arvicanthis* were injected at 75, 100 or 150 mg/kg b.w. dose. Rats were always injected at a 75 mg/kg b.w. dose.

N.B. It is important to keep in mind during the entire procedure of preparation and injection, that MNU is a toxic and highly carcinogenic compound promoting tumours across many animal species via different mean of application (i.p., sub-cutaneous and oral). In humans, it is probable that it acts as a carcinogen and may also cause reproductive harm.

4. Morpho-Structural Analysis

4.1. Histology

4.1.1. Tissue Samplings

Retinas to be analysed by Western blotting were collected in Eppendorf tubes, snap frozen in liquid nitrogen (-195.79°C), and then kept in a freezer at -80°C until protein extraction.

Eyes taken for immunohistochemistry were quickly removed for immersion fixation in buffered 2 or 4 % paraformaldehyde in 0.01 M Phosphate Buffered Saline (PBS), pH 7.4. They were kept at 4°C in the dark for 4-h or overnight and then transferred into fresh PBS 0.01 M for minimum 1-h. For orientation purpose and to facilitate penetration of fixative to the retina, a hole was made in the nasal pole of the *ora serrata* using a 25 G needle before removal. Eyes were dissected under a binocular dissecting microscope: cornea, lens and vitreous were removed. Histological analyses were either performed on retinal sections or on entire flat-mounted retinas. If sections were to be made, eye cups were bisected by making a cut with a clean scalpel blade, running through the optic nerve head along a superior to inferior axis (using the nasal hole as a reference).

4.1.2. Tissue Treatments

Routine histological examination (and selected immunohistochemistical studies, if the given antigen resisted the embedding procedure; see Figure 20) was performed on paraffin wax-embedded eyes. For this purpose, they were first transferred in ethanol 70° for 30 min (two changes), 2-ethoxyethanol for 1-h (two changes) and butanol solution overnight. Then the semi-eye cups were transferred to fresh butanol solutions for 1-h (two changes) and finally for 2-h in paraffin (two changes) (Histosec® pastilles without DMSO, Merck KGaA, Darmstadt, Germany) at 60°C. Eyes were then oriented in the paraffin mold with the optic nerve head facing down. Paraffin blocks were cut by microtome (Reichert-Jung Biocut 2030, Leica, Heidelberg, Germany) at 4 µm, and sections floated on 40°C hot water before being mounted on gelatin-coated glass slides. Before performing immunohistochemistry and histological staining, paraffin was removed from sections using solutions of toluene (2 x 10 min) and descending solutions of ethanol gradient (100, 90, 80, 70 and 50°) and then PBS.

Frozen sections, were embedded in Tissue-Tek® O.C.T™ compound (Sakura Finetek Europe, Zoeterwoude, The Netherlands). Prior to embedding, semi eye-cups were transferred to an ascending gradient of sucrose solutions (10, 20 and 30 %) for cryoprotection until the

tissue was totally immerged. Specimens were then put in a mold in Tissue-Tek® O.C.T™ compound and frozen on liquid nitrogen. Sections of 10 µm were made using the Leica CM3050 S cryostat (Leica Instruments, Heidelberg, Germany), mounted on gelatin-coated glass slides and kept at -20°C until needed for histological staining.

Retinal flatmounts were prepared after fixation and dissection, and washed in PBS 0.01 M.

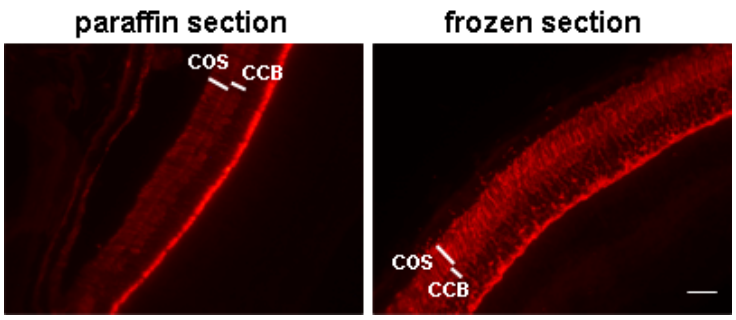

Figure 20 Immunofluorescent labelling on paraffin and frozen sections.

Paraffin and frozen sections were both incubated with anti-cone arrestin antibody. Staining is much apparent on frozen than on paraffin section. Scale: 20 µm.

COS: cone outer segments; CCB: cone cell bodies.

4.1.3. Hematoxylin/Eosin (H/E) staining and Construction of Spider Graphs

Deparaffinized sections were briefly washed in distilled water. They were then stained with Mayer's or Carazzi's hematoxylin 6.67 mg/L solution for 5 minutes. Sections were washed in warm running tap water for 3 minutes to allow stain to develop. Sections were rinsed in distilled water and dipped in hydrochloric acid (HCl) 0.37 % for 10 sec to adjust staining, especially outside the nucleus. In a second step, sections were counterstained with eosin (0.25 % in acetic acid 0.16 %) for 30 seconds. Dehydration was made through ascending baths of 5 min of ethanol solutions from 70 to 100 %. Ethanol was cleared with two baths of toluene of 5 min each and sections were then covered with coverslips in xylene based mounting medium (Eukitt®; O. Kindler GmBH, Fribourg, Switzerland).

Retinas were used for morphometric examination (measurement of retinal layer thickness) to identify any loss of specific cell types. Sections were taken in a systematic manner along the vertical meridian at the level of ONH across the entire retinal surface in order to construct spider graphs to demonstrate topographical changes retinal cell layers. Measurements were made at 275 µm intervals extending from the ONH in both superior and inferior *ora serrata*, using the ImageJ analysis software (version 1.37v; National Institutes of Health, USA) (Figure 21).

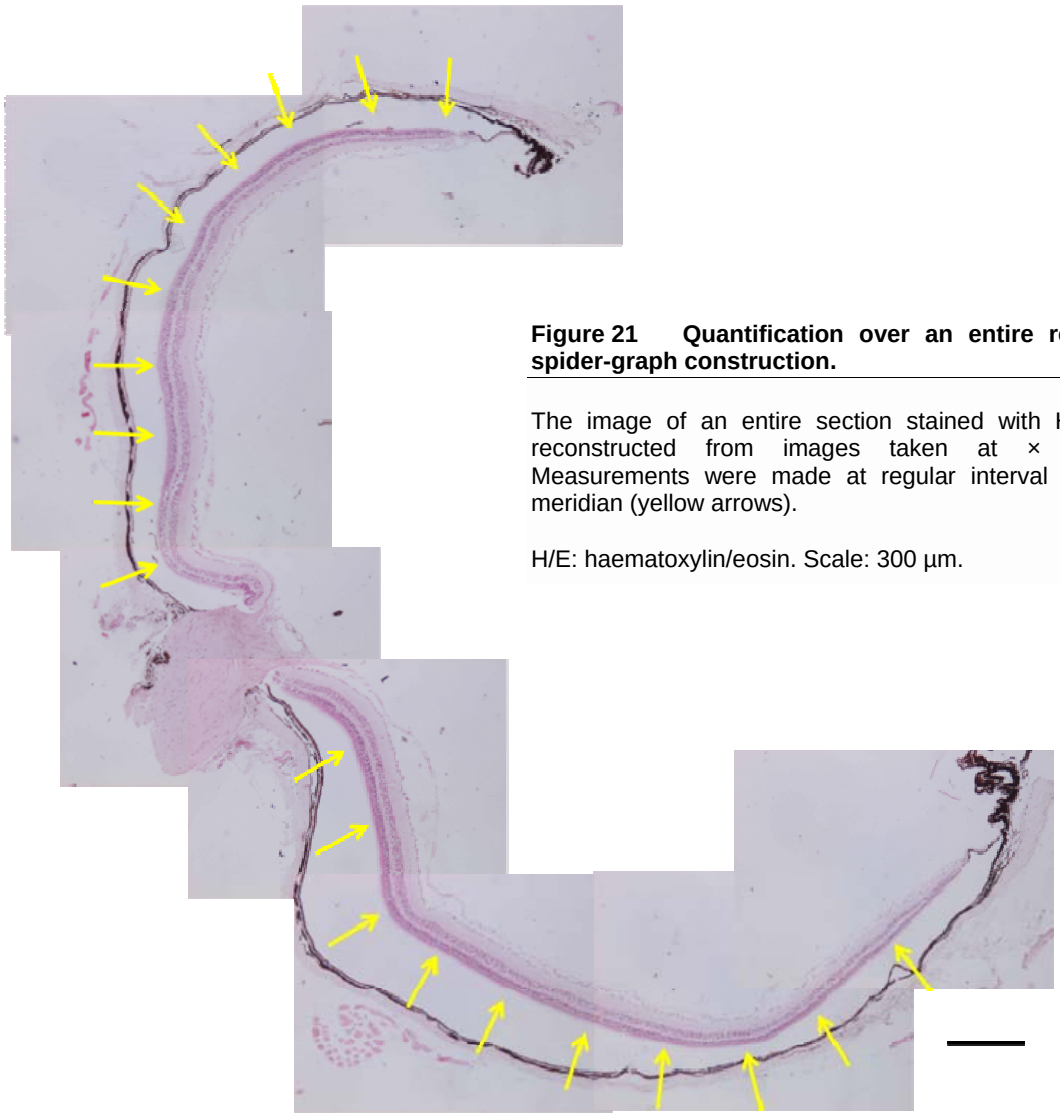

Figure 21 Quantification over an entire retina section for spider-graph construction.

The image of an entire section stained with H/E of retina was reconstructed from images taken at × 5 magnification. Measurements were made at regular interval along the vertical meridian (yellow arrows).

H/E: haematoxylin/eosin. Scale: 300 µm.

4.1.4. Immunohistochemistry

Immunohistochemistry was performed on sections or flatmounted retinas.

Sections were permeabilized with 0.1 % Triton X-100 for 5 minutes and then saturated with PBS 0.01 M, pH 7.4, containing 3 % BSA, 0.05 % Tween-20, and 0.1 % sodium azide (NaN_3) for 30 minutes. The primary antibody was diluted in the saturation buffer and left overnight at 4°C. Primary antibodies used for immunohistochemistry are reported in the Table 1. Sections were washed three times for 10 min with 0.01 M PBS. Secondary antibody incubation was performed at room temperature for 2-h with Alexa goat anti-rabbit or anti-mouse IgG-conjugated antibodies coupled with 594 or 488 Alexa (Molecular Probes Ltd., Eugene, OR, USA; 5 µg/mL). Cell nuclei were stained with 4,6-diamino-phenyl-indolamine (DAPI; Sigma) diluted at 1:500. The sections were again washed three times with PBS 0.01 M and then mounted using a glycerol/PBS solution 1:1 volume/volume.

ANTIBODIES (anti-)		Antigen	Type	Reference	Structures stained	Concentration/ (Dilution)
rhodopsin	Rho4D2	N-terminal	monoclonal	(Hicks and Molday, 1986)	ROS +++ and RCB +	1 µg/mL (1:200)
rod-transducin ($G_{\alpha t1}$)	K-20	Human peptide	polyclonal (rabbit)	Santa Cruz: sc-389	RCB	4 µg/mL (1:50)
cone-transducin ($G_{\alpha t2}$)	I-20	Bovine peptide	polyclonal (rabbit)	Santa Cruz: sc-390	CCB	4 µg/mL (1:50)
MW opsin	-	Mouse peptide	polyclonal (rabbit)	(Zhu et al., 2003)	COS	1 µg/mL (1:200)
cone arrestin (c-arr.)	-	Mouse peptide	polyclonal (rabbit)	(Zhu et al., 2002)	CCB	1 µg/mL (1:50)
GFAP	-	GFAP isolated from cow spinal cord	Polyclonal (rabbit)	DAKO: No. Z 0334	astrocyte	10.25 µg/mL (1:400)
melanopsin	-	Synthetic peptide corresponding to aa 1-19 of rat	polyclonal (rabbit)	Abcam: ab19306	entire cell	5 µg/mL (1:200)

Table 1 Primary antibodies used for immunohistochemistry staining.

aa: amino-acid; c-arr: cone arrestin; CCB: cone cell body; COS: cone outer segment; $G_{\alpha t1}$: rod-transducin; $G_{\alpha t2}$: cone-transducin; GFAP: glial fibrillary acidic protein; RCB: rod cell body; ROS: rod outer segment
Abcam, Cambridge, UK; DAKO A/S, Glostrup, Denmark; Santa Cruz Biotechnology, Inc. Santa Cruz, CA, USA

For wholemount immunohistochemistry, retinas were permeabilized in 0.3 % Triton X-100 for 1-h, saturated in blocking buffer overnight and incubated with primary antibodies for 3 days at 4°C under gentle agitation. After extensive washing (8-h with six changes of PBS solution), retinas were incubated with the same secondary antibody as mentioned above for 2-h at room temperature and flattened under coverslips in 1:1 PBS-glycerol.

4.1.5. *IN SITU* CELL DEATH DETECTION (TUNEL ANALYSIS)

Several methods have been described to identify apoptotic cells. Endonucleolysis is considered as the key biochemical event of apoptosis, resulting in cleavage of nuclear DNA into oligonucleosome-sized fragments. Therefore, this process is commonly used for detection of apoptosis by the typical "DNA ladder" on agarose gels during electrophoresis. This method however can not provide information regarding apoptosis in individual cells nor relate cellular apoptosis to histological localization.

In our experiments, apoptosis was assessed by an enzymatic *in situ* cell death detection technique, using the "Cell Death Detection Kit" (Roche Diagnostics, Basel, Switzerland). The principle of the method is based on the cleavage of genomic DNA during apoptosis that may yield double-stranded, low molecular weight DNA fragments ("nicks") in high molecular weight DNA. Those DNA strand breaks can be identified by labelling in an enzymatic reaction involving Terminal deoxynucleotidyl Transferase (TdT), which catalyzes

polymerization of labelled modified nucleotides to free 3'-OH DNA ends in a template-independent manner. The tailing reaction using TdT is called TUNEL for "TdT-mediated dUTP nick end labelling". In a second step, fluorescein labels are incorporated in nucleotide polymers.

Practically, the kit is composed of two components (Enzyme Solution and Label Solution). The TUNEL mixture is prepared immediately before use and kept on ice. The solution mixture is placed on sections in a dark humid chamber at 37°C for 1-h according to the manufacturer instructions guideline. Sections are then washed twice with PBS and mounted with PBS:glycerol 1:1.

4.1.6. Combined Fluorescent Immunohistochemistry and TUNEL Techniques

To assess with certainty the identity of TUNEL-positive cells, we combined IHC with *in situ* cell death detection.

For this purpose, the TUNEL reaction was performed between incubation with primary antibody and incubation with secondary antibody.

Briefly, sections were permeabilized with 0.1 % Triton X-100 for 5 minutes and then saturated with the saturation buffer for 30 minutes. The primary antibody was diluted in the saturation buffer and let overnight at 4°C. Sections were washed three times for 10 min with 0.01 M PBS. Freshly prepared TUNEL reaction mixture was applied on each section and left in a humid dark chamber for 1-h at 37°C. Sections were then washed thoroughly and incubation was performed in a dark humid chamber at room temperature for 2-h with DAPI and corresponding secondary antibody. Sections were again washed three times with PBS 0.01 M and finally mounted in a glycerol/PBS solution 1:1.

4.2. *in vivo* Imaging

Imaging techniques were realized after ERG recordings on still anesthetised animals. Imagery procedures along with some of the ERG experiments were performed in the group of Prof. Mathias Seeliger in Tubingen.

4.2.1. Scanning Laser Ophthalmoscopy (SLO)

Dr. Susanne Beck was in charge of the SLO imaging technique. Retinas of the still anaesthetized *Arvicanthis* were observed by SLO imaging with a Heidelberg Retina

Angiograph (HRA I, Heidelberg Engineering, Germany), a confocal scanning-laser ophthalmoscope (SLO), according to previously described procedures (Seeliger et al., 2005). The HRA features two argon wavelengths (488 nm and 514 nm) in the short wavelength range and two infrared diode lasers (795 nm and 830 nm) in the long wavelength range. Laser wavelengths used for fundus visualization were: 830 nm (IR, infrared channel), 514 nm (RF, red-free channel) and 488 nm for autofluorescent images (AF). Additionally, the 488 nm and 795 nm lasers were used for fluorescein (FL) and indocyanine green (ICG) angiography, respectively. ICG injections were performed in the ventral tail vessel by Dr. Edda Fahl. Appropriate barrier filters of 500 and 800 nm, respectively, were used to remove the reflected light with unchanged wavelength and only allow passage of light emitted by the dye upon stimulation. Two device settings for the field of view were used: for fundus overview, the focus was adjusted to 20°; and for magnification and detailed view, the focus was set at 10°.

4.2.2. Optical Coherence Tomography (OCT)

Spectral Domain Optical Coherence Tomography (SD-OCT) imaging was done with a commercially available Spectralis™ HRA + OCT device from Heidelberg Engineering featuring a broadband super-luminescent diode at λ = 870 nm as low coherent light source. Each two-dimensional B-Scan recorded at 30° field of view consists of 1536 A-scans, which are acquired at a speed of 40,000 scans per second. Optical depth resolution is approximately 7 µm with digital resolution reaching 3.5 µm (Wolf-Schnurrbusch et al., 2008). Imaging was performed using the proprietary software package Eye Explorer (version 3.2.1.0, Heidelberg Engineering, Germany). Outer and inner retinal layers thickness was quantified using horizontal slides, located 1,500 µm distant from the optic nerve head. Outer retina was defined as proximal of the highly reflective layer presumably representing the RPE/choriocapillary complex up to the OPL; inner retina as proximal of the OPL up to the inner limiting membrane.

5. Western Blot Analysis

Retinas were immediately frozen in liquid nitrogen and maintained at -80°C until protein extraction.

Samples were prepared in an extraction buffer solution containing 20 mM Tris-Base, 150 mM NaCl, 1 % Triton X-100, 1 mM EDTA, pH 7.4. Just before use, 4 % of protease inhibitor cocktail (Roche Diagnostics GmbH. Roche Applied Science, Mannheim, Germany) and 1 mM DTT were added to the buffer. A volume of 200 µL of buffer was added for one retina and incubated on ice for 30 min. Retinas were then mechanically dissociated using an ultrasonic ultrasound power generator (Vibra-Cell 75186, Sonics & Materials, Newtown, CT, USA): 15 sec, pulse 30/10 and amplitude 50 %.

Protein content of the extracts was determined using the Lowry method (Lowry et al., 1951), using Bovine Serum Albumin (BSA) as standard (ascending concentrations 0.125, 0.250, 0.500, 0.750 and 1 mg/mL).

Retinal proteins were separated by loading onto SDS-polyacrylamide gels (4-10 %) and running in a gel tank (Bio-Rad, Munich, Germany) in electrophoresis buffer, for 2-h at 100 V. Proteins were then transferred to a PVDF (Polyvinylidene Fluoride) membrane with a transblotter cell (1-h, 90 V) (Bio-Rad) (Figure 22). Composition of gels and buffers are reported in Table 2. After blotting, the membrane was washed in methanol and dried for 15 min. After the membrane is totally dry, it is put back in methanol and then rinsed with Tris Buffer Sodium (TBS). This step is necessary to clean the membrane of any remaining blotting buffer. Membranes were first blocked with TBS containing 0.1 % Tween 20 and 3 % fat-free powdered milk (pH 7.3) for 1-h at room temperature. In a second step, membranes were incubated with the primary antibodies and incubated overnight at 4°C under agitation (for antibodies description, see Table 3). The membranes were washed thoroughly and then incubated with secondary antibody coupled to horseradish peroxidase diluted to a final concentration of 0.08 µg/mL (1:10,000; Jackson ImmunoResearch Laboratories, West Grove, PA, USA). Immunoreactive bands were visualized with chemiluminescence (Immobilon™ Western, Millipore, Bedford, MA, USA), according to the manufacturer's instructions. Apparent molecular masses were estimated by comparison to pre-stained molecular size markers (Invitrogen-Life Technologies, Gaithersburg, MD, USA). When needed, the membranes were incubated with Restore™ Western Blot Stripping Buffer (Thermo Fisher Scientific, Rockford, IL, USA) 20 min at room temperature, and the same procedure as described above was performed.

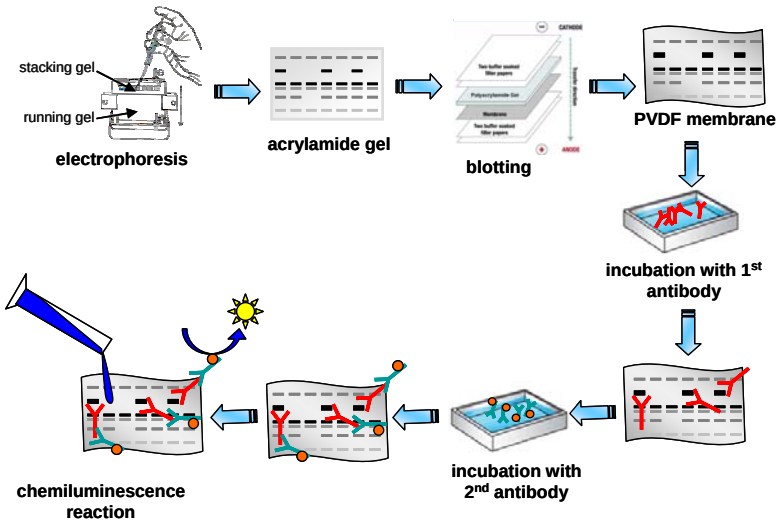

Figure 22 Western blot analysis procedure.

Samples are loaded on a polyacrylamide gel. Electrophoresis is run and proteins are subsequently transferred on a PVDF membrane. The membrane is latter incubated with primary antibody, washed, and incubated with secondary antibody. Chemiluminescence reaction with adequate substrate reveals stained bands.

PVDF: Polyvinylidene Fluoride.

	Composition	pH
10 % Acrylamide Running Gel	Tris-HCl 0.37 M; SDS 0.1 %; Acrylamide 10 % /Bis Acrylamide 0.27 %; APS 0.1 %; TEMED 0.1 %	8.8
4 % Acrylamide Stacking Gel	Tris-HCl 0.12 M; SDS 0.1 %; Acrylamide 4 % / Bis Acrylamide 0.1 %; APS 0.1 %; TEMED 0.1 %	6.8
Electrophoresis Buffer	Tris 0.025 M; Glycine 1.44 %; SDS 2.5 %	8.3
Blotting Buffer	Tris 20 mM; Glycine 192 mM; Methanol 20 %	7.4
Tris Buffer Sodium	NaCl 14.6 %; Tris 1.2 %	7.4

Table 2 Buffers used for Western Blot analysis.

APS: Ammonium persulfate; SDS: sodium dodecyl sulfate; TEMED: Tetramethylethylenediamine.

		Antigen	Type	Reference	Concentration/ (Dilution)
cone arrestin (c-arr.)	-	Mouse peptide	polyclonal (rabbit)	(Zhu et al., 2002)	0.008 µg/mL (1:6,000)
cone-transducin ($G_{\alpha t2}$)	I-20	Bovine peptide	polyclonal (rabbit)	Santa cruz: sc-390	0.004 µg/mL (1 :50,000)
melanopsin	-	Synthetic peptide corresponding to aa 1-19 of rat	polyclonal (rabbit)	Abcam: ab19306	0.004 µg/mL (1:250,000)
NF-68	8A1	Human brain peptide	monoclonal (mouse)	Santa Cruz: sc-20012	50 µg/mL (1:4,000)
rhodopsin	Rho4D2	N-terminal	monoclonal (mouse)	(Hicks and Molday, 1986)	0.04 µg/mL (1:5,000)
rod-transducin ($G_{\alpha t1}$)	K-20	Human peptide	polyclonal (rabbit)	Santa cruz: sc-389	0.0004 µg/mL (1:50,000)

Table 3 Primary antibodies used for Western-blot analysis.

aa: amino-acid.

Abcam, Cambridge, UK; DAKO A/S, Glostrup, Denmark; Santa Cruz Biotechnology, Inc. Santa Cruz, CA, USA.

Films were developed and fixed using an automatic film processor, (Hyperprocessor RNP 1700, Amersham, Les Ulis, France). Protein band densities were determined by scanning the blots on a professional scanner (Epson Perfection 4990 Photo, Seiko Epson Co., Nagano, Japan) at 1,200 dpi resolution. Each image was subjected to quantification using the ImageJ analysis software (version 1.37v; National Institutes of Health, USA).

6. ELECTRORETINOGRAPHY

Electroretinography experiments were performed in collaboration with two partner laboratories. The initial ERG recordings were made with Dr. Niyazi Acar (Eye and Nutrition group, UMR FLAVIC, INRA, Dijon, France). Subsequent experiments were performed with Dr. Naoyuki Tanimoto in the group of Prof. Mathias Seeliger (University Hospital, Tubingen, Germany). Both of the teams possess all the equipment, technical and theoretical expertise necessary for ERG recordings. This section describes the materials used in Prof. Seeliger's group, but similar material is found in the laboratory in Dijon.

Animals were dark adapted overnight before the experiments and their pupils were dilated with tropicamide (Mydriaticum Stulln; Pharma Stulln, Nabburg, Germany) and phenylephrine 5 % (Neosynephrin-POS 5 %; Ursapharm, Saarbruecken, Germany) eye drops. Animals were anaesthetised by intraperitoneal injection of a combination of ketamine (Virbac, Carros, France) at 150 mg/kg b.w. and xylazine (Rompun® 2 %, Bayer Pharma, Puteaux, France) at 10 mg/kg b.w.

Animals were positioned on a temperature controlled (38°C) cushion on a sliding platform. Silver needle electrodes served as reference (forehead) and ground (tail) electrodes, and gold-wire ring electrodes as active electrodes. Methylcellulose (Methocel; Ciba Vision, Wessling, Germany) was applied to ensure good electrical contact and to keep the cornea hydrated during the entire procedure.

ERGs were performed according to previously described procedures (Seeliger et al., 2001; Tanimoto et al., 2009). The ERG equipment consisted of a Ganzfeld bowl, a direct current amplifier, and a PC-based control and recording unit (Multiliner Vision; VIASYS Healthcare GmbH, Hoechberg, Germany). ERGs were recorded from both eyes simultaneously after the animals were placed in the Ganzfeld bowl. Band-pass filter width was 1 to 300 Hz for single-flash and flicker-stimuli recordings. Band-pass filter cutoff frequencies were 0.1 and 3,000 Hz. Single-flash and flicker recordings were obtained both under dark-adapted (scotopic) and light-adapted (photopic) conditions. Light-adaptation was performed with a background illumination of 30 cds/m^2 presented 10 minutes before recording to reach a stable level of the photopic responses. Illumination strength was varied using different actinic filters placed below the lamp housing. Single white-flash stimulus intensity ranged from -4 to 1.5 log cd×s/m^2 under scotopic and from -2 to 1.5 log cd×s/m^2 under photopic conditions, divided into 10 and 8 steps, respectively. Ten responses were

averaged with an inter-stimulus interval of either 5 seconds (for -4, -3, -2, -1.5, -1 and -0.5 log cd×s/m^2) or 17 seconds (for 0, 0.5, 1 and 1.5 log cd×s/m^2)

7. ACTIMETRY

Wheel-running activity of singly housed animals was recorded continuously and data (number of revolutions) were stored in 10 min bins using the data acquisition system CAMS (Circadian Activity Monitoring System, INSERM, France).

Behavioural re-entrainment was analyzed using the Clocklab software package (Actimetrics, Evanston, IL, USA). The time of locomotor activity onset was determined using the onset fit algorithm. Animals were considered re-entrained to the new LD cycle when their activity onset remained stable for at least the following five days, and when the period of activity was close to the 24-h period of the new LD cycle. Period was calculated with a χ^2 periodogram analysis (ClockLab, Actimetrics Software, Evanston, IL, USA).

The phase angle of entrainment (ψ) was defined as the time of the onset of activity relative to the time of lights off. To evaluate differences in the phase angle of entrainment between groups, we compared the mean of the ψ for the last five days of each LD cycle in both groups.

Quantification of activity during the light period was performed for each cycle. To avoid any effect of the transition cycle, only the period at which animals were fully entrained was considered. An exception was made for animals that did not synchronize even after extended periods.

8. Light Intensity Measurements

We measured light intensity with a Digital Light Meter (DLM2000AC, General Tools & Instruments Co., New York, NY, USA) providing light levels in **lux** covering a 0 to 20,000 lux range. The lux is the International Unit of **illuminance**. It is used in photometry as a measure of the *apparent* intensity of light hitting or passing through a surface. Some examples of illuminance correspondences can be found in Table 4.

Illuminance	Example
10^{-5} lux	Light from the brightest star (Sirius)
10^{-4} lux	Total starlight, overcast sky
0.002 lux	Moonless clear night sky with airglow
0.01 lux	Quarter moon
0.27 lux	Full moon on a clear night[f]
1 lux	Full moon overhead at tropical latitudes
3.4 lux	Dark limit of civil twilight under a clear sky
50 lux	Family living room
80 lux	Hallway/toilet
100 lux	Very dark overcast day
320 lux	Recommended office lighting
400 lux	Sunrise or sunset on a clear day. Well-lit office area
500 lux	Lighting level for an office according to the European law UNI EN 12464.
1,000 lux	Overcast day typical TV studio lighting
10,000–25,000 lux	Full daylight (not direct sun)
32,000–130,000 lux	Direct sunlight

Table 4 **Examples of illuminance correspondences.**

Sources: Paul Schlyter, Radiometry and photometry in astronomy FAQ (2006); "Petzl reference system for lighting performance" (2007): http://en.petzl.com; (Bunning and Moser, 1969); "Electro-Optics Handbook"; Pears, Alan (June, 1998), "Chapter 7: Appliance technologies and scope for emission reduction", Strategic Study of Household Energy and Greenhouse Issues, Australian Greenhouse Office (2008); Australian Greenhouse Office (2005), "Chapter 5: Assessing lighting savings".

Like all photometric measures, illuminance has a corresponding "radiometric" measure: **irradiance**. Irradiance is measured in **watt/metre^2**. The difference between illuminance and irradiance is that irradiance is based on physical power, with all wavelengths being weighted equally, while illuminance takes into account the fact that the eye is more sensitive to some wavelengths than others, and accordingly every wavelength is given a different weight. Therefore, there is no single conversion factor between lux and watt/metre^2;

there is a different conversion factor for every wavelength, and it is not possible to make a conversion unless one knows the spectral composition of the light.

The peak of the luminosity function is at 555 nm (green) as the human eye is more sensitive to light of this wavelength than any other. For monochromatic light of this wavelength, the irradiance needed to make one lux is minimal at 1.464 mW/m^2. That is, one obtains 683.002 lux per W/m^2 (or lumens per watt) at this wavelength. Other wavelengths of visible light produce fewer lumens per watt. The luminosity function falls to zero for wavelengths outside the visible spectrum.

To further complicate the situation, older publications use other units to express illuminance such as **foot candles**.

In practical applications, as when measuring room illumination, it is very difficult to measure illuminance more accurately than ± 10 %, and getting precise measures of light intensity in the cage of an animal is quite impossible. Therefore, when illuminance was measured at the level of a cage, 3 measures were taken at 3 different points and the average was computed.

For ERG experiments, light intensity is given in **candela per square metre** (cd/m^2). This is the unit of **luminance**, a photometric measure that describes the amount of light emitted from a particular area, and falling within a given solid angle (the solid angle subtended by the eye's pupil). Luminance is used to characterize emission or reflection from diffuse surfaces and indicates how much luminous power will be perceived by an eye looking at the surface from a particular angle of view indicating how bright the surface will appear. In the case of ERG, luminance represents the amount of light re-emitted via the interior of the Ganzfeld bowl (Figure 23). The Table 4 gives some example of natural scene luminance levels in cd/m^2. The Table 5 shows the physiological processes in the retina in relation with different luminance levels.

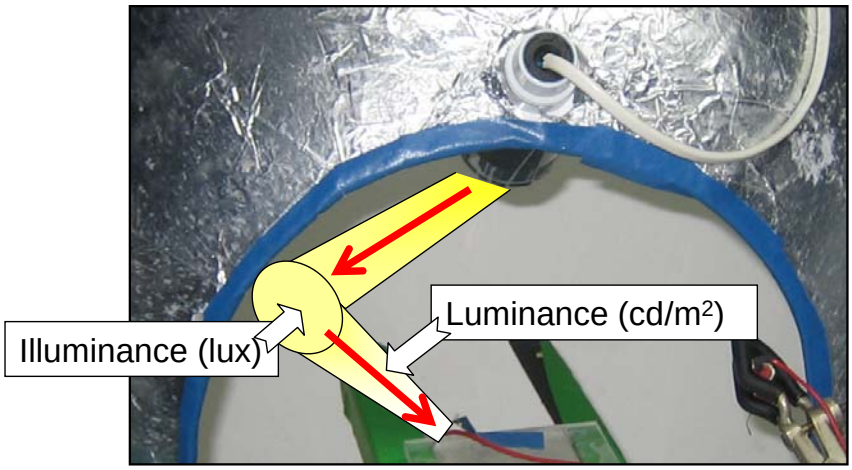

Figure 23 Representation of illuminance and luminance measures within a Ganzfeld bowl.

Light emitted within the Ganzfeld bowl hits the interior of the bowl. The total luminous flux incident on the interior surface, per unit area is called **illuminance** and is measure in **lux** unit. The amount of light that is emitted from this area, and falls within a given solid angle is called **luminance** and is measured in **candela per square metre (cd/m^2)**.

Environment	Luminance level (cd/m^2)
Clear sky at noon	10^4
Cloudy sky at noon	10^3
Grey sky at noon	10^2
Cloudy sky at sunset	10
Clear sky, a quarter hour after sunset	1
Clear sky, a half hour after sunset	10^{-1}
Night sky - Full moon	10^{-2}
Night sky - Clear without moon	10^{-3}
Night sky - Cloudy without moon	10^{-4}

Table 5 Examples of luminance correspondences.

Approximate luminance of the sky near the horizon in cd/m^2.

Source: (Middleton, 1952).

Significance	Lum level (log cd/m^2)
Absolute Threshold	-6
Scotopic Start	-
Cone Threshold	-3
Scotopic End	-
Mesopic Begin	-
Rod Saturation Begins	2
~ Mesopic End	-
~ Photopic Begin	-
Damage Possible	8

Table 6 Levels of luminances and their corresponding significance at the level of retinal physiology.

Rods are activated at ~ -6 log cd/m^2 before cones, which need a ~ -3 log cd/m^2 luminance level to be active. The condition in which only rods are active is called scotopic. When both cells are active, this is the mesopic condition. When rods saturate at ~ -2 log cd/m^2 it is the inititation of the photopic condition.

Source: (Hood and Finkelstein, 1986).

RESULTS

D. Results

1. Further Characterization of *Arvicanthis* Retina

2. (No) Light-Induced RD in *Arvicanthis* (?)

3. MNU-Induced PR Degeneration in *Arvicanthis* (1st article)

4. RD and Photoentrainment: MNU-injected Rats Lost in the Twilight Zone… (2nd article)

1. Further Characterization of *Arvicanthis* Retina

In a previous study, our group described the structure of *Arvicanthis* retina and particularly the PR layer (Bobu et al., 2006). The rod to cone ratio was quantified and the distribution of SW cones investigated. Through application of complementary techniques, we investigated new features of the *Arvicanthis* retina.

1.1. Structural Features Investigated with Real-Time Imaging Techniques

1.1.1. Scanning Laser Ophthalmoscopy (SLO)

Arvicanthis fundus visualization was accomplished by SLO imaging, and photographs were compared with those of C57Bl6 mice and Wistar rats (Figure 24). Fundus visualization with IR and RF channels did not reveal any major changes in *Arvicanthis* fundus compared to mice and rats. None of the species show AF materials. Angiography with both FL, displaying mainly the retinal vessels, and ICG which allows analysis of the choroidal vessels additionally, did not reveal any striking differences in the retinal vascular anatomy among species.

However, on the *Arvicanthis* fundus, a region located in the median part of the superior hemisphere (located at the inferior part of the picture because SLO pictures are shown inverted) appears lighter than the rest of the retina (region surrounded in red; Figure 24). This region is not seen in retinas of rat and mouse, but resembles the visual streak found in other species.

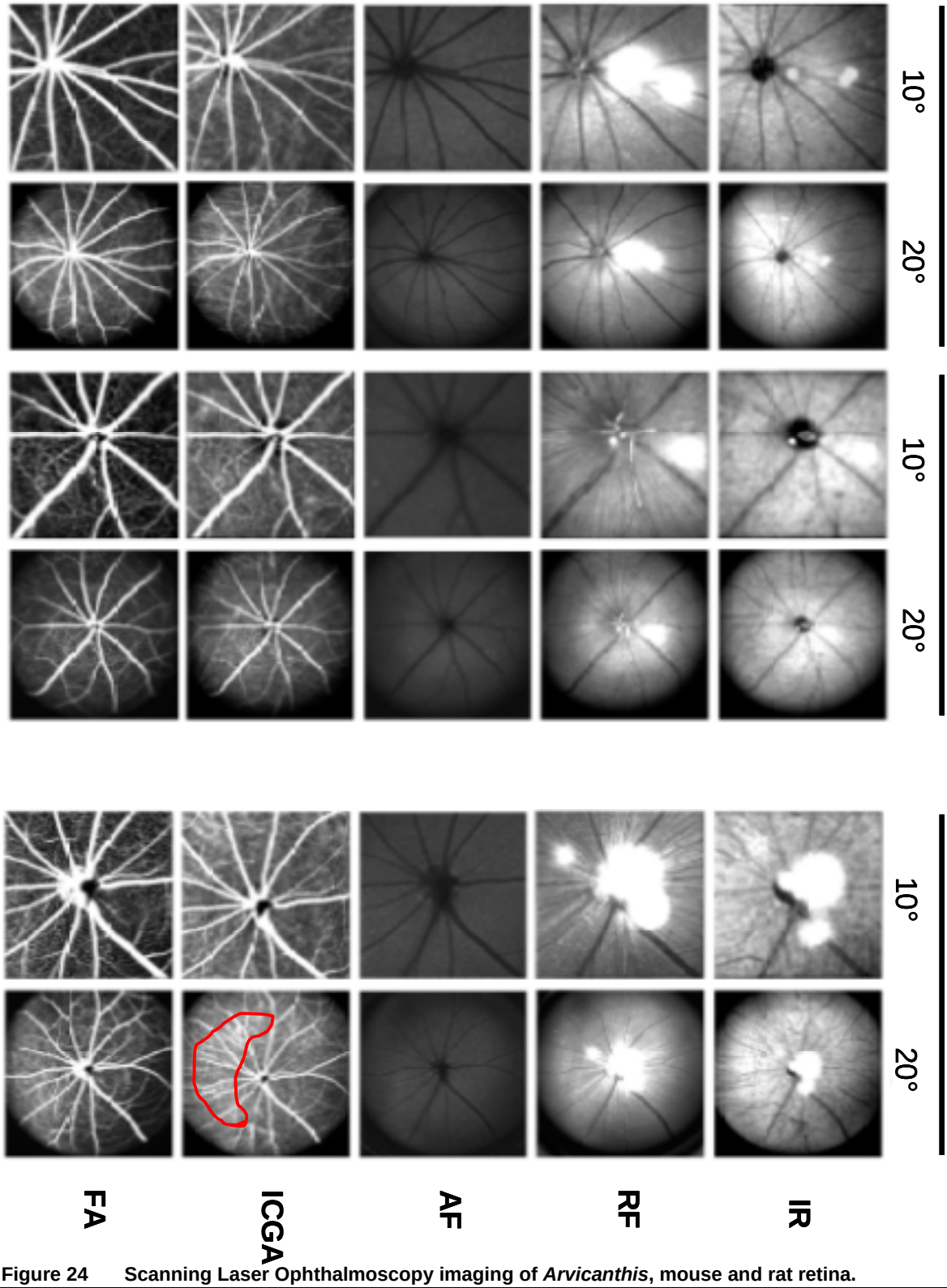

Figure 24 Scanning Laser Ophthalmoscopy imaging of *Arvicanthis*, mouse and rat retina.

SLO imaging of *Arvicanthis*, mouse and rat retinas with different excitation channels taken at 10° and 20° focus setting. Overall fundus structure along with retinal vessels appears very similar among the three species. A light zone (**red line**) reveals a putative visual streak in the superior hemisphere of the *Arvicanthis* retina, which is not seen in mouse or rat.

AF: autofluorescence; FA: fluorescein angiography; ICG: indocyanine green angiography; IR: infrared; RF: red-free; SLO: scanning laser ophthalmoscopy.
Images: Dr. Susanne C. Beck.

1.1.2. Optical Coherence Tomography (OCT)

OCT imaging was used to study the structure of *Arvicanthis* retina *in vivo*, and particularly the transversal structure. On OCT photographs, very dense structures (such as nuclear layers) appear white whereas diffuse structures (such as synaptic layers) appear dark.

In Figure 25, an image taken with OCT technique is compared with two microscope pictures of tissue sections after cryostat sectioning and H/E staining.

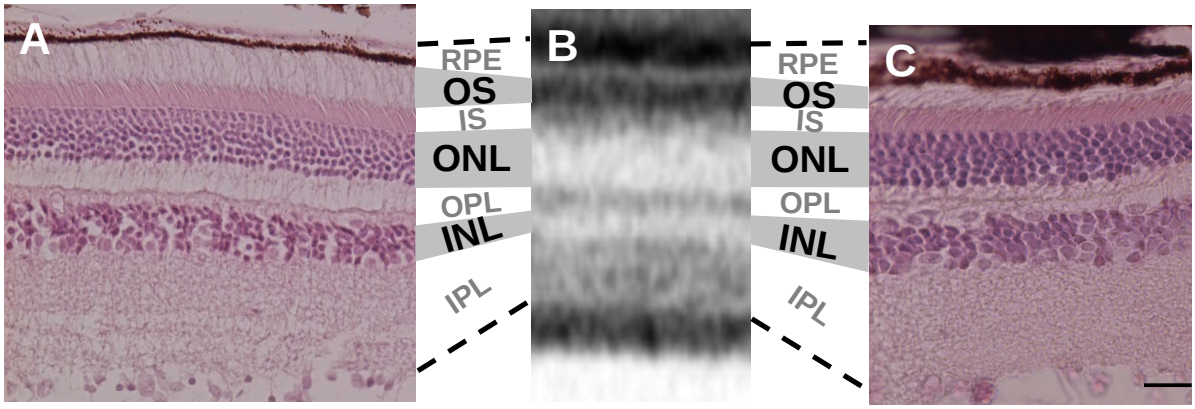

Figure 25 Optical Coherence Tomography imaging picture of *Arvicanthis* retina compared to two pictures of H/E stained retinal sections.

A and **C**: images of two retina sections of *Arvicanthis* stained with H/E compared to **B**: OCT imaging image of *Arvicanthis* retina. Depending on the section, layers can be enlarged compared to *in vivo* layers.

H/E: haematoxylin/eosin; INL: inner retina layer; IPL: interplexiform layer; IS: inner segment; OCT: optical coherence tomography; ONL: outer nuclear layer; OPL: outer plexiform layer; RPE: retinal pigmentary epithelium.
Scale: 30 µm.
OCT images: Gesine Hubert.

It should be noted that tissue treatment/sectioning can lead to artefactual appearance of layers more or less detached from one another (Figure 25A and C). When comparing histological sections (Figure 25A and C) with OCT image (Figure 25B), the first notable observation is that overall *Arvicanthis* retina after tissue processing and histological staining is wider than the retina observed *in vivo* in real time with OCT imaging, due to swelling. Particularly, the IPL appears much wider in histological sections.

1.2. Electrophysiological Responses of the *Arvicanthis* retina: when Cones do not go Unnoticed

To assess the functional characteristics of *Arvicanthis* retina, ERG data were compared to those of mice and rats.

Under **dark-adapted conditions** (scotopic conditions; Figure 26 upper panels), *Arvicanthis* responses appear totally different compared to those of mice and rats. It is important to note that the ERG responses of mice and rats constitute very characteristic "signatures". Responses to stimuli of -2.0 log cd×s/m² and below are generated exclusively by the rod system (Seeliger et al., 2001; Tanimoto et al., 2009). In this low intensity range, flash ERG responses in *Arvicanthis* were significantly smaller than those of mice. In the intensity range above -1.0 log cd×s/m², response onset and amplitudes of a- and b-waves were quite similar for both species. However, a prominent difference was that the b-wave in *Arvicanthis* was considerably shorter in duration.

Under **light-adapted conditions** (photopic conditions, Figure 26 bottom panels), where rods are normally saturated by background light, single flash responses of *Arvicanthis* became apparent at lower intensities (-1.5 log cd×s/m^2) compared to those of mice and rats (-0.5 log cd×s/m^2). Also, the latency time of *Arvicanthis* responses was smaller, suggesting higher sensitivity of cones. B-waves of *Arvicanthis* are shorter, have larger amplitudes and are accompanied by larger a-waves than those of mice and rats. The small, high frequency oscillations superimposed on the b-wave, called oscillatory potentials, were in contrast less evident in *Arvicanthis* than in mouse.

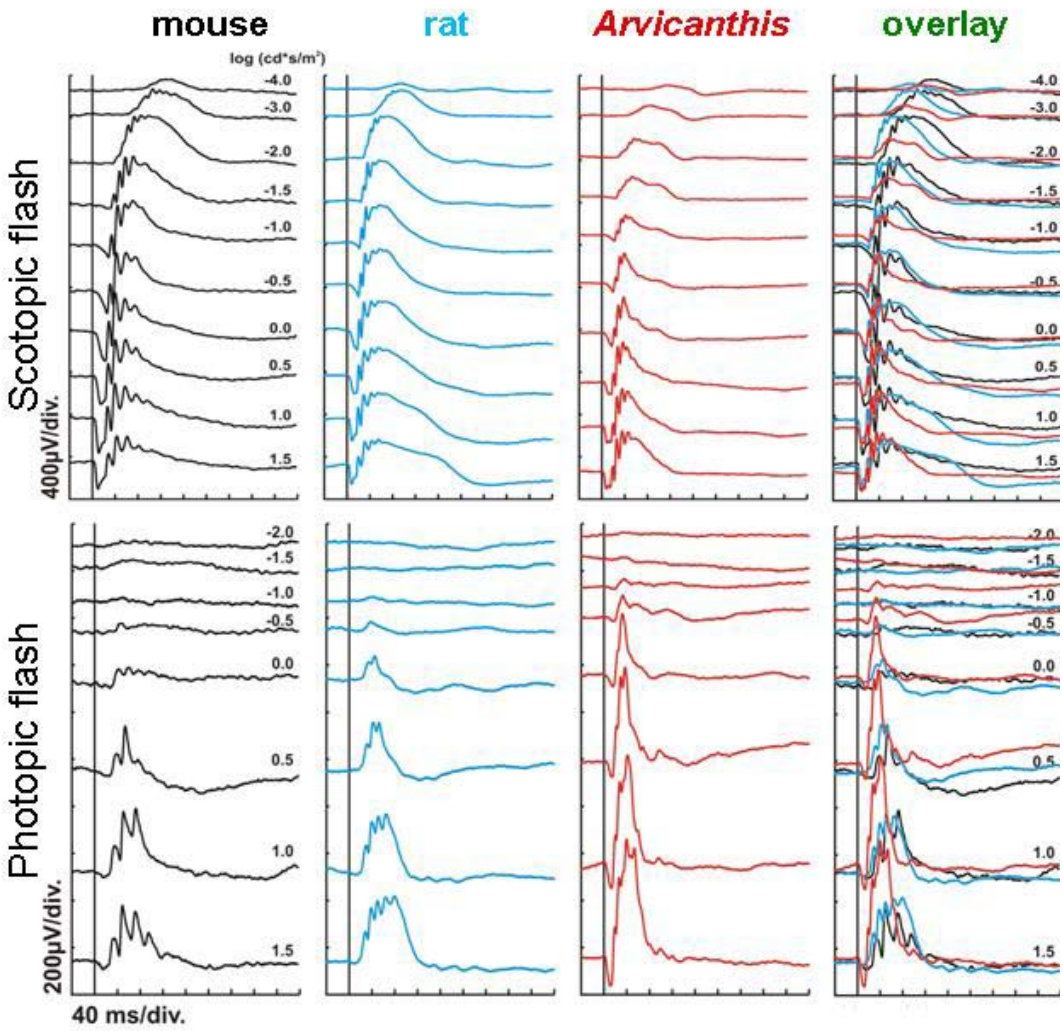

Figure 26 ERG responses of *Arvicanthis*, mouse and rats with single flash scotopic and photopic protocols.

Mouse (black), rat (blue) and *Arvicanthis* (red) ERG responses obtained with a single flash protocol under scotopic or photopic conditions. Mouse and rat responses are very similar whereas *Arvicanthis* are drastically different. Responses of both nocturnal rodents are much higher than *Arvicanthis'* in scotopic conditions at low intensities whereas in photopic conditions *Arvicanthis* responses are much higher than those of mice and rats.

Recordings: Dr. Naoyuki Tanimoto.

Responses to **Flicker stimulations** at different frequencies were also registered for the three rodent species (Figure 27). By comparing scotopic and photopic Flicker responses of *Arvicanthis*, we observed that the scotopic Flicker response at 2 Hz is similar to that of photopic responses. Therefore, we can assume that the scotopic response at 2 Hz is generated entirely by cones. This is not the case for other species whose scotopic and photopic responses are totally different below 10 Hz frequency, with particularly the b-wave being longer in scotopic conditions. Also, the a-wave is clearly visible in *Arvicanthis* for all frequencies and under both conditions. This is not the case for mice and rats whose a-wave is not visible in photopic conditions, or in scotopic conditions above 1 Hz for rats, and 7 Hz for mice. This again suggests a much higher sensitivity of the cone system in *Arvicanthis*. It is also interesting to note that the **critical flicker fusion frequency** (**CFF**), the frequency that the visual system can no longer resolve is at about 30 Hz in both mice and rats whereas it is much higher in *Arvicanthis*, whose responses do not show a major drop in amplitude at 30 Hz. This demonstrates the enhanced visual frequency resolution of *Arvicanthis*, typical for diurnal species.

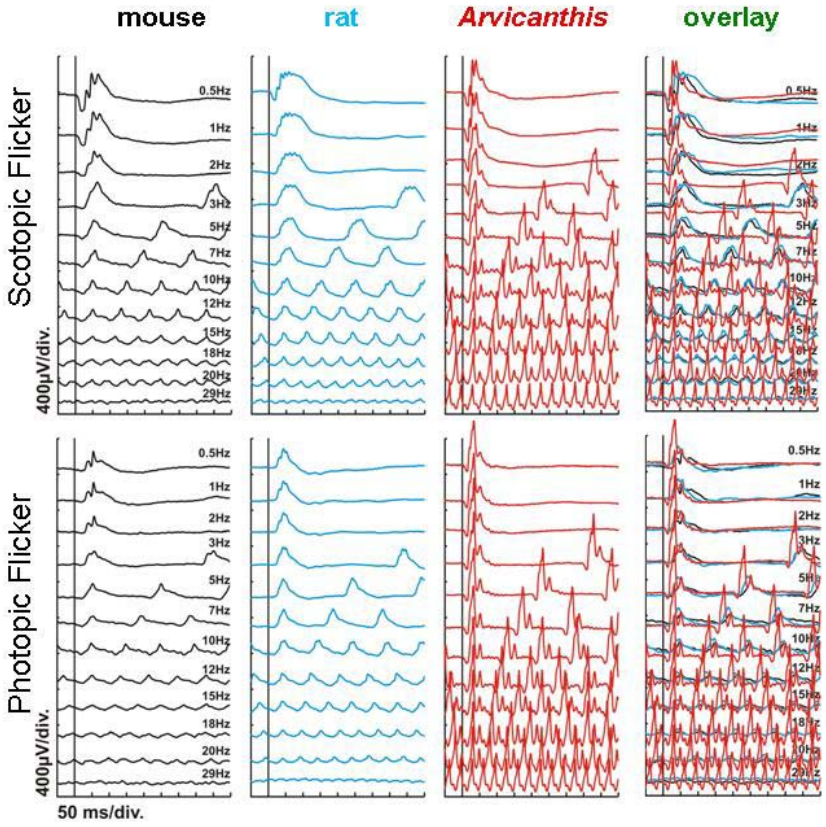

Figure 27 ERG responses of *Arvicanthis*, mouse and rats with scotopic and photopic Flicker protocols.

Mouse (black), rat (blue) and *Arvicanthis* (red) ERG responses obtained with a Flicker protocol under scotopic or photopic conditions. The sustained response at high frequencies stimulation for *Arvicanthis* is striking.

Recordings: Dr. Naoyuki Tanimoto.

Responses to a **6 Hz Flicker protocol** (flash frequency kept at 6 Hz while increasing light intensity), show that at low intensities, where principally rods are activated, responses of *Arvicanthis* resemble those of mice (Figure 28). Responses for higher intensities, where cones are active, are totally different for both species. *Arvicanthis* cones begin to respond around 0.4 to 1 cd×s/m^2 (log -3). Amplitudes of the responses are much higher than those of mice.

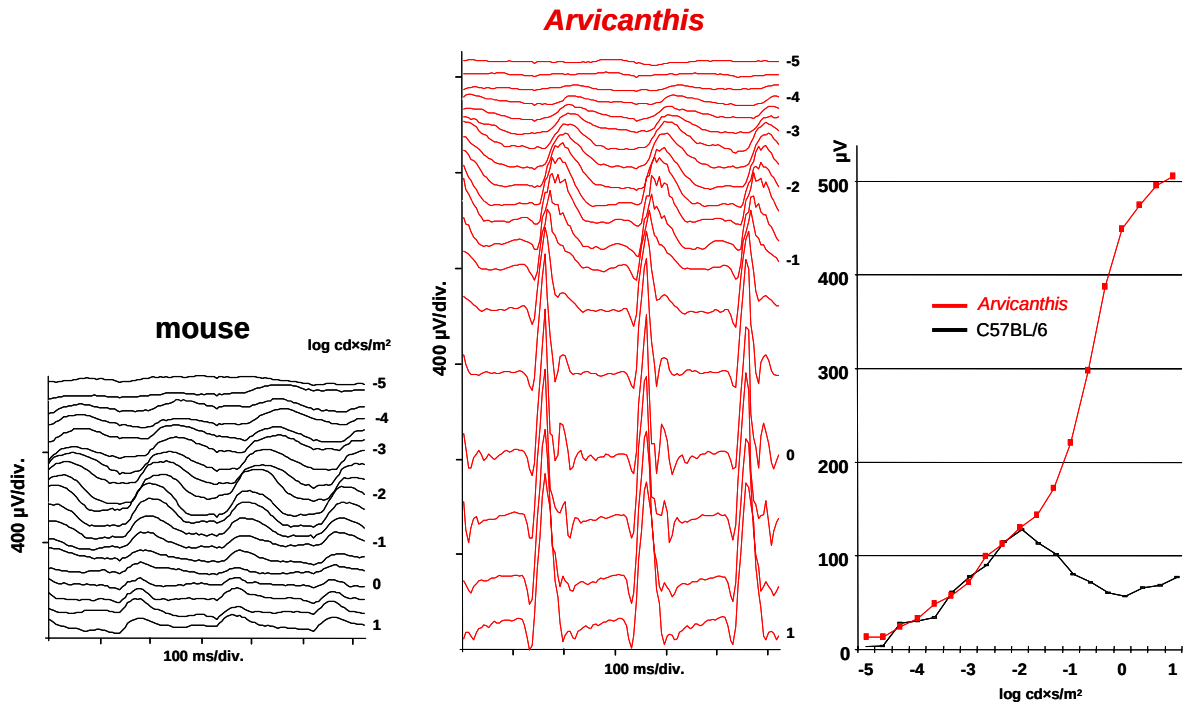

Figure 28 ERG responses of mouse and *Arvicanthis* with 6 Hz Flicker protocol.

Mouse (black) and *Arvicanthis* (red) ERG responses obtained with a Flicker protocol at 6 Hz with increasing intensities. Responses are much higher in *Arvicanthis* compared to those of the mouse. Right panel: Representation of the amplitude of b-waves shown in left panels. Responses of mice show a first peak at -2 log cd×s/m^2 corresponding to the rod response. Only the ascending portion of cone peak response is visible at 1 log cd×s/m^2. On *Arvicanthis*, only one peak is visible.

Recordings: Dr. Niyazi Acar.

2. (No) Light-Induced RD in *Arvicanthis* (?)

After the *in vivo* examination of non-pathological *Arvicanthis* retinas, our second goal was to produce RD in *Arvicanthis* in order to obtain a reproducible model to study rod and cone pathophysiological processes.

The first approach we used was the **bright light exposure**.

All experiments using light exposures were conducted after full pupil dilation (see Materials and Methods section). Some experiments were performed with free moving animals which were housed in individual cages. Also, during exposure the litter was removed and no food or water was left on the cage grill, to avoid any shadow formation within the cage.

Except for the experiments described in the section "2.7: Use of Classical Rodents as (Positive) Controls", all exposure experiments were performed on young adult male or female (depending on availability among the colony) *Arvicanthis ansorgei*.

Control animals were kept in the same conditions as exposed animals, but while exposed animals were undergoing bright light exposure, control animals remained in light with intensity equal to that during rearing.

The same device was used for broad band white light exposures (see Materials and Methods 2.2.), except for the experiment described in 2.4. where optic fibres were used, and 2.5. where blue light was used.

In order to induce RD, several parameters were tested.

2.1. Use of Classical Parameters

2.1.1. Basic Parameters

In our first experiment, we used parameters found in the literature known to induce RD in rats and mice and used them on *Arvicanthis*.

Arvicanthis were exposed to either 5,000 lux or 12,000 lux during 30 min, 1-h or 2-h. One control animal was unexposed to light. Animals were sacrificed 60 min or 30-h after exposure.

Eyes were fixed, cut and sections were prepared for histological analysis. None of the exposed retinas showed any structural or morphological changes compared to the unexposed retinas (Figure 29). No TUNEL staining was seen on sections of exposed retinas taken 30-h after exposure. Moreover, there was no overexpression of GFAP.

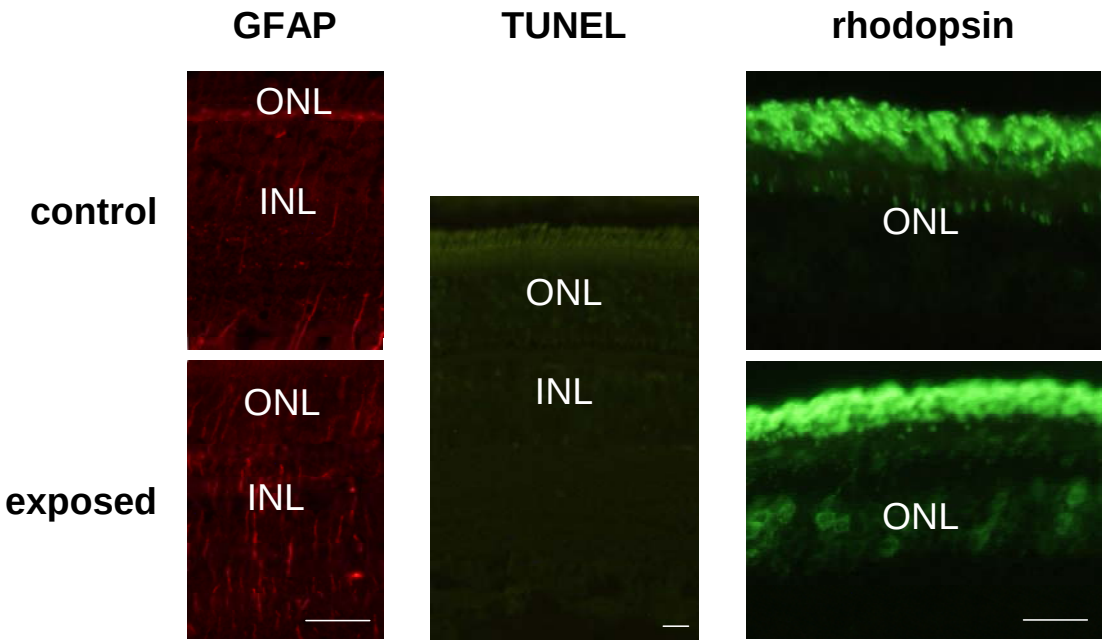

Figure 29 IHC and TUNEL staining on unexposed control and exposed (12,000 lx for 120 min) *Arvicanthis* retinas.

No difference was seen between exposed and control animals in GFAP expression. On exposed retina, no TUNEL positive cells were found. Only a delocalization of rhodopsin normally located to the OS was seen around the nucleus in the ONL in exposed retinas.

GFAP: glial fibrillary acidic protein; INL: inner retina layer; ONL: outer nuclear layer; OS: outer segment; TUNEL: TdT-mediated dUTP nick end labelling. Scale: 10 µm.

The only noticeable difference is a slight delocalization of rhodopsin present in the cell bodies of exposed retinas, compared to the retinas of unexposed animals where rhodopsin is localised to the OS. Redistribution of proteins has been seen to occur in other PR degenerations (Hagstrom et al., 1999).

2.1.2. Increased Time after Exposure

Since 30-h was maybe too late to detect apoptotic nuclei by the TUNEL method, and too early to see structural changes, we exposed animals for 8 h and sacrificed them at 12 h, 24 h, 36 h, 48 h, 60 h or one week after exposure. Intensity was also increased to 15,000 lux.

All the exposed retinas showed a normal regular structure and an absence of TUNEL staining (Figure 30).

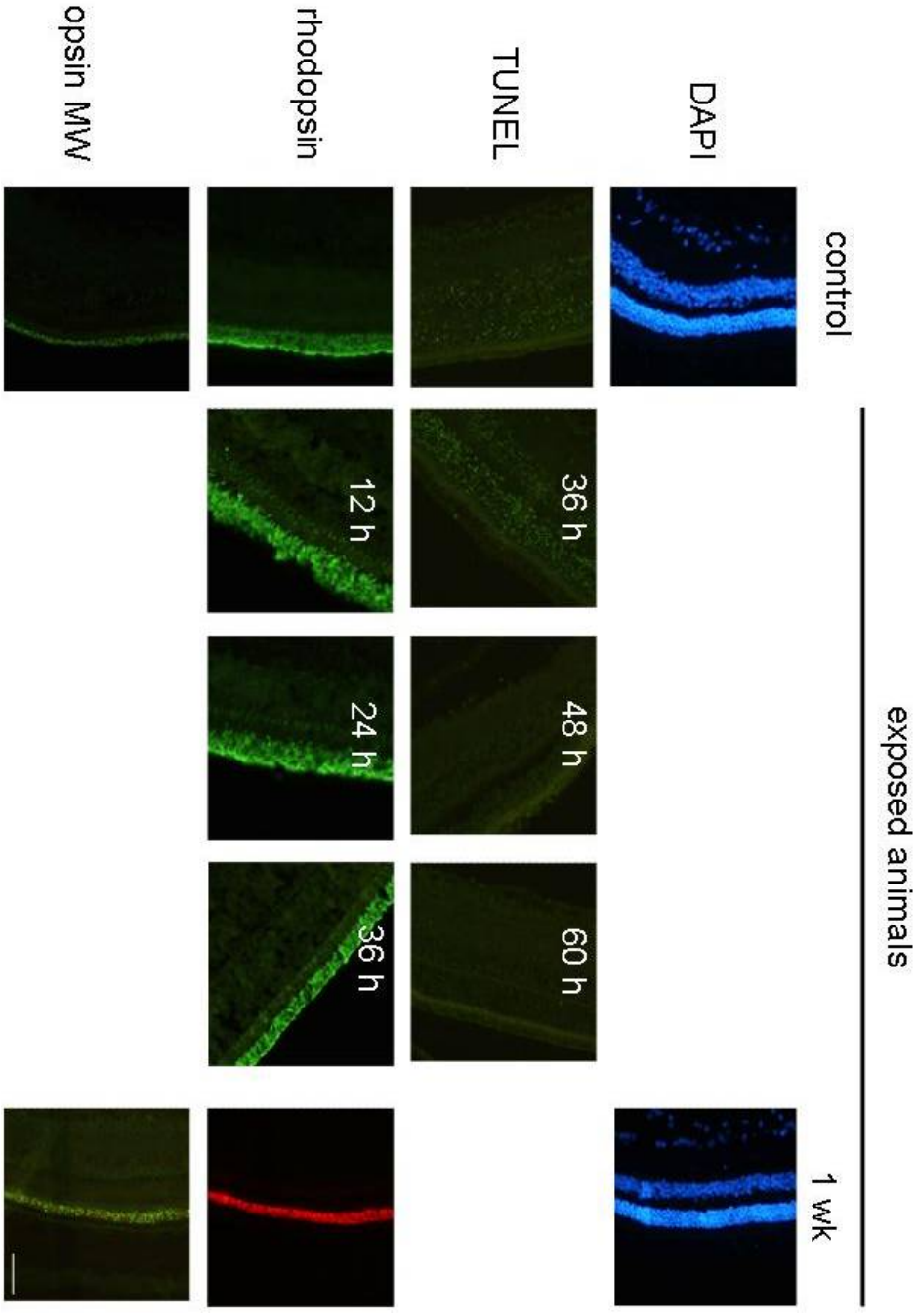

Figure 30 Structural and phenotypic aspects of *Arvicanthis* retinas taken at different times after an 8-h light exposure at 15,000 lux.

Eyes of *Arvicanthis* were taken at 36 h, 48 h, 60 h and 1 week after exposure. DAPI staining shows that 1 week after exposure, the overall retina structure remains intact. No TUNEL expression was seen at anytime after exposure. Rhodopsin and MW opsin staining did not show any decrease in the time course. (At 1 week exposure, secondary antibodies were reversed and rhodopsin staining is shown in red.)

DAPI: 4',6-diamidino-2-phenylindole dihydrochloride; MW opsin: middle-wave opsin; TUNEL: TdT-mediated dUTP nick end labelling. Scale: 30 µm.

2.1.3. Exposure under Anaesthesia

To avoid the possibility that animals were sheltering their eyes from light during previous experiments, animals were exposed under anaesthesia. It has been shown that halothane mediated anaesthesia protects the retina from light-induced damage (Keller et al., 2001), and thus animals were anaesthetised through an intraperitoneal route with Zoletil/Rompun (same dose as rats). Sedated animals were carefully positioned below the lamp under an intensity of about 6'000 lux. A drop of ophthalmic gel (Methocel®) was gently put on both corneas to prevent desiccation. The animal's head was placed on the side so that only the left eye was exposed to direct light. Right eyes were hidden from light so that each animal served as its own control. Exposure lasted 9-h.

H/E staining on sections showed that all left exposed retinas had the same structure as their contralateral unexposed retinas (not shown).

2.1.4. One Week Exposure

All the experiments mentioned so far involved exposures lasting between 30 min and 8-h. In a fourth experiment, the duration of exposure was increased to one week. Animals were exposed at 5,000 lux for one week and sacrificed 36-h after the end of exposure.

It is known that under constant light conditions (LL), the circadian system is severely disturbed (Ohta et al., 2005; Bobu and Hicks, 2009). To make sure any putative observed damage was really due to light effects and not to problems of circadian system malfunction, control animals were kept in LL at 20 lux during the same time as bright light exposed animals.

No structural change could be seen on any of the exposed retinas (not shown).

2.2. Influence of the Circadian Time

It has been shown for rats that light damage is under circadian control, since exposure during the night leads to far greater damage than the same exposure conditions during the daytime (Organisciak et al., 2000). This differential effect is maintained under DD conditions (animals exposed during subjective day or subjective night), and can be phase-shifted (Vaughan et al., 2002). Such effects are completely unexplored for a diurnal species, or for possible cone effects. It is plausible that diurnal animals, analogous to nocturnal species, would be more sensitive to retinal light-induced damage during their active phase (in this case during daytime). In our studies to date, animals were always exposed during daytime and no

degeneration was observed. However, it is more likely that the circadian mechanism modulating light damage susceptibility does not depend on the active phase of the species, but is synchronised with fluctuations in ambient light. Therefore, *Arvicanthis* would also be more sensitive when exposed during night time.

In a new series of experiments, animals were all exposed for 4-h at 1,500 lux. One group was exposed during the middle of the active phase (5-h after lights on, ZT 5), and one group was exposed during the middle of the resting period (5-h after lights off, ZT 17). Animals were killed 50-h after exposure.

None of the exposed retina showed differences compared to unexposed controls as revealed by classical histological staining, rhodopsin and MW opsin immunostaining. Moreover, no positive TUNEL staining was seen (not shown).

2.3. Influence of Light Rearing History

It is known that the light-rearing environment is a factor that greatly influences the extent of retinal light damage. It has also been known for many years that light history of an animal affects its susceptibility to light-induced apoptosis.

Early studies by Noell and Albrecht found that the retinas of albino rats raised in darkness conditions were more damaged than those from animals raised in cyclic light (Noell and Albrecht, 1971; Birch and Jacobs, 1980). Dark-reared animals also had longer ROS with a higher density of rhodopsin packing than light-reared animals. However, animals placed in DD have their circadian system in a particular state, and therefore dim LD cycle is a better choice to rear animals. Later, Penn *et al.* reported that albino rats born and raised in bright cyclic light (800 lux) were protected from light damage, whereas rats born and raised in 5 lux cyclic light were not (Penn et al., 1987). There were also significant morphological changes in the retinas of the dim light-reared animals: outer segments were shorter and much more disorganized in these animals, and cells had the appearance of impending cell death. This observation was also made with mice; retinas of albino mice are protected from light-induced apoptosis when reared in bright-cyclic light: retinas of mice raised in 400 lux cyclic light are more protected from light damage than animals born and raised in 5 lux cyclic light (Kaldi et al., 2003).

In our animal facility, light intensity at the level of the cage varies between 50 and 300 lux depending on the location of the cages on the shelf and the proximity to the lamp. Thus, the lack of degeneration seen so far with *Arvicanthis* could be due to a protection coming from a bright light rearing condition.

In a new experiment, animals were reared in LD cycles with dim light (20-50 lux) during 4 weeks before 8-h exposure at 6,000 lux. As for the previous experiments, animals remained in the dark for 12-h immediately prior to exposure.

None of the dim light-reared retina sections showed typical apoptotic staining (not showed).

2.4. Influence of Light Intensity

Another possibility to explain the lack of visible degeneration was that light intensity was not sufficient to induce damage in *Arvicanthis'* retina. Therefore, animals were exposed to higher light intensities. As our frame device could not generate more than 15,000 lux at the corneal level, we used directed illumination from optical fibre lamps (as used for dissection with binocular microscopes). Fibre guides were adjusted in a manner such that anaesthetised animals received 20,000 lux at the level of the left cornea.

Animals were reared for 10 days in dim light (20 lux), then anaesthetised and exposed for 2-h during their active phase (daytime) at 20,000 lux.

No structural damage was seen in any of the bright light exposed retinas (not shown).

2.5. Influence of Wavelength: Blue light Exposure

It is known that the spectral quality of light radiation is an important parameter of retinal damage: broad white or narrow spectrum green light (~ 550 nm) normally leads mainly to acute PR damage; short wavelength blue light (~ 400 nm) leads to damage of the RPE and PR. There are some data that suggest blue light may be particularly injurious to cones (Sperling, 1986; Reme, 2005). The potential differential effects of wavelength upon rod and cone damage in a diurnal animal are however unknown.

We tested *Arvicanthis* for retinal blue light damage. Sample conditions were chosen based on consultation with the laboratory of Prof. Grimm (City University Hospital, Zurich, Switzerland). From their experience, 1 min exposure is sufficient to induce threshold damage with blue light of 410 nm at 30 mW/cm^2 at the corneal level on pigmented and albino mice. Being aware of the potential light damage resistance of *Arvicanthis*, we chose to expose animals during 5, 15 or 45 min.

The global structures of the exposed retinas are shown in Figure 31. Only the retina exposed for 45 min showed a degeneration of a localized spot ~ 1-2 mm^2 in the central retina. Within this area, there was complete degeneration of all three cell layers, as seen by H/E and DAPI staining.

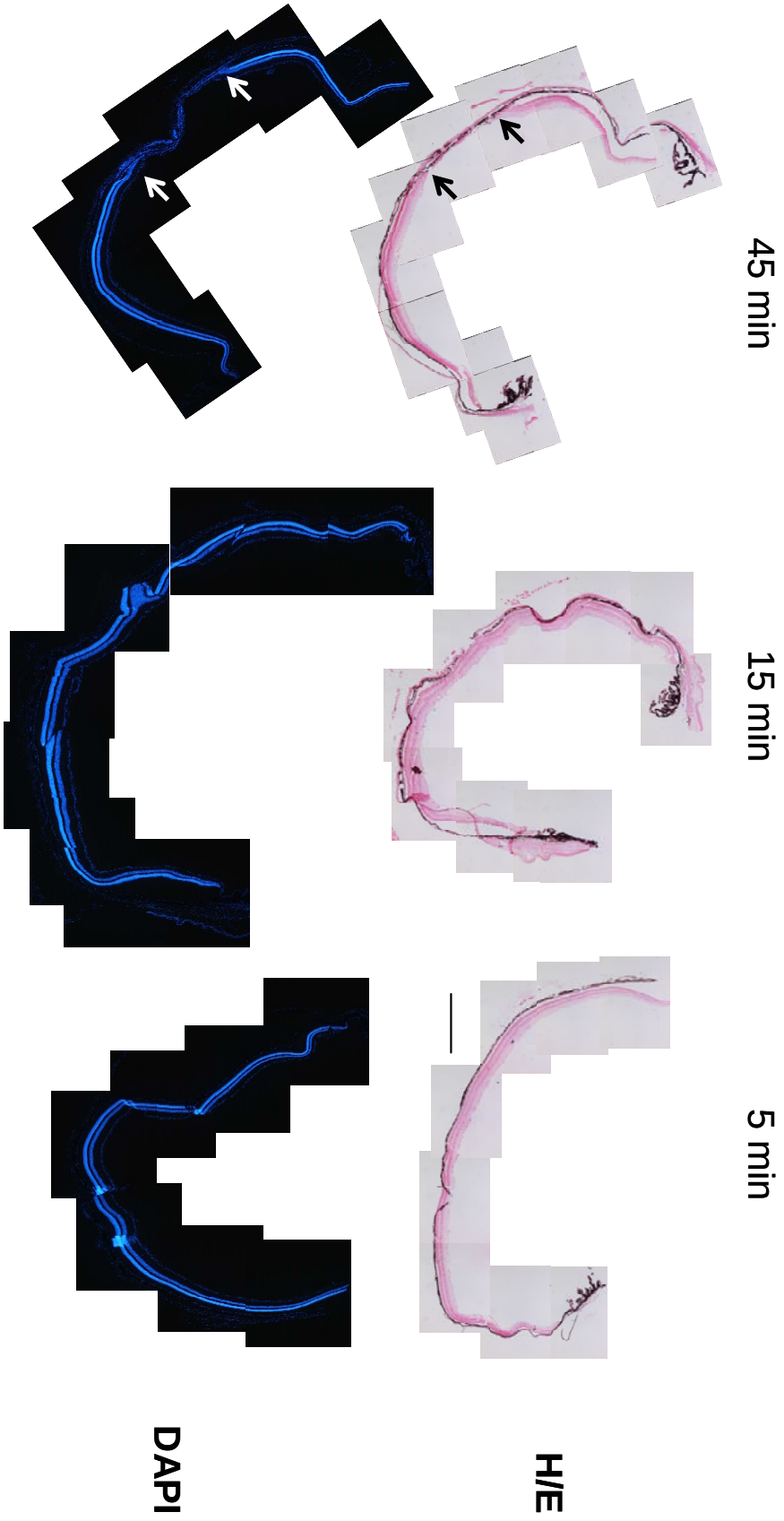

Figure 31 Overall structural aspects of sections of *Arvicanthis* retinas after blue light exposure.

Animals were exposed during 5, 15 or 45 min with narrow spectrum blue light (403 ± 10 nm). Sections were stained with H/E or DAPI. Only the retina exposed for 45 min showed a complete RD at a very precise spot (arrows).

DAPI: 4',6-diamidino-2-phenylindole dihydrochloride; HE: haematoxylin/eosin. Scale: 1,000 µm.

Expression of rhodopsin, c-arr and GFAP was also investigated in these retinas. In the retina exposed for 45 min, at the level of the injury there was disappearance of PR markers, along with a generalised upregulation of GFAP expression across the retina (Figure 32). Retinas exposed for 5 to 15 minutes did not show any differences compared with controls.

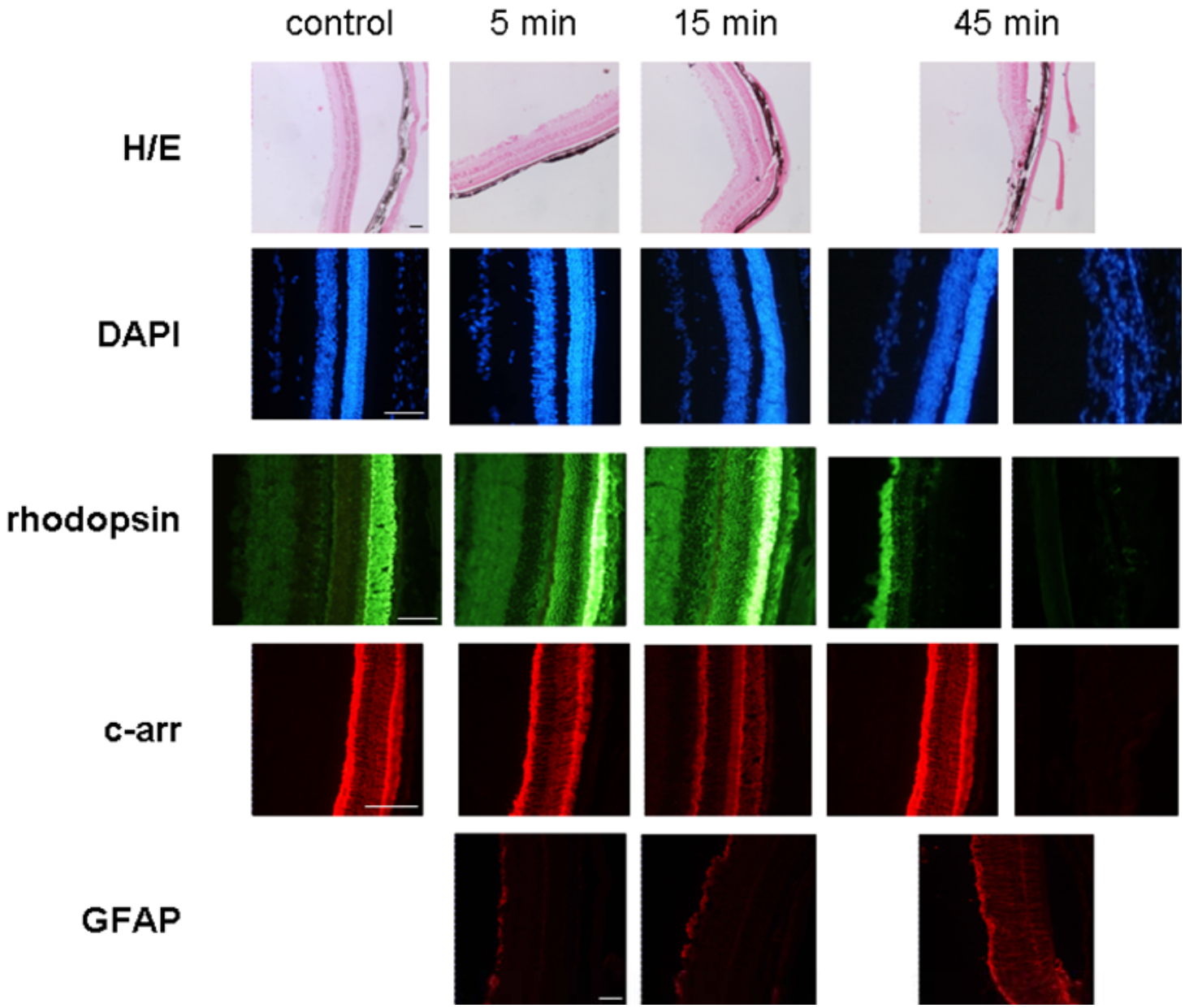

Figure 32 Structural and phenotypic aspects of *Arvicanthis* retina after blue light exposure.

Retinal structure of *Arvicanthis* exposed for 5 or 15 min with narrow band blue light (403 ± 10 nm) did not differ from control retina as seen with H/E and DAPI staining; expression of rod (rhodopsin) and cone (cone opsin) specific proteins was not different from control, neither did expression of GFAP. After 45 min exposure, the retina of *Arvicanthis* appeared much damaged at a small central spot, in which the entire retina is missing as seen with H/E staining and right panels of DAPI, rhodopsin and c-arr. Also, GFAP expression is upregulated throughout the cytoplasm of Müller glia.

c-arr: cone arrestin; DAPI: 4',6-diamidino-2-phenylindole dihydrochloride; GFAP: glial fibrillary acidic protein; H/E: haematoxylin/eosin Scale: 40 µm.

2.6. ERG Recordings

Except in the experiment with 45 minutes exposure to intense blue light, histological evaluation of light-exposed retinas of *Arvicanthis* did not show any detectable damage. We hypothesized that damaging treatments maybe were not visible by structural analysis, but could still have a functional impact. Therefore, exposed animals were tested for retinal electrophysiological responses. Animals were reared in dim light (20 lux) before an 8-h exposure at 6,000 lux during active phase.

ERGs were performed in Dijon with Dr. Niyazi Acar. Seven exposed animals and 6 controls were analyzed for their retinal electrophysiological responses. Two protocols were used. For one group of animals, composed of 3 control and 4 exposed animals, regular scotopic and Flicker protocols were used. A second group composed of 3 exposed and 3 control animals were submitted to the 6 Hz protocol.

The scotopic responses did not show any difference between exposed and control animals, either for latency time or for amplitudes (Figure 33). For photopic responses, there was no difference between groups. However, for low intensities, exposed animals showed an increased latency time of the b-wave. This may indicate early effects of degeneration that affected only a particular population or a different response mechanism (i.e. the one for low intensities), as the latency time was similar between test and control groups at high light intensities.

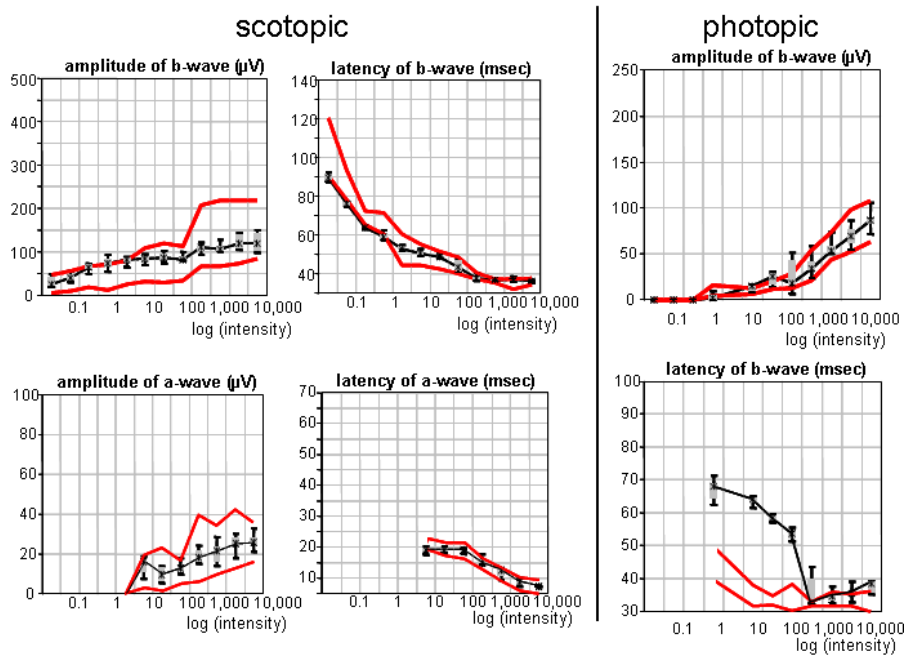

Figure 33 ERG responses of control and light-exposed *Arvicanthis* with scotopic and photopic single flash protocol.

Data of exposed animals (n = 4) are represented with box-plots. The upper line corresponds to the results of 95 % exposed, the bottom line to 5 % exposed animals and the grey box to 50 % exposed animals. × represents the median. Red lines indicate data of control animals (n = 3), the upper line corresponding to 95 % and the bottom line to 5 % control animals.

Recordings: Dr. Niyazi Acar.

The second group was submitted to a 6 Hz protocol. Except at high intensities for which the b-wave amplitude is smaller in exposed animals, there were no major differences between control and exposed animals on this protocol (Figure 34).

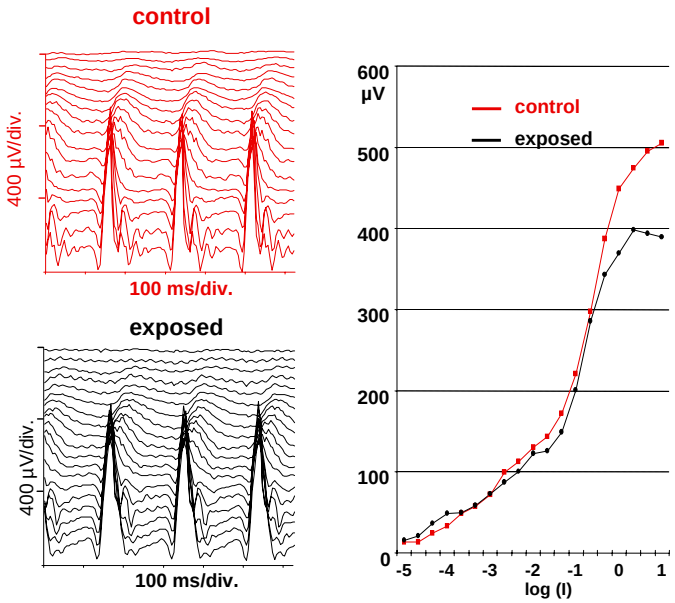

Figure 34 ERG responses of control and light-exposed *Arvicanthis* with 6 Hz protocol.

Responses of control and exposed animals did not differ greatly. Only amplitudes of b-waves were slightly reduced at higher intensities (right panel) for the exposed animals.

Recordings: Dr. Niyazi Acar.

2.7. Use of Classical Rodents as (Positive) Controls

Our protocol, light device and evaluation of retinal integrity method were verified through the use of mice and rats, classic models of light-induced RD.

2.7.1. Exposure of Mice

In a first experiment we tested our TUNEL kit on sections of control and exposed BALBc mice (provided by Dr. Andrea Wenzel, Zürich). Mice had been exposed for 1-h at 5,000 lux during their sleeping phase with broad band white light, and killed after 72-h. No positive TUNEL reaction was seen on control sections, while in light-exposed animals the majority of PR nuclei show intense TUNEL staining, reflecting a high number of apoptotic cells (Figure 35).

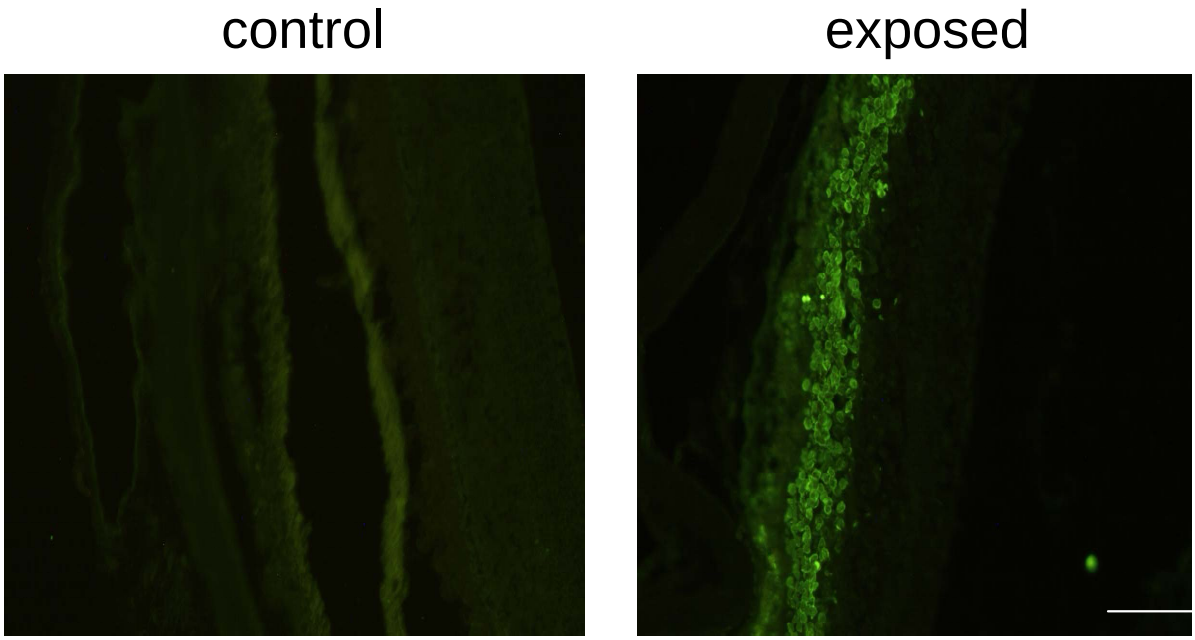

Figure 35 ***in situ*** **cell detection by TUNEL method in control and BALB/c exposed mice exposed in Zürich.**

No TUNEL positive cells are seen on control retina sections. Almost all the PRs of the exposed retinal section are stained.

TUNEL: TdT-mediated dUTP nick end labelling. Scale: 50 µm.
Sections: Dr. Andrea Wenzel.

To check if our exposure device was effective, we exposed the same strain of BALBc mice using our own broad band exposure apparatus. Animals were exposed at 5,000 lux for 1-h and recovered for 36-h before sacrifice. Intense TUNEL positive staining was seen on exposed sections (Figure 36).

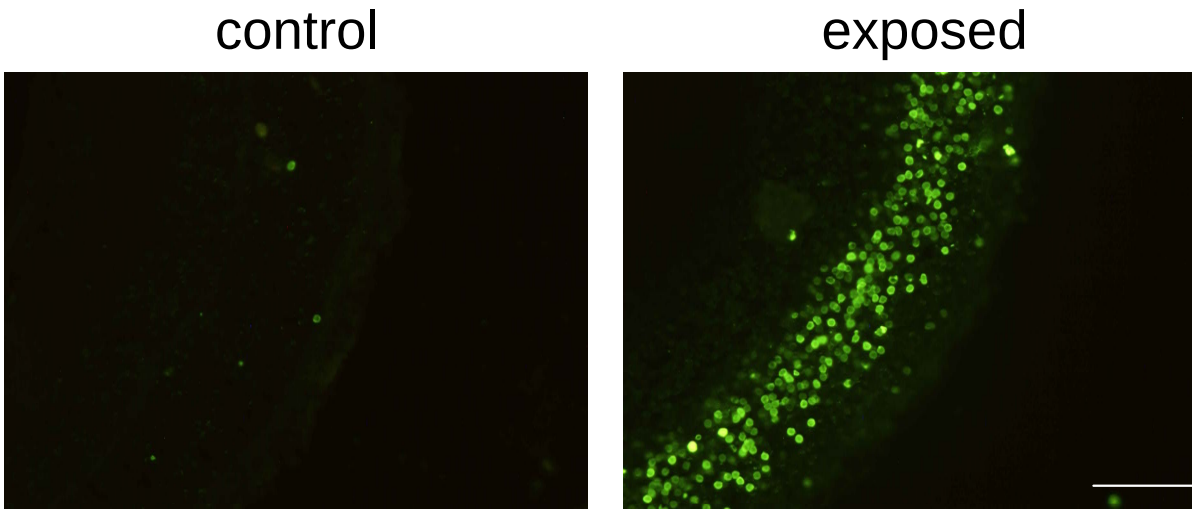

Figure 36 ***in situ*** **cell detection by TUNEL method in control and exposed BALB mice.**

Retinal sections of exposed BALB/c mice from Harlan Laboratories showed several apoptotic nuclei at the ONL level as revealed by TUNEL method.

ONL: outer nuclear layer; TUNEL: TdT-mediated dUTP nick end labelling. Scale: 30 µm.

2.7.2. Exposure of Rats

Wistar rats were exposed to 12,000 lux white light for 3-h during their sleeping phase (daytime). They recovered for 24-h before sacrifice. DAPI staining of sections of exposed retinas revealed a normal ONL structure and thickness. Rhodopsin staining showed that OS length was slightly reduced upon exposure (Figure 37). MW opsin staining showed normal OS length. However, exposed animals had rhodopsin staining around the PR nucleus whereas control animals had rhodopsin localized exclusively in the OS. No overexpression of GFAP was seen in exposed animals.

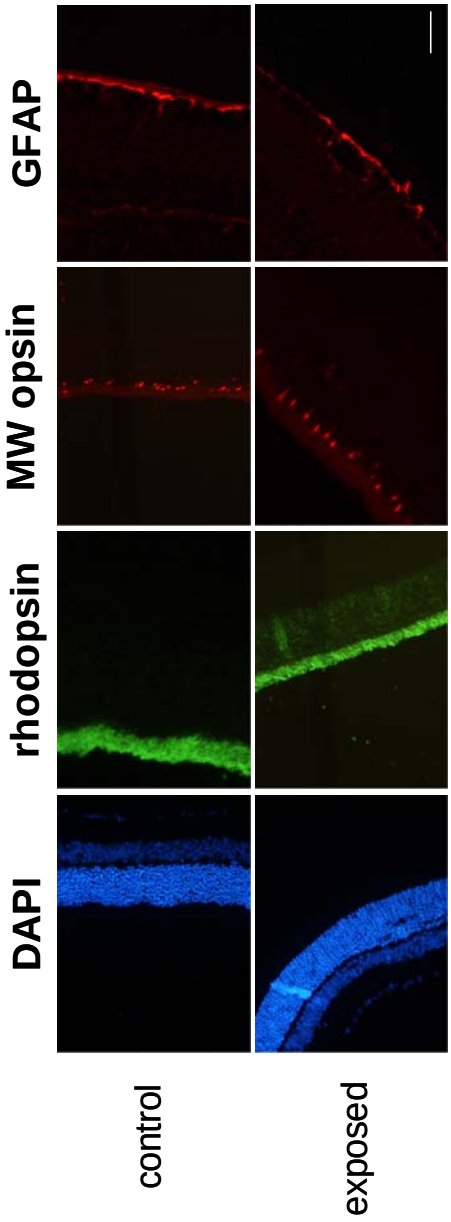

Figure 37 Retinal structure and rod/cone-specific protein expression in control and bright light exposed rat retinas.

DAPI staining showed a regular layer structure of the rat retina even after a 12,000 lux exposure. Rhodopsin staining showed a decrease of OS length in exposed rats. GFAP was not over-expressed upon exposure.

DAPI: 4',6-diamidino-2-phenylindole dihydrochloride; GFAP: glial fibrillary acidic protein; OS: outer segment. Scale: 30 µm.

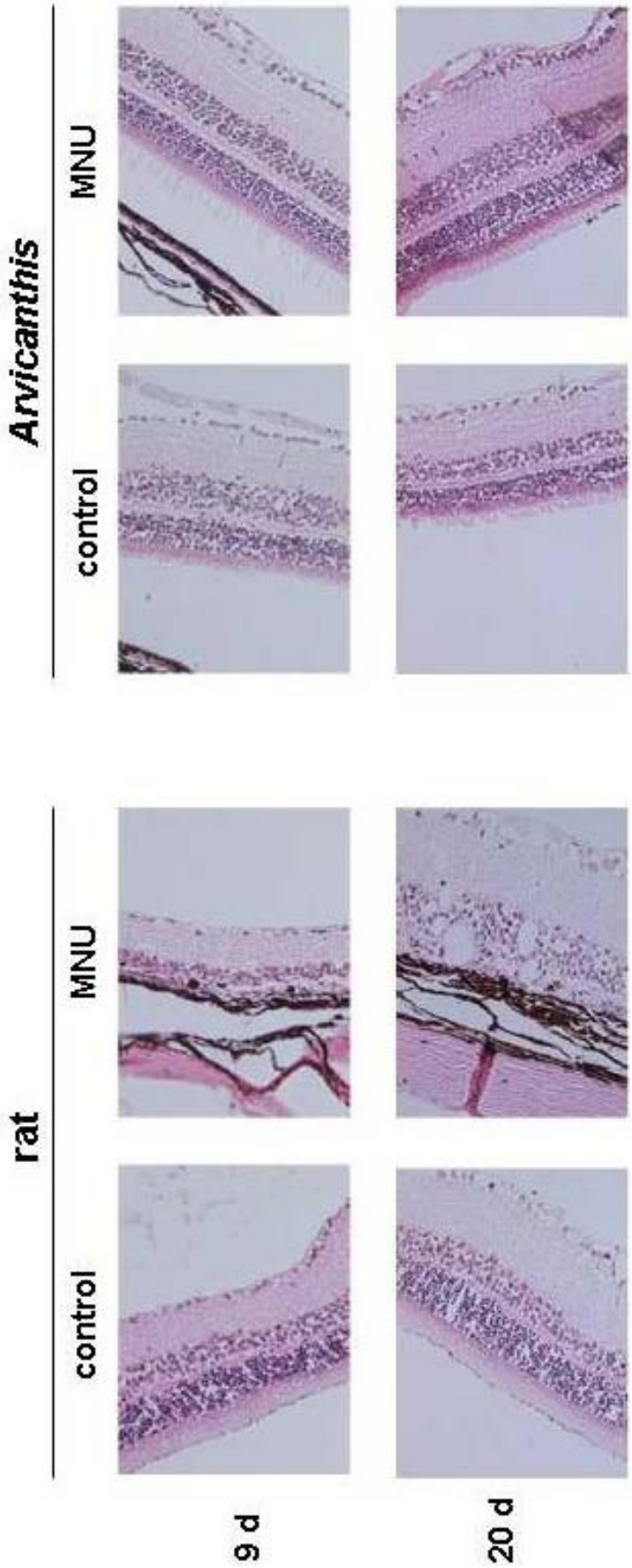

Figure 38 General structure of rat and *Arvicanthis* retinas at 9 and 20 d.p.i. of MNU at 75 mg/kg.

Sections of Long-Evans rat and *Arvicanthis* retinas were stained with H/E after a MNU injection at 75 mg/kg. At 9 d.p.i., MNU-treated rat retinas appeared drastically degenerated. ONL thickness was much reduced and RPE was attached to the remaining INL. At 20 d.p.i., ONL was quasi-absent. In contrast, MNU-treated *Arvicanthis* retina appears unchanged at 9 and 20 d.p.i.

HE: haematoxylin/eosin; MNU: *N*-methyl-*N*-nitrosourea; ONL: outer nuclear layer. Scale: 30 µm.

3. MNU-INDUCED PR DEGENERATION IN *ARVICANTHIS*

The findings on light-induced stress indicate that *Arvicanthis* is remarkably resistant to this kind of trauma. In order to test whether this species is resistant to other types of retinal stress and to achieve our initial goal of developing a model of cone degeneration, we used another approach to induce degeneration of cones and rods: MNU i.p. injection.

3.1. Regular MNU doses: is Retina of *Arvicanthis* an Ironclad Structure???

Arvicanthis were injected with a 75 mg/kg dose of MNU. Wistar and Long Evans rats were also injected with the same dose, to serve as positive controls. Animals were sacrificed 9 and 20 days post injection (d.p.i.).

Sections of rat and *Arvicanthis* retinas were stained with H/E. At 9 d.p.i., MNU-treated rat retinas appeared greatly affected and the ONL was virtually absent (Figure 38). The same features were observed at 20 d.p.i. In contrast, MNU-treated *Arvicanthis* retinas did not show any difference with controls at 9 d.p.i. or 20 d.p.i.

3.2. Stronger MNU Doses: Achille's Heel of the *Arvicanthis* Retina!

In a second set of experiments *Arvicanthis* were injected with 33 or 100 % higher doses of MNU (i.e. 100 and 150 mg/kg respectively) and the effects were analyzed at the structural and functional levels.

First Article

(under submission)

Structural and Functional Characterization of Rod and Cone Breakdown in Chemically-Induced Retinal Degeneration

Domitille L. Boudard[1], Naoyuki Tanimoto[2], Gesine Huber[2], Susanne C. Beck[2], Mathias W. Seeliger[2], David Hicks[1*]

[1.] Department of Neurobiology of Rhythms, Institute of Cellular and Integrative Neurosciences, Centre National de la Recherche Scientifique, University of Strasbourg, Strasbourg, France.

[2.] Ocular Neurodegeneration Research Group, Centre for Ophthalmology, Institute for Ophthalmic Research, University of Tuebingen, Schleichstrasse 4/3, D-72076 Tuebingen, Germany.

[*] Corresponding author: photoreceptor67@hotmail.com

Abstract

Background: Cone photoreceptor breakdown underlies vision loss in many blinding diseases. Cone loss is often secondary to that of rods, but little experimental data are available on the relationship between the two populations. We used a cone-rich rodent to explore changes in rod and cone survival and function during induced retinal degeneration.

Methodology/Principal Findings: Adult *Arvicanthis ansorgei* – a cone-rich rodent species – were injected with N-methyl-N-nitrosourea (MNU), and changes in retinal histology, phenotype, apoptosis (TUNEL staining) and functionality (scotopic and photopic electroretinography) were monitored as a function of post-treatment time and retinal topography. Control animals were injected with solvent solution. Injected animals showed time-, region- and population-specific changes as measured by morphological, immunochemical and functional criteria. Histological and phenotypical modifications were first observed in superior central retina, in rods before cones, and gradually spread peripherally into the inferior hemisphere. Rods showed clear signs of apoptosis whereas cones were unaffected in many samples. Electroretinographic measures performed at late post-injection times showed that both rod and cone functions were severely compromised by 3 months post-treatment.

Conclusions/Significance: MNU-induced retinal degeneration in *Arvicanthis* follows a predictable spatial and temporal pattern allowing clear separation of rod- and cone-specific pathogenic mechanisms.

Introduction

Age-related Macular Degeneration (AMD) and Retinitis Pigmentosa (RP), two retinal pathologies responsible for a major part of blindness in Western countries (World Health Organization 2008 data), are both characterized at a structural level by retinal degeneration (RD). The deficit that is most debilitating in RD is the loss of central vision (high acuity discrimination) in daylight, mediated by foveal cone photoreceptors (PRs). It has become apparent that death of cone PRs occurs secondarily to that of rods in several forms of RD, both in animal models (e.g. *rd1*, rho$^{-/-}$) and humans [1], and that malfunction and degeneration of cones actually form the major reason for visual handicap even in diseases not directly concerning them. For example, although mutations in rod-specific genes underlie the majority of forms of RP, most severe vision loss occurs from secondary cone death [2]. Similarly, debilitating blindness in AMD is due to cone death within the central cone-rich macula. Elucidating the mechanisms involved in the dysfunction of cones is thus of paramount importance. Little is known concerning cone PRs pathophysiology in part because suitable experimental animal models have not been available. The principal laboratory models, rats and mice, are rod-dominated animals (~ 97 % rods of the total PRs) [3,4,5]. A few "pure" cone-rich species have been characterized [6] but these species exhibit various drawbacks for experimentation, such as lack of pre-existing antibodies or databank sequence information, or captive rearing. Cone-rich transgenic mouse models, e.g. Nrl knock-out mice, have become available [7], but cones in such strains may not be fully normal (although recent data show that they display typical cone features by a wide range of structural and functional criteria [8]). Moreover, in all-cone species, due to the absence of rods, the surrounding tissue environment of cones must be different from the human macula. In order to determine true relative rates of degeneration, one must obtain comparable information for both rods and cones at matched locations in the same well-characterized species.

In addition to genetic models of RD [9], several approaches involving "environmental" insults exist. RD can be induced by light [10], modified diet [11], increased intraocular pressure [12] or toxic chemicals [13,14,15,16,17,18,19]. In all these models, data on cones are very limited or lacking. The scarce references pertaining to cone phototoxicity are contradictory, indicating either decreased [20] or increased [21] toxicity compared to rods. Among retinotoxic agents, the alkylating derivative N-methyl-N-nitrosourea (MNU), appears suitable for inducing RD because: 1. A single intraperitoneal injection induces a PR-specific degeneration; 2. Dosage and post-injection time can be varied to obtain differential effects on visual structure and function; 3. Onset and progression of the degeneration are

usually very rapid [22,23,24]; 4. MNU injections induce comparable effects in a wide variety of many mammalian species [25].

Our team recently described the retina of *Arvicanthis ansorgei*, a murid rodent from West Africa whose retina presents two important characteristics: a high cone content (33 % of the total PRs or tenfold higher than classic laboratory rodents), and their organization into a strict double cell row layer at the scleral surface of the outer nuclear layer (ONL) [26], resembling somewhat the human peripheral macula [27]. Here, we characterized the morphological, structural and functional effects of an acute injection of MNU on the retina of *Arvicanthis ansorgei*. We observed a clear separation of rod and cone responses to chemical poisoning, in terms of structure, phenotype and function.

Results

Growth and Food Intake

Because MNU is known to induce tumours [28] and was injected via an intra-peritoneal route, overall physiology was observed. Control and treated *Arvicanthis* appeared in good health, with equivalent levels of locomotor activity (wheel-running activity, data not shown) and no animals were moribund. We monitored MNU-injected animals for potential feeding difficulties and growth (Figure 1A and B). After the injection, control animals did not show any difference in their daily food intake (Figure 1A; **dark symbols**). In the treated group, one animal showed no change in daily food intake and two animals showed a reduction of a few grams of their daily food intake, that returned to normal around 10 days post-injection (d.p.i.). In the MNU group, a slight body weight (b.w.) loss: less than 7 % occurred compared with injection day and reaching a maximal decrease at 9 d.p.i., but thereafter the animals in this group gained body weight similar to those injected with solvent (Figure 1B).

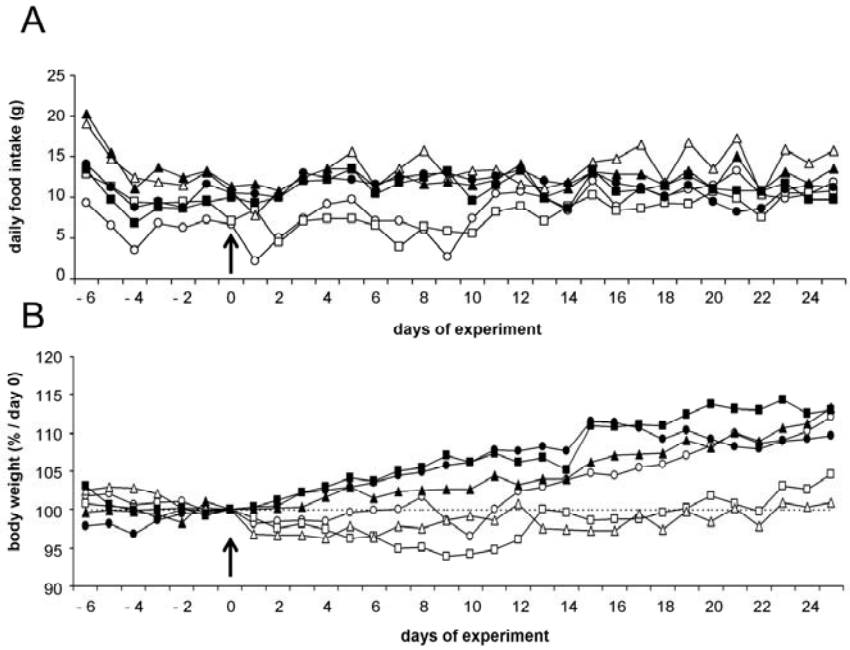

Figure 1 **Growth and food intake of control and MNU-treated animals over a 25 days period.**

Daily food intake (**A**) has been measured 6-7 days before and 25 days after **solvent** (**dark symbols**) or MNU at 150 mg/kg (open symbols) injections for three animals for each group. Body weights have been computed over the same period (**B**) and are presented as a percentage of body weight at the day of injection (day 0; arrow).

MNU: *N*-methyl-*N*-nitrosourea.

Morphology of *Arvicanthis* MNU-degenerated retina

In order to measure the temporal progression of induced degeneration, we performed morphometry on retinal histology at 3, 5, 8, 11, 15 and 20 d.p.i. after a 150 mg/kg MNU injection, and 3 months after a 100 mg/kg MNU injection. None of the control animals killed at the end of the experiment exhibited any structural changes of the retina.

The first change observed at 3 d.p.i. of MNU was a slight decrease in OS length (Figure 2A). This shortening progressed with time, followed by a gradual continuous decrease in the PR layer thickness. It is important to note that the other layers: inner nuclear layer (INL) and ganglion cell layer (GCL), remained unaffected.

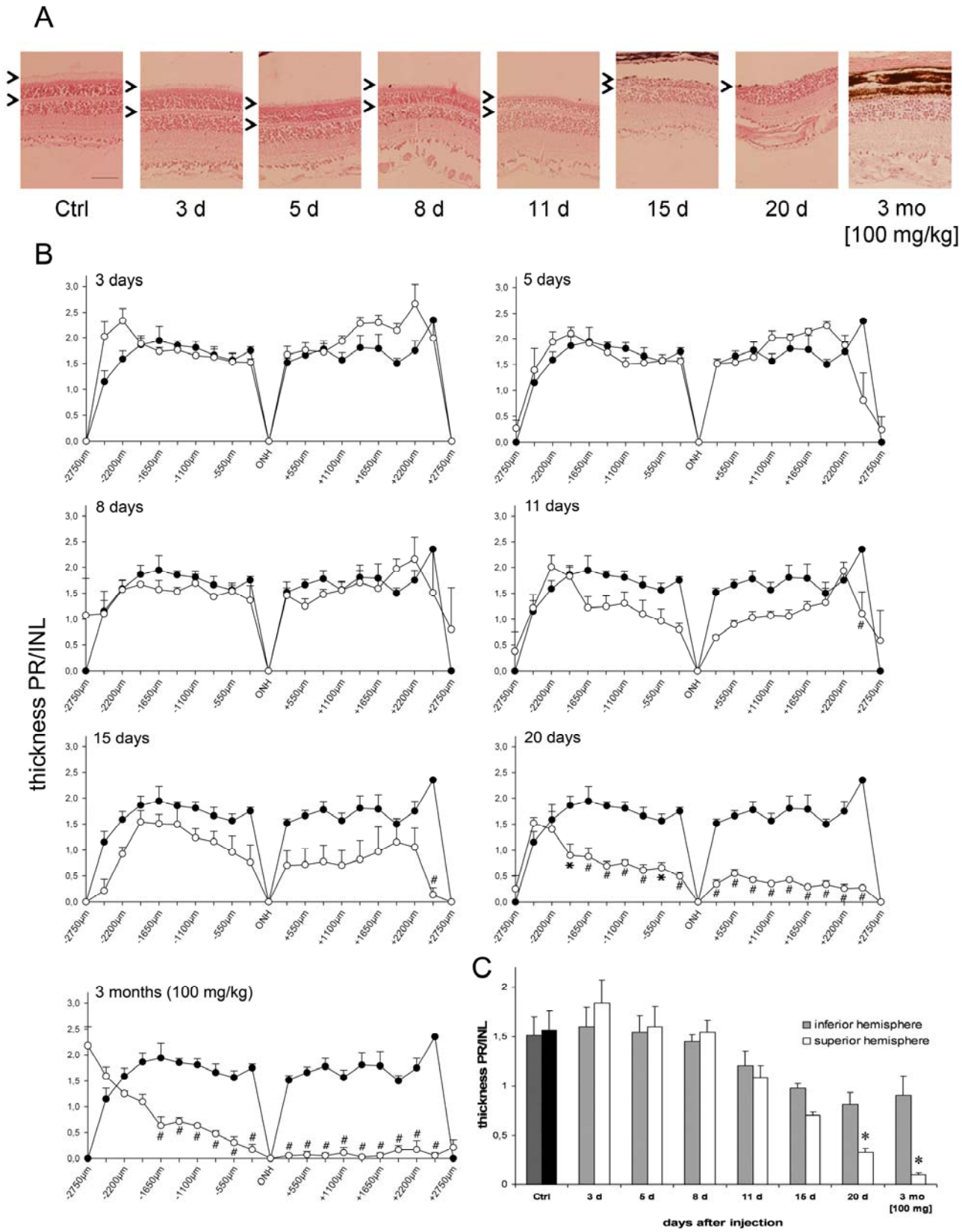

Figure 2 **Morphometric analysis of retinas of control and MNU-treated *Arvicanthis*.**

Control and MNU-treated retinas 3, 5, 8, 11, 15 and 20 d.p.i. at 150 mg/kg, and 3 months after a 100 mg/kg injection. **A**. Representative photomicrographs of haematoxylin/eosin-stained paraffin sections. The area comprised between the two arrowheads corresponds to the PR layer. Scale bar: 50 µm. **B**. Spider-graph representations of the measurements of PR thickness (after normalisation to INL width) along the vertical meridian. Means ± SEM for control (open symbol; n = 3) and **MNU** (**close symbol**; n = 3) animals are shown. Symbols represent statistical difference for the same point between control and MNU group: * $P < 0.05$; # $P < 0.01$. **C**. Graphic representation of the averaged measurements over superior and inferior hemispheres at different d.p.i. (* $P < 0.05$).

INL: inner nuclear layer; MNU: *N*-methyl-*N*-nitrosourea; PR, photoreceptor.

To assess whether the degeneration was generalised or localised to a particular region of the retina, topographic analysis of the degeneration was performed (Figure 2B). There was no significant difference between control and MNU-treated animals in PR cell loss, as reflected by PR layer thickness measurements, until 11 d.p.i. of MNU. ONL reduction started at 11 d.p.i., thereafter decreasing constantly to reach very advanced cell loss by 20 d.p.i. However, PR layer thickness reduction was not uniform along the vertical meridian, with greater loss seen in the superior compared to inferior quadrants: at 11 d.p.i., the PR layer of MNU-treated animals was significantly different to that of control animals in both central inferior and central superior regions ($P = 0.017$ and $P = 0.005$ respectively). At 15 d.p.i., the difference between the thickness of PR layer of MNU-treated and control retina was significant in the far superior region ($P = 0.026$). At 20 d.p.i., all regions were statistically different between MNU and control retinas ($P < 0.001$), except the far inferior region ($P = 0.121$). Interestingly, within the 20 d.p.i.-MNU group, PR layer thickness of median and far regions over the superior hemisphere differed significantly from the corresponding regions in the inferior hemisphere ($P = 0.017$ and $P < 0.001$ respectively). At 3 months post-injection, the results were similar to those at 20 days: all regions of MNU-treated and control retinas differ significantly ($P < 0.001$) except the far inferior region ($P = 0.878$); and within the MNU group, median and far regions differ significantly with respect to their belonging to superior or inferior hemisphere ($P = 0.006$ and $P < 0.001$ respectively). It is important to note that none of the regions was statistically different between retinas of the group MNU 20 days injected at 150 mg/kg and MNU 3 months injected at 100 mg/kg ($P = 1$). The difference between superior and inferior hemispheres for the combined far, median and central regions is represented graphically in Figure 2C. The difference is statistically significant for 20 days and 3 months post-injection ($P = 0.001$ and $P < 0.001$ respectively).

Progressive loss of rod- and cone-specific proteins

Analysis on retinal sections

To determine whether rods or cones were selectively affected by the degeneration, we performed immunohistochemistry with rod specific (rhodopsin, rod transducin) and cone specific- (MW opsin and cone arrestin) protein antibodies on adjacent sections of a control retina and a retina 3 months after a 100 mg/kg MNU injection (Figure 3). Eight regions of interest located at different points of the MNU-treated retinal section were selected, based on the distance from the optic nerve head and differential expression of rod and cone proteins. Control retina showed a normal morphology, with DAPI-stained nuclei aligned into the three regular layers, and rhodopsin labelling located mainly in the OS, and rod transducin staining in the cell bodies, of the rods. MW cone opsin was abundant and restricted to the OS of cones. Cone arrestin was located throughout the cone cell bodies, from the OS to the synapse. Region A (inferior far periphery) showed no difference in aforementioned protein staining to control retinas. In region B (inferior medial/far periphery), a reduction of ONL thickness was seen with DAPI staining, rhodopsin and rod transducin staining were reduced and patchy, while MW cone opsin and cone arrestin staining did not show differences to either region A or control retina. At region C (inferior medial periphery), only faint scattered rod immunostaining remained, and the ONL was only two cell rows thick. At region D (inferior centre), only one row of cells remained in the ONL, rod staining was no longer present and immunostaining of cones began to decrease as well. In region E, close to the optic nerve head (ONH) in the inferior hemisphere, rod immunostaining was absent and cone staining was almost gone. Region F, located close to the ONH in the superior hemisphere, also seemed void of both rod and cone PRs. Regions G and H (superior mid- and far periphery respectively) were characterized by an almost complete lack of rod staining and sparse cone staining.

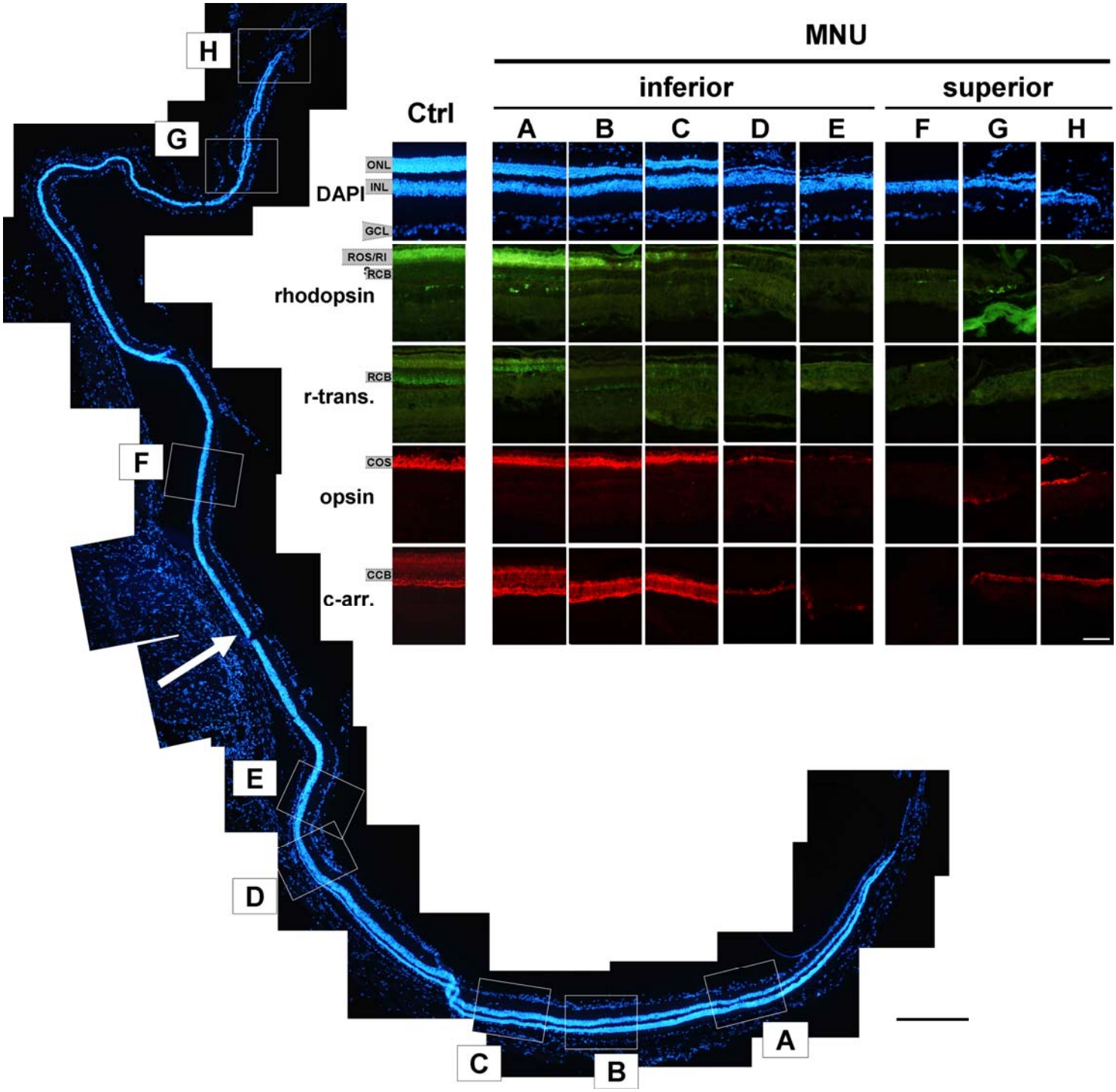

Figure 3 **Immunohistochemistry labelling showing progressive loss of rod- and cone-specific proteins.**

Fluorescence microscopy of an entire retinal section of 3 months 100 mg/kg MNU-treated *Arvicanthis* stained with DAPI (scale: 250 µm) showing the gradient of the degeneration along the vertical meridian from superior (top) to inferior (bottom) hemisphere. The entire section has been reconstructed with adjacent images taken at × 20 magnification. Focus on eight different regions (**A-H**) of this section is shown (scale: 50 µm). **A-E** regions are located at the inferior hemisphere and **F-H** regions are located at the superior hemisphere. Optic nerve head is shown with a white arrow. Same regions of adjacent sections labelled with rhodopsin, MW opsin, rod transducin (r-trans.) and cone arrestin (c-arr.) are shown in small panels. Control (Ctrl) retina labelled with the same antibodies is given as a reference.

DAPI: 4',6-diamidino-2-phenylindole; INL: inner nuclear layer; MNU: *N*-methyl-*N*-nitrosourea; MW: middle-wave; ONH: optic nerve head; ONL: outer nuclear layer; R/C-CB: rod/cone cell bodies; R/C-IS: rod/cone inner segments; R/C-OS: rod/cone outer segments.

Western-Blot analysis

We quantified the relative amounts of rhodopsin and cone arrestin in retinas of control and MNU-treated animals. A representative immunoblot after 20 d.p.i. is given in Figure 4, and shows the expression of both proteins was highly reduced in MNU-treated animals compared to controls. In order to measure the comparative degeneration of rods and cones, we calculated the ratio of immunoreactive rhodopsin and cone arrestin in control and MNU-treated animals. This ratio was significantly smaller in MNU-treated animals, indicating the greater loss of rods compared to cones during this period ($P = 0.001$).

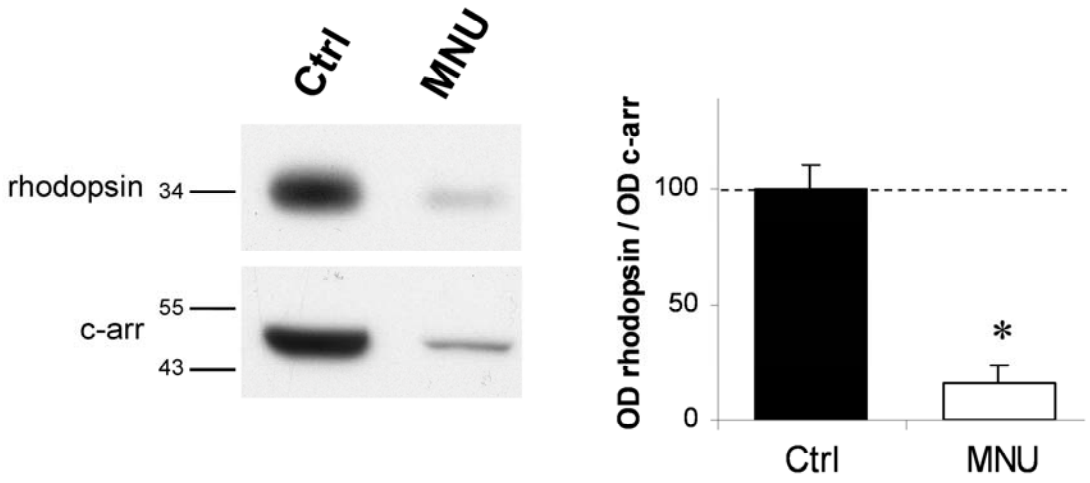

Figure 4 **Rod *vs.* cone proteins expression in control and 20 d.p.i. of MNU 150 mg/kg *Arvicanthis* retinas.**

Western-blot analysis on retinas shows that rhodopsin and c-arr reactivity bands are greatly reduced in MNU-treated retinas. The graphic representation shows that the rhodopsin to cone arrestin optic density ratio is reduced after MNU treatment (n = 6; t_4 = 8.08; P = 0.001).

c-arr: cone arrestin; MNU: *N*-methyl-*N*-nitrosourea; MW: middle-wave.

Characterization of the degeneration

Detection of apoptosis was performed *in situ* with the TUNEL method. Control retina did not show any positive TUNEL staining, as neither did sections from 5 d.p.i. retina. By 11 d.p.i. apoptotic figures were evident across the retina, with an asymmetrical distribution as seen above. In the inferior hemisphere, TUNEL-positive nuclei were localized within the innermost rows of the ONL, corresponding to the position of rod cell bodies. In contrast, in the superior hemisphere, TUNEL staining was seen throughout the entire depth of the ONL. This pattern was also seen at 15 and 20 d.p.i., with increasing numbers of TUNEL-positive nuclei appearing. Semi-quantitative analysis of the numbers and distribution of TUNEL-positive cells showed a spreading wave, moving from rods only within the inferior hemisphere to both rods and cones in the superior hemisphere (Table 1). In no cases were TUNEL-positive nuclei seen in either the INL or GCL. However, generalised retinal stress was induced by MNU treatment, as testified by a widespread up-regulation in GFAP levels in treated retinas compared to controls (Figure 5).

rod/cone	5 d	11 d	15 d	20 d	3 mo
Far Sup	-/-	-/-	++/++	++/++	-/-
Med Sup	-/-	+++/+	+++/++	+++/+++	-/-
Centr Sup	-/-	+++/++	+++/++	+++/+++	-/-
Centr Inf	-/-	++/-	++/-	+++/++	-/-
Med Inf	-/-	+/-	+/-	+++/-	-/-
Far Inf	-/-	-/-	-/-	-/-	-/-

Table 1 **TUNEL positive cells (rod/cone) across complete sections of 150 mg/kg MNU-treated retinas at 11, 15 and 20 d.p.i. and 100 mg/kg 3 months after injection.**

Rods and cones are discriminated according to their position across the ONL. - corresponds to no positive cells and +++ corresponds to a situation where virtually all the PRs of one type are stained. Cells have been counted on n = 6 (11 d), n = 10 (15 d) and n = 7 (20 d) sections.

ONL: outer nuclear layer; MNU: *N*-methyl-*N*-nitrosourea; PRs: photoreceptors

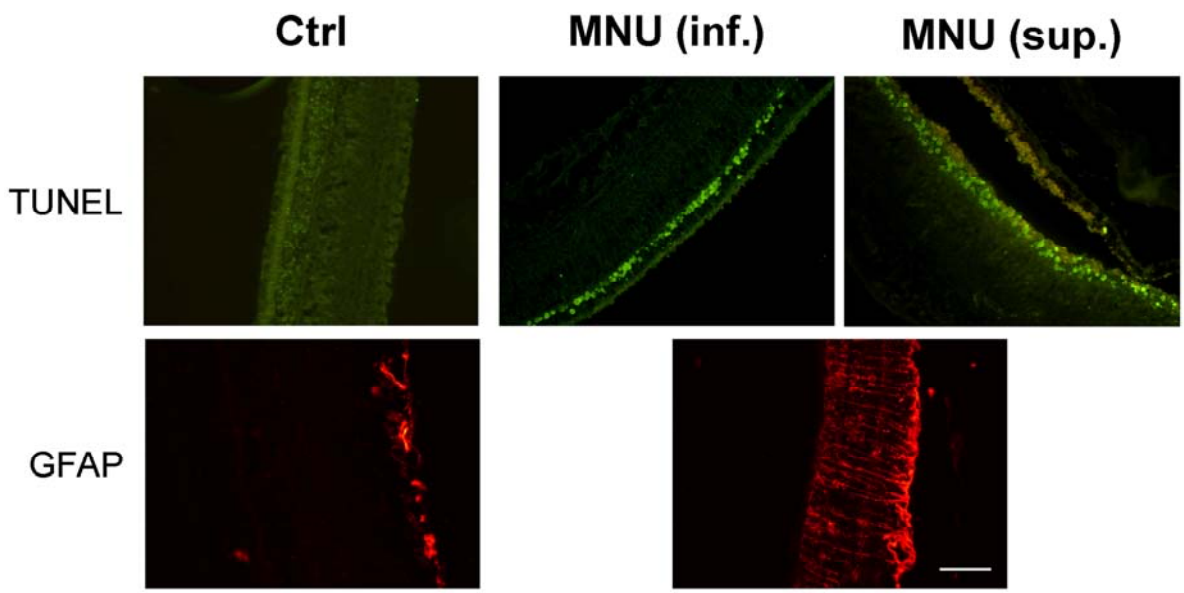

Figure 5 **Characterization of the *Arvicanthis* retinal degeneration induced by MNU.**

Sections of control retinas were compared with those of retinas at 20 d.p.i of MNU at 150 mg/kg. *in situ* cell death was detected with the TUNEL method. TUNEL staining is absent from the control retinas. In the inferior retina, the most inner region of the outer nuclear layer is stained, whereas in the superior retina, the whole remaining of the ONL cells are stained. GFAP is overexpressed in MNU-treated retina. Scale: 10 µm.

GFAP, glial fibrillary acidic protein; MNU, N-methyl-nitrosourea; ONL, outer nuclear layer; TUNEL, terminal deoxynucleotidyl transferase mediated dUTP Nick End Labeling.

Functional effects of MNU injection in *Arvicanthis*

To correlate deleterious structural changes in rods and cones with retinal function, single flash ERGs were recorded from control and 100 mg/kg MNU-treated animals (3 months post-injection) under scotopic and photopic conditions (Figure 6 MNU-treated *Arvicanthis* showed significant reductions in amplitudes of both scotopic (85% decrease at maximum intensities, Figure 6A) and photopic (70% loss at maximum intensities, Figure 6B) ERG responses, indicating alterations of both rod and cone system components. As the initial portion of the a-wave (open arrows) reflects the primary light response of PRs, the remarkable attenuation of the a-wave up to the highest intensity (i.e., 1.5 log cd×s/m^2) observed in MNU-treated *Arvicanthis* indicates almost complete PR dysfunction. The b-wave (solid arrows) and the oscillatory potentials, markers for retinal circuitry downstream to the PRs, were also strongly reduced. Figsure 6C and D show graphic representations of averaged b-wave amplitudes for control and MNU groups under scotopic and photopic conditions respectively.

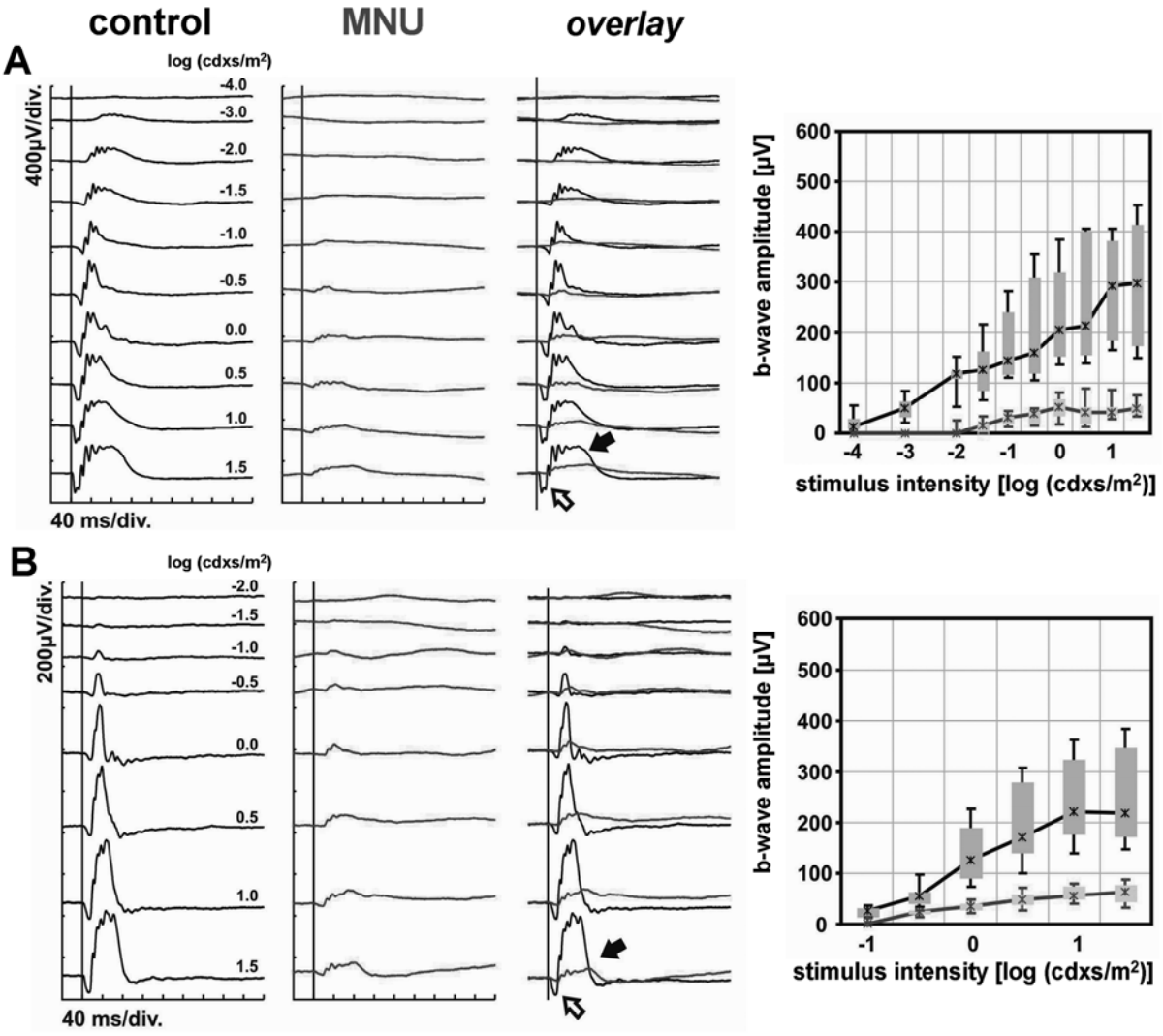

Figure 6 **Electroretinographic data from control and MNU-treated *Arvicanthis*.**

ERGs of control and 100 mg/kg MNU-treated animals at 3 months post-injection are shown under scotopic (**A**; dark-adapted) and photopic (**B**; light-adapted) conditions for single flash stimuli. Box plot representation of scotopic and photopic b-wave amplitudes of **control** (**black**, *n* = 5) and MNU-treated animals (grey, *n* = 5) as a function of the logarithm of the flash intensity are shown. Boxes indicate the 25 % and 75 % quantiles range, whiskers indicate the 5 % and 95 % quantiles; the × symbol indicate the median of the data.

ERG: electroretinogram; MNU: *N*-methyl-*N*-nitrosourea.

Scanning Laser Ophthalmoscopy (SLO)

Some RDs lead to degenerative changes in vasculature, and we examined the aspect of the retinal circulation in MNU-treated *Arvicanthis*. Control animals showed a normal structure of retina, retinal blood vessels and nerve fibre layer (Figure 7A; control In contrast, 100 mg/kg MNU-treated animals displayed distinct changes associated with the degenerative processes, namely reduction of retinal vessel diameter, "optical gaps" corresponding to the visualisation of deep structures behind the RPE and choroid, and lipofuscin and related autofluorescent (AF) material (Figure 7A; MNU). AF analysis in control animals (Figure 7B) showed a regular, diffuse baseline "glow" due to the normal lipid amount and distribution. In MNU-treated animals, bright AF patches were present, typical for the deposits formed from PR debris during retinal degenerative processes.

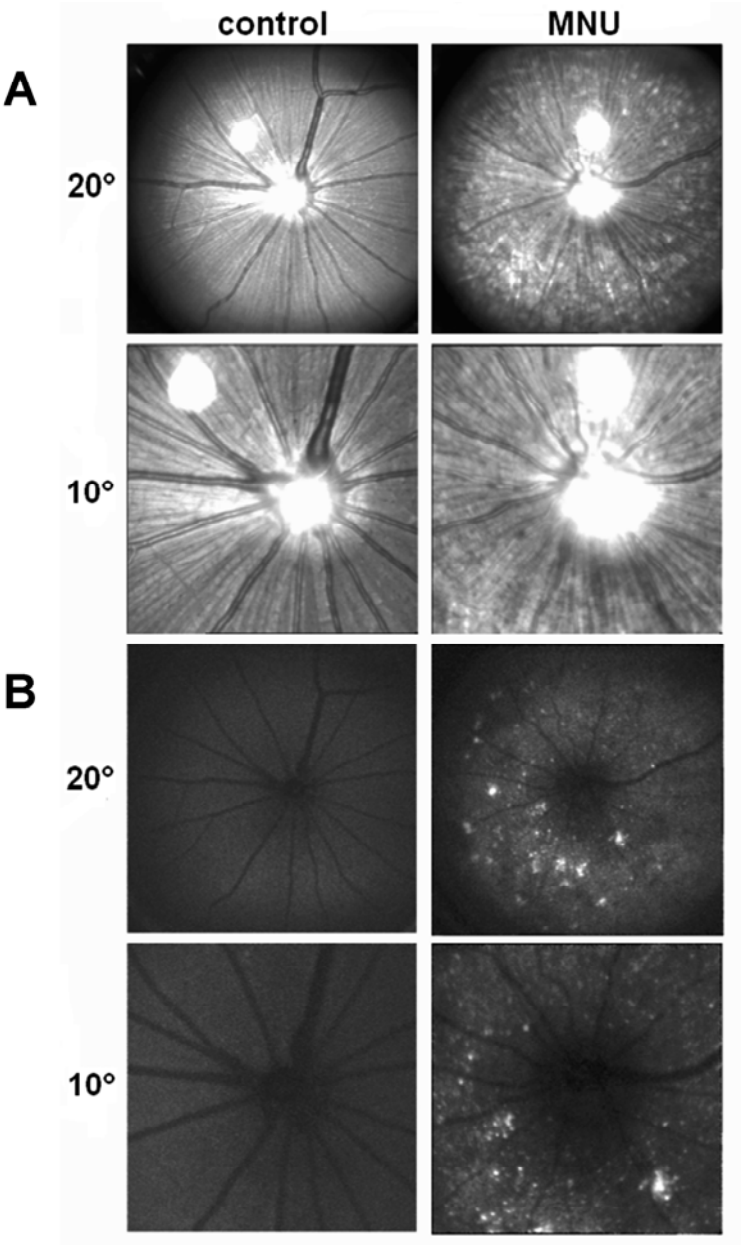

Figure 7 Scanning Laser Ophthalmoscopy (SLO) imaging of control and MNU-treated *Arvicanthis*.

MNU animals were examined at 3 months after a 100 mg/kg injection. Native SLO images obtained with 514 nm excitation (**A**) or AF (488 nm; **B**). Photographs were taken either with 20° magnification for fundus overview, or with 10° magnification for more precise observation of the retinal centre. MNU-treated retinas show typical signs of degenerative processes particularly in the superior hemisphere (lower part of the images).

AF: autofluorescence; MNU: *N*-methyl-*N*-nitrosourea; SLO, scanning laser ophthalmoscopy.

Optical Coherence Tomography (OCT)

Morphological alterations in the retina of MNU-treated *Arvicanthis* were also identified with optical coherence tomography (OCT; Figure 8). This technique provides histology-analogue vertical sections *in vivo*. Enlarged images (Figure 8C and E) demonstrate that inner retina (IR) thickness is virtually unchanged, whereas the PR layer is essentially degenerated. Figure 8G shows averaged IR and OR thicknesses for both groups, highly significantly different for PR ($P < 0.00001$) and not significant for IR ($P = 0.79$) thickness.

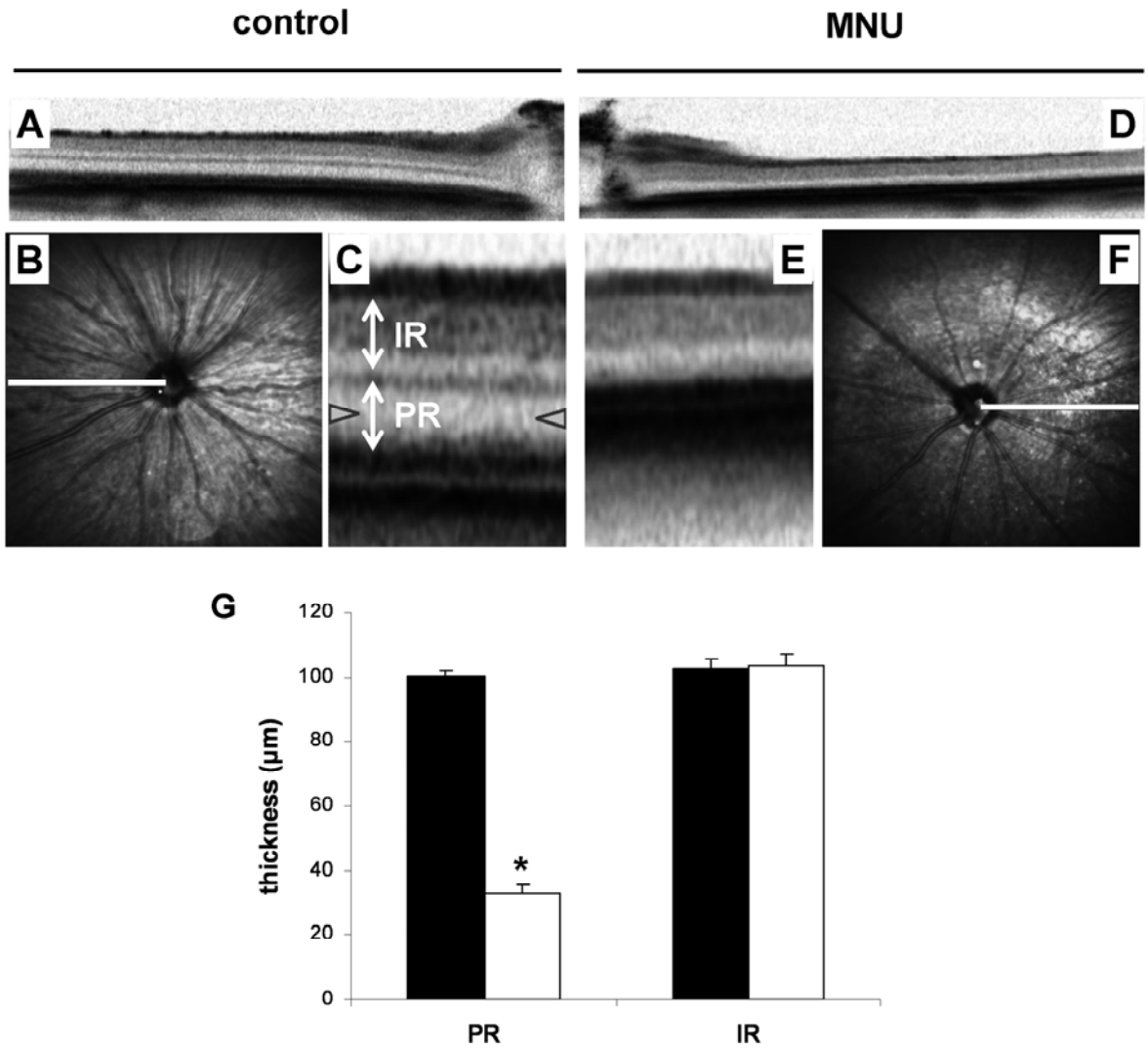

Figure 8 **Optical Coherence Tomography (OCT) imaging of control and MNU-treated *Arvicanthis*.**

Control (**A-C**) and MNU-treated (**D-F**) *Arvicanthis* (300 mg/kg, 3 months post-injection) OCT imaging are shown. **A**, **D**: Vertical histology-analog OCT sections at positions indicated on the corresponding fundus images (**B**, **F**). The horizontal white line indicates the position of the section (**A**, **D**). Details of retinal layers (**C**, **E**) indicate the quasi complete loss of the PR layer (arrowheads) in the MNU-treated animals (**E**). IR layers appear unchanged. **G**: Graphic representation of measurements taken from OCT imaging. OR and IR thicknesses were determined in control and MNU-treated *Arvicanthis*. Layer thickness difference between both groups was significant for OR ($t_8 = 23.24$; $P < 0.00001$) and not significant for IR ($t_8 = -0.28$; $P = 0.79$).

IR: inner retina; MNU, *N*-methyl-*N*-nitrosourea; OCT: optical coherence tomography: OR, outer retina.

Discussion

Our study describes a novel informative model for RD: MNU-treated *Arvicanthis*. In this model, degeneration is localized exclusively to the ONL, and rod and cone PR degenerate with markedly different kinetics and topography. Notably, cones display a remarkable resistance to trauma, although both the structural and functional integrity of retinas are eventually impaired by MNU-injections.

It has been established that in many retinal pathologies, cone death occurs secondarily to that of rods. This is seen in the rd1 mouse, in which initial rapid rod death is followed by a second slower decline in cone survival [29,30]. It has also been documented in human RP, where careful counting of PR numbers reveals that loss of more than 75 % rod OS is necessary before detectable cone loss is seen [1]. Rod loss is also reported to precede cone loss in AMD, where methodical counting of PRs in the perifoveal ring reveals significant rod disappearance prior to cone death [31]. Secondary cone loss is also seen in animal models in which degeneration is induced by light damage [32]. Secondary cone death is proposed to be either due to deprivation of essential neurotrophic factors, such as "rod derived cone viability factor" [33,34] or insulin [35]; or to "poisoning" by oxidative stress [36,37] or iron [38]. All of these animal studies have relied upon mice, in which the cone population is very minor [4]. Although cone behaviour and responses can be isolated, their paucity and distribution renders analyses difficult. On the other hand, use of cone-rich animals such as the zebrafish has given somewhat different results: in a zebrafish light damage model, rod and cone degeneration seem to proceed together (although rod breakdown is more complete and rapid than that of cones) [39,40]. So far, to the best of our knowledge, a practical, reproducible mammalian model of retinal degeneration permitting detailed longitudinal analysis of rod and cone fate does not exist. We took advantage of the high cone content and clear laminated distribution of the retina of *Arvicanthis* [26] to discriminate rod and cone fates after MNU-injection. The data show that rod and cone degeneration are clearly separable events, as seen with rod- and cone-specific protein expression and localization of TUNEL positive cells in the ONL. In human retina, macular cones are surrounded by large numbers of rods. In this respect the retina of *Arvicanthis* is quite similar to the situation in the human macula, and it can be speculated that pathogenic events may occur in a similar manner between the two tissues.

MNU-induced degeneration exhibits a distinct and reproducible spatial- and temporal-dependent progression. The initial signs of ONL changes occur within the upper hemisphere, while the lower hemisphere remains intact for several more days. This asymmetry of cell loss has been previously reported in studies using intense light exposure to induce RD

[41,42,43,44,45]. It is hypothesized that the superior retina receives more light from overhead illumination, and it is plausible that the same phenomenon happens here, a double insult of light damage and chemically-induced lesion being necessary to induce cell loss. However, in inherited animal models of RD like the rd1 mouse, the superior quadrant is the most resistant, with patches of late-surviving cones [30]. In addition, regional loss of PRs is also reported in RP [1]. In the present studies it is remarkable that this topographical difference is visible from early in degeneration, and does not seem to reflect a temporal delay in inferior relative to superior regions. This is because apoptosis is visible throughout the ONL in superior retina from the earliest time points, and that within the inferior hemisphere cones persist even many months later, a situation without parallel in other MNU-injected species. Impairment of rod-mediated ERG responses is consistent with the quasi-total disappearance of rod PRs. However, the residual cone population could permit cone function to persist. This was not the case, as also in photopic conditions visual responses were very reduced for MNU-treated animals. However, it is known that rod and cone pathways are anatomically connected or coupled by gap junctions [46,47], a type of electrical synapse at which rod or cone input can enter the cone or rod circuit respectively and thereby reach ganglion cells. Therefore, the more rapid disappearance of rods would have functional consequences on cone-mediated visual responses. Moreover, ERG response decreases could also be linked to damage of second order neurons due to MNU injection. In the event the IR was also affected, a selective reduction of these components relative to the PR component would be present. However, in a situation where input signals from PR are much reduced, all downstream responses are similarly low too, so it is not possible to investigate a potential additional functional impairment of the IR.

To our knowledge, this is the first study presenting *in vivo* images of *Arvicanthis* retina. SLO was used to observe overall fundus integrity along with retinal vessel structure in control retinas. In MNU-treated retinas, the predominant loss of PRs leads to a reduced demand for oxygen and metabolites, which becomes visible as a marked reduction of retinal vessel diameter in comparison to controls. Translucent areas become visible as bright spots in fundoscopy, suggesting the existence of “optical gaps” that allow to visualize deeply lying structures below the RPE and choroid. These optical gaps are due to reduced metabolism inducing changes in the RPE/choroidal interface. Lipofuscin and related AF material are prominent in AF imaging [48] and suggest PR degeneration, particularly of their lipid-rich outer segments. Despite these changes, the dramatic changes in PR survival are unlikely to be due to vascular remodelling. OCT was used to assess the PR thickness reduction *in vivo*.

Histological approaches, even though essential to study several structural and phenotypical aspects, do not give an absolute indication of structure in living tissue as processing usually leads to structural changes (such as thickness or degradation). Therefore, the OCT technique is a useful supplementary approach to allow ongoing non-invasive assessment of RD. The technique confirmed the drastic decrease in PR thickness and showed that the IR was not structurally affected by MNU injection, and that MNU leads to specific destruction of PRs.

In summary, no previously described mammalian model allows such a clean separation of rod and cone pathogenic changes, and the use of *Arvicanthis* retina will greatly facilitate analysis of PR type specific pathways underlying demise and death.

Materials and Methods

Animals

Young adults, 2 to 6 month old, male (~ 150 g) *Arvicanthis ansorgei* were obtained from our breeding colony raised in our animal facilities in Strasbourg. Animals were kept in an air-conditioned room at 22 ± 2 °C under a 12:12 h light/dark cycle. Half of the cages with experimental animals were put on the top shelf (where room light intensity is higher) and the other half on the bottom shelf (where light intensity was minimal). The same was done for control cages as to prevent any bias from a light intensity effect on MNU-induced degeneration [49]. Animals were supplied *ad libitum* with water and standard rat chow. Animal treatment and experimentation adhered to rules established within our institution, and guidelines in the ARVO Statement for the Use of Animals in Ophthalmic and Vision Research. Food intake and body weight were recorded on a daily basis during the entire experiment. Animals were humanely killed after CO_2 anaesthesia at different time points after MNU injection.

MNU injections

MNU was purchased from Sigma-Aldrich Chemie S.a.r.l. (Saint-Quentin Fallavier, France) and kept at 4°C in the dark.

Immediately before use, MNU powder was dissolved in physiological saline at 10 mg/mL. Experimental *Arvicanthis ansorgei* received a single intraperitoneal injection of 100 or 150 mg/kg body weight MNU. Control animals were injected with a corresponding bolus of physiological saline combined with 0.05 % of acetic acid, as contained in the commercial MNU compound.

Morphologic Evaluation by Quantitative Histology

Eyes were quickly removed for immersion fixation in buffered 4 % paraformaldehyde for 4 h. A hole was made in the nasal *ora serrata* with a 25 G needle to facilitate entry of fixative to the retina and for orientation purposes. Eyes were then transferred in 0.01 M Phosphate Buffered Saline pH 7.4 (PBS). Fixed eyes were bisected along the superior-to-inferior axis, to access the vertical meridian of each hemisphere, embedded in paraffin, and 4 µm thick sections were taken along the vertical meridian, to allow comparison of all regions of the retina in the superior and inferior hemispheres. Sections were then stained with haematoxylin/eosin staining and examined by light microscopy.

For morphometry, we used a modified version of a method previously described [50]. Adjacent pictures were taken × 20 magnification and entire sections were reconstructed using the Microsoft® Office Power Point® 2003 version. Measurements of retinal layers thickness were made at 275 µm intervals extending from the optic nerve head in both superior and inferior ora serrata, using the ImageJ analysis software (version 1.37v; National Institutes of Health, USA). PR layer thickness was considered as the sum of outer segments, inner segments and outer nuclear layer thicknesses. The ratio of PR thickness to the inner nuclear layer thickness was used for analysis to account for obliquely cut sections. Averaged layer thicknesses at each point were calculated from three sections of three animals per MNU d.p.i. group and plotted as a function of eccentricity from the ONH, producing a morphometric profile across the vertical meridian ("spider graph"). For convenience reasons, the retina was divided in 6 regions: central inferior and superior, medial inferior and superior, and far inferior and superior. Central region was comprised between ONH and ± 825 µm; medial region was comprised between ± 825 µm and ± 1,650 µm; and far region was between ± 1,650 µm and 2,475 µm.

Immunohistochemistry

Eyes were fixed overnight in 4 % paraformaldehyde at 4°C, transferred to an ascending series of sucrose solutions (10 %, 20 %, and 30 %, each for 2 h) and embedded in Tissue-Tek (Sakura Finetek, Tokyo, Japan). Ten µm thick cryostat sections were prepared and stored at -20°C until ready for use. The sections were permeabilized with Triton X-100 (0.1 % in PBS for 5 minutes) and then saturated with PBS containing 0.1 % BSA, 0.3 % Tween-20, and 0.1 % sodium azide for 30 minutes. Sections were incubated overnight at 4°C with the following primary antibodies diluted in the buffer used for saturation. Antibodies used were monoclonal anti-rhodopsin antibody Rho-4D2 [51] diluted to ~ 2 µg/mL, polyclonal anti-mouse MW-

cone opsin and anti-mouse cone arrestin (MW opsin and c-arr.; both gifts from Dr. Cheryl Craft, Doheny Eye Institute, Univ. Southern California, Los Angeles, USA) used at 1 µg/mL final concentration (Zhu et al., 2002) and polyclonal GFAP antibody (Z 0334; DAKO, Glostrup, Denmark) used at 10.25 µg/mL final concentration. Polyclonal anti- rod ($G_{\alpha\ t1}$) and cone ($G_{\alpha\ t2}$) transducin (sc-389, sc-390; Santa Cruz Biotechnology Inc., Santa Cruz, CA, USA) were diluted to a final concentration of 4 µg/mL. Secondary antibody incubation was performed at room temperature for 2 h with Alexa (488 or 594) goat anti-rabbit or anti-mouse IgG-conjugated antibodies (Molecular Probes Ltd., Eugene, OR, USA; 5 µg/mL). Cell nuclei were stained with DAPI (Invitrogen). Slides were washed thoroughly, mounted in PBS and glycerol (1:2), and observed with a confocal laser scanning microscope (LSM 510 ver. 2.5; Carl Zeiss Meditec, Jena, Germany) or a fluorescence microscope light microscope (Leica DMRB; Leica). Images were relayed by charge-coupled device camera video capture (Olympus DP50; Olympus) to a dedicated computer.

in situ cell death detection

Apoptosis was assessed by terminal deoxynucleotidyltransferase-mediated dUTP nick end labeling (TUNEL; Roche Diagnostics) according to the manufacturer's instructions. In accordance with the manufacturer's instructions, sections were treated as for immunohistochemistry with 0.1 % Triton X-100. After washing, sections were then incubated with the TUNEL mixture (terminal deoxynucleotidyltransferase enzyme, phycoerythrin-dUTP and dNTP nucleotides). After 60 min at 37 °C in a humid dark chamber, sections were washed three times in wash PBS and mounted under coverslips in 1:2 PBS-glycerol

Western Blot Analysis

To quantify the degeneration of rods and cones, we performed WB on control Arvicanthis and Arvicanthis killed at 20 d.p.i. of MNU. Retinas were collected and homogenized in lysis buffer (20 mM Tris-HCl [pH 7.4], 150 mM NaCl, 1% Triton X-100, 0.1% SDS, 1 mM EDTA) containing a protease inhibitor cocktail (Roche Molecular Biochemicals, Meylan, France). As degenerated retinas contain less protein than control retinas, and as we were more interested in the ratio of rod to cone protein rather than the absolute quantity, lanes were loaded on a per retina basis rather than protein concentration. Samples (10 µL/lane or about ~ 20 µg for control and ~ 16 µg for MNU retinas) were separated by 10 % SDS-polyacrylamide gel electrophoresis and transferred to nitrocellulose membranes with a trans blotter cell (Bio-Rad, Munich, Germany). The membrane was blocked with TBS containing 0.1 % Tween 20

and 3 % fat-free powdered milk (pH 7.3) for 1 h at room temperature. Membranes were incubated with polyclonal anti-mouse cone arrestin diluted to a final concentration of 0.008 µg/mL, and incubated overnight at 4°C on agitation. The membrane was washed thoroughly and then incubated with goat anti-rabbit IgG-horseradish peroxidase secondary antibodies (0.08 µg/mL; Jackson ImmunoResearch Laboratories, West Grove, PA). Immunoreactive bands were visualized with chemiluminescence (Super Signal ECL kit; West Pico; Pierce, Rockford, IL), according to the manufacturer's instructions. Apparent molecular masses were estimated by comparison to pre-stained molecular size markers (Invitrogen-Life Technologies, Gaithersburg, MD). The membrane was incubated with RestoreTM Western Blot Stripping Buffer (Thermo Fisher Scientific, Rockford, IL, USA) 35 min at 37°C. The membrane was washed thoroughly and then the same procedure as described above was performed with monoclonal anti-rhodopsin antibody Rho-4D2 diluted to a final concentration of ~ 0.04 µg/mL. The secondary antibody was a goat anti-mouse IgG-horseradish peroxidase (0.08 µg/mL).

Electroretinographic Analysis

ERGs were performed according to previously described procedures [52,53]. The ERG equipment consisted of a Ganzfeld bowl, a direct current amplifier, and a PC-based control and recording unit (Multiliner Vision; VIASYS Healthcare GmbH, Hoechberg, Germany). Animals were dark-adapted overnight and anaesthetised by intraperitoneal injection of a combination of ketamine (Virbac, Carros, France) at 150 mg/kg body weight and xylazine (12.5 mg/kg; KVP Pharma und Veterinaer-Produkte GmbH, Kiel, Germany) at 10 mg/kg body weight. Pupils were dilated with tropicamide (Mydriaticum Stulln; Pharma Stulln, Nabburg, Germany) and phenylephrine (Neosynephrin-POS 5%; Ursapharm, Saarbruecken, Germany). Silver needle electrodes served as reference (forehead) and ground (tail) electrodes, and gold-wire ring electrodes as active electrodes. Methylcellulose (Methocel; Ciba Vision, Wessling, Germany) was applied to ensure good electrical contact and to keep the eye hydrated during the entire procedure. Single flash ERG responses were obtained under dark-adapted (scotopic) and light-adapted (photopic) conditions. Light adaptation was accomplished with a background illumination of 30 candela (cd) per square meter starting 10 minutes before recording. Single white-flash stimulus intensity ranged from -4 to 1.5 log cd×s/m2 under scotopic and from -2 to 1.5 log cd×s/m2 under photopic conditions, divided into 10 and 8 steps, respectively. Ten responses were averaged with an inter-stimulus interval of either 5 seconds (for -4, -3, -2, -1.5, -1, and -0.5 log cd×s/m2) or 17 seconds (for 0, 0.5, 1,

and 1.5 log cd×s/m2). The range of intensities used in the protocol was 2.0 to 4.1 log cd×s/m2.

Scanning Laser Ophthalmoscopy

After ERG recording the retinal structures of the still anesthetized Arvicanthis were visualized via SLO imaging with a Heidelberg Retina Angiograph (HRA I, Heidelberg Engineering, Germany) and a confocal scanning-laser ophthalmoscope, according to previously described procedures [54]. The HRA features two argon wavelengths (488 nm and 514 nm) in the short wavelength range and two infrared diode lasers (795 nm and 830 nm) in the long wavelength range. Laser wavelengths used for fundus visualization were: 514 nm (RF, red-free channel), and 488 nm for autofluorescent images (AF), with a barrier filter at 500 nm. Two device settings for the field of view were used: for fundus overview, the focus was adjusted to 20°, and for magnification and detailed view, the focus was set at 10°.

Spectral Domain-Optical Coherence Tomography

Spectral Domain-Optical Coherence Tomography (SD-OCT) imaging was done with a commercially available Spectralis™ HRA + OCT device from Heidelberg Engineering featuring a broadband superluminescent diode at λ = 870 nm as low coherent light source. Each two-dimensional B-Scan recorded at 30° field of view consists of 1,536 A-scans, which are acquired at a speed of 40,000 scans per second. Optical depth resolution is approximately 7 µm with digital resolution reaching 3.5 µm [55]. Imaging was performed using the proprietary software package Eye Explorer (version 3.2.1.0, Heidelberg Engineering, Germany). Retinal thickness was quantified using horizontal slides, located 1,500 µm distant from the optic nerve head in the temporal hemisphere (?). PR was defined as proximal of the highly reflective layer presumably representing the RPE/choriocapillary complex up to the outer plexiform layer; IR as proximal of the OPL up to the inner limiting membrane.

Statistical Analysis

Data are expressed as mean ± SEM. For comparison of two groups, we used a Student's t-test. For multiple factors analysis, we used two-way analysis of variance (ANOVA) for independent measures, followed by Tukey's HSD (Honestly Significant Difference) post-hoc tests. The -2,750 µm point was not included in the statistical analysis.

A statistical evaluation of the ERG data was performed.

Acknowledgments

The authors thank Dr. Edda Fahl for her help with SLO imaging and Prof. Christian Grimm for his advices with retinal degenerations issues. We gratefully thank Alcon® for their financial support. D.Boudard is a recipient of a doctoral fellowship from Région Alsace.

Abbreviations

AMD, aged macular degeneration; AF, autofluorescence; b.w., body weight; CFF, critical flicker fusion frequency; DAPI, 4',6-diamidino-2-phenylindole; d.p.i., day post-injection; ERG, electroretinogram; GCL, ganglion cell layer; GFAP, glial fibrillary acidic protein, INL, inner nuclear layer; IR, inner retina; IS, inner segments; MNU, N-methyl-nitrosourea; MW, middle-wave; ONH: optic nerve head; ONL, outer nuclear layer; OPL, outer plexiform layer; OR, outer retina; OS, outer segments; PBS, phosphate buffer saline; PR(s), photoreceptor(s); R/C-CB, rod/cone cell bodies; R/C-IS, rod/cone inner segments; R/C-OS, rod/cone outer segments; RD(s): retinal degeneration(s); RF, red-free channel; RP, retinitis pigmentosa; (SD) OCT, (spectral domain-) optical coherence tomography; SLO, scanning laser ophthalmoscopy; TUNEL, terminal deoxynucleotidyl transferase mediated dUTP Nick End Labeling assay

References

1. Cideciyan AV, Hood DC, Huang Y, Banin E, Li ZY, et al. (1998) Disease sequence from mutant rhodopsin allele to rod and cone photoreceptor degeneration in man. Proc Natl Acad Sci U S A 95: 7103-7108.
2. Hartong DT, Berson EL, Dryja TP (2006) Retinitis pigmentosa. Lancet 368: 1795-1809.
3. Carter-Dawson LD, LaVail MM (1979) Rods and cones in the mouse retina. II. Autoradiographic analysis of cell generation using tritiated thymidine. J Comp Neurol 188: 263-272.
4. Jeon CJ, Strettoi E, Masland RH (1998) The major cell populations of the mouse retina. J Neurosci 18: 8936-8946.
5. Szel A, Rohlich P (1992) Two cone types of rat retina detected by anti-visual pigment antibodies. Exp Eye Res 55: 47-52.
6. Williams DS, Colley NJ, Farber DB (1987) Photoreceptor degeneration in a pure-cone retina. Effects of cyclic nucleotides, and inhibitors of phosphodiesterase and protein synthesis. Invest Ophthalmol Vis Sci 28: 1059-1069.

7. Mears AJ, Kondo M, Swain PK, Takada Y, Bush RA, et al. (2001) Nrl is required for rod photoreceptor development. Nat Genet 29: 447-452.

8. Daniele LL, Lillo C, Lyubarsky AL, Nikonov SS, Philp N, et al. (2005) Cone-like morphological, molecular, and electrophysiological features of the photoreceptors of the Nrl knockout mouse. Invest Ophthalmol Vis Sci 46: 2156-2167.

9. Fauser S, Luberichs J, Schuttauf F (2002) Genetic animal models for retinal degeneration. Surv Ophthalmol 47: 357-367.

10. Noell WK, Walker VS, Kang BS, Berman S (1966) Retinal damage by light in rats. Invest Ophthalmol 5: 450-473.

11. Scott PP, Greaves JP, Scott MG (1964) Nutritional Blindness In The Cat. Exp Eye Res 3: 357-364.

12. Seidehamel RJ, Dungan KW (1974) Characteristics and pharmacologic utility of an intraocular pressure (IOP) model in unanesthetized rabbits. Invest Ophthalmol 13: 319-322.

13. Kiuchi K, Yoshizawa K, Shikata N, Moriguchi K, Tsubura A (2002) Morphologic characteristics of retinal degeneration induced by sodium iodate in mice. Curr Eye Res 25: 373-379.

14. Noell WK (1977) Some animal models of retinitis pigmentosa. Adv Exp Med Biol 77: 87-91.

15. Matsumura M, Ohkuma M, Tsukahara I (1986) Experimental chloroquine retinopathy. Ophthalmic Res 18: 172-179.

16. Alkemade PP (1968) Phenothiazine-retinopathy. Ophthalmologica 155: 70-76.

17. Lee KP, Gibson JR, Sherman H (1979) Retinopathic effects of 2-aminooxy propionic acid derivatives in the rat. Toxicol Appl Pharmacol 51: 219-232.

18. Lee KP, Valentine R (1990) Retinotoxicity of 1,4,-bis(4-aminophenoxy)-2-phenylbenzene (2-phenyl-APB-144) in albino and pigmented rats. Arch Toxicol 64: 135-142.

19. Bellhorn RW, Bellhorn M, Friedman AH, Henkind P (1973) Urethan-induced retinopathy in pigmented rats. Invest Ophthalmol 12: 65-76.

20. Cicerone CM (1976) Cones survive rods in the light-damaged eye of the albino rat. Science 194: 1183-1185.

21. Cortina MS, Gordon WC, Lukiw WJ, Bazan NG (2003) Light-induced photoreceptor damage triggers DNA repair: differential fate of rods and cones. Adv Exp Med Biol 533: 229-240.

22. Nakajima M, Yuge K, Senzaki H, Shikata N, Miki H, et al. (1996) Photoreceptor apoptosis induced by a single systemic administration of N-methyl-N-nitrosourea in the rat retina. Am J Pathol 148: 631-641.

23. Taomoto M, Nambu H, Senzaki H, Shikata N, Oishi Y, et al. (1998) Retinal degeneration induced by N-methyl-N-nitrosourea in Syrian golden hamsters. Graefes Arch Clin Exp Ophthalmol 236: 688-695.

24. Nambu H, Taomoto M, Ogura E, Tsubura A (1998) Time-specific action of N-methyl-N-nitrosourea in the occurrence of retinal dysplasia and retinal degeneration in neonatal mice. Pathol Int 48: 199-205.

25. Tsubura A, Yoshizawa K, Kiuchi K, Moriguchi K (2003) N-Methyl-N-nitrosourea-induced Retinal Degeneration in Animals. Acta Histochem Cytochem 36: 263-270.

26. Bobu C, Craft CM, Masson-Pevet M, Hicks D (2006) Photoreceptor organization and rhythmic phagocytosis in the nile rat Arvicanthis ansorgei: a novel diurnal rodent model for the study of cone pathophysiology. Invest Ophthalmol Vis Sci 47: 3109-3118.

27. Curcio CA, Sloan KR, Kalina RE, Hendrickson AE (1990) Human photoreceptor topography. J Comp Neurol 292: 497-523.

28. Gullino PM, Pettigrew HM, Grantham FH (1975) N-nitrosomethylurea as mammary gland carcinogen in rats. J Natl Cancer Inst 54: 401-414.

29. Carter-Dawson LD, LaVail MM, Sidman RL (1978) Differential effect of the rd mutation on rods and cones in the mouse retina. Invest Ophthalmol Vis Sci 17: 489-498.

30. Jimenez AJ, Garcia-Fernandez JM, Gonzalez B, Foster RG (1996) The spatio-temporal pattern of photoreceptor degeneration in the aged rd/rd mouse retina. Cell Tissue Res 284: 193-202.

31. Curcio CA, Medeiros NE, Millican CL (1996) Photoreceptor loss in age-related macular degeneration. Invest Ophthalmol Vis Sci 37: 1236-1249.

32. Krebs MP, White DA, Kaushal S (2009) Biphasic Photoreceptor Degeneration Induced by Light in a T17M Rhodopsin Mouse Model of Cone Bystander Damage. Invest Ophthalmol Vis Sci.

33. Mohand-Said S, Deudon-Combe A, Hicks D, Simonutti M, Forster V, et al. (1998) Normal retina releases a diffusible factor stimulating cone survival in the retinal degeneration mouse. Proc Natl Acad Sci U S A 95: 8357-8362.

34. Leveillard T, Mohand-Said S, Lorentz O, Hicks D, Fintz AC, et al. (2004) Identification and characterization of rod-derived cone viability factor. Nat Genet 36: 755-759.

35. Punzo C, Kornacker K, Cepko CL (2009) Stimulation of the insulin/mTOR pathway delays cone death in a mouse model of retinitis pigmentosa. Nat Neurosci 12: 44-52.

36. Shen J, Yang X, Dong A, Petters RM, Peng YW, et al. (2005) Oxidative damage is a potential cause of cone cell death in retinitis pigmentosa. J Cell Physiol 203: 457-464.

37. Komeima K, Rogers BS, Lu L, Campochiaro PA (2006) Antioxidants reduce cone cell death in a model of retinitis pigmentosa. Proc Natl Acad Sci U S A 103: 11300-11305.

38. Rogers BS, Symons RC, Komeima K, Shen J, Xiao W, et al. (2007) Differential sensitivity of cones to iron-mediated oxidative damage. Invest Ophthalmol Vis Sci 48: 438-445.

39. Vihtelic TS, Hyde DR (2000) Light-induced rod and cone cell death and regeneration in the adult albino zebrafish (Danio rerio) retina. J Neurobiol 44: 289-307.

40. Vihtelic TS, Soverly JE, Kassen SC, Hyde DR (2006) Retinal regional differences in photoreceptor cell death and regeneration in light-lesioned albino zebrafish. Exp Eye Res 82: 558-575.

41. LaVail MM, Gorrin GM, Repaci MA, Yasumura D (1987) Light-induced retinal degeneration in albino mice and rats: strain and species differences. Prog Clin Biol Res 247: 439-454.

42. Rapp LM, Smith SC (1992) Morphologic comparisons between rhodopsin-mediated and short-wavelength classes of retinal light damage. Invest Ophthalmol Vis Sci 33: 3367-3377.

43. Reme CE, Malnoe A, Jung HH, Wei Q, Munz K (1994) Effect of dietary fish oil on acute light-induced photoreceptor damage in the rat retina. Invest Ophthalmol Vis Sci 35: 78-90.

44. Organisciak DT, Darrow RA, Barsalou L, Darrow RM, Lininger LA (1999) Light-induced damage in the retina: differential effects of dimethylthiourea on photoreceptor survival, apoptosis and DNA oxidation. Photochem Photobiol 70: 261-268.

45. Ranchon I, LaVail MM, Kotake Y, Anderson RE (2003) Free radical trap phenyl-N-tert-butylnitrone protects against light damage but does not rescue P23H and S334ter rhodopsin transgenic rats from inherited retinal degeneration. J Neurosci 23: 6050-6057.

46. Raviola E, Gilula NB (1973) Gap junctions between photoreceptor cells in the vertebrate retina. Proc Natl Acad Sci U S A 70: 1677-1681.

47. Bloomfield SA, Dacheux RF (2001) Rod vision: pathways and processing in the mammalian retina. Prog Retin Eye Res 20: 351-384.

48. Schmitz-Valckenberg S, Holz FG, Bird AC, Spaide RF (2008) Fundus autofluorescence imaging: review and perspectives. Retina 28: 385-409.

49. Smith SB, Hashimi W, Yielding KL (1988) Retinal degeneration in the mouse induced transplacentally by N-methyl-N-nitrosourea: effects of constant illumination or total darkness. Exp Eye Res 47: 347-359.

50. Vaughan DK, Coulibaly SF, Darrow RM, Organisciak DT (2003) A morphometric study of light-induced damage in transgenic rat models of retinitis pigmentosa. Invest Ophthalmol Vis Sci 44: 848-855.

51. Hicks D, Molday RS (1986) Differential immunogold-dextran labeling of bovine and frog rod and cone cells using monoclonal antibodies against bovine rhodopsin. Exp Eye Res 42: 55-71.

52. Seeliger MW, Grimm C, Stahlberg F, Friedburg C, Jaissle G, et al. (2001) New views on RPE65 deficiency: the rod system is the source of vision in a mouse model of Leber congenital amaurosis. Nat Genet 29: 70-74.

53. Tanimoto N, Muehlfriedel RL, Fischer MD, Fahl E, Humphries P, et al. (2009) Vision tests in the mouse: Functional phenotyping with electroretinography. Front Biosci 14: 2730-2737.

54. Seeliger MW, Beck SC, Pereyra-Munoz N, Dangel S, Tsai JY, et al. (2005) In vivo confocal imaging of the retina in animal models using scanning laser ophthalmoscopy. Vision Res 45: 3512-3519.

55. Wolf-Schnurrbusch UE, Enzmann V, Brinkmann CK, Wolf S (2008) Morphologic changes in patients with geographic atrophy assessed with a novel spectral OCT-SLO combination. Invest Ophthalmol Vis Sci 49: 3095-3099.

4. RD & PHOTOENTRAINMENT: MNU-INJECTED RATS LOST IN THE TWILIGHT ZONE…

Experiments described pages 121-122 showed that **rats** injected with MNU lose their ONL within 9 days. In addition, a study published in 2006 showed that MNU-treated rats had a down regulation of the expression of melanopsin (Wan et al., 2006), a visual pigment thought to be highly involved in the photic synchronization of the circadian system. Hence, in a new study, we studied the ability of MNU-treated rats characterized by a loss of PR and low melanopsin expression to synchronize to different LD cycles.

Second Article

(under submission)

Signalement bibliographique ajouté par le :

UNIVERSITÉ DE STRASBOURG

Service Commun de Documentation

Loss of photic entrainment at low illuminances in rats with acute photoreceptor degeneration

Domitille L. BOUDARD, Jorge MENDOZA and David HICKS

European Journal of Neuroscience, 2009, vol. 30, n° 8, pages 1527-1536

Pages 152-176 :

La publication présentée ici dans la thèse est soumise à des droits détenus par un éditeur commercial.

Les utilisateurs de l'UdS peuvent consulter cette publication sur le site de l'éditeur :
http://dx.doi.org/10.1111/j.1460-9568.2009.06935.x

La version imprimée de cette thèse peut être consultée à la bibliothèque ou dans un autre établissement via une demande de prêt entre bibliothèques (PEB) auprès de nos services :
http://www-sicd.u-strasbg.fr/services/peb/

UNIVERSITÉ DE STRASBOURG

GENERAL

DISCUSSIONS

E. General Discussions

1. Of *Arvicanthis* and Men… Is *Aa* Retina a good Model for the Study of Human Retina?

2. Rods, Cones and ipRGCs: the Winning Combination for an Ideal Photic Entrainement?

3. NIF Functions Based Tests: another Way to Evaluate Retinal Damage?

1. Of *Arvicanthis* and Men… Is *Aa* Retina a good Model for the Study of Human Retina?

1.1. Closeness to Human Retina in Non-Pathological Situations

Arvicanthis ansorgei is a diurnal rodent and as such combines two interesting characteristics for biological studies aimed at understanding human physiology: easy maintenance and experimentation, and an activity rhythm profile similar to humans. Adaptation of *Arvicanthis* to diurnal life has almost certainly been accompanied by adaptation to the high ambient light intensity conditions endured in particular by the eye. But are these characteristics sufficient enough to make *Arvicanthis* a good model of human vision or, more precisely, to make *Arvicanthis* retina a good model of human retina?

1.1.1. Topography of Cellular Types across the Retina

Probably the strongest argument in favour of *Arvicanthis* as an interesting model of human vision is the proportion of the different types of PR. *Arvicanthis* retina contains a high percentage of cones compared to other (nocturnal) rodents (about ten fold). However, human retina actually possesses only 5 % of cones, a percentage closer to that of mice and rats, than to *Arvicanthis*. The difference with rat and mice retinas is that human cones are not distributed homogenously across the retina, but concentrated in an area 6 mm in diameter: the macula. The human macula can be further sub-divided into an inner ring called the fovea, and a central cone-pure foveola only 0.8 mm in diameter, totally devoid of rods and in which cones are packed tightly together and connected on a 1:1 basis to second and third order neurons. The special architecture of the macula underlies high acuity vision and good daylight eyesight. It is surrounded by a rod-dominated parafoveal ring (Curcio et al., 2000). In *Arvicanthis* retina, cones are distributed uniformly throughout the retina and their cell bodies lie in the outer (scleral) part of the outer nuclear layer, above the rod cell bodies (Bobu et al., 2006). In these retinas, the cone to rod ratio is approximately constant, at roughly 1:3. Thus, even if the percentage of cones in *Arvicanthis* retina is far higher than that found in the human retina, and the distribution of cones is very different, *Arvicanthis* retina could be considered to represent a region of the human retina equivalent to the medial part of the macula, of great importance for human vision.

Although our earlier histological studies indicated that retinal architecture is uniform in *Arvicanthis*, in the work presented here SLO examination of their retina revealed a non-homogeneous aspect of the fundus. Indeed, a curved band located in the superior hemisphere appears lighter than the rest of the retina, resembling specialized regions found in other vertebrates and corresponding to regions of high visual acuity where cones are more highly concentrated. In species such as cats and dogs, images focus to a central specialized area or *area centralis*, where cones predominate (Rapaport and Stone, 1984). Also, the retinas of mammals such as rabbits and squirrels, as well as those of non mammalians like turtles, have a long, horizontal strip of specialized cells above the optic nerve called the visual streak (Normann and Kolb, 1981), thought necessary to detect the fast and fleeting movements of predators relative to the horizon. In *Arvicanthis*, SW cone distribution displays a central to periphery gradient, but no other areas of higher SW cone density were seen (Bobu et al., 2006). However, the distribution of MW cones, the most common cone type in *Arvicanthis* (Bobu et al., 2006), has not been studied. The light area found in SLO images of *Arvicanthis* fundus could also be due to a higher density of other cell types such as second order neurons or RGCs. In this case, such a specialized area could also be responsable for higher visual acuity by leading to a lower PR to second or third order cell ratio for example. Further studies need to be performed to address this issue.

1.1.2. ERG Responses

Our data represent the first functional recordings obtained from retina of *Arvicanthis ansorgei*. ERG responses of *Arvicanthis* were recorded in different stimulation conditions and compared to those of rats and mice. As these signals correspond to global responses from all cellular types within the retina, a high cone to rod ratio should influence greatly the responses seen by ERG. Indeed, in all tested conditions, the responses of *Arvicanthis* retina drastically differed from those of "classic" rodents. At low intensities and in scotopic conditions where principally rods are activated, *Arvicanthis* responses were very small, while in photopic conditions, where cone-mediated responses only are visible, responses were very rapid and their amplitude was increased. In these respects, *Arvicanthis* responses are closer to humans (Henkes, 1958). The very high amplitudes of *Arvicanthis* ERG responses make this animal species very interesting to describe the functional impact of early RD or the protective effects of a therapeutic agent on the cone system, as slight decreases or increases in ERG wave amplitudes are readily visible compared to the small ERG responses of mice and rats.

When the frequency of retinal stimulation using flashing light of moderate intensity is increased from 1 to 30 flashes per second during an ERG protocol, some photoreceptive cells within the retina become incapable of responding. The stimulus frequency at which separate responses can no longer be recorded is the critical fusion frequency (CFF), which in rats and mice is around 30 Hz. In *Arvicanthis*, CFF is clearly greater than this value, as with this frequency the individual wave responses could still be distinguished. In humans, it is known that up to approximately 20 flashes per second, rods can respond with a separate response for each flash, whereas cones can generate separate responses to flash stimulus rates as high as 70 flashes per second (Heck, 1957). Measurement of both CFF and the amplitudes seen at faster stimulus frequencies is of value in the diagnosis of eye diseases, in which these parameters have been explored for more than a century. Braunstein was one of the first to investigate CFF in cases of optic atrophy, optic neuritis, amblyopia, glaucoma, and chorioretinitis (Braunstein, 1903). Since then, flicker measurements have been shown to be sensitive indicators of optic nerve or retinal diseases such as macular dystrophy, serous retinopathy or Leber's disease when other clinical tests remain unaffected (Simonson and Wohlrabe, 1963; Babel et al., 1969; Massof et al., 1977; Han et al., 1985; Nakamura and Yamamoto, 2000). In this context, the particularly high CFF of *Arvicanthis* could be a useful feature for the diagnostic of retinal or other ocular pathologies.

Using glutamate analogues to obtain relatively selective blockage of either on- or off-bipolar cells of the monkey retina, Bush and Sieving found a major contribution from postsynaptic or second-order neurons (essentially bipolar cells) to the photopic fast-flicker ERG response (Bush and Sieving, 1994). Characterization of cone and rod on- and off-bipolar cells in the retina of *Arvicanthis* should be investigated in more detail to determine their differences with those of mice and rats, and potential similarities to humans.

When comparing *Arvicanthis* ERG responses with those of mice and rats, it is important to remember that *Arvicanthis* are diurnal animals, whereas mice and rats are nocturnal. Before experiments, animals are kept at least 12 h in complete dark. But recordings are usually performed during daytime for the convenience of the experimenter, and the subjective daytime for animals. Therefore, *Arvicanthis* responses are recorded during their active phase while those for rats and mice are recorded during their sleeping phase. It is known that anaesthetics have a chronobiotic effect (Reinberg, 1986), and hence the physiological status and the effect of anaesthesia could be different on *Arvicanthis vs*. nocturnal species at the time of recordings. As depth of anaesthesia may affect the b-wave amplitude to variable degrees, depending on the nature of the drug (Raitta et al., 1979), it is

important to keep this aspect in mind while comparing *Arvicanthis* ERG responses with those of nocturnal species. Also, for the same reason, comparing *Arvicanthis* and human ERG responses might be more straight forward.

More generally, the different components of ERG responses in *Arvicanthis* and the contribution of the different cell types in the generation of these components, are analyzed in the light of knowledge from studies in mice, in which synaptic blockers have been used to analyze rod and cone responses under different conditions. However, it is legitimate to ask whether findings obtained in mice can be applied to *Arvicanthis* and humans. For example, the intensity and duration of background light used to saturate rods in photopic conditions may be slightly different with types and numbers of cones, and maybe cones of *Arvicanthis* and mice are not physiologically identical. Only systematic pharmacological approaches using different blockers could help to answer these questions.

1.2. Pathology: the Resistance Hypothesis Based on Light Experiments

We used intense light exposure to attempt to induce RD in *Arvicanthis*. We tested several parameters of exposure (duration, intensity), conditions of animals (previous light history, circadian time) and nature of the light (spectrum), but failed to obtain characteristic or reproducible RD damage as described in published studies with rat or mice (de Raad et al., 1996; Hafezi et al., 1997). Among the multiple protocols we tested, only extended exposure to very intense blue light induced unambiguous damage to a small region of retina, visible as complete destruction of all layers. This pattern does not resemble what is classically observed after blue light exposure in rats, where only PR are damaged (Grimm et al., 2001). It is hence doubtful that the mechanisms responsable for the damage that occurred in this paradigm are the same as those observed by other groups. In short, we were unable to induce retinal damage in *Arvicanthis* through any light-based strategy.

To explain such resistance in *Arvicanthis* retina following light exposure, two hypotheses can be advanced: either retinal damage after exposure indeed occurred but our methods were either not sensitive enough or the nature of damage was so different to conventional experimental rodents that we were unable to detect it; or no damage occurred.
With respect to the first possibility, we used primarily histological observation of thin (10 μm) sections by light or fluorescent microscopy. Maybe embedding of tissue in Epon and making semi-thin (0.5 μm) or thin (50-60 nm) sections (the latter observed by electron

microscopy), could have allowed detection of fine features characteristic of retinal damage such as damaged OS and condensation of RIS with swollen mitochondria. Also, through the use of gene array techniques we might have detected up- or down-regulation of molecules implicated in cell death (such as pro- or anti- apoptotic genes). It is also possible that some changes specific to a cone-rich species (eg. re-distribution of cone opsins) may have been overlooked. However, use of appropriate positive controls clearly showed a complete absence of TUNEL staining in light-exposed *Arvicanthis*, indicating that apoptotic pathways are not activated. Furthermore, light microscopy is perfectly satisfactory for providing a general picture of the extent and site of damage for most purposes (and was adequate for alternative forms of induced RD: see below). To see whether functional approaches might reveal lesions undetectable by structural examination, we also recorded ERG responses of *Arvicanthis* previously exposed to light. In 1966, Noell *et al.* already used ERG to evaluate functional deficit after light exposure in rats (Noell et al., 1966) and found that both a- and b- waves were drastically reduced after exposure. In our study, no significant functional impairment was seen in retinas of exposed *Arvicanthis*. As ERG allows early detection of retinal damage (Ben-Shlomo et al., 2005), it is unlikely that functional evaluation performed at later stages would have led to different results. Also, it is risky to correlate ERG responses with visual capacities (Nagy et al., 2008). Therefore, even if no structural or functional damage of *Arvicanthis* retina has been demonstrated after light exposure, we cannot conclude formerly that visual capacities of *Arvicanthis* are not impaired after light exposure, and use of carefully designed visually-based behavioural tests are necessary to fully answer this question.

Arvicanthis could be particularly resistant to light damage. This may be related to its natural ecology, as it lives in semi-arid sub-tropical regions and forages during daytime. *Animals* active in high ambient light conditions should probably have evolved protective mechanisms. This relative resistance could be due to its particular ocular anatomy, general mechanisms within the eye or local mechanisms at the level of retina. *Arvicanthis* has a different corneal curvature (observation made when adjusting the external lens necessary for SLO examination), and hence the amount of light entering the eye might be reduced. Optical characteristics of cornea and lens could decrease the amount of light received by the retina or block the passage of particular wavelengths (Boettner, 1962). Lenses of many diurnal vertebrates possess UV light filtering characteristics, an adaptation to the potential damaging levels of short wavelength radiation (Zigman, 1989). This aspect could be tested by measuring the transmission index of these structures.

Resistance of *Arvicanthis* retina could also be due to particularities at the level of the retina. The cone to rod ratio could be one of the reasons: due to the large number of cones, maybe spectrogram and intensities of light should be adjusted for this particular species. Also, it has been demonstrated that light damage occurs via a rhodopsin-dependent mechanism (Grimm et al., 2000). The high number of cones in the *Arvicanthis* retina necessarily leads to a lower number of rods and hence rhodopsin, and could tend to protect the tissue. Also, it is known that phagocytosis protects from light-induced damage by clearing free radicals and cellular debris (Winkler, 2008). It has recently been seen that constant light rapidly induces a more intense cone shedding rate in *Arvicanthis* (Bobu and Hicks, 2009). *Arvicanthis* may possess higher levels of specific factors known to protect retinal PR from light-induced apoptosis, such as stress and sex hormones (O'Steen, 1980; O'Steen and Donnelly, 1982), growth hormones/cytokines (Faktorovich et al., 1990; LaVail et al., 1992) and anti-oxidants (Organisciak et al., 1985; Organisciak et al., 1992; Ranchon et al., 2001).

Natural protection against light damage in *Arvicanthis* retina appears as a plausible interpretation to explain the outcome of our studies compared to the numerous published studies showing degeneration in rats and mice. However, we can also reverse the question and wonder whether light-induced retinal damage would actually be very specific to some animal strains or to animals reared in controlled conditions. Excessive exposure to visible light causes photochemical lesions in zebrafish (Vihtelic et al., 2006), mice (Hao et al., 2002), rats (de Raad et al., 1996), rabbits (Hoppeler et al., 1988) or monkeys (Sykes et al., 1981). However, tested animals all need to be examined in particular conditions to show clear retinal damage after exposure. Indeed, the work of several laboratories, especially those of LaVail, Katz, Organisciak and Remé, has led to the realisation that phototoxicity is a complicated pathological phenomenon implicating multiple signalling mechanisms depending on parameters such as light intensity, duration of exposure, spectral composition, daily timing of exposure, recent light history, genetic susceptibility, regional factors and species. Notably from the studies of Remé's group, it is apparent that at least two forms of cell death can be triggered by light exposure, one rhodopsin- and AP-1-dependent, the other rhodopsin-dependent but AP-1 independent (Reme, 2005; Wenzel et al., 2005).

Eye pigmentation is a critical factor, as albino animals raised in constant light or bright cyclic light show greater damage than pigmented animals (Rapp and Williams, 1980; Williams et al., 1985). This is due to the light absorbing and free radical scavenging properties of melanin in pigmented RPE. Hence pigmented animals are rarely used, even if it has been reported that the same damage observed in albino strains can be found in pigmented

animals upon increasing intensity or duration of exposure (Williams et al., 1985). Also, the extent of damage differs among inbred strains, implying that modifier genes are able to regulate the processes that result in damage (LaVail et al., 1987b; LaVail et al., 1987a). The amount of bleachable rhodopsin available during light exposure, determined by the rate of rhodopsin regeneration after bleaching, is a major factor influencing susceptibility to light damage (Wenzel et al., 2005). Therefore, mouse strains with slow metabolic rhodopsin regeneration rates are more resistant to light damage than mouse strains with fast regeneration kinetics (Grimm et al., 2001). Indeed, polymorphisms in the visual cycle retinal isomerase RPE65 generate mice strains which have slowed rhodopsin regeneration kinetics and greater resistance to light damage (Wenzel et al., 2001). Our group sequenced *Arvicanthis* RPE65 (M.P. Felder, unpublished data) and found only the normal Leu-450 form, so the increased resistance is not due to visual cycle differences.

Light-induced damage depends highly on experimental parameters such as light intensity, continuity of the light source (Organisciak et al., 1989) or time of exposure relative to the light cycle (Organisciak et al., 2000). Also, the pre-exposure history is a very important factor to take into account (Penn and Anderson, 1987; Penn et al., 1987). Light experience of individual animals can affect their sensitivity to phototoxicity; light of 130-270 lux above the light intensity under which they were raised has been reported to be near the threshold of retinal damage in some individual albino rats according to histologic, morphometric, and electrophysiologic evidence (Semple-Rowland and Dawson, 1987). The ensemble of these studies suggests that light damage effects are highly context specific. Hence, we can wonder to what extent light-induced RD is involved in human retinal health, a (usually) pigmented diurnal species active in high ambient light levels. The role of photic lesions in the aetiology of human retinal diseases such as AMD remains controversial: epidemiological studies have failed to establish a link between light exposure and retinal breakdown (Delcourt et al., 2001; Wang et al., 2003; Tomany et al., 2004; Paskowitz et al., 2006). However, these studies require re-examination following identification of a high susceptibility locus (the complement factor H gene) (Haddad et al., 2006) which might bias sampling groups. Aggression by light could be an additive risk factor in some forms of inherited RD (e.g. Stargardt's disease (Radu et al., 2004)). To this extent, the difficulty of inducing light damage in *Arvicanthis* could actually be considered as an argument in favour of *Arvicanthis* as a good model for human retina.

1.3. *Arvicanthis* and the MNU Model

Although damage was difficult to induce in *Arvicanthis* retina, it was nevertheless achieved when animals were injected with either 150 mg/kg or 100 m/kg MNU doses. Several interesting aspects derive from these experiments.

As for other species in which MNU has been used (Tsubura et al., 2003), we observed on histological sections and OCT images that the degeneration was restricted to the PR layer. Degeneration of PR is progressive but INL and GCL integrity remains structurally normal. This apparent specificity may be due to the high metabolic activity of PR, with a turnover of OS within 10 days rendering them highly sensitive to DNA intercalating agents. Additionally, proximity of the PR to the choroidal vascularisation, and therefore to the release site of MNU, may play a role. Although the retina is also irrigated by another vessel system, the retinal circulation at the level of the nerve fiber layer, the blood flow is much less than that of choroidal circulation (Sugiyama et al., 1999).

One of the most interesting aspects of our results is the clear temporal and spatial segregation of pathological responses of the two PR types: rod degeneration is seen at early stages, and is then followed by cone breakdown. Such a sequence of events is seen in many RD models, such as the rd1 mouse in which initial rapid rod death is followed by a second slower decline in cone survival (Carter-Dawson et al., 1978; Jimenez et al., 1996). It has also been documented in human RP, where careful counting of PR numbers reveals that loss of more than 75 % rod OS is necessary before detectable cone loss is seen (Cideciyan et al., 1998). Rod loss is also reported to precede cone loss in AMD, where methodical counting of PR in the perifoveal ring reveals significant rod disappearance prior to cone death (Curcio et al., 1996). Secondary cone loss is also seen in animal models in which degeneration is induced by light damage (Krebs et al., 2009). Secondary cone death is proposed to be either due to deprivation of essential neurotrophic factors, such as “rod derived cone viability factor” (Mohand-Said et al., 1998; Leveillard et al., 2004) or insulin (Punzo et al., 2009); or to “poisoning” by oxidative stress (Shen et al., 2005; Komeima et al., 2006) or iron (Rogers et al., 2007). However, in all these cases rod and cone demise still occur as intermingled events, making it very difficult to analyse potential specific pathogenic pathways in either cell type. To the best of our knowledge, a practical, reproducible mammalian model of retinal degeneration permitting detailed longitudinal analysis of rod and cone fate does not exist. The MNU-induced RD *Arvicanthis* model, in conjunction with laser capture micro-dissection techniques and hybridisation against relevant gene arrays should yield very valuable data.

Topographical mapping of structural damage across the entire retina showed that the degeneration was not uniform, with damage appearing early in the superior compared to the inferior hemisphere, and the superior hemisphere being significantly more damaged compared to inferior hemisphere. This regional variation is probably not due to intrinsic differences as their distribution is homogenous over the retina, but it could be due to several factors. Possibly choroidal and retinal vessels are distributed in a non-uniform manner across the *Arvicanthis* retina. But SLO examination showed that it was not the case. A second hypothesis could be that light aggression constitutes a requisite co-factor of the pathogenic process. Some studies have suggested that MNU-induced damage requires secondary insults such as light, to amplify the lesions (Smith et al., 1988). Photons reaching the retina come mainly from light reflected from the ground, and therefore impact on the superior hemisphere. Interestingly, the onset of apoptosis occurred roughly simultaneously in rods and cones in the superior hemisphere, while it was distinctly delayed in cones in the inferior retina. Based on these observations, it can be speculated that MNU treatment on its own is more specifically toxic to rods, while a "double hit" of MNU poisoning and light damage is detrimental to both populations. In addition, cone loss was almost total in retinas of MNU-injected rats, while many such cells survived in *Arvicanthis*. Therefore, intrinsic differences cannot entirely account for the resistance of *Arvicanthis* retina to structural damage.

The impact of rod and cone breakdown on the global electrical activity of retina in response to light stimuli is clearly seen by ERG analysis. It is interesting to see that at late stages of degeneration, responses in both scotopic and photopic conditions are reduced. The dramatic decrease of ERG response amplitudes at high intensities show that, although cones appear structurally spared relative to rods, there is a severe functional deficit. As ERG recordings correspond to global electrical activity, decreased responses can be linked to degeneration of many cell types within the retina. We cannot exclude that cells in the inner retina (bipolar, amacrine cells or even RGCs) could be affected by MNU. However, we did not see any structural changes in the inner retina, neither by histology nor by OCT imaging. However, other types of changes not visible with these techniques could occur. For example, it has been shown that melanopsin expression in ipRGCs is down regulated after MNU injection (Wan et al., 2006). This down-regulation is an indirect effect of PR degeneration. By analogy, electrophysiological properties of some IR cells could be down- or up-regulated after PR degeneration induced by MNU.

We mentioned above the difficulty of inducing light damage in *Arvicanthis* and hypothesized it could be due to endogenous protection mechanisms in accordance with its

natural ecology. However, the relative resistance to MNU suggests a general robustness to insults. Indeed MNU used at doses published as inducing damage in other species were completely ineffective in *Arvicanthis*. The dose had to be increased by 50-100 % to induce any damage. Furthermore, even at high doses apoptotic nuclei were not observed before 11 d.p.i. By contrast, in other species apoptotic nuclei are detected very rapidly and at 7 d.p.i. virtually the entire ONL is gone (Yang et al., 2005) (in our study, the rat ONL was totally gone after 9 d.p.i of a 75 mg/kg MNU injection). Interestingly, this signifies that not only cones disappear later in *Arvicanthis* than in the rat, but that rods also have slower progression of damage. *Arvicanthis* retina hence expresses a high resistance to two different type of stress in which underlying pathogenic mechanisms are different. Light exposure induces retinal degeneration by mechanisms likely to involve oxidative stress (Gordon et al., 2002). Excessive light stimulates shedding of rod outer segments that are phagocytosed by RPE cells in a process that generates an excess of reactive oxygen and nitrogen species (Miceli et al., 1994; Tate et al., 1995; Sun et al., 2006). Intense light exposure induces increased expression of the DNA polymerase β base excision repair enzyme (Gordon et al., 2002). In contrast, MNU is a S_N1 type alkylating agent which reacts with both oxygen and nitrogen in DNA to form 3 major adducts: 7-methylguanine, O^6-methylguanine, and 3-methyladenine. A recent study showed that MNU-induced retinal cytotoxicity is likely to be induced by O^6-methylguanine. Characterization of the molecular mechanisms underlying retinal resistance in *Arvicanthis* might shed light on important strategies for neuroprotection in human RD.

2. Rods, Cones and ipRGCs: the Winning Combination for an Ideal Photic Entrainment?

It has been clearly shown by Hattar et *al.* that rods, cones and melanopsin expressing ipRGCs account for all NIF functions (Hattar et al., 2003). The role of ipRGCs in the generation of some of these functions has also been established (Panda et al., 2002). But the contribution of cones and rods for these same roles is still under discussion, and some studies suggest that rods and cones do not play a role (Foster et al., 1991; Freedman et al., 1999) while others show that mice with loss of all or one type of PR show impairment of NIF functions (Ebihara and Tsuji, 1980; Dkhissi-Benyahya et al., 2007).

In our study control and MNU-treated rats with virtually no PR were tested for their ability to photoentrain. Animals were exposed to successive jet-lags of 6 h associated with a decrease in light intensity. It is first interesting to note that all control animals were able to synchronize their rhythmic activity to all LD cycles even at very low light intensity (~ 1 lux). At such very low intensities, cones and ipRGCs are not activated by photons (Berson et al., 2002), and only rods can detect and respond to such stimuli. Therefore, we propose that at such low intensities rods are responsable for transmitting photic signals for synchronization of locomotor activity. This is confirmed by the fact that MNU-treated animals, which possess virtually no rods, do not entrain at low intensities. Our proposed model is that when light levels are sufficiently high, the ipRGC contribution to photoentrainment is predominant. This is confirmed by the fact that MNU-treated animals, which still possess melanopsinergic RGC albeit less than controls, do not show an impaired ability to photoentrain at high intensity. The data are consistent with rods accounting for photoentrainment in dim light. Whether MNU-treated animals fail to detect light at low intensities, or do not detect the transition between the low intensity white light phase and the red, very low intensity light, phase remains to be determined. Whether impaired photoentrainment is due to perturbation of the retinal circadian clock, or from a decoupling of the SCN from the retinal clock after PR destruction, cannot be answered.

Other studies have shown that mice lacking melanopsin show a reduction of the amplitude of phase shift when a light pulse is given (Panda et al., 2002). Light pulses are commonly given in DD at a particular moment of the active phase of the animal. In these

precise conditions, melanopsin should also play an important role in the photic resetting of the circadian clock.

Although the MNU model is not as "clean" as transgenic models to study the contribution of rod, cone and ipRGCs on NIF functions, the advantages are that induction of retinal degeneration occurs during adulthood, hence avoiding synaptic remodelling and compensatory mechanisms that can occur in transgenic models (Cho et al., 2007). The recent models using either conjugation of an anti-melanopsin antibody to saporin (Goz et al., 2008), introduction of a gene encoding attenuated diphtheria toxin A subunit (Guler et al., 2008) or the use of the Cre-inducible diphtheria toxin receptor (Hatori et al., 2008) are not prone to the above mentioned drawbacks, but they were used to eliminate ipRGCs and not rods and cones. These latter approaches are all technically demanding, whereas MNU injection requires no particular expertise or equipment. Importantly, the type of damage induced by MNU is more likely to represent what happens in clinic during retinal degeneration (first part of the General Discussion section) than engineered animal models with a particular type of cell damage. Last, circadian photosensitivity has been shown to vary between two strains of rd mice, suggesting that this sensitivity is under genetic control (Yoshimura et al., 2002), another issue encountered when working with genetic models and that we can overcome with a model of induced degeneration.

3. NIF Functions-Based Tests: Another Way to Evaluate Retinal Damage?

Vision is considered the most vital sense in humans, and the most debilitating handicap of people suffering ocular damage is loss of visual function. Hence, in research, behavioural tests used to assess retinal integrity or evaluate the extent of retinal damage are based on visual capacities and visual discrimination ability. As the visual system is responsable for accomplishing many tasks with a wide range of complexity, ranging from tracking moving targets to discerning spatial details and colours in the objects being viewed, there is not one single behavioural test able to serve as a comprehensive test of visual function. Maze-based tests like the Morris water maze or eight-arm radial maze have been used to characterize visually guided behaviour (Ammassari-Teule et al., 1993; Paylor et al., 1994; Owen et al., 1997). In these tests, rodents are trained to move toward a visual stimulus and are tested following manipulation of a stimulus property. Other tests, such as visual cliff and elevated plus maze, are based on the reluctance for heights. The cued fear conditioning takes place in response to a sensory cue in which a sensory stimulus, that can be light, is made to precede an aversive stimulus (Bolivar et al., 2001). In the visual placing test, the animal is lifted by the base of the tail to a height of approximately 15 cm and above ground and lowered to a wire-mesh grid within 1/2 to 1 s, decelerating as the grid is approached. Scoring is based on the distance of the animal's nose from the grid before extending the forelimbs toward it (Stewart and Chauhan, 1995). To properly evaluate visual function of an animal using behavioural tests in optimal conditions, it is necessary that the motor apparatus remains intact and functional, and that interactions between the visual system and other physiological systems are normal (Clapcote et al., 2005).

Visual ability-based tests have been widely used to evaluate the effect of retinal damage or the ability of a therapeutic agent to help recover normal retinal function (McGill et al., 2004a; McGill et al., 2004b; Hoelter et al., 2008). However, image formation, as mentioned in the Introduction section, is not the only function of the eye. Retina also functions to sense light and transmit the light-dark signal to dedicated structures. Therefore RD can entrain perturbations beyond image formation impairment, and blind people can suffer from troubles other than direct blindness. For example, some blind persons present disrupted rhythms of melatonin secretion (Nakagawa et al., 1992; Sack et al., 1992; Czeisler et al., 1995), cortisol synthesis (Krieger and Rizzo, 1971; Bodenheimer et al., 1973), core body temperature (Stavosky et al., 1980) and the sleep/wake cycle (Miles and Wilson, 1977;

Tabandeh et al., 1998; Skene and Arendt, 2007). These examples show that in some cases, visual impairment is associated with disruption of NIF functions.

In our study, we showed that rats with virtually no remaining PR, and presumably no visual capacities, could still photoentrain at high and moderate light intensities. Hence, as the contribution of each type of PR to these two functions might differ depending on the environmental conditions, visual damage does maybe not necessarily mean deficits in NIF functions. Moreover, the two functions do not feed forward to the same superior structures: lateral geniculate nucleus, intergeniculate leaflet and visual cortex for the image forming system; and OPN and EW for PLR, SCN and pineal gland for circadian rhythms. Depending on the extent of ocular damage, an eye can sense light without sight.

A natural example of this situation is the case for the subcutaneous minute eye of the blind mole-rat *Spalax ehrenbergi*. This animal lack external eyes but possesses paired rudimentary ocular structures found embedded in the Harderian glands and covered by the skin and fur of the head. The ganglion cell and PR layers are relatively thin, and there is a very small unmyelinated optic nerve containing approximately 900 to 1000 fibres (Sanyal et al., 1990; Bronchti et al., 1991; Cooper et al., 1993). The animal has lost all image processing capability and yet is able to entrain its daily locomotor activity rhythms to light/dark cycles and some individuals also show entrainment to daily cycles of ambient temperature (Goldman et al., 1997). A study by Hannibal *et al.* has shown that its retina expresses melanopsin in RGCs projecting to the SCN (Hannibal et al., 2002).

In visually handicapped humans it is difficult to evaluate the impairment of NIF functions on the basis of direct interrogation since NIF perception, in contrast to vision, is mostly unconscious. Even though patients may be annoyed by impairment to photoentrain, some are not aware of the troubles they endure and of the strategies they build to compensate the difficulties. Some blind people with free-running rhythms give up trying to sleep at night; instead, they sleep “in tune” with their body clock on a non-24-h sleep/wake schedule. Because they synchronise their sleep with other body rhythms, they presumably have less insomnia and sleep deprivation (Sack and Lewy, 2001).

In the clinic, careful evaluation of the integrity of NIF functions would be essential to diagnose the extent of retinal damage, but also complement decisions made only on the basis of visual functions. For example, measures to limit trauma and the further deterioration of useful sight would be prudent for patients in whom the pathway of light input to the SCN is intact. Enucleation after a trauma, sometimes performed for cosmetic reasons or to alleviate residual pain, should be reconsidered given the consequent disruption of photic entrainment of

the circadian pacemaker. Before bilateral enucleation is performed, a comprehensive evaluation of residual visual function, including light-induced melatonin suppression, regulation of circadian timing, masking behaviour, and the PLR should be done. This also might help to assist in identifying blind patients at risk of chronic, recurring insomnia and other symptoms associated with the loss of circadian synchronization to the 24 h day. Third, as visual and NIF functions depend on two different pathways, combination of such evaluations with common visual tests might help to locate the damaged structures and even the cell types. Finally, methods currently under investigation to cure blindness should consider the re-establishment of NIF functions in the case of a completely dysfunctional eye. The artificial retina project for example is based on the study of electrophysiological properties of the retina during detection of shapes and colours but does it take into account the light sensing property of melanopsin cells? Using a combination of tests based on both visual and NIF abilities, the global consequences of retinal damage on quality of life could be evaluated.

In research studies, tests based not on visual but on light/dark signal sensing capacity could also be used to evaluate retinal damage. Ability for PLR, photoentrainment and phase shifting of circadian rhythms could be evaluated. In 2008, Drouyer *et al.* showed that experimentally induced glaucoma in rats leads to alterations in the circadian timing system and particularly that glaucomatous animals require more time to adjust to shifted LD cycles and show significantly greater variability in activity onset in comparison with normal rats (Drouyer et al., 2008). This parameter could hence be used to evaluate the extent of the visual impairment correlated to the RGC loss induced by glaucoma in rodents. Also optokinetic nystagmus (OKN) reflexes are often tested. OKN is elicited by a moving stimulus, and consists of tracking eye movements with a slow component in the direction of stimulus movement and an interleaved rapid component in the opposite direction. Like the PLR, OKN also uses pathways that include a specific minor set of RGCs (Kato et al., 1992) and a set of pretectal and accessory optic terminal nuclei.

Hence evaluating NIF functions could be of value to assess retinal integrity or evaluate extent of RD, and provide valuable information on possible effects on quality of life. However, even though image forming and NIF functions are distinct in their pathways and expression, they actually overlap and analysis of two kinds of tests might be difficult to interpret independently. First, at the experimental level, visual and NIF functions are difficult to separate. For example, in an animal with a defect in PLR, the pupil will not be able to constrict compared to an animal with no defect. At high light intensities, irradiance at the

retinal level will be much higher than that of normal animals. The animal could subsequently be handicapped by glare, and if submitted to a vision-based behavioural test will maybe not perform optimally. The same problem might be encountered if the pupil becomes fully constricted and visual cues can not be seen. In other words, a low score on these tasks does not necessarily reflect impairment of the visual pathway, but rather a problem with a NIF function. In the same manner, we can postulate that an animal with defective photic entrainment will have troubles with learning tasks, since the time at which tests are conducted will not necessarily correspond either to that of control animals or even to other lesioned animals. Similar issues could be faced with photoentrainment protocols, in which it is difficult to compare photoentrainment abilities of an animal with a defect in the PLR and control animals, as the level of retinal irradiance will dictate the ability to photoentrain. This problem could be overcome with the use of pupil dilators with which control and experimented animals will have the same amount of light reaching the retina. However, pupil dilators have a limited action time course and application to a large group of animals for actimetry experiments generally lasting over long periods of time is not so straight forward. For the same reasons, the cell types activated by light entering eyes through fully open pupils might not be similar to those in controls. Cones and ipRGCs need relatively high light intensities for activation and may be preferentially stimulated in animals with defective PLR, whereas control animals will only have their rods activated. The contrary situation can occur if pupils are less open than normal leading to limited entry of light and activation of rods only. Finally, animals whose photoentrainment ability is impaired might have a disrupted circadian retinal clock which could impinge on processes essential for good image formation, and also cognitive functions necessary in visual tests.

Second, pathways mediating image forming and NIF processes might share similarities. For example, lesions in the IGL, a structure a priori dedicated to visual function, have consequences on circadian rhythms (Edelstein and Amir, 1999; Redlin et al., 1999; Morin and Pace, 2002). Also, visual cortex lesions increase the masking response to light, another NIF function (Redlin et al., 2003). Also for photoreceptive cells in which segregation ostensibly appears clear between those dedicated to image-forming (rod and cone) and NIF (ipRGCs), the reality is more complicated. It has been shown that melanopsin regulates visual processing in the mouse retina (Barnard et al., 2006), probably due to the fact that ipRGCs receive rod and cone synaptic input (Guler et al., 2008) and may provide the brain with different information in series, separated by complex spatial and temporal dynamics and having the ability to adapt to both light and darkness. The same study showed that ipRGCs

can also influence retinal physiology, possibly changing the functional properties of retinal circuitry. Even though ipRGCs project mainly to the SCN (Gooley et al., 2001), sensitive mapping of their projections by targeting tau-lacZ to the melanopsin gene locus in mice have revealed that ipRGC project also to the dorsal division of the lateral geniculate nucleus (LGN) and the superior colliculus (SC), both structures involved in image forming vision (Hattar et al., 2006) (Hattar, Kumar et al. 2006). These findings suggest that in addition to their known role in regulating visual reflexes, ipRGCs may play an as yet unknown role in shaping conscious visual perception. Interestingly, Dacey *et al.* found that in primates, ipRGCs could be retrolabeled by injecting fluorescent tracers into the LGN, and that these "giant" melanopsin-expressing ganglion cells display colour opponent receptive fields (Dacey et al., 2005). In 2007, Zaidi *et al.* showed that patients with neither rods nor cones showed sensitivity and conscious perception of SW light (Zaidi et al., 2007).

Taking all these considerations into account, NIF tests could allow valuable additional insights into retinal damage. However, their use in assessing integrity of retinal function or evaluating the extent of retinal damage predicates great care in experimental design, for example choice of stimulus strength.

CONCLUSIONS

AND

PERSPECTIVES

The work presented in this manuscript brings new data regarding retinal degeneration and their structural, functional and behavioural consequences:

1. Further characterization of the *Arvicanthis* retina, particularly at the functional level through the use of ERG approach;
2. The relative resistance of the *Arvicanthis* retina to RD compared to rats and mice;
3. The establishment of a model for the study of induced cone degeneration allowing comparison of time course of degeneration of the two types of PR within the same retina;
4. Structural and functional characterization of the effects of MNU on the *Arvicanthis* retina;
5. Evidence of an impairment of the photoentrainment in rats with an MNU-degenerated retina.

In the first part of our work where we compared the ERG responses of *Arvicanthis* with those of rats and mice, we saw several differences in multiple conditions. To help understand *Arvicanthis* ERG responses and the contribution of cone system on the global electrical activity of the retina, a histological study of *Arvicanthis* retina should be further conducted. Analysis of the wiring connections between cones and cone bipolar cells would be useful. Also, the proposition of cone bipolar cells would be a value of much interest. It will notably help to understand the high CFF value found in *Arvicanthis*.

The contribution of a high cone ratio in the retina of *Arvicanthis* should also be investigated at the level of visual ability with the use of behavioural tests (based on colour discrimination for example).

During our work, we notice that *Arvicanthis* was particularly resistant to retinal damage induced by light as well as that induced by MNU. In *Arvicanthis*, analysis of the expression of factors susceptible to protect retinas from multiple types of damage, as neurotrophic factors for example will help understanding how the retina of *Arvicanthis* is protected and what kind of strategies could be use to protect PR from degenerating.

We established a complete structural, physiological and behavioural analysis of MNU effects on high rod and high cone retina rodents. Screening neuroprotective strategies requires reproducible, convenient, cost-effective experimental models. The MNU model could serve to evaluate the therapeutic value of potential retinoprotectants. Many

pharmacological substances are known to slow or protect rods against degeneration, but similar data for cone survival are very limited. Our experiments argue that *Arvicanthis* is well suited for providing such a model for cone pathogenesis.

MNU model has certain drawbacks that could be worked on. Injections of MNU can lead to different results, no always reproducible and some MNU-induced animals can have intact retinas while others will have a complete RD. The delivering procedures have to be improved. Also, MNU is a highly toxic chemical and its use has to be done with extreme caution. Its tumorigenic property is not convenient for long term studies as tumours can occur a few months after injection and, in the case of photoentrainment studies, locomotor activity might be impaired or animals might even die after a few months. Maybe the problem of toxicity could be overcome by using lower dose of MNU combined with another type of stress. Light might be crucial to exacerbate pre-existent damage. Maybe by combining injection of a low dose of MNU with high intensity light exposure, RD could be achieved with no risk of lethality problems. With this approach, light would only constitute a helping factor for MNU-induced effect, and this situation, would be closer to what is found in humans.

Finally, we showed that MNU-treated rats were impaired in their ability to photoentrain to LD cycles of low intensities. The ability of the same animals to phase-shift after a light pulse of different intensities will also be an important data to obtain. Also, a confirmation of the perturbation of photic input at the retina level could be done by evaluating the PLR of these same animals or dosing their plasmatic melatonin over a 24-h period. Finally, our results show unequivocally that MNU injections in *Arvicanthis* lead to initial rod degeneration and secondary cone loss (at least in the inferior hemisphere). Therefore it would be interesting to check for photoentrainment ability under conditions in which only functional cones remain to analyse in more detail the role of cones in photoentrainment.

REFERENCES

A

Adler R, Curcio C, Hicks D, Price D, Wong F (1999) Cell death in age-related macular degeneration. Mol Vis 5:31.

Ahnelt PK, Kolb H (2000) The mammalian photoreceptor mosaic-adaptive design. Prog Retin Eye Res 19:711-777.

al-Ubaidi MR, Font RL, Quiambao AB, Keener MJ, Liou GI, Overbeek PA, Baehr W (1992) Bilateral retinal and brain tumors in transgenic mice expressing simian virus 40 large T antigen under control of the human interphotoreceptor retinoid-binding protein promoter. J Cell Biol 119:1681-1687.

Alkemade PP (1968) Phenothiazine-retinopathy. Ophthalmologica 155:70-76.

Allikmets R, Shroyer NF, Singh N, Seddon JM, Lewis RA, Bernstein PS, Peiffer A, Zabriskie NA, Li Y, Hutchinson A, Dean M, Lupski JR, Leppert M (1997) Mutation of the Stargardt disease gene (ABCR) in age-related macular degeneration. Science 277:1805-1807.

Ambati J, Ambati BK, Yoo SH, Ianchulev S, Adamis AP (2003) Age-related macular degeneration: etiology, pathogenesis, and therapeutic strategies. Surv Ophthalmol 48:257-293.

Ammassari-Teule M, Hoffmann HJ, Rossi-Arnaud C (1993) Learning in inbred mice: strain-specific abilities across three radial maze problems. Behav Genet 23:405-412.

B

Babel J, Rey P, Stangos N, Meyer JJ, Guggenheim P (1969) The functional examination of the macular and perimacular region with the aid of flicker-fusion thresholds. Doc Ophthalmol 26:248-256.

Barlow HB, Levick WR (1969) Three factors limiting the reliable detection of light by retinal ganglion cells of the cat. J Physiol 200:1-24.

Barnard AR, Hattar S, Hankins MW, Lucas RJ (2006) Melanopsin regulates visual processing in the mouse retina. Curr Biol 16:389-395.

Bellhorn RW, Bellhorn M, Friedman AH, Henkind P (1973) Urethan-induced retinopathy in pigmented rats. Invest Ophthalmol 12:65-76.

Ben-Shlomo G, Bakalash S, Lambrou GN, Latour E, Dawson WW, Schwartz M, Ofri R (2005) Pattern electroretinography in a rat model of ocular hypertension: functional evidence for early detection of inner retinal damage. Exp Eye Res 81:340-349.

Bennett J (2000) Gene therapy for retinitis pigmentosa. Curr Opin Mol Ther 2:420-425.

Bernard DJ, Maurizis JC, Chassagne J, Chollet P, Plagne R (1986) N-nitroso-N-methylurea-induced mammary carcinogenesis: effect of prolactin on expression of Ia antigen by tumor cells. J Natl Cancer Inst 76:1237-1242.

Berson DM (2003) Strange vision: ganglion cells as circadian photoreceptors. Trends Neurosci 26:314-320.

Berson DM, Dunn FA, Takao M (2002) Phototransduction by retinal ganglion cells that set the circadian clock. Science 295:1070-1073.

Bhatti MT (2006) Retinitis pigmentosa, pigmentary retinopathies, and neurologic diseases. Curr Neurol Neurosci Rep 6:403-413.

Biel M, Seeliger M, Pfeifer A, Kohler K, Gerstner A, Ludwig A, Jaissle G, Fauser S, Zrenner E, Hofmann F (1999) Selective loss of cone function in mice lacking the cyclic nucleotide-gated channel CNG3. Proc Natl Acad Sci U S A 96:7553-7557.

Birch DG, Jacobs GH (1980) Light-induced damage to photopic and scotopic mechanisms in the rat depends on rearing conditions. Exp Neurol 68:269-283.

Bloomfield SA, Dacheux RF (2001) Rod vision: pathways and processing in the mammalian retina. Prog Retin Eye Res 20:351-384.

Bobu C, Hicks D (2009) Retinal Photoreceptor Phagocytosis in a Diurnal Mammal Is Regulated by Circadian Clocks and Ambient Lighting. Invest Ophthalmol Vis Sci.

Bobu C, Craft CM, Masson-Pevet M, Hicks D (2006) Photoreceptor organization and rhythmic phagocytosis in the nile rat Arvicanthis ansorgei: a novel diurnal rodent model for the study of cone pathophysiology. Invest Ophthalmol Vis Sci 47:3109-3118.

Bobu C, Lahmam M, Vuillez P, Ouarour A, Hicks D (2008) Photoreceptor organisation and phenotypic characterization in retinas of two diurnal rodent species: potential use as experimental animal models for human vision research. Vision Res 48:424-432.

Bodenheimer S, Winter JS, Faiman C (1973) Diurnal rhythms of serum gonadotropins, testosterone, estradiol and cortisol in blind men. J Clin Endocrinol Metab 37:472-475.

Boettner EA (1962) Transmission of the ocular media. Inves Ophthal 1:776-783.

Bogenmann E, Lochrie MA, Simon MI (1988) Cone cell-specific genes expressed in retinoblastoma. Science 240:76-78.

Bolivar VJ, Pooler O, Flaherty L (2001) Inbred strain variation in contextual and cued fear conditioning behavior. Mamm Genome 12:651-656.

Bourne MC, Campbell DA, Tansley K (1938) Hereditary Degeneration of the Rat Retina. Br J Ophthalmol 22:613-623.

Bowmaker JK, Dartnall HJ (1980) Visual pigments of rods and cones in a human retina. J Physiol 298:501-511.

Bowmaker JK, Heath LA, Wilkie SE, Hunt DM (1997) Visual pigments and oil droplets from six classes of photoreceptor in the retinas of birds. Vision Res 37:2183-2194.

Braunstein EF (1903) Beitrag zur lehre des intermittierendem lichtreizes der gesuden und kranken. Z Psychol 33:241-288.

Bronchti G, Rado R, Terkel J, Wollberg Z (1991) Retinal projections in the blind mole rat: a WGA-HRP tracing study of a natural degeneration. Brain Res Dev Brain Res 58:159-170.

Bunning E, Moser I (1969) Interference of Moonlight with the Photoperiodic Measurement of Time by Plants, and Their Adaptive Reaction. Proc Natl Acad Sci U S A 62:1018-1022.

Bush RA, Sieving PA (1994) A proximal retinal component in the primate photopic ERG a-wave. Invest Ophthalmol Vis Sci 35:635-645.

C

Cajal SRY (1892) El nuevo concepto de la histologia de los centros nerviosos. Rev Cienc Méd Barcelona 18:457-476.

Cameron DA, Carney LH (2000) Cell mosaic patterns in the native and regenerated inner retina of zebrafish: implications for retinal assembly. J Comp Neurol 416:356-367.

Carter-Dawson LD, LaVail MM (1979a) Rods and cones in the mouse retina. I. Structural analysis using light and electron microscopy. J Comp Neurol 188:245-262.

Carter-Dawson LD, LaVail MM (1979b) Rods and cones in the mouse retina. II. Autoradiographic analysis of cell generation using tritiated thymidine. J Comp Neurol 188:263-272.

Carter-Dawson LD, LaVail MM, Sidman RL (1978) Differential effect of the rd
mutation on rods and cones in the mouse retina. Invest Ophthalmol Vis Sci 17:489-498.

Challet E, Pitrosky B, Sicard B, Malan A, Pevet P (2002) Circadian organization in a diurnal rodent, Arvicanthis ansorgei Thomas 1910: chronotypes, responses to constant lighting conditions, and photoperiodic changes. J Biol Rhythms 17:52-64.

Chang B, Hawes NL, Hurd RE, Davisson MT, Nusinowitz S, Heckenlively JR (2002) Retinal degeneration mutants in the mouse. Vision Res 42:517-525.

Cho JH, Klein WH, Tsai MJ (2007) Compensational regulation of bHLH transcription factors in the postnatal development of BETA2/NeuroD1-null retina. Mech Dev 124:543-550.

Chong NH, Keonin J, Luthert PJ, Frennesson CI, Weingeist DM, Wolf RL, Mullins RF, Hageman GS (2005) Decreased thickness and integrity of the macular elastic layer of Bruch's membrane correspond to the distribution of lesions associated with age-related macular degeneration. Am J Pathol 166:241-251.

Cibis GW, Morey M, Harris DJ (1980) Dominantly inherited macular dystrophy with flecks (Stargardt). Arch Ophthalmol 98:1785-1789.

Cicerone CM (1976) Cones survive rods in the light-damaged eye of the albino rat. Science 194:1183-1185.

Cideciyan AV, Hood DC, Huang Y, Banin E, Li ZY, Stone EM, Milam AH, Jacobson SG (1998) Disease sequence from mutant rhodopsin allele to rod and cone photoreceptor degeneration in man. Proc Natl Acad Sci U S A 95:7103-7108.

Clapcote SJ, Lazar NL, Bechard AR, Roder JC (2005) Effects of the rd1 mutation and host strain on hippocampal learning in mice. Behav Genet 35:591-601.

Coleman JE, Zhang Y, Brown GA, Semple-Rowland SL (2004) Cone cell survival and downregulation of GCAP1 protein in the retinas of GC1 knockout mice. Invest Ophthalmol Vis Sci 45:3397-3403.

Cooper HM, Herbin M, Nevo E (1993) Visual system of a naturally microphthalmic mammal: the blind mole rat, Spalax ehrenbergi. J Comp Neurol 328:313-350.

Cortina MS, Gordon WC, Lukiw WJ, Bazan NG (2003) Light-induced photoreceptor damage triggers DNA repair: differential fate of rods and cones. Adv Exp Med Biol 533:229-240.

Curcio CA, Medeiros NE, Millican CL (1996) Photoreceptor loss in age-related macular degeneration. Invest Ophthalmol Vis Sci 37:1236-1249.

Curcio CA, Owsley C, Jackson GR (2000) Spare the rods, save the cones in aging and age-

related maculopathy. Invest Ophthalmol Vis Sci 41:2015-2018.

Curcio CA, Sloan KR, Kalina RE, Hendrickson AE (1990) Human photoreceptor topography. J Comp Neurol 292:497-523.

Curcio CA, Millican CL, Allen KA, Kalina RE (1993) Aging of the human photoreceptor mosaic: evidence for selective vulnerability of rods in central retina. Invest Ophthalmol Vis Sci 34:3278-3296.

Curcio CA, Allen KA, Sloan KR, Lerea CL, Hurley JB, Klock IB, Milam AH (1991) Distribution and morphology of human cone photoreceptors stained with anti-blue opsin. J Comp Neurol 312:610-624.

Czeisler CA, Shanahan TL, Klerman EB, Martens H, Brotman DJ, Emens JS, Klein T, Rizzo JF, 3rd (1995) Suppression of melatonin secretion in some blind patients by exposure to bright light. N Engl J Med 332:6-11.

D

D'Cruz PM, Yasumura D, Weir J, Matthes MT, Abderrahim H, LaVail MM, Vollrath D (2000) Mutation of the receptor tyrosine kinase gene Mertk in the retinal dystrophic RCS rat. Hum Mol Genet 9:645-651.

Dacey DM, Liao HW, Peterson BB, Robinson FR, Smith VC, Pokorny J, Yau KW, Gamlin PD (2005) Melanopsin-expressing ganglion cells in primate retina signal colour and irradiance and project to the LGN. Nature 433:749-754.

Daniele LL, Lillo C, Lyubarsky AL, Nikonov SS, Philp N, Mears AJ, Swaroop A, Williams DS, Pugh EN, Jr. (2005) Cone-like morphological, molecular, and electrophysiological features of the photoreceptors of the Nrl knockout mouse. Invest Ophthalmol Vis Sci 46:2156-2167.

Dardente H, Menet JS, Challet E, Tournier BB, Pevet P, Masson-Pevet M (2004) Daily and circadian expression of neuropeptides in the suprachiasmatic nuclei of nocturnal and diurnal rodents. Brain Res Mol Brain Res 124:143-151.

Das S, Lin D, Jena S, Shi A, Battina S, Hua DH, Allbaugh R, Takemoto DJ (2008) Protection of retinal cells from ischemia by a novel gap junction inhibitor. Biochem Biophys Res Commun 373:504-508.

de Raad S, Szczesny PJ, Munz K, Reme CE (1996) Light damage in the rat retina: glial fibrillary acidic protein accumulates in Muller cells in correlation with photoreceptor damage. Ophthalmic Res 28:99-107.

Delcourt C, Carriere I, Ponton-Sanchez A, Fourrey S, Lacroux A, Papoz L (2001) Light exposure and the risk of age-related macular degeneration: the Pathologies Oculaires Liees a l'Age (POLA) study. Arch Ophthalmol 119:1463-1468.

DeVries SH, Qi X, Smith R, Makous W, Sterling P (2002) Electrical coupling between mammalian cones. Curr Biol 12:1900-1907.

Di Polo A, Farber DB (1995) Rod photoreceptor-specific gene expression in human retinoblastoma cells. Proc Natl Acad Sci U S A 92:4016-4020.

Dkhissi-Benyahya O, Sicard B, Cooper HM (2000) Effects of irradiance and stimulus duration on early gene expression (Fos) in the suprachiasmatic nucleus: temporal summation and reciprocity. J Neurosci 20:7790-7797.

Dkhissi-Benyahya O, Gronfier C, De Vanssay W, Flamant F, Cooper HM (2007) Modeling the role of mid-wavelength cones in circadian responses to light. Neuron 53:677-687.

Doonan F, Donovan M, Cotter TG (2003) Caspase-independent photoreceptor apoptosis in mouse models of retinal degeneration. J Neurosci 23:5723-5731.

Drouyer E, Dkhissi-Benyahya O, Chiquet C, WoldeMussie E, Ruiz G, Wheeler LA, Denis P, Cooper HM (2008) Glaucoma alters the circadian timing system. PLoS ONE 3:e3931.

Ducroz JF, Volobouev V, Granjon L (1998) A molecular perspective on the systematics and evolution of the genus Arvicanthis (Rodentia, Muridae): inferences from complete cytochrome b gene sequences. Mol Phylogenet Evol 10:104-117.

E

Ebihara S, Tsuji K (1980) Entrainment of the circadian activity rhythm to the light cycle: effective light intensity for a Zeitgeber in the retinal degenerate C3H mouse and the normal C57BL mouse. Physiol Behav 24:523-527.

Edelstein K, Amir S (1999) The role of the intergeniculate leaflet in entrainment of circadian rhythms to a skeleton photoperiod. J Neurosci 19:372-380.

F

Faktorovich EG, Steinberg RH, Yasumura D, Matthes MT, LaVail MM (1990) Photoreceptor degeneration in inherited retinal dystrophy delayed by basic fibroblast growth factor. Nature 347:83-86.

Farber DB, Souza DW, Chase DG (1983) Cone visual cell degeneration in ground squirrel retina: disruption of morphology and cyclic nucleotide metabolism by lodoacetic acid. Invest Ophthalmol Vis Sci 24:1236-1249.

Farber DB, Kozak CA, Danciger M (1989) Assignment to mouse chromosomes of candidate genes for the rd mutation. Prog Clin Biol Res 314:143-153.

Fauser S, Luberichs J, Schuttauf F (2002) Genetic animal models for retinal degeneration. Surv Ophthalmol 47:357-367.

Fleisch VC, Schonthaler HB, von Lintig J, Neuhauss SC (2008) Subfunctionalization of a retinoid-binding protein provides evidence for two parallel visual cycles in the cone-dominant zebrafish retina. J Neurosci 28:8208-8216.

Foster RG, Provencio I, Hudson D, Fiske S, De Grip W, Menaker M (1991) Circadian photoreception in the retinally degenerate mouse (rd/rd). J Comp Physiol [A] 169:39-50.

Freedman MS, Lucas RJ, Soni B, von Schantz M, Munoz M, David-Gray Z, Foster R (1999) Regulation of mammalian circadian behavior by non-rod, non-cone, ocular photoreceptors. Science 284:502-504.

Frumkes TE, Eysteinsson T (1987) Suppressive rod-cone interaction in distal vertebrate retina: intracellular records from Xenopus and Necturus. J Neurophysiol 57:1361-1382.

G

Gaillard F, Bonfield S, Gilmour GS, Kuny S, Mema SC, Martin BT, Smale L, Crowder N, Stell WK, Sauve Y (2008) Retinal anatomy and visual performance in a diurnal cone-rich laboratory rodent, the Nile grass rat (Arvicanthis niloticus). J Comp Neurol 510:525-538.

Gehrs KM, Anderson DH, Johnson LV, Hageman GS (2006) Age-related macular degeneration--emerging pathogenetic and therapeutic concepts. Ann Med 38:450-471.

Goldman BD, Goldman SL, Riccio AP, Terkel J (1997) Circadian patterns of locomotor activity and body temperature in blind mole-rats, Spalax ehrenbergi. J Biol Rhythms 12:348-361.

Gonzalez CM, Bervig T, Podlasek C, Huang CF, McKenna KE, McVary KT (1999) Sildenafil causes a dose- and time-dependent downregulation of phosphodiesterase type 6 expression in the rat retina. Int J Impot Res 11 Suppl 1:S9-14.

Gooley JJ, Lu J, Chou TC, Scammell TE, Saper CB (2001) Melanopsin in cells of origin of the retinohypothalamic tract. Nat Neurosci 4:1165.

Gordon WC, Casey DM, Lukiw WJ, Bazan NG (2002) DNA damage and repair in light-induced photoreceptor degeneration. Invest Ophthalmol Vis Sci 43:3511-3521.

Goto Y, Peachey NS, Ziroli NE, Seiple WH, Gryczan C, Pepperberg DR, Naash MI (1996) Rod phototransduction in transgenic mice expressing a mutant opsin gene. J Opt Soc Am A Opt Image Sci Vis 13:577-585.

Goz D, Studholme K, Lappi DA, Rollag MD, Provencio I, Morin LP (2008) Targeted destruction of photosensitive retinal ganglion cells with a saporin conjugate alters the effects of light on mouse circadian rhythms. PLoS ONE 3:e3153.

Graf V, Norren DV (1974) A blue sensitive mechanism in the pigeon retina: lambda max 400 nm. Vision Res 14:1203-1209.

Graham DM, Wong KY, Shapiro P, Frederick C, Pattabiraman K, Berson DM (2008) Melanopsin ganglion cells use a membrane-associated rhabdomeric phototransduction cascade. J Neurophysiol 99:2522-2532.

Grimm C, Reme CE, Rol PO, Williams TP (2000a) Blue light's effects on rhodopsin: photoreversal of bleaching in living rat eyes. Invest Ophthalmol Vis Sci 41:3984-3990.

Grimm C, Wenzel A, Hafezi F, Yu S, Redmond TM, Reme CE (2000b) Protection of Rpe65-deficient mice identifies rhodopsin as a mediator of light-induced retinal degeneration. Nat Genet 25:63-66.

Grimm C, Wenzel A, Williams T, Rol P, Hafezi F, Reme C (2001) Rhodopsin-mediated blue-light damage to the rat retina: effect of photoreversal of bleaching. Invest Ophthalmol Vis Sci 42:497-505.

Guler AD, Ecker JL, Lall GS, Haq S, Altimus CM, Liao HW, Barnard AR, Cahill H, Badea TC, Zhao H, Hankins MW, Berson DM, Lucas RJ, Yau KW, Hattar S (2008) Melanopsin cells are the principal conduits

for rod-cone input to non-image-forming vision. Nature 453:102-105.

Gullino PM, Pettigrew HM, Grantham FH (1975) N-nitrosomethylurea as mammary gland carcinogen in rats. J Natl Cancer Inst 54:401-414.

Gurevich L, Slaughter MM (1993) Comparison of the waveforms of the ON bipolar neuron and the b-wave of the electroretinogram. Vision Res 33:2431-2435.

H

Haddad S, Chen CA, Santangelo SL, Seddon JM (2006) The genetics of age-related macular degeneration: a review of progress to date. Surv Ophthalmol 51:316-363.

Hafezi F, Marti A, Munz K, Reme CE (1997) Light-induced apoptosis: differential timing in the retina and pigment epithelium. Exp Eye Res 64:963-970.

Hagstrom SA, Duyao M, North MA, Li T (1999) Retinal degeneration in tulp1-/- mice: vesicular accumulation in the interphotoreceptor matrix. Invest Ophthalmol Vis Sci 40:2795-2802.

Halstenberg S, Lindgren KM, Samagh SP, Nadal-Vicens M, Balt S, Fernald RD (2005) Diurnal rhythm of cone opsin expression in the teleost fish Haplochromis burtoni. Vis Neurosci 22:135-141.

Han DP, Thompson HS, Folk JC (1985) Differentiation between recently resolved optic neuritis and central serous retinopathy. Use of tests of visual function. Arch Ophthalmol 103:394-396.

Hannibal J, Hindersson P, Nevo E, Fahrenkrug J (2002a) The circadian photopigment melanopsin is expressed in the blind subterranean mole rat, Spalax. Neuroreport 13:1411-1414.

Hannibal J, Hindersson P, Knudsen SM, Georg B, Fahrenkrug J (2002b) The photopigment melanopsin is exclusively present in pituitary adenylate cyclase-activating polypeptide-containing retinal ganglion cells of the retinohypothalamic tract. J Neurosci 22:RC191.

Hao W, Wenzel A, Obin MS, Chen CK, Brill E, Krasnoperova NV, Eversole-Cire P, Kleyner Y, Taylor A, Simon MI, Grimm C, Reme CE, Lem J (2002) Evidence for two apoptotic pathways in light-induced retinal degeneration. Nat Genet 32:254-260.

Harrington ME (1997) The ventral lateral geniculate nucleus and the intergeniculate leaflet: interrelated structures in the visual and circadian systems. Neurosci Biobehav Rev 21:705-727.

Hartong DT, Berson EL, Dryja TP (2006) Retinitis pigmentosa. Lancet 368:1795-1809.

Hatori M, Le H, Vollmers C, Keding SR, Tanaka N, Buch T, Waisman A, Schmedt C, Jegla T, Panda S (2008) Inducible ablation of melanopsin-expressing retinal ganglion cells reveals their central role in non-image forming visual responses. PLoS ONE 3:e2451.

Hattar S, Liao HW, Takao M, Berson DM, Yau KW (2002) Melanopsin-containing retinal ganglion cells: architecture, projections, and intrinsic photosensitivity. Science 295:1065-1070.

Hattar S, Kumar M, Park A, Tong P, Tung J, Yau KW, Berson DM (2006) Central projections of melanopsin-expressing retinal ganglion cells in the mouse. J Comp Neurol 497:326-349.

Hattar S, Lucas RJ, Mrosovsky N, Thompson S, Douglas RH, Hankins MW, Lem J, Biel M, Hofmann F, Foster RG, Yau KW (2003) Melanopsin and rod-cone photoreceptive systems account for all major accessory visual functions in mice. Nature 424:76-81.

Heck J (1957) The flicker electroretinogram of the human eye. Acta Physiol Scand 39:158-166.

Hendrickson A, Hicks D (2002) Distribution and density of medium- and short-wavelength selective cones in the domestic pig retina. Exp Eye Res 74:435-444.

Henkes HE (1958) Differentiation and evaluation of rod and cone system responses in the human electroretinogram. Ophthalmologica 135:138-146.

Herrold KM (1967) Pigmentary degeneration of the retina induced by N-methyl-N-nitrosourea. An experimental study in syrian hamsters. Arch Ophthalmol 78:650-653.

Heywood R, Gopinath C (1990) Morphological assessment of visual dysfunction. Toxicol Pathol 18:204-217.

Hicks D, Molday RS (1986) Differential immunogold-dextran labeling of bovine and frog rod and cone cells using monoclonal antibodies against bovine rhodopsin. Exp Eye Res 42:55-71.

Hoelter SM, Dalke C, Kallnik M, Becker L, Horsch M, Schrewe A, Favor J, Klopstock T, Beckers J, Ivandic B, Gailus-Durner V, Fuchs H, Hrabe de Angelis M, Graw J, Wurst W (2008) "Sighted C3H" mice--a tool for analysing the influence of vision on mouse behaviour? Front Biosci 13:5810-5823.

Homma K, Osakada F, Hirami Y, Jin ZB, Mandai M, Takahashi M (2009) Detection of localized retinal malfunction in retinal degeneration model using a multielectrode array system. J Neurosci Res.

Hood DC, Finkelstein (1986) Sensitivity to light: New York, NY: John Wiley & Sons.

Hood DC, Birch DG (1996) Beta wave of the scotopic (rod) electroretinogram as a measure of the activity of human on-bipolar cells. J Opt Soc Am A Opt Image Sci Vis 13:623-633.

Hoppeler T, Hendrickson P, Dietrich C, Reme C (1988) Morphology and time-course of defined photochemical lesions in the rabbit retina. Curr Eye Res 7:849-860.

Hultborn H, Mori K, Tsukahara N (1978) The neuronal pathway subserving the pupillary light reflex. Brain Res 159:255-267.

Humphries MM, Rancourt D, Farrar GJ, Kenna P, Hazel M, Bush RA, Sieving PA, Sheils DM, McNally N, Creighton P, Erven A, Boros A, Gulya K, Capecchi MR, Humphries P (1997) Retinopathy induced in mice by targeted disruption of the rhodopsin gene. Nat Genet 15:216-219.

Humphries P, Farrar GJ, Kenna P, McWilliam P (1990) Retinitis pigmentosa: genetic mapping in X-linked and autosomal forms of the disease. Clin Genet 38:1-13.

Hyatt GA, Schmitt EA, Fadool JM, Dowling JE (1996) Retinoic acid alters photoreceptor development in vivo. Proc Natl Acad Sci U S A 93:13298-13303.

J

Jackson GR, Owsley C, Curcio CA (2002) Photoreceptor degeneration and dysfunction in aging and age-related maculopathy. Ageing Res Rev 1:381-396.

Jacobs GH (1998) A perspective on color vision in platyrrhine monkeys. Vision Res 38:3307-3313.

Jacobs GH, Calderone JB, Sakai T, Lewis GP, Fisher SK (2002) An animal model for studying cone function in retinal detachment. Doc Ophthalmol 104:119-132.

Jeon CJ, Strettoi E, Masland RH (1998) The major cell populations of the mouse retina. J Neurosci 18:8936-8946.

Jimenez AJ, Garcia-Fernandez JM, Gonzalez B, Foster RG (1996) The spatio-temporal pattern of photoreceptor degeneration in the aged rd/rd mouse retina. Cell Tissue Res 284:193-202.

Joselevitch C, Kamermans M (2007) Interaction between rod and cone inputs in mixed-input bipolar cells in goldfish retina. J Neurosci Res 85:1579-1591.

K

Kaldi I, Martin RE, Huang H, Brush RS, Morrison KA, Anderson RE (2003) Bright cyclic rearing protects albino mouse retina against acute light-induced apoptosis. Mol Vis 9:337-344.

Kanan Y, Moiseyev G, Agarwal N, Ma JX, Al-Ubaidi MR (2007) Light induces programmed cell death by activating multiple independent proteases in a cone photoreceptor cell line. Invest Ophthalmol Vis Sci 48:40-51.

Kato I, Okada T, Watanabe S, Sato S, Urushibata T, Takeyama I (1992) Retinal ganglion cells related to optokinetic nystagmus in the rat. Acta Otolaryngol 112:421-428.

Keeler CE, Sutcliffe E, Chaffee EL (1928) Normal and "Rodless" Retinae of the House Mouse with Respect to the Electromotive Force Generated through Stimulation by Light. Proc Natl Acad Sci U S A 14:477-484.

Keller C, Grimm C, Wenzel A, Hafezi F, Reme C (2001) Protective effect of halothane anesthesia on retinal light damage: inhibition of metabolic rhodopsin regeneration. Invest Ophthalmol Vis Sci 42:476-480.

Kelley MW, Turner JK, Reh TA (1995) Ligands of steroid/thyroid receptors induce cone photoreceptors in vertebrate retina. Development 121:3777-3785.

Kiuchi K, Yoshizawa K, Shikata N, Moriguchi K, Tsubura A (2002) Morphologic characteristics of retinal degeneration induced by sodium iodate in mice. Curr Eye Res 25:373-379.

Kiuchi K, Kondo M, Ueno S, Moriguchi K, Yoshizawa K, Miyake Y, Matsumura M, Tsubura A (2003) Functional rescue of N-methyl-N-nitrosourea-induced retinopathy by nicotinamide in Sprague-Dawley rats. Curr Eye Res 26:355-362.

Kolb H, West RW (1977) Synaptic connections of the interplexiform cell in the retina of the cat. J Neurocytol 6:155-170.

Komeima K, Rogers BS, Lu L, Campochiaro PA (2006) Antioxidants reduce cone cell death in a model of retinitis pigmentosa. Proc Natl Acad Sci U S A 103:11300-11305.

Krebs MP, White DA, Kaushal S (2009) Biphasic Photoreceptor Degeneration Induced by

Light in a T17M Rhodopsin Mouse Model of Cone Bystander Damage. Invest Ophthalmol Vis Sci.

Krieger DT, Rizzo F (1971) Circadian periodicity of plasma 11-hydroxycorticosteroid levels in subjects with partial and absent light perception. Neuroendocrinology 8:165-169.

Krishnamoorthy RR, Crawford MJ, Chaturvedi MM, Jain SK, Aggarwal BB, Al-Ubaidi MR, Agarwal N (1999) Photo-oxidative stress down-modulates the activity of nuclear factor-kappaB via involvement of caspase-1, leading to apoptosis of photoreceptor cells. J Biol Chem 274:3734-3743.

Kryger Z, Galli-Resta L, Jacobs GH, Reese BE (1998) The topography of rod and cone photoreceptors in the retina of the ground squirrel. Vis Neurosci 15:685-691.

L

Larison KD, Bremiller R (1990) Early onset of phenotype and cell patterning in the embryonic zebrafish retina. Development 109:567-576.

LaVail MM, Gorrin GM, Repaci MA, Yasumura D (1987a) Light-induced retinal degeneration in albino mice and rats: strain and species differences. Prog Clin Biol Res 247:439-454.

LaVail MM, Gorrin GM, Yasumura D, Matthes MT (1999) Increased susceptibility to constant light in nr and pcd mice with inherited retinal degenerations. Invest Ophthalmol Vis Sci 40:1020-1024.

LaVail MM, Gorrin GM, Repaci MA, Thomas LA, Ginsberg HM (1987b) Genetic regulation of light damage to photoreceptors. Invest Ophthalmol Vis Sci 28:1043-1048.

LaVail MM, Unoki K, Yasumura D, Matthes MT, Yancopoulos GD, Steinberg RH (1992) Multiple growth factors, cytokines, and neurotrophins rescue photoreceptors from the damaging effects of constant light. Proc Natl Acad Sci U S A 89:11249-11253.

Lee KP, Valentine R (1990) Retinotoxicity of 1,4,-bis(4-aminophenoxy)-2-phenylbenzene (2-phenyl-APB-144) in albino and pigmented rats. Arch Toxicol 64:135-142.

Lee KP, Gibson JR, Sherman H (1979) Retinopathic effects of 2-aminooxy propionic acid derivatives in the rat. Toxicol Appl Pharmacol 51:219-232.

Lei B, Perlman I (1999) The contributions of voltage- and time-dependent potassium conductances to the electroretinogram in rabbits. Vis Neurosci 16:743-754.

Leskov IB, Klenchin VA, Handy JW, Whitlock GG, Govardovskii VI, Bownds MD, Lamb TD, Pugh EN, Jr., Arshavsky VY (2000) The gain of rod phototransduction: reconciliation of biochemical and electrophysiological measurements. Neuron 27:525-537.

Leveillard T, Mohand-Said S, Lorentz O, Hicks D, Fintz AC, Clerin E, Simonutti M, Forster V, Cavusoglu N, Chalmel F, Dolle P, Poch O, Lambrou G, Sahel JA (2004) Identification and characterization of rod-derived cone viability factor. Nat Genet 36:755-759.

Li W, DeVries SH (2004) Separate blue and green cone networks in the mammalian retina. Nat Neurosci 7:751-756.

Lin B, Koizumi A, Tanaka N, Panda S, Masland RH (2008) Restoration of visual function in retinal degeneration mice by ectopic expression of melanopsin. Proc Natl Acad Sci U S A 105:16009-16014.

Linberg KA, Sakai T, Lewis GP, Fisher SK (2002) Experimental retinal detachment in the cone-dominant ground squirrel retina: morphology and basic immunocytochemistry. Vis Neurosci 19:603-619.

Long KO, Fisher SK, Fariss RN, Anderson DH (1986) Disc shedding and autophagy in the cone-dominant ground squirrel retina. Exp Eye Res 43:193-205.

Low JC (1987) The corneal ERG of the heterozygous retinal degeneration mouse. Graefes Arch Clin Exp Ophthalmol 225:413-417.

Lowry OH, Rosebrough NJ, Farr AL, Randall RJ (1951) Protein measurement with the Folin phenol reagent. J Biol Chem 193:265-275.

Lucas RJ, Douglas RH, Foster RG (2001) Characterization of an ocular photopigment capable of driving pupillary constriction in mice. Nat Neurosci 4:621-626.

Lucas RJ, Hattar S, Takao M, Berson DM, Foster RG, Yau KW (2003) Diminished pupillary light reflex at high irradiances in melanopsin-knockout mice. Science 299:245-247.

Lyubarsky AL, Pugh EN, Jr. (1996) Recovery phase of the murine rod photoresponse reconstructed from electroretinographic recordings. J Neurosci 16:563-571.

Lyubarsky AL, Falsini B, Pennesi ME, Valentini P, Pugh EN, Jr. (1999) UV- and midwave-sensitive cone-driven retinal responses of the mouse: a possible phenotype for

coexpression of cone photopigments. J Neurosci 19:442-455.

M

Machida S, Kondo M, Jamison JA, Khan NW, Kononen LT, Sugawara T, Bush RA, Sieving PA (2000) P23H rhodopsin transgenic rat: correlation of retinal function with histopathology. Invest Ophthalmol Vis Sci 41:3200-3209.

Massof RW, Fleischman JA, Fine SL, Yoder F (1977) Flicker fusion thresholds in Best macular dystrophy. Arch Ophthalmol 95:991-994.

Mata NL, Weng J, Travis GH (2000) Biosynthesis of a major lipofuscin fluorophore in mice and humans with ABCR-mediated retinal and macular degeneration. Proc Natl Acad Sci U S A 97:7154-7159.

Matsumura M, Ohkuma M, Tsukahara I (1986) Experimental chloroquine retinopathy. Ophthalmic Res 18:172-179.

Mazzoni F, Novelli E, Strettoi E (2008) Retinal ganglion cells survive and maintain normal dendritic morphology in a mouse model of inherited photoreceptor degeneration. J Neurosci 28:14282-14292.

McCall MA, Gregg RG, Merriman K, Goto Y, Peachey NS, Stanford LR (1996) Morphological and physiological consequences of the selective elimination of rod photoreceptors in transgenic mice. Exp Eye Res 63:35-50.

McGill TJ, Douglas RM, Lund RD, Prusky GT (2004a) Quantification of spatial vision in the Royal College of Surgeons rat. Invest Ophthalmol Vis Sci 45:932-936.

McGill TJ, Lund RD, Douglas RM, Wang S, Lu B, Prusky GT (2004b) Preservation of vision following cell-based therapies in a model of retinal degenerative disease. Vision Res 44:2559-2566.

Mears AJ, Kondo M, Swain PK, Takada Y, Bush RA, Saunders TL, Sieving PA, Swaroop A (2001) Nrl is required for rod photoreceptor development. Nat Genet 29:447-452.

Meijer JH, Schwartz WJ (2003) In search of the pathways for light-induced pacemaker resetting in the suprachiasmatic nucleus. J Biol Rhythms 18:235-249.

Melyan Z, Tarttelin EE, Bellingham J, Lucas RJ, Hankins MW (2005) Addition of human melanopsin renders mammalian cells photoresponsive. Nature 433:741-745.

Mendoza J, Revel FG, Pevet P, Challet E (2007) Shedding light on circadian clock resetting by dark exposure: differential effects between diurnal and nocturnal rodents. Eur J Neurosci 25:3080-3090.

Miceli MV, Liles MR, Newsome DA (1994) Evaluation of oxidative processes in human pigment epithelial cells associated with retinal outer segment phagocytosis. Exp Cell Res 214:242-249.

Middleton W (1952) Vision through the atmosphere. University of Toronto Press.

Miles LEM, Wilson MA (1977) High incidence of cyclic sleep/wake distribution in blind subjetcs with and without sleep complaints. Sleep Res 6.

Mohand-Said S, Deudon-Combe A, Hicks D, Simonutti M, Forster V, Fintz AC, Leveillard T, Dreyfus H, Sahel JA (1998) Normal retina releases a diffusible factor stimulating cone survival in the retinal degeneration mouse. Proc Natl Acad Sci U S A 95:8357-8362.

Morin LP, Pace L (2002) The intergeniculate leaflet, but not the visual midbrain, mediates hamster circadian rhythm response to constant light. J Biol Rhythms 17:217-226.

Mrosovsky N (2003) Contribution of classic photoreceptors to entrainment. J Comp Physiol A Neuroethol Sens Neural Behav Physiol 189:69-73.

Muller B, Peichl L (1989) Topography of cones and rods in the tree shrew retina. J Comp Neurol 282:581-594.

Murthy AS, Vawter GF, Kopito L, Rossen E (1972) Retinal atrophy and cataract in rats following administration of N-methyl-N-nitrosourea. Proc Soc Exp Biol Med 139:84-87.

N

Nagy D, Schonfisch B, Zrenner E, Jagle H (2008) Long-term follow-up of retinitis pigmentosa patients with multifocal electroretinography. Invest Ophthalmol Vis Sci 49:4664-4671.

Nakagawa H, Sack RL, Lewy AJ (1992) Sleep propensity free-runs with the temperature, melatonin and cortisol rhythms in a totally blind person. Sleep 15:330-336.

Nakajima M, Nambu H, Shikata N, Senzaki H, Miki H, Tsubura A (1996a) Pigmentary degeneration induced by N-methyl-N-nitrosourea and the fate of pigment epithelial cells in the rat retina. Pathol Int 46:874-882.

Nakajima M, Yuge K, Senzaki H, Shikata N, Miki H, Uyama M, Tsubura A (1996b)

Photoreceptor apoptosis induced by a single systemic administration of N-methyl-N-nitrosourea in the rat retina. Am J Pathol 148:631-641.

Nakamura M, Yamamoto M (2000) Variable pattern of visual recovery of Leber's hereditary optic neuropathy. Br J Ophthalmol 84:534-535.

Nambu H, Taomoto M, Ogura E, Tsubura A (1998) Time-specific action of N-methyl-N-nitrosourea in the occurrence of retinal dysplasia and retinal degeneration in neonatal mice. Pathol Int 48:199-205.

Narfstrom K, Ehinger B, Bruun A (2001) Immunohistochemical studies of cone photoreceptors and cells of the inner retina in feline rod-cone degeneration. Vet Ophthalmol 4:141-145.

Nathans J (1999) The evolution and physiology of human color vision: insights from molecular genetic studies of visual pigments. Neuron 24:299-312.

Nathans J, Thomas D, Hogness DS (1986) Molecular genetics of human color vision: the genes encoding blue, green, and red pigments. Science 232:193-202.

Nelson DE, Takahashi JS (1991) Comparison of visual sensitivity for suppression of pineal melatonin and circadian phase-shifting in the golden hamster. Brain Res 554:272-277.

Nelson R (1977) Cat cones have rod input: a comparison of the response properties of cones and horizontal cell bodies in the retina of the cat. J Comp Neurol 172:109-135.

Nelson RJ, Zucker I (1981) Photoperiodic control of reproduction in olfactory-bulbectomized rats. Neuroendocrinology 32:266-271.

Nishiwaki Y, Komori A, Sagara H, Suzuki E, Manabe T, Hosoya T, Nojima Y, Wada H, Tanaka H, Okamoto H, Masai I (2008) Mutation of cGMP phosphodiesterase 6alpha'-subunit gene causes progressive degeneration of cone photoreceptors in zebrafish. Mech Dev 125:932-946.

Noell WK (1977) Some animal models of retinitis pigmentosa. Adv Exp Med Biol 77:87-91.

Noell WK, Albrecht R (1971) Irreversible effects on visible light on the retina: role of vitamin A. Science 172:76-79.

Noell WK, Walker VS, Kang BS, Berman S (1966) Retinal damage by light in rats. Invest Ophthalmol 5:450-473.

Normann RA, Kolb H (1981) Anatomy and physiology of the horizontal cells of the visual streak region of the turtle retina. Vision Res 21:1585-1588.

O

O'Steen WK (1980) Hormonal influences on retinal photodamage. New-York: Plenum Press.

O'Steen WK, Donnelly JE (1982) Antagonistic effects of adrenalectomy and ether/surgical stress on light-induced photoreceptor damage. Invest Ophthalmol Vis Sci 22:1-7.

Ogino H, Ito M, Matsumoto K, Yagyu S, Tsuda H, Hirono I, Wild CP, Montesano R (1993) Retinal degeneration induced by N-methyl-N-nitrosourea and detection of 7-methyldeoxyguanosine in the rat retina. Toxicol Pathol 21:21-25.

Ohta H, Yamazaki S, McMahon DG (2005) Constant light desynchronizes mammalian clock neurons. Nat Neurosci 8:267-269.

Oka T, Nakajima T, Tamada Y, Shearer TR, Azuma M (2007) Contribution of calpains to photoreceptor cell death in N-methyl-N-nitrosourea-treated rats. Exp Neurol 204:39-48.

Okano T, Fukada Y, Artamonov ID, Yoshizawa T (1989) Purification of cone visual pigments from chicken retina. Biochemistry 28:8848-8856.

Olson JL, Prall FR, Ciardella AP (2006) Bilateral foveal neurosensory detachment in hypertensive retinopathy demonstrated by optical coherence tomography. Eye 20:1370-1371.

Olsson JE, Gordon JW, Pawlyk BS, Roof D, Hayes A, Molday RS, Mukai S, Cowley GS, Berson EL, Dryja TP (1992) Transgenic mice with a rhodopsin mutation (Pro23His): a mouse model of autosomal dominant retinitis pigmentosa. Neuron 9:815-830.

Organisciak DT, Wang HM, Li ZY, Tso MO (1985) The protective effect of ascorbate in retinal light damage of rats. Invest Ophthalmol Vis Sci 26:1580-1588.

Organisciak DT, Jiang YL, Wang HM, Pickford M, Blanks JC (1989) Retinal light damage in rats exposed to intermittent light. Comparison with continuous light exposure. Invest Ophthalmol Vis Sci 30:795-805.

Organisciak DT, Darrow RM, Jiang YI, Marak GE, Blanks JC (1992) Protection by dimethylthiourea against retinal light damage in rats. Invest Ophthalmol Vis Sci 33:1599-1609.

Organisciak DT, Darrow RA, Barsalou L, Darrow RM, Lininger LA (1999) Light-induced damage in the retina: differential effects of dimethylthiourea on photoreceptor survival, apoptosis and DNA oxidation. Photochem Photobiol 70:261-268.

Organisciak DT, Darrow RM, Barsalou L, Kutty RK, Wiggert B (2000) Circadian-dependent retinal light damage in rats. Invest Ophthalmol Vis Sci 41:3694-3701.

Osterberg G (1935) Topography of the layer of rods and cones in the human retina. Acta Ophtal 6:1-103.

Owen EH, Logue SF, Rasmussen DL, Wehner JM (1997) Assessment of learning by the Morris water task and fear conditioning in inbred mouse strains and F1 hybrids: implications of genetic background for single gene mutations and quantitative trait loci analyses. Neuroscience 80:1087-1099.

P

Panda S, Nayak SK, Campo B, Walker JR, Hogenesch JB, Jegla T (2005) Illumination of the melanopsin signaling pathway. Science 307:600-604.

Panda S, Sato TK, Castrucci AM, Rollag MD, DeGrip WJ, Hogenesch JB, Provencio I, Kay SA (2002) Melanopsin (Opn4) requirement for normal light-induced circadian phase shifting. Science 298:2213-2216.

Papaioannou M, Ocaka L, Bessant D, Lois N, Bird A, Payne A, Bhattacharya S (2000) An analysis of ABCR mutations in British patients with recessive retinal dystrophies. Invest Ophthalmol Vis Sci 41:16-19.

Paskowitz DM, LaVail MM, Duncan JL (2006) Light and inherited retinal degeneration. Br J Ophthalmol 90:1060-1066.

Paylor R, Johnson RS, Papaioannou V, Spiegelman BM, Wehner JM (1994) Behavioral assessment of c-fos mutant mice. Brain Res 651:275-282.

Peachey NS, Goto Y, Quiambao AB, al-Ubaidi MR (1995) Functional consequences of oncogene-induced photoreceptor degeneration in transgenic mice. Vis Neurosci 12:513-522.

Peichl L (2005) Diversity of mammalian photoreceptor properties: adaptations to habitat and lifestyle? Anat Rec A Discov Mol Cell Evol Biol 287:1001-1012.

Penn JS, Anderson RE (1987) Effect of light history on rod outer-segment membrane composition in the rat. Exp Eye Res 44:767-778.

Penn JS, Naash MI, Anderson RE (1987) Effect of light history on retinal antioxidants and light damage susceptibility in the rat. Exp Eye Res 44:779-788.

Poznanski RR (2005) Biophysical mechanisms and essential topography of directionally selective subunits in rabbit's retina. J Integr Neurosci 4:341-361.

Provencio I, Cooper HM, Foster RG (1998a) Retinal projections in mice with inherited retinal degeneration: implications for circadian photoentrainment. J Comp Neurol 395:417-439.

Provencio I, Rollag MD, Castrucci AM (2002) Photoreceptive net in the mammalian retina. This mesh of cells may explain how some blind mice can still tell day from night. Nature 415:493.

Provencio I, Jiang G, De Grip WJ, Hayes WP, Rollag MD (1998b) Melanopsin: An opsin in melanophores, brain, and eye. Proc Natl Acad Sci U S A 95:340-345.

Provencio I, Rodriguez IR, Jiang G, Hayes WP, Moreira EF, Rollag MD (2000) A novel human opsin in the inner retina. J Neurosci 20:600-605.

Prusky GT, West PW, Douglas RM (2000) Experience-dependent plasticity of visual acuity in rats. Eur J Neurosci 12:3781-3786.

Pugh EN, Jr., Baehr W, Zrenner E (2005) Neuroimaging the retina. Vision Res 45:3431.

Punzo C, Kornacker K, Cepko CL (2009) Stimulation of the insulin/mTOR pathway delays cone death in a mouse model of retinitis pigmentosa. Nat Neurosci 12:44-52.

Q

Qiu X, Kumbalasiri T, Carlson SM, Wong KY, Krishna V, Provencio I, Berson DM (2005) Induction of photosensitivity by heterologous expression of melanopsin. Nature 433:745-749.

R

Rabin AR, Hayes KC, Berson EL (1973) Cone and rod responses in nutritionally induced retinal degeneration in the cat. Invest Ophthalmol 12:694-704.

Radu RA, Mata NL, Nusinowitz S, Liu X, Travis GH (2004) Isotretinoin treatment inhibits lipofuscin accumulation in a mouse model of recessive Stargardt's macular degeneration. Novartis Found Symp 255:51-63; discussion 63-57, 177-178.

Raitta C, Karhunen U, Seppalainen AM, Naukkarinen M (1979) Changes in the electroretinogram and visual evoked

potentials during general anaesthesia. Albrecht Von Graefes Arch Klin Exp Ophthalmol 211:139-144.

Rakoczy EP, Yu MJ, Nusinowitz S, Chang B, Heckenlively JR (2006) Mouse models of age-related macular degeneration. Exp Eye Res 82:741-752.

Ranchon I, Chen S, Alvarez K, Anderson RE (2001) Systemic administration of phenyl-N-tert-butylnitrone protects the retina from light damage. Invest Ophthalmol Vis Sci 42:1375-1379.

Ranchon I, LaVail MM, Kotake Y, Anderson RE (2003) Free radical trap phenyl-N-tert-butylnitrone protects against light damage but does not rescue P23H and S334ter rhodopsin transgenic rats from inherited retinal degeneration. J Neurosci 23:6050-6057.

Rapaport DH, Stone J (1984) The area centralis of the retina in the cat and other mammals: focal point for function and development of the visual system. Neuroscience 11:289-301.

Rapp LM, Williams TP (1980) The role of ocular pigmentation in protecting against retinal light damage. Vision Res 20:1127-1131.

Rapp LM, Smith SC (1992) Morphologic comparisons between rhodopsin-mediated and short-wavelength classes of retinal light damage. Invest Ophthalmol Vis Sci 33:3367-3377.

Raviola E, Gilula NB (1973) Gap junctions between photoreceptor cells in the vertebrate retina. Proc Natl Acad Sci U S A 70:1677-1681.

Rebrik TI, Korenbrot JI (2004) In intact mammalian photoreceptors, Ca2+-dependent modulation of cGMP-gated ion channels is detectable in cones but not in rods. J Gen Physiol 123:63-75.

Redlin U, Vrang N, Mrosovsky N (1999) Enhanced masking response to light in hamsters with IGL lesions. J Comp Physiol [A] 184:449-456.

Redlin U, Cooper HM, Mrosovsky N (2003) Increased masking response to light after ablation of the visual cortex in mice. Brain Res 965:1-8.

Reinberg A (1986) Circadian rhythms in effects of hypnotics and sleep inducers. Int J Clin Pharmacol Res 6:33-44.

Reme CE (2005) The dark side of light: rhodopsin and the silent death of vision the proctor lecture. Invest Ophthalmol Vis Sci 46:2671-2682.

Reme CE, Malnoe A, Jung HH, Wei Q, Munz K (1994) Effect of dietary fish oil on acute light-induced photoreceptor damage in the rat retina. Invest Ophthalmol Vis Sci 35:78-90.

Ribelayga C, Cao Y, Mangel SC (2008) The circadian clock in the retina controls rod-cone coupling. Neuron 59:790-801.

Robinson J, Schmitt EA, Dowling JE (1995) Temporal and spatial patterns of opsin gene expression in zebrafish (Danio rerio). Vis Neurosci 12:895-906.

Robson JG, Frishman LJ (1995) Response linearity and kinetics of the cat retina: the bipolar cell component of the dark-adapted electroretinogram. Vis Neurosci 12:837-850.

Robson JG, Frishman LJ (1996) Photoreceptor and bipolar cell contributions to the cat electroretinogram: a kinetic model for the early part of the flash response. J Opt Soc Am A Opt Image Sci Vis 13:613-622.

Rodieck RW, Rushton WA (1976) Cancellation of rod signals by cones, and cone signals by rods in the cat retina. J Physiol 254:775-785.

Rogers BS, Symons RC, Komeima K, Shen J, Xiao W, Swaim ME, Gong YY, Kachi S, Campochiaro PA (2007) Differential sensitivity of cones to iron-mediated oxidative damage. Invest Ophthalmol Vis Sci 48:438-445.

Roorda A, Williams DR (1999) The arrangement of the three cone classes in the living human eye. Nature 397:520-522.

Rozet JM, Gerber S, Ghazi I, Perrault I, Ducroq D, Souied E, Cabot A, Dufier JL, Munnich A, Kaplan J (1999) Mutations of the retinal specific ATP binding transporter gene (ABCR) in a single family segregating both autosomal recessive retinitis pigmentosa RP19 and Stargardt disease: evidence of clinical heterogeneity at this locus. J Med Genet 36:447-451.

Ruby NF, Brennan TJ, Xie X, Cao V, Franken P, Heller HC, O'Hara BF (2002) Role of melanopsin in circadian responses to light. Science 298:2211-2213.

Rudolph G, Kalpadakis P, Bechmann M, La Rocca G, Hormann C, Berninger T (2002) Scanning laser ophthalmoscope-evoked multifocal-ERG (SLO-m-ERG) by using short m-sequences. Eur J Ophthalmol 12:109-116.

Ruggiero L, Allen CN, Lane Brown R, Robinson DW (2009) The development of melanopsin-containing retinal ganglion cells in mice with early retinal degeneration. Eur J Neurosci 29:359-367.

S

Sack RL, Lewy AJ (2001) Circadian rhythm sleep disorders: lessons from the blind. Sleep Med Rev 5:189-206.

Sack RL, Lewy AJ, Blood ML, Keith LD, Nakagawa H (1992) Circadian rhythm abnormalities in totally blind people: incidence and clinical significance. J Clin Endocrinol Metab 75:127-134.

Sakamoto K, Liu C, Tosini G (2004) Classical photoreceptors regulate melanopsin mRNA levels in the rat retina. J Neurosci 24:9693-9697.

Sanyal S, Jansen HG, de Grip WJ, Nevo E, de Jong WW (1990) The eye of the blind mole rat, Spalax ehrenbergi. Rudiment with hidden function? Invest Ophthalmol Vis Sci 31:1398-1404.

Schmitz-Valckenberg S, Holz FG, Bird AC, Spaide RF (2008) Fundus autofluorescence imaging: review and perspectives. Retina 28:385-409.

Scott PP, Greaves JP, Scott MG (1964) Nutritional Blindness In The Cat. Exp Eye Res 3:357-364.

Seeliger MW, Grimm C, Stahlberg F, Friedburg C, Jaissle G, Zrenner E, Guo H, Reme CE, Humphries P, Hofmann F, Biel M, Fariss RN, Redmond TM, Wenzel A (2001) New views on RPE65 deficiency: the rod system is the source of vision in a mouse model of Leber congenital amaurosis. Nat Genet 29:70-74.

Seeliger MW, Beck SC, Pereyra-Munoz N, Dangel S, Tsai JY, Luhmann UF, van de Pavert SA, Wijnholds J, Samardzija M, Wenzel A, Zrenner E, Narfstrom K, Fahl E, Tanimoto N, Acar N, Tonagel F (2005) In vivo confocal imaging of the retina in animal models using scanning laser ophthalmoscopy. Vision Res 45:3512-3519.

Seidehamel RJ, Dungan KW (1974) Characteristics and pharmacologic utility of an intraocular pressure (IOP) model in unanesthetized rabbits. Invest Ophthalmol 13:319-322.

Semo M, Peirson S, Lupi D, Lucas RJ, Jeffery G, Foster RG (2003) Melanopsin retinal ganglion cells and the maintenance of circadian and pupillary responses to light in aged rodless/coneless (rd/rd cl) mice. Eur J Neurosci 17:1793-1801.

Semple-Rowland SL, Dawson WW (1987) Cyclic light intensity threshold for retinal damage in albino rats raised under 6 lx. Exp Eye Res 44:643-661.

Shen J, Yang X, Dong A, Petters RM, Peng YW, Wong F, Campochiaro PA (2005) Oxidative damage is a potential cause of cone cell death in retinitis pigmentosa. J Cell Physiol 203:457-464.

Simonson E, Wohlrabe RG (1963) The flicker fusion frequency in different testing arrangements, of healthy older persons, of patients with cataracts and patients with retinal disorders. Am J Ophthalmol 55:1023-1032.

Skene DJ, Arendt J (2007) Circadian rhythm sleep disorders in the blind and their treatment with melatonin. Sleep Med 8:651-655.

Smith SB, Yielding KL (1986) Retinal degeneration in the mouse. A model induced transplacentally by methylnitrosourea. Exp Eye Res 43:791-801.

Smith SB, Hashimi W, Yielding KL (1988) Retinal degeneration in the mouse induced transplacentally by N-methyl-N-nitrosourea: effects of constant illumination or total darkness. Exp Eye Res 47:347-359.

Soucy E, Wang Y, Nirenberg S, Nathans J, Meister M (1998) A novel signaling pathway from rod photoreceptors to ganglion cells in mammalian retina. Neuron 21:481-493.

Sparrow JR, Boulton M (2005) RPE lipofuscin and its role in retinal pathobiology. Exp Eye Res 80:595-606.

Spekreijse H, Wietsma JJ, Neumeyer C (1991) Ethambutol-induced color-blindness in goldfish: a behavioral, electrophysiological and morphological study. Neurosci Res Suppl 15:S77-89.

Sperling HG (1986) Spectral sensitivity, intense spectral light studies and the color receptor mosaic of primates. Vision Res 26:1557-1571.

Stavosky JM, Rosekind MR, England WR, Miles LEM, Dement WC (1980) Circadian rhythms of body
temperature and sleep latency in
blind subjects with sleep/wake complaints. Sleep Res 9:277.

Steinberg RH, Reid M, Lacy PL (1973) The distribution of rods and cones in the retina of the cat (Felis domesticus). J Comp Neurol 148:229-248.

Stewart WC, Chauhan BC (1995) Newer visual function tests in the evaluation of glaucoma. Surv Ophthalmol 40:119-135.

Sugita Y, Tasaki K (1988) The activation of cones in scotopic and rods in photopic vision. Tohoku J Exp Med 156:311-317.

Sugiyama K, Gu ZB, Kawase C, Yamamoto T, Kitazawa Y (1999) Optic nerve and peripapillary choroidal microvasculature of the rat eye. Invest Ophthalmol Vis Sci 40:3084-3090.

Sun M, Finnemann SC, Febbraio M, Shan L, Annangudi SP, Podrez EA, Hoppe G, Darrow R, Organisciak DT, Salomon RG, Silverstein RL, Hazen SL (2006) Light-induced oxidation of photoreceptor outer segment phospholipids generates ligands for CD36-mediated phagocytosis by retinal pigment epithelium: a potential mechanism for modulating outer segment phagocytosis under oxidant stress conditions. J Biol Chem 281:4222-4230.

Sykes SM, Robison WG, Jr., Waxler M, Kuwabara T (1981) Damage to the monkey retina by broad-spectrum fluorescent light. Invest Ophthalmol Vis Sci 20:425-434.

Szel A, Rohlich P (1992) Two cone types of rat retina detected by anti-visual pigment antibodies. Exp Eye Res 55:47-52.

Szel A, Rohlich P, Van Veen T (1993) Short-wave sensitive cones in the rodent retinas. Exp Eye Res 57:503-505.

T

Tabandeh H, Lockley SW, Buttery R, Skene DJ, Defrance R, Arendt J, Bird AC (1998) Disturbance of sleep in blindness. Am J Ophthalmol 126:707-712.

Tan E, Ding XQ, Saadi A, Agarwal N, Naash MI, Al-Ubaidi MR (2004) Expression of cone-photoreceptor-specific antigens in a cell line derived from retinal tumors in transgenic mice. Invest Ophthalmol Vis Sci 45:764-768.

Tanimoto N, Muehlfriedel RL, Fischer MD, Fahl E, Humphries P, Biel M, Seeliger MW (2009) Vision tests in the mouse: Functional phenotyping with electroretinography. Front Biosci 14:2730-2737.

Taomoto M, Nambu H, Senzaki H, Shikata N, Oishi Y, Fujii T, Miki H, Uyama M, Tsubura A (1998) Retinal degeneration induced by N-methyl-N-nitrosourea in Syrian golden hamsters. Graefes Arch Clin Exp Ophthalmol 236:688-695.

Tate DJ, Jr., Miceli MV, Newsome DA (1995) Phagocytosis and H2O2 induce catalase and metallothionein gene expression in human retinal pigment epithelial cells. Invest Ophthalmol Vis Sci 36:1271-1279.

Tian N, Slaughter MM (1995) Correlation of dynamic responses in the ON bipolar neuron and the b-wave of the electroretinogram. Vision Res 35:1359-1364.

Tomany SC, Cruickshanks KJ, Klein R, Klein BE, Knudtson MD (2004) Sunlight and the 10-year incidence of age-related maculopathy: the Beaver Dam Eye Study. Arch Ophthalmol 122:750-757.

Tournier BB, Dardente H, Vuillez P, Pevet P, Challet E (2007) Expression of Tgfalpha in the suprachiasmatic nuclei of nocturnal and diurnal rodents. Neuroscience 145:1138-1143.

Traverso V, Kinkl N, Grimm L, Sahel J, Hicks D (2003) Basic fibroblast and epidermal growth factors stimulate survival in adult porcine photoreceptor cell cultures. Invest Ophthalmol Vis Sci 44:4550-4558.

Travis GH, Sutcliffe JG, Bok D (1991) The retinal degeneration slow (rds) gene product is a photoreceptor disc membrane-associated glycoprotein. Neuron 6:61-70.

Travis GH, Golczak M, Moise AR, Palczewski K (2007) Diseases caused by defects in the visual cycle: retinoids as potential therapeutic agents. Annu Rev Pharmacol Toxicol 47:469-512.

Trevino SG, Villazana-Espinoza ET, Muniz A, Tsin AT (2005) Retinoid cycles in the cone-dominated chicken retina. J Exp Biol 208:4151-4157.

Tsubura A, Yoshizawa K, Kiuchi K, Moriguchi K (2003a) N-methyl-N-nitrosourea-induced Retinal Degeneration in Animals. Acta Histochem Cytochem 36:263-270.

Tsubura A, Yoshizawa K, Kiuchi K, Moriguchi K (2003b) N-Methyl-N-nitrosourea-induced Retinal Degeneration in Animals. Acta Histochem Cytochem 36:263-270.

U

Ulshafer RJ, Clausnitzer EL, Sherry DM, Szel A, Rohlich P (1990) Immunocytochemical identification of outer segment proteins in the rd chicken. Exp Eye Res 51:209-216.

Umino Y, Everhart D, Solessio E, Cusato K, Pan JC, Nguyen TH, Brown ET, Hafler R, Frio BA, Knox BE, Engbretson GA, Haeri M, Cui L, Glenn AS, Charron MJ, Barlow RB (2006) Hypoglycemia leads to age-related loss of vision. Proc Natl Acad Sci U S A 103:19541-19545.

Usukura J, Khoo W, Abe T, Breitman ML, Shinohara T (1994) Cone cells fail to develop normally in transgenic mice showing ablation of rod photoreceptor cells. Cell Tissue Res 275:79-90.

V

Vaughan DK, Nemke JL, Fliesler SJ, Darrow RM, Organisciak DT (2002) Evidence for a circadian rhythm of susceptibility to retinal light damage. Photochem Photobiol 75:547-553.

Vihtelic TS, Hyde DR (2000) Light-induced rod and cone cell death and regeneration in the adult albino zebrafish (Danio rerio) retina. J Neurobiol 44:289-307.

Vihtelic TS, Soverly JE, Kassen SC, Hyde DR (2006) Retinal regional differences in photoreceptor cell death and regeneration in light-lesioned albino zebrafish. Exp Eye Res 82:558-575.

W

Wan J, Zheng H, Hu BY, Xiao HL, She ZJ, Chen ZL, Zhou GM (2006) Acute photoreceptor degeneration down-regulates melanopsin expression in adult rat retina. Neurosci Lett 400:48-52.

Wang JJ, Jakobsen K, Smith W, Mitchell P (2003) Five-year incidence of age-related maculopathy in relation to iris, skin or hair colour, and skin sun sensitivity: the Blue Mountains Eye Study. Clin Experiment Ophthalmol 31:317-321.

Wenzel A, Grimm C, Samardzija M, Reme CE (2005) Molecular mechanisms of light-induced photoreceptor apoptosis and neuroprotection for retinal degeneration. Prog Retin Eye Res 24:275-306.

Wenzel A, Reme CE, Williams TP, Hafezi F, Grimm C (2001) The Rpe65 Leu450Met variation increases retinal resistance against light-induced degeneration by slowing rhodopsin regeneration. J Neurosci 21:53-58.

Wiechmann AF (1996) Recoverin in cultured human retinoblastoma cells: enhanced expression during morphological differentiation. J Neurochem 67:105-110.

Wilhelm M, Gabriel R (1999) Functional anatomy of the photoreceptor and second-order cell mosaics in the retina of Xenopus laevis. Cell Tissue Res 297:35-46.

Williams DS, Colley NJ, Farber DB (1987) Photoreceptor degeneration in a pure-cone retina. Effects of cyclic nucleotides, and inhibitors of phosphodiesterase and protein synthesis. Invest Ophthalmol Vis Sci 28:1059-1069.

Williams RA, Howard AG, Williams TP (1985) Retinal damage in pigmented and albino rats exposed to low levels of cyclic light following a single mydriatic treatment. Curr Eye Res 4:97-102.

Winkler BS (2008) An hypothesis to account for the renewal of outer segments in rod and cone photoreceptor cells: renewal as a surrogate antioxidant. Invest Ophthalmol Vis Sci 49:3259-3261.

Witkovsky P, Stone S, Tranchina D (1989) Photoreceptor to horizontal cell synaptic transfer in the Xenopus retina: modulation by dopamine ligands and a circuit model for interactions of rod and cone inputs. J Neurophysiol 62:864-881.

Wolf-Schnurrbusch UE, Enzmann V, Brinkmann CK, Wolf S (2008) Morphologic changes in patients with geographic atrophy assessed with a novel spectral OCT-SLO combination. Invest Ophthalmol Vis Sci 49:3095-3099.

Wolf G (2004) The visual cycle of the cone photoreceptors of the retina. Nutr Rev 62:283-286.

X

Xu J, Dodd RL, Makino CL, Simon MI, Baylor DA, Chen J (1997) Prolonged photoresponses in transgenic mouse rods lacking arrestin. Nature 389:505-509.

Xu X, Quiambao AB, Roveri L, Pardue MT, Marx JL, Rohlich P, Peachey NS, Al-Ubaidi MR (2000) Degeneration of cone photoreceptors induced by expression of the Mas1 protooncogene. Exp Neurol 163:207-219.

Y

Yacob A, Kunz YW (1977) 'Disk shedding' in the cone outer segments of the teleost, Poecilia reticulata P. Cell Tissue Res 181:487-492.

Yang JN, Luo L, Lin SC, Chen JM, Li D, Hu SX (2005) N-methyl-N-nitrosourea-induced apoptosis of photoreceptor cells in Sprague-Dawley rats via nuclear factor-kappaB. Chin Med J (Engl) 118:1081-1086.

Yang L, Li D, Chen J, Yang J, Xue L, Hu S, Wu K (2007) Microarray expression analysis of the early N-methy-N-nitrosourea-induced retinal degeneration in rat. Neurosci Lett 418:38-43.

Yasukawa T, Wiedemann P, Hoffmann S, Kacza J, Eichler W, Wang YS, Nishiwaki A, Seeger J, Ogura Y (2007) Glycoxidized

particles mimic lipofuscin accumulation in aging eyes: a new age-related macular degeneration model in rabbits. Graefes Arch Clin Exp Ophthalmol 245:1475-1485.

Yoshimura T, Yokota Y, Ishikawa A, Yasuo S, Hayashi N, Suzuki T, Okabayashi N, Namikawa T, Ebihara S (2002) Mapping quantitative trait loci affecting circadian photosensitivity in retinally degenerate mice. J Biol Rhythms 17:512-519.

Yoshizawa K, Tsubura A (2005) [Characteristics of N-methyl-N-nitrosourea-induced retinal degeneration in animals and application for the therapy of human retinitis pigmentosa]. Nippon Ganka Gakkai Zasshi 109:327-337.

Yoshizawa K, Nambu H, Yang J, Oishi Y, Senzaki H, Shikata N, Miki H, Tsubura A (1999) Mechanisms of photoreceptor cell apoptosis induced by N-methyl-N-nitrosourea in Sprague-Dawley rats. Lab Invest 79:1359-1367.

Yoshizawa K, Yang J, Senzaki H, Uemura Y, Kiyozuka Y, Shikata N, Oishi Y, Miki H, Tsubura A (2000) Caspase-3 inhibitor rescues N -methyl- N -nitrosourea-induced retinal degeneration in Sprague-Dawley rats. Exp Eye Res 71:629-635.

Yuge K, Nambu H, Senzaki H, Nakao I, Miki H, Uyama M, Tsubura A (1996) N-methyl-N-nitrosourea-induced photoreceptor apoptosis in the mouse retina. In Vivo 10:483-488.

Z

Zaidi FH, Hull JT, Peirson SN, Wulff K, Aeschbach D, Gooley JJ, Brainard GC, Gregory-Evans K, Rizzo JF, 3rd, Czeisler CA, Foster RG, Moseley MJ, Lockley SW (2007) Short-wavelength light sensitivity of circadian, pupillary, and visual awareness in humans lacking an outer retina. Curr Biol 17:2122-2128.

Zhang K, Nguyen TH, Crandall A, Donoso LA (1995) Genetic and molecular studies of macular dystrophies: recent developments. Surv Ophthalmol 40:51-61.

Zhu X, Ma B, Babu S, Murage J, Knox BE, Craft CM (2002) Mouse cone arrestin gene characterization: promoter targets expression to cone photoreceptors. FEBS Lett 524:116-122.

Zhu X, Brown B, Li A, Mears AJ, Swaroop A, Craft CM (2003) GRK1-dependent phosphorylation of S and M opsins and their binding to cone arrestin during cone phototransduction in the mouse retina. J Neurosci 23:6152-6160.

Zigman S (1989) Special features of the lens relative to the environment. Lens Eye Toxic Res 6:807-821.

In the vertebrate retina, the cells whose role is to detect photons are called photoreceptors. Two types of "classical photoreceptors" (PRs) can be distinguished based on their structure and function: rods and cones. Because of their primordial role in visual acuity, integrity of cones is essential for good vision. The study of physiology and pathology of cones is hence crucial but hampered in classic laboratory rodents (mice and rats) due to their rod dominant retinas (97-99 %). Our laboratory possesses the world's only breeding colony of the diurnal rodent: *Arvicanthis ansorgei,* whose retina has 33 % of cones.

The aims of the study were: 1st, **to establish an *in vivo* model of retinal degeneration in which cone pathogenesis can be easily observed, permitting comparison with that of rods**; and 2nd, **to characterize the effects of degeneration at the structural, physiological and behavioural levels**.

To induce retinal degeneration, two types of published approaches were used: bright light exposure and *N*-methyl-*N*-nitrosourea (MNU) injections. Exposure of *Arvicanthis* to bright light, irrespective of the paradigm used, never induced any reproducible retinal damage either at the structural or functional level. In an alternative approach, high doses of MNU were injected into *Arvicanthis* to induce retinal degeneration. At the structural level, the degeneration commenced approximately 11 days after injection, and presented regional variability in that the upper hemisphere was damaged first, followed by the degeneration of the inferior one. Cones were markedly more resistant than rods during the degeneration process. ERG recordings at late post-treatment times showed decreased amplitudes of responses driven by either rods or cones, demonstrating that visual function is highly compromised. However, because retinal degeneration was never complete in Arvicanthis, in order to examine the effects of MNU-induced retinal degeneration on light-evoked behaviour, we chose to use rats in which photoreceptor loss is total. Abilities of control and MNU-treated rats to photoentrain to light/dark cycles of different light intensities were compared. Results showed that MNU-treated rats did not entrain their locomotor activity when light intensity was low whereas control rats were still synchronized.

The ensemble of this work has provided: 1st, extensive characterization of *Arvicanthis ansorgei* retina, particularly at the functional level; 2nd, evidence for remarkably high resistance of *Arvicanthis* to retinal damage; 3rd, establishment of a validated model for the study of rod and cone degeneration within the same retina; 4th, extensive description of structural and functional characteristics of MNU-induced retinal degeneration in *Arvicanthis;* and 5th, evidence of an impaired photoentrainment ability in MNU-treated rats.